

AD-A041 204

UNITED TECHNOLOGIES RESEARCH CENTER EAST HARTFORD CONN

F/G 20/5

LONG RANGE CHAIN LASER STUDIES, PHASE I STUDIES. (U)

JUN 77 L R BOEDEKER, P A BONZYK, J J HINCHEN

F29601-75-C-0139

UNCLASSIFIED

UTRC/R77-952198-58

AFWL-TR-77-43

NL

3 OF 4
AD
A041204



AFWL-TR-77-43

AFWL-TR-
77-43

AD A041204

LONG RANGE CHAIN LASER STUDIES

Phase I Studies

United Technologies Research Center
East Hartford, CT 06108

June 1977



Final Report

Approved for public release; distribution unlimited.

Prepared for
ADVANCED RESEARCH PROJECTS AGENCY
1400 Wilson Boulevard
Arlington, VA 22

AIR FORCE WEAPONS LABORATORY
Air Force Systems Command
Kirtland Air Force Base, NM 87117

DDO
RECEIVED
JUL 5 1977
REGISTRY

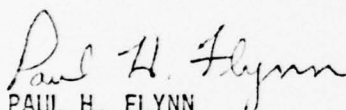
UDC FILE COPY

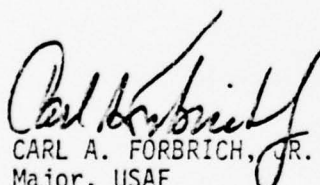
This final report was prepared by United Technologies Research Center, East Hartford, Connecticut, under Contract F29601-75-C-0139, Job Order 27610605 with the Air Force Weapons Laboratory, Kirtland Air Force Base, New Mexico. Captain Paul H. Flynn (ALC) was the Laboratory Project Officer-in-Charge.

When US Government drawings, specifications, or other data are used for any purpose other than a definitely related Government procurement operation, the Government thereby incurs no responsibility nor any obligation whatsoever, and the fact that the Government may have formulated, furnished, or in any way supplied the said drawings, specifications, or other data is not to be regarded by implication or otherwise as in any manner licensing the holder or any other person or corporation or conveying any rights or permission to manufacture, use, or sell any patented invention that may in any way be related thereto.

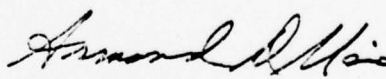
This report has been reviewed by the Office of Information (OI) and is releasable to the National Technical Information Service (NTIS). At NTIS, it will be available to the general public, including foreign nations.

This technical report has been reviewed and is approved for publication.


PAUL H. FLYNN
Captain, USAF
Project Officer


CARL A. FORBRICH, JR.
Major, USAF
Chief, Chemical Laser Branch

FOR THE COMMANDER


ARMAND D. MAIO
Lt Colonel, USAF
Chief, Advanced Laser Technology Div

UNCLASSIFIED

SECURITY CLASSIFICATION OF THIS PAGE (When Data Entered)

REPORT DOCUMENTATION PAGE		READ INSTRUCTIONS BEFORE COMPLETING FORM	
1. REPORT NUMBER AFWL-TR-77-43	2. GOVT ACCESSION NO.	3. RECIPIENT'S CATALOG NUMBER	
4. TITLE (and Subtitle) LONG RANGE CHAIN LASER STUDIES, Phase I Studies		5. TYPE OF REPORT & PERIOD COVERED Final Report	
6. AUTHOR(s) L. R. Boedeker, P. A. Bonzyk, J. J. Hinchey, R. Tripodi, C. J. Ultee		7. PERFORMING ORG. REPORT NUMBER R77-952198-58	
8. PERFORMING ORGANIZATION NAME AND ADDRESS United Technologies Research Center East Hartford, CT 06108		9. CONTRACT OR GRANT NUMBER(s) F29601-75-C-0139 new	
10. CONTROLLING OFFICE NAME AND ADDRESS Advanced Research Projects Agency Arlington, VA 22209		11. PROGRAM ELEMENT, PROJECT, TASK AREA & WORK UNIT NUMBERS 62301F/27610605	
12. MONITORING AGENCY NAME & ADDRESS (if different from Controlling Office) Air Force Weapons Laboratory (ALC) Kirtland Air Force Base, NM 87117		13. REPORT DATE June 1977	
		14. NUMBER OF PAGES 314	
		15. SECURITY CLASS. (of this report) UNCLASSIFIED	
		16. DECLASSIFICATION/DOWNGRADING SCHEDULE	
17. DISTRIBUTION STATEMENT (of this Report) Approved for public release; distribution unlimited.			
18. DISTRIBUTION STATEMENT (of the abstract entered in Block 20, if different from Report)			
19. SUPPLEMENTARY NOTES			
20. KEY WORDS (Continue on reverse side if necessary and identify by block number) Chain Reaction Vibrational Relaxation Kinetics Rate Constants Laser HF			
21. ABSTRACT (Continue on reverse side if necessary and identify by block number) The chemical and vibrational kinetics of the H_2-F_2 chain reaction were studied to improve the description of the evolution of the various vibrational levels in order to better predict chain-reaction-laser performance. Two types of experiments were performed: (1) flow tube, and (2) pulsed reaction. In the flow tube experiments, fluorine atoms were produced by passing F_2 through a mass heater. The F_2 and F emanating from the heater were mixed with additional F_2 , Ar, and H_2 to achieve the desired stoichiometry. The concentrations (OVER)			

DD FORM 1 JAN 73 1473

EDITION OF 1 NOV 65 IS OBSOLETE

UNCLASSIFIED

SECURITY CLASSIFICATION OF THIS PAGE (When Data Entered)

UNCLASSIFIED

SECURITY CLASSIFICATION OF THIS PAGE (When Data Entered)

20. ABSTRACT

of the HF vibrational levels from 0 through 6 were monitored as the mixture flowed through a 5 cm diameter tube through the use of a gain probe, fundamental band IR emission spectroscopy and $\Delta v=3$ overtone emission spectroscopy. In the pulsed-reaction experiments a predetermined mixture of F_2 , H_2 and Ar was sealed in a small constant-volume test cell. The reaction was initiated by the dissociation of a small fraction of the F_2 with a frequency doubled pulsed ruby laser. Pressure changes were monitored with a Kistler gauge and ground state HF with a probe laser. Vibrational levels 1 through 6 were observed by fluorescence measurements. In addition, gain was measured on the 1-0 and 2-1 transitions and laser tests performed which achieved lasing as high as the 5-4 transition.

The results of the study indicate no significant changes need be made to the rates normally used for the hot and cold reactions. Vibrational deactivation rates must be scaled up rapidly with quantum number, however, to adequately describe the measured distributions. A viable deactivation model is presented and possible improvements discussed. It appears that the HF chain reaction is of limited usefulness as a cw laser device.

ACCESSION for	
NTIS	White Spotter <input checked="" type="checkbox"/>
DDC	Buff Spotter <input type="checkbox"/>
UNANNOUNCED	<input type="checkbox"/>
JUSTIFICATION	
BY	
DISTRIBUTION/AVAILABILITY CODES	
Dist.	AVAIL. and/or SPECIAL
A	

DDC
RECEIVED
JUL 5 1977
REGISTRATION
D

UNCLASSIFIED

SECURITY CLASSIFICATION OF THIS PAGE (When Data Entered)

SUMMARY

In order to better understand the physical mechanisms important in chain reaction lasers and their effect on performance, a basic study was initiated, comprised of identification of the problem areas, experimental testing, and subsequent improvement of theoretical models.

The major problem areas were identified as uncertainty of the values for and effects of (1) the chemical pumping reaction rate coefficients ($H + F_2 \rightarrow HF + F$, $F + H_2 \rightarrow HF + H$), (2) HF-HF vibrational deactivation, and (3) H atom deactivation of HF. Potentially significant problem areas also included wall effects, back reactions, hot-atom effects, and chain branching.

The laboratory experiments to study these problem areas fell under two categories: cw flow-tube experiments and stationary-gas pulsed-reaction experiments.

The cw flow-tube chain-reaction experiment was initiated by the thermal dissociation of small quantities of F_2 , subsequently mixed with F_2 , H_2 , and Ar in a flowing situation. As the reaction progressed through the flow tube population distributions of the various v and J levels were measured.

Initial F-atom concentrations were measured with metered HCl titration and HF probe laser absorption. This technique was verified by separate electron-spin-resonance tests performed under the subject contract. Initial temperature profiles were measured with a thermocouple probe, and velocity profiles with a pitot probe. These results were incorporated in the analysis. Ground state HF was measured with probe laser absorption, whereas for vibrational level populations in $v = 1, 2, 3, 4$ absolute IR, $\Delta v = 1$, emission spectroscopy was used. Vibrational levels $v = 3, 4, 5, 6$ were determined with overtone emission spectroscopy using $\Delta v = 3$.

Tests were performed over a range of H_2/F_2 ratios with a fixed initial F-atom concentration in order to obtain reaction rate and vibrational deactivation information. Some HF was added initially to enhance self-deactivation effects. Subsequent tests involved variation of the initial F-atom concentration while trying to maintain the same net HF production rate in order to isolate the influence of H-HF collisions.

The pulsed reaction experiments were used to study H_2-F_2 chain reaction kinetics in a closed volume containing premixed H_2 and F_2 . The reaction was initiated by producing fluorine atoms in the mixture by dissociating F_2 with pulsed UV radiation from a doubled frequency ruby laser. Three types of

experiments were performed: First, a study was made of the temporal development of populations in vibrational states of HF produced from the reaction. Fluorescence measurements were used to track excited state populations and absorption of cw radiation to follow ground state formation. Second, small signal gain was determined for $v(1-0)$ and $v(2-1)$ transitions by use of a gain probe. Third, pulsed laser radiation from the reacting mixture was studied using a laser configuration.

The rationale for these experiments was that they would serve as an experimental check on the laser computer program as modified by results from flow-tube experiments and other available data. Pulsed experiments were chosen as being relatively simple in that the problems attendant with mixing and flow are not present, the reaction is initiated over the total volume in a short time period and changes in temperature and pressure could be monitored in a constant volume cell.

Analysis of the data from the two sets of experiments has indicated that no drastic changes need be made to the chemical reaction rates now in use. The cold reaction rate was found to lie between 1.0 and 2.0 times the nominal value, and the hot reaction rate between 0.5 and 1.3 times its nominal value. Other effects (back reactions, chain branching, hot-atom enhancement) could not be easily isolated, but appear to be of minor importance. Under some circumstances (such as these experiments) wall effects can be nonnegligible.

The original vibrational-deactivation model was found to be inadequate in describing upper level vibrational populations. Much better agreement has been achieved by adopting a model allowing for rapid deactivation of upper vibrational levels via multiquanta V-T transitions. Single quantum V-V exchange is then found to be somewhat slower than expected, but in any case to weakly influence the population distributions. Remaining deficiencies in the fit of the model to the data indicate, however, that multiquanta V-V exchange may be the key to even better agreement. Such a possibility should be explored further.

The direct influence of H atoms on vibrational deactivation proved difficult to isolate due to the strong influence of HF self-deactivation, which is still not completely understood, in the test conditions feasible in these experiments. Hence, no new conclusions were reached with regard to such rates, now believed to be very rapid for $v \geq 3$.

The laser model as modified was employed to predict the performance potential of chain-reaction lasers. It was found that operation in a fluorine-rich condition tended to give the best gains and powers, in agreement with experimental observation. Nonetheless, the enhanced vibrational deactivation was sufficient to reduce predicted output power to the extent that chain-reaction lasers are not competitive with cold-reaction lasers for high altitude applications.

TABLE OF CONTENTS

<u>Section</u>		<u>Page</u>
I	INTRODUCTION	1
II	CW FLOW TUBE REACTOR EXPERIMENT	3
	Introduction	3
	Description of Experimental Configuration	3
	Test Program and Instrumentation for CW Flow Tube	7
	Reactor Experiment	
	Summary of Conditions	7
	Experiment and Results	11
	Vacuum Pumping Arrangement	11
	Setting of Gas Flows	11
	Pressure Distribution in Flow Tube	14
	Velocity Profiles Along Flow Tube	14
	Gas Temperature Uniformity	16
	HF Probe Laser Absorption	21
	Titration for F Atoms	27
	Emission Spectroscopy Measurements	32
	Contaminants	32
	Discussion and Recommendations	33
	Summary and Conclusions	35
III	PULSED REACTION EXPERIMENTS	37
	Pulsed Fluorescence Experiment	37
	Pulsed Fluorescence Data	45
	Pulsed Gain Measurements	71
	Pulsed Laser Tests	73
IV	DATA ANALYSIS	87
	Chemical Reactions	87
	Flow Tube	87
	Pulsed-Fluorescence	100
	Vibrational Deactivation	148
	Flow Tube	148
	Pulsed-Fluorescence	189
	Performance Calculations	220
	Discussion	229
	Chemical Reactions	229
	Vibrational Deactivation	232
	Chain Reaction Laser Performance	239

TABLE OF CONTENTS (CONT'D)

<u>Section</u>	<u>Page</u>
V ESR TITRATION EXPERIMENT	241
Summary	241
Introduction	241
Apparatus	243
Results	243
O ₂ Calibration Spectra	243
F Spectra	246
(F+HCl) Spectra	249
Conclusion	249
REFERENCES	255
APPENDIX A: NOMINAL RATE PACKAGE	259
APPENDIX B: STEADY-STATE SOLUTION	271
APPENDIX C: ACCOUNTING FOR TWO-DIMENSIONAL VELOCITY VARIATIONS IN PIPE FLOWS	277
APPENDIX D: ESTIMATES OF WALL ADSORPTION EFFECTS	289
LIST OF SYMBOLS	298

LIST OF ILLUSTRATIONS

<u>Figure</u>	<u>Page</u>
1. HF Chain Reaction Flow Tube Experiment	4
2. HF Chain Kinetics Mixer	6
3. Flow Tube Reactor Experimental Arrangement	10
4. Pressure Distribution Along Flow Tube	15
5. Velocity Profile Measurement	17
6. Flow Tube Velocity Distribution Data	18
7. Flow Tube Velocity Distribution Data	19
8. Effect of Purge Gas Flow Rate on Flow Tube Temperature Distribution	20
9. Effect of Mass Heater on Flow Tube Temperature Distribution	22
10. HF Probe Laser Absorption Diagnostic	23
11. Probe Laser Absorption Signal	24
12. Probe Laser Absorption Signal	25
13. Probe Laser Absorption Data Acquisition	26
14. Probe Laser Absorption Calibration Check by HF Addition	28
15. HCl Titration for F	29
16. HCl Titration for F	30
17. Initial F Atom Concentration from HCl Titration	31
18. Fluorescence Experiment	38
19. Fluorescence Experiment	39

LIST OF ILLUSTRATIONS (CONT'D)

<u>Figure</u>		<u>Page</u>
20.	Calibration-Kistler Gauge vs Capacitance	41
21.	Variation of Exit Throat Area with Chamber Pressure	44
22.	Absorption of $1P_4$ Radiation by HF and HF in Argon	46
23.	Effect of Argon on HF Linewidth	47
24.	Effect of 100 Torr Ar on Apparent HF Pressure	48
25.	Fluorescence Traces	49
26.	Fluorescence Traces	50
27.	HF Number Density and Temperature Histories - Pulsed-Fluorescence Case A10	51
28.	HF Number Density and Temperature Histories - Pulsed-Fluorescence Case B4	53
29.	HF Number Density and Temperature Histories - Pulsed-Fluorescence Case C7	54
30.	HF Number Density and Temperature Histories - Pulsed-Fluorescence Case DH4	55
31.	HF Number Density and Temperature Histories - Pulsed-Fluorescence Case EF2	56
32.	HF Number Density and Temperature Histories - Pulsed-Fluorescence Case FF2	57
33.	Reaction on an H_2-F_2 Mixture	68
34.	Effect of Initial F-Atom on H_2-F_2 Reactions	69
35.	Effect of Initial F-Atom on Reaction - 0.02 Torr HF Present	70

LIST OF ILLUSTRATIONS (CONT'D)

<u>Figure</u>		<u>Page</u>
36.	Gain Traces	72
37.	Gain vs. Laser Transition	75
38.	Gain vs. Pulse Energy	76
39.	Gain LP ₄ - Various Mixtures	77
40.	Laser Experiments	79
41.	Pulsed Laser Output	81
42.	Variation of Total HF	89
43.	Comparison Between Model and Experiment	91
44.	Comparison Between Model and Experiment	92
45.	Comparison Between Model and Experiment	93
46.	Comparison Between Model and Experiment	94
47.	Comparison Between Model and Experiment	95
48.	Comparison Between Model and Experiment	96
49.	Comparison Between Model and Experiment	97
50.	Comparison Between Model and Experiment	98
51.	Composite HF Temporal Behavior	103
52.	Composite HF Temporal Behavior	104
53.	Composite HF Temporal Behavior	105
54.	Composite HF Temporal Behavior	106
55.	Composite HF Temporal Behavior	107

LIST OF ILLUSTRATIONS (CONT'D)

<u>Figure</u>		<u>Page</u>
56.	Composite HF Temporal Behavior	108
57.	Variation of Maximum HF Produced with Pulse Energy	109
58.	Variation of Maximum HF Produced with Pulse Energy	110
59.	Variation of Maximum HF Produced with Pulse Energy	111
60.	Variation of Maximum HF Produced with Pulse Energy	112
61.	Variation of Maximum HF Produced with Pulse Energy	113
62.	Variation of Maximum HF Produced with Pulse Energy	114
63.	Comparison of Model with Experiment	118
64.	Comparison of Model with Experiment	119
65.	Comparison of Model with Experiment	120
66.	Comparison of Model with Experiment	121
67.	Comparison of Model with Experiment	122
68.	Comparison of Model with Experiment	123
69.	Comparison of Model with Experiment	124
70.	Comparison of Model with Experiment	125
71.	Comparison of Model with Experiment	126
72.	Comparison of Model with Experiment	127
73.	Comparison of Model with Experiment	128
74.	Comparison of Model with Experiment	129
75.	Comparison of HF Histories	131

LIST OF ILLUSTRATIONS (CONT'D)

<u>Figure</u>		<u>Page</u>
76.	Comparison of Temperature Histories	132
77.	Comparison of HF Histories	133
78.	Comparison of Model with Experiment	134
79.	Comparison of Model with Experiment	135
80.	Comparison of Model with Experiment	136
81.	Comparison of Model with Experiment	137
82.	Comparison of Model with Experiment	138
83.	Comparison of Model with Experiment	139
84.	Comparison of Model with Experiment	140
85.	Comparison of Model with Experiment	141
86.	Comparison of Model with Experiment	142
87.	Comparison of Model with Experiment	143
88.	Comparison of Model with Experiment	144
89.	Comparison of Model with Experiment	145
90.	Comparison with Model	151
91.	Comparison with Model	152
92.	Comparison with Model	153
93.	Comparison with Model	154
94.	Comparison with Model	155
95.	Comparison with Model	156

LIST OF ILLUSTRATIONS (CONT'D)

<u>Figure</u>		<u>Page</u>
96.	Comparison with Model	157
97.	Comparison with Model	158
98.	Comparison with Model	159
99.	Comparison with Model	160
100.	Comparison with Model	161
101.	Comparison with Model	162
102.	Comparison with Model	163
103.	Comparison with Model	164
104.	Comparison with Model	165
105.	Comparison with Model	166
106.	Comparison with Model	167
107.	Comparison with Model	168
108.	Comparison with Model	169
109.	Comparison with Model	170
110.	Comparison with Model	171
111.	Influence of V-V Rates	173
112.	Influence of V-V Rates	174
113.	Comparison with Model	175
114.	Comparison with Model	176
115.	Comparison with Model	177

LIST OF ILLUSTRATIONS (CONT'D)

<u>Figure</u>		<u>Page</u>
116.	Comparison with Model	178
117.	Comparison with Model	179
118.	Comparison with Model	180
119.	Comparison with Model	181
120.	Comparison with Model	182
121.	Comparison with Model	183
122.	Comparison with Model	184
123.	Comparison with Model	185
124.	Comparison with Model	186
125.	Comparison with Model	187
126.	Comparison with Model	188
127.	Variation of Total HF	195
128.	Vibrational Population Distributions	196
129.	Vibrational Population Distributions	197
130.	Vibrational Population Distributions	198
131.	Vibrational Population Distributions	199
132.	Comparison of Model with Experiment	203
133.	Comparison of Model with Experiment	204
134.	Comparison of Model with Experiment	205
135.	Comparison of Model with Experiment	206

LIST OF ILLUSTRATIONS (CONT'D)

<u>Figure</u>		<u>Page</u>
136.	Comparison of Model with Experiment	207
137.	Comparison of Model with Experiment	208
138.	Comparison of Model with Experiment	209
139.	Comparison of Model with Experiment	210
140.	Comparison of Model with Experiment	211
141.	Comparison of Model with Experiment	212
142.	Comparison of Model with Experiment	213
143.	Comparison of Model with Experiment	214
144.	Comparison of Model with Experiment	215
145.	Comparison of Model with Experiment	216
146.	Comparison of Model with Experiment	217
147.	Comparison of Model with Experiment	218
148.	Comparison of Model with Experiment	219
149.	ESR F-Atom Titration Apparatus	244
150.	Molecular Oxygen ESR Signal	245
151.	Spectrometer Calibration Curve	247
152.	Atomic Fluorine ESR Signal	252
153.	HCl Titration of F-Atom ESR Signal	253
C1.	Effective Rate Coefficient Multiplier	282
C2.	One Dimensional Simulation of Reacting Pipe Flow	283

LIST OF ILLUSTRATIONS (CONT'D)

<u>Figure</u>		<u>Page</u>
C3.	One Dimensional Simulation of Reacting Pipe Flow	284
C4.	One Dimensional Simulation of Reacting Pipe Flow	285
C5.	Prescribed Velocity and Rate Modifier for Flow Tube Calculations	287
D1.	Normalized Number Density Time History	291
D2.	Normalized Number Density Time History	295

LIST OF TABLES

<u>Table</u>		<u>Page</u>
1.	Instrumentation	8
2.	Summary of Conditions	9
3.	Summary of Conditions	12
4.	Argon Feed Distribution to Flow Tube	13
5.	Pulsed Fluorescence Data with Premixed Gases	58
6.	Summary of Preliminary Pulse Experiments	63
7.	Data from Gain Measurements	74
8.	Pulsed Laser Test Data	82
9.	Initial Conditions - Flow Tube Simulation	88
10.	Initial Conditions - Pulsed Fluorescence Simulation	101
11.	Initial Conditions - Pulsed Fluorescence Experiment	117
12.	x = 4 cm - Port 1	190
13.	x = 8 cm - Port 2	191
14.	x = 12.1 cm - Port 3	192
15.	x = 21.4 cm - Port 4	193
16.	x = 31 cm - Port 5	194
17.	Initial Conditions - Pulsed Fluorescence	201
18.	Comparison of Predicted and Measured Gain Input Conditions	202
19.	Predicted Gain	221
20.	Comparison of Predicted and Measured Gain	222

LIST OF TABLES (CONT'D)

<u>Table</u>		<u>Page</u>
21.	Input Conditions	224
22.	Predicted Performance - Cold Reaction Laser	225
23.	Input Conditions - Design Point Chain Reaction Laser	226
24.	Input Conditions - Representative Chain Reaction Laser	227
25.	Predicted Performance - Design Point Chain Reaction Laser	228
26.	Predicted Performance - Representative Chain Reaction Laser	228
27.	Input Conditions - Chain Reaction Pressure Variation Studies	230
28.	Predicted Performance - Effect of Pressure Variation	231
29.	Predicted Performance - Effect of Fluorine	231
30.	Recommended Chemical Rates	233
31.	Recommended Changes to Original Vibrational Relaxation Rate Package	236
32.	Summary of HCl Titration of F via $\text{HCl} + \text{F} \rightarrow \text{HF} + \text{Cl}$	251
A1.	Chemical Reactions Considered and Nominal Rates	260
A2.	V-T Relaxation Times	263
A3.	V-T Multiple-Quanta Transitions: $v \rightarrow v-n$, n Arbitrary	264
A4.	H_2 Deactivation	269
B1.	Steady State Solution	274

LIST OF TABLES (CONT'D)

<u>Table</u>		<u>Page</u>
B2.	Steady State Solution	275
C1.	Input Conditions - Effective Rate Test Cases	281
D1.	Possible HF Wall Loss Effects in Pulsed-Fluorescence Tests	296

SECTION I. INTRODUCTION

The work described in this report covers the research carried out under Phase I of the subject contract. Phase I was a technology development program designed to improve the ability to predict analytically the performance potential of chain reaction lasers, and to assess their feasibility, particularly with respect to high altitude missions. The program comprised three tasks: (1) identification of kinetic problem areas in model predictions, (2) experimental testing to study those problem areas, (3) analysis of the data and resultant modification of existing computer models to assess performance potential.

The details of the various experiments, the subsequent analysis and code modification, and the resulting conclusions will be presented below.

SECTION II. CW FLOW TUBE REACTOR EXPERIMENT

Introduction

The CW flow tube reactor was selected as one of the experiments to be conducted because populations in the various V and J levels and the ground state are readily obtained under steady state conditions (Refs. 1-3). Results of Task I, Problem Area Identification (Ref. 4) indicated that the chemical and relaxation processes probably account for a major share of the observed discrepancy between predictions and experiment. Results of Task I also indicated a practical range of conditions over which flow tube results likely could provide rate information for the overall reaction and molecular energy transfer processes that are occurring. A discussion of the flow tube research conducted to obtain this information is presented in the following sections. In general, significant data results on vibrational level populations and total HF formation are included in the discussion under Section IV of this report.

Description of Experimental Configuration

The apparatus components employed in the tests were essentially those described in References 1 through 3 with suitable modifications of a minor nature to achieve additional required data and improved accuracy of results. A schematic of the major components as employed here is shown in Figure 1.

Fluorine mixed with a constant purge flow of argon makes three passes in a nickel tube assembly through the heated zone of a well regulated commercial tube furnace. At low pressure significant dissociation of F_2 ($\alpha_{F_2} = 1-40$ percent) can occur thermally (Ref. 3) at temperatures under $1000^{\circ}K$, a safe

1. UTRC Report P-R89, "Proposal for Long-Range HF Chain Laser Studies, Part I, Technical Proposal," and "Part II, Addendum," East Hartford, CT, April 1975.
2. UTRC Report P-R89-2, "Answers to Questions Addressed to United Technologies Research Center Concerning Proposal P-R89-1, East Hartford, CT, May 1975.
3. Boedeker, L. R., J. F. Verdick, and R. J. Hall, "HF Chain Reaction Laser," Final Technical Report, Contract N00014-74-C-0379 (NRL/ONR), UTRC Report R75-951883-4, East Hartford, CT, May 1975.
4. Ultee, C. J., "HF Long-Range Chain Laser Studies, Proposed Research Plan," Contract F29601-75-C-0139, UTRC Report R75-952198-5, East Hartford, CT, August 1975.

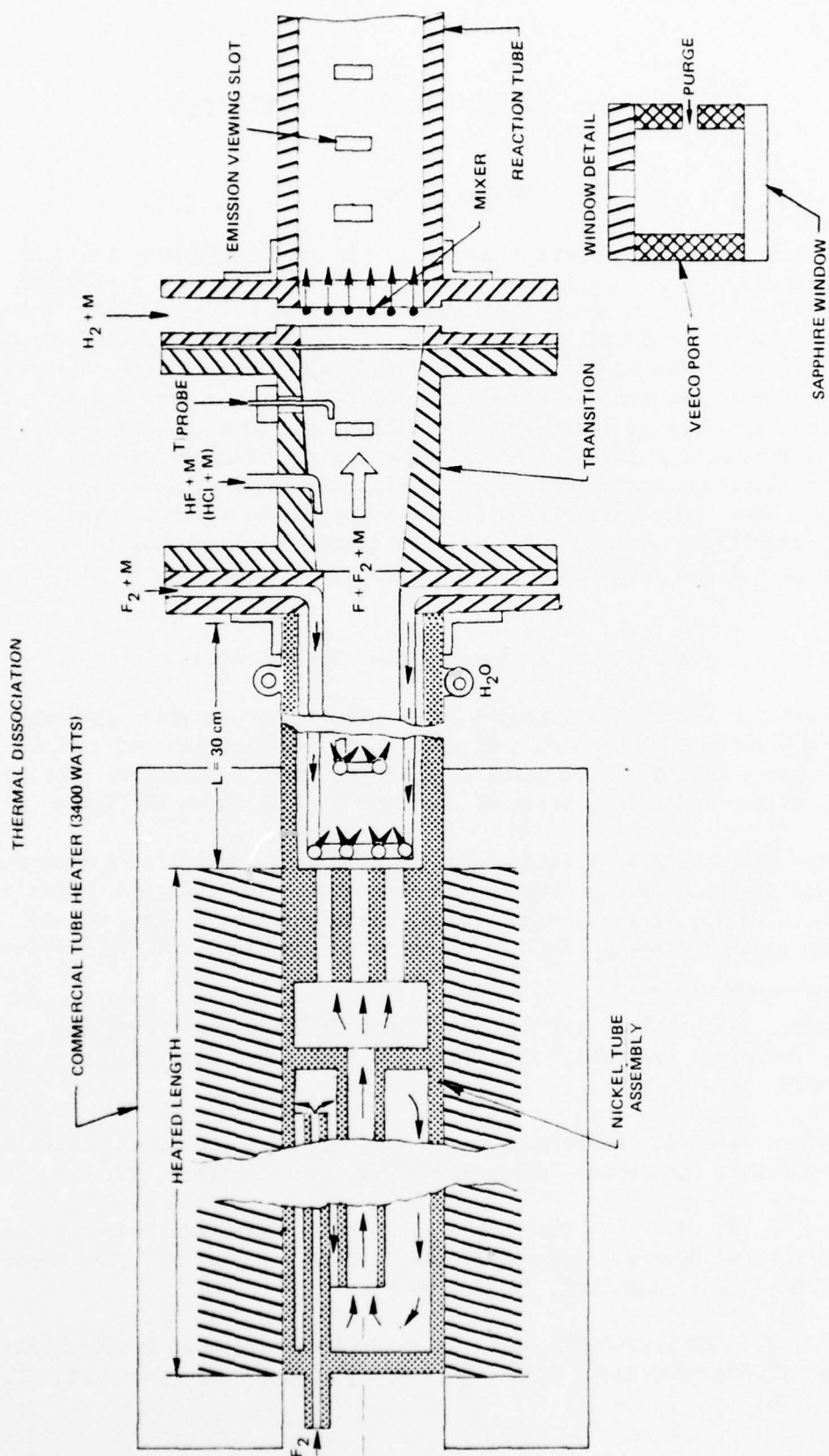


FIGURE 1 HF CHAIN REACTION FLOW TUBE EXPERIMENT

working level for nickel. The hot, partially dissociated F_2 passes rapidly out of the heated zone through an array of seven holes and the translational temperature is reduced rapidly to near room temperature by mixing with argon introduced through a fine scale injector ring placed close to the end of the heated length. This injector is supported by a length of copper pipe which is water cooled (not shown in Fig. 1) and does not touch the hot nickel tube assembly except at the flange joint 30 cm downstream of the heated zone and outside the tube heater where all components are water cooled. The translational temperature of the F_2 is lowered rapidly enough here to preserve F atoms in flow from the mass heater to the H_2 injector (Refs. 1-3). In order to adjust the overall level of dissociation, additional F_2 is added to the argon diluent flow which thus bypasses the mass heater.

An auxiliary injector ring was located in the F_2 dilution section through which metered flows of HF or HCl were added upstream of the H_2 injector.

Before the H_2 injector, a transition section was placed to adjust the diameter of the flow smoothly to the diameter of the reaction zone $d = 5$ cm. The H_2 mixer is an array of small tubes, Figure 2, with small injection holes angled 30° downstream to avoid impingement of the injectant on adjacent tubes and backstreaming effects. The H_2 is mixed with a large amount of argon and large penetration occurs. The characteristic mixing tends to be between layers separated by about 1.5 mm, the hole spacing along each tube, thus assuring mixing in 1 to 2 cm (Refs. 1-4).

Viewing ports were placed along the reaction tube at $x = 4, 8, 12, 24, 31, 41, 51$ cm from the H_2 injector. One viewing port was placed 4 cm upstream of the H_2 injector to check for backstreaming. Each set of viewing ports was purged with a metered flow of argon. The viewing ports contained narrow slots cut through to the reaction zone. Thus, maximum spontaneous emission could be collected by aligning the spectrometer slit with the long side of the slot while minimizing distortion of the flow velocity profile.

The inside of the reaction tube and transition were coated with Teflon to inhibit H atom recombination on the wall (Ref. 5). The particular coating that gave best application results contained about 13 percent TiO_2 as pigment. Substantial reduction in H atom recombination would be expected, however, compared to pure copper based on exposed surface area of Teflon. Present tests are also at a factor of 4 higher pressure than previously (Ref. 3) reported. Experimental results must be examined closely, however, to see if an H atom

-
5. Wood, R. J. and H. Wise, "Kinetics of Hydrogen Atom Recombination on Surfaces," J. Chem. Phys., 65, 1976, 1961.

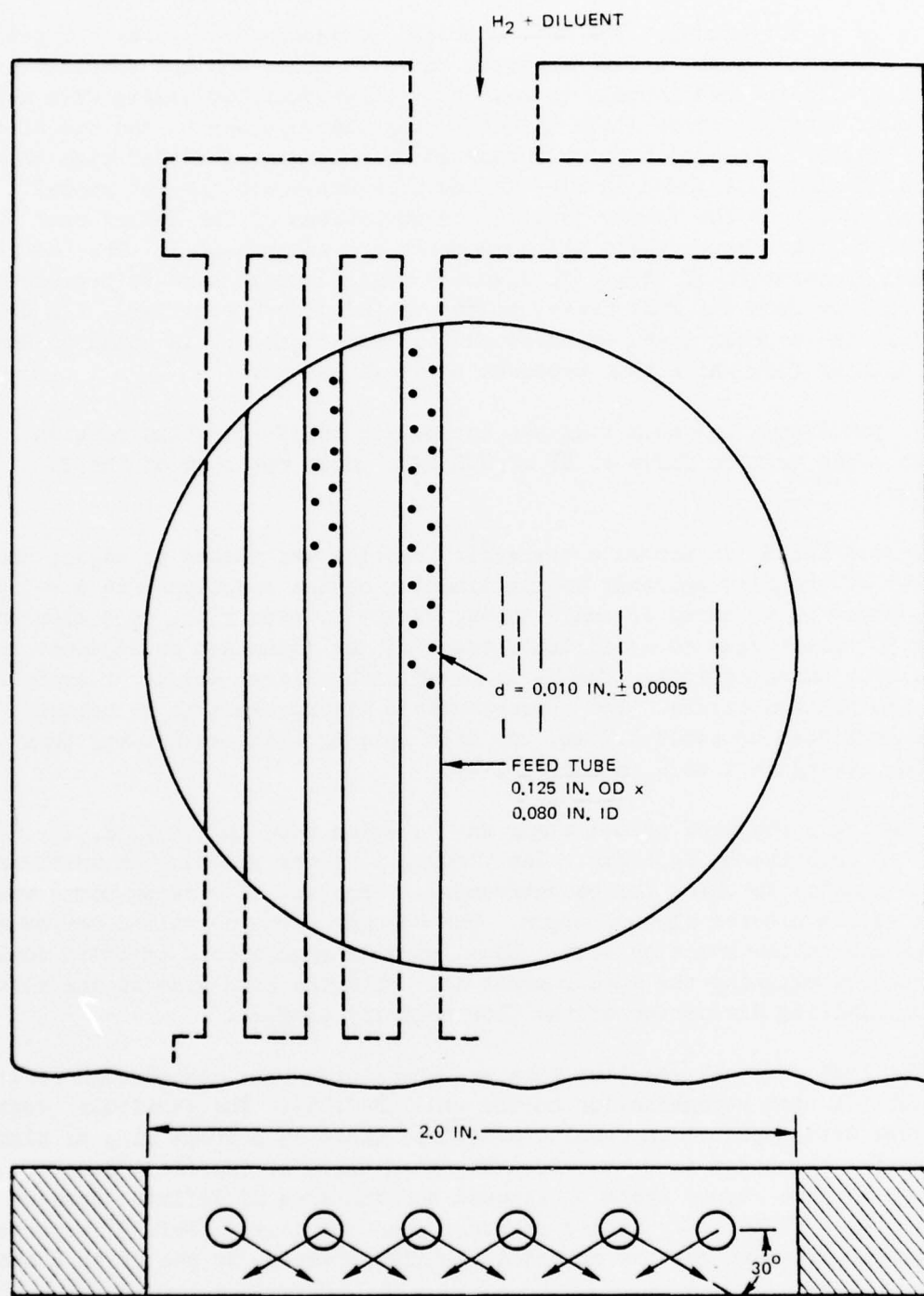


FIGURE 2 HF CHAIN KINETICS MIXER

or other wall effect exists at large distances or F_2/H_2 ratios. At present, calculations and examination of results in Section IV do not indicate wall effects to be a factor unless the H atom loss was unity and then the effect would be limited to 25 percent.

Test Program and Instrumentation for CW Flow Tube Reactor Experiment

Flow tube experiments were directed towards (1) acquisition of F atom titration data with HCl addition and HF probe laser absorption in order to calibrate the mass heater and verify establishment of desired low levels of initial F_2 dissociation and (2) acquisition at several stations along the flow tube reaction zone of ground state and vibrational level population information from probe laser absorption; $\Delta v = 1$ and $\Delta v = 3$ emission spectroscopy data for conditions determined from Task I studies in order to provide relevant fits to the model that would yield improved information on rates for the hot reaction; HF V-V, V-T self-relaxation; and H atom deactivation. In initial work, the Proposed Research Plan (Ref. 4) for flow tube experiments was prepared, and based on the results of Task I and discussion with AFWL and Aerospace personnel, increased emphasis was placed on verification of velocity and temperature uniformity with most testing conducted at higher pressure, up to $p = 20$ torr, at velocity $v \sim 10^4$ cm/sec with a useful reaction zone length $L \sim 50$ cm. A summary of instrumentation is given in Table 1. The overall arrangement of the instrumentation and the apparatus is shown in Figure 3. Detailed discussion of each diagnostic and results is given after the overall conditions that were attained are summarized in the next section.

Summary of Conditions

The objectives of the experiment were sought in two series of tests:

(1) In the first series operation over a wide range of F_2/H_2 about unity was sought maintaining fixed F in order to obtain information about the hot and cold reaction rates near room temperature. Conditions attained are summarized in Table 2. This series also provided HF:HF interaction information since HF production varied over a wide range and generally HF:HF appeared to dominate H:HF interaction where effects were measurable. Such HF:HF information was supplemented by direct addition of HF to the flow tube for these cases.

(2) In the second series operation was sought at a higher level of F and F_2 dissociation maintaining constant H_2 and nearly constant HF production. Such a condition was sought by decreasing the level of F_2 proportional to the increase in F. The relative effect of H:HF collisions is enhanced as a result.

TABLE 1. INSTRUMENTATION

1. Probe Laser Absorption: $v = 0$, initial F
2. Overtone Spectroscopy $\Delta v = 3$, EMI S-1 Photodetector ($T = -50^{\circ}\text{C}$ controlled): $v = 3, 4, 5, 6$
3. IR Spectroscopy $\Delta v = 1$, PbS Detector (LN_2 cooled): $v = 1, 2, 3, 4$
4. Pitot and wall pressure distributions: gas velocity and pressure
5. Gas Temperature Radial Distribution
6. Gas feed rates, inert argon, H_2 and corrosive F_2 , HF, HCl: species concentrations.

TABLE 2. SUMMARY OF CONDITIONS*

I) Chemical Rates and HF additive

$$p = 20.0 \pm 0.4 \text{ torr}$$

$$T_i = 308 \pm 4^\circ\text{K}$$

$$\bar{v} = (\text{graph given}) + 0$$

$$- 6\%$$

Case	F_i	Initial Conditions			$F/2F_2$
		F_2^{**} scc/min (torr)	H_2 scc/min (torr)	Ar sl/min	
1	$0.0021 \pm .002$	1130 ± 40 (.0950)	135 ± 3 (.0113)	238 ± 12	0.011
2	$0.0021 \pm .002$	640 ± 30 (.0538)	200 ± 5 (.0168)	238 ± 12	0.020
3	$0.0021 \pm .002$	250 ± 15 (.0210)	400 ± 10 (.0336)	238 ± 12	0.050
4	$0.0021 \pm .002$	60 ± 5 (.0050)	800 ± 20 (.0672)	238 ± 12	0.210

*These conditions are the average values and maximum uncertainty of quantities that were recorded as each case was repeated for the separate probe laser, overtone emission, IR emission and F atom titration measurements.

**Total F_2 feed to experiment

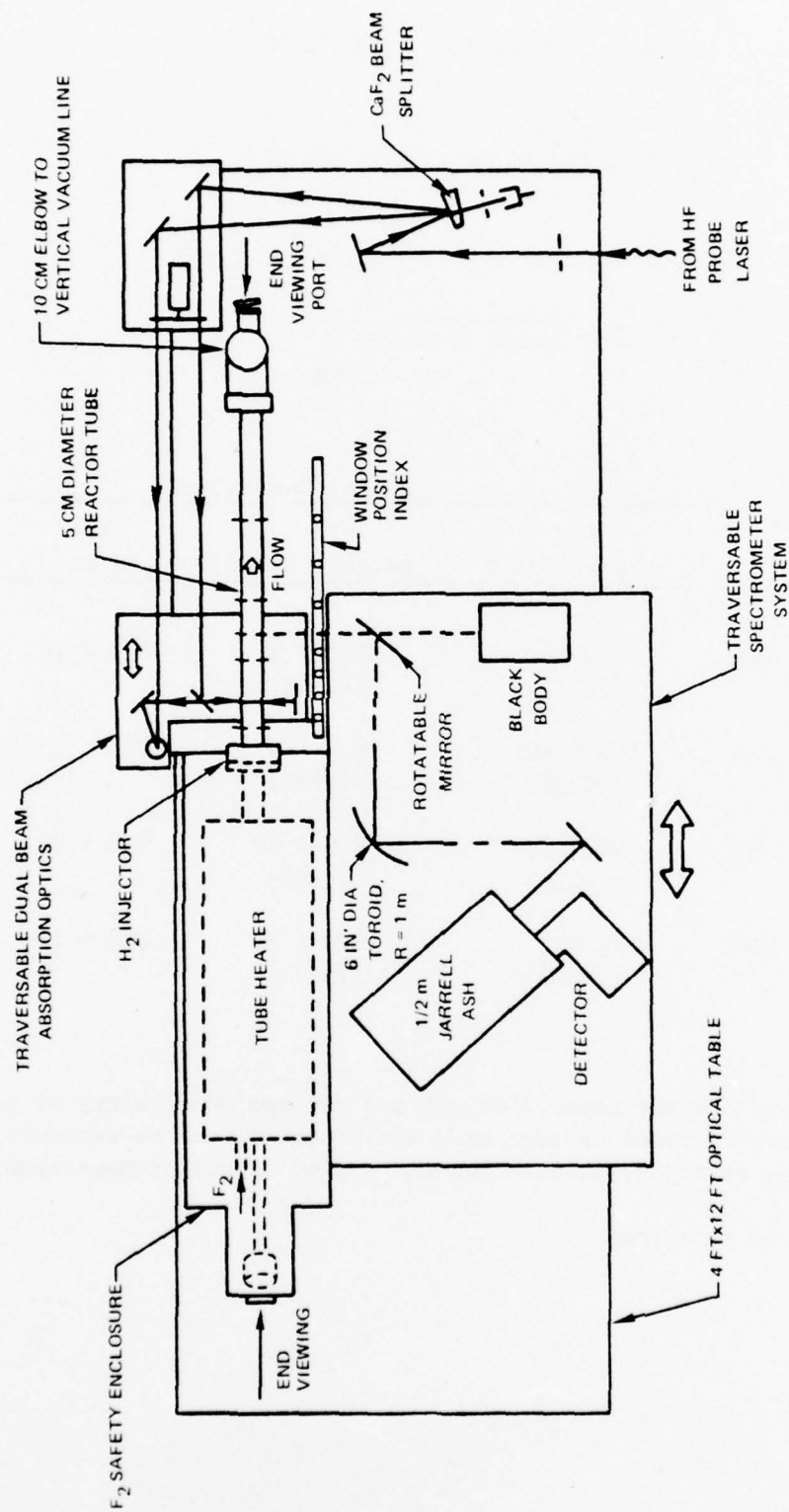


FIGURE 3 FLOW TUBE REACTOR EXPERIMENTAL ARRANGEMENT

Actual initial conditions attained for the two resulting cases are summarized in Table 3. Results for HF production and vibrational level changes are given in Section IV.

Experiment and Results

Vacuum Pumping Arrangement

The experiment was connected through a 4 in. vacuum line (with in-line LN₂ trap, isolation valve and throttle valve) to a 3000 CFM mechanical blower backed by two 450 CFM trochiodal pumps.

Setting of Gas Flows

Diluent argon for 5 cm diameter flow tube at p = 20 torr

Argon was selected as the diluent for the experiment instead of helium because its higher molecular weight at constant velocity results in higher Reynolds number flow, thinner boundary layers and a more uniform velocity profile in the reaction zone. This minimizes corrections that have to be applied in the analysis to account for diffusion of HF(v) to the walls and for streamlines in the flow having different velocities and time histories. Uniform velocity is enhanced for the present flow tube since the pressure and velocity are moderately high, $p \sim 20$ torr and $v \sim 10^4$ cm/sec. The combination of these conditions permits operation here with a tube diameter small relative to the reaction zone length $D/L = 0.1$.

A listing of the argon feed distribution along the flow tube is given in Table 4: (1) Argon flow to the mass heater is needed to overcome a slight ejector effect at the F₂ dilution injector and maintain the pressure in the mass heater higher than in the F₂ dilution stage. This assures uniform distribution in the mass heater F₂ effluent in the seven hole array (Fig. 1) in the presence of small radial pressure gradients at the F₂ dilution injector. Such purge also serves to clear the system of F₂ rapidly when establishing reference levels for absorption measurements. (2) The argon flow to the F₂ dilution injector is limited at present by a pressure limit in the F₂ system which supplies additional cold F₂ for mixing with this diluent. (3) The argon flow in the H₂ injector is higher than in the F₂ dilution injector to make up for this limit in F₂ dilution injector flow. Also, velocity profile tests gave slightly more favorable results with more argon in the H₂ injector. (4) Purge in the annular dead zone between the F₂ dilution injector and nickel mass heater was thought to be necessary, but had to be kept to a low value to maintain temperature uniformity as discussed later in this section. (5) Steady purge of the HF(HCl) injector assured attainment of a fast probe laser

TABLE 3. SUMMARY OF CONDITIONS*

II) H Atom Deactivation

$$p = 2 \pm 0.4 \text{ torr}$$

$$T_i = 308 \pm 4^\circ\text{K}$$

$$\bar{v} = (\text{graph given}) + 0$$

- 6%

Case	Initial Conditions				$F/2F_2$
	F torr	F_2^{**} scc/min	H_2 scc/min	Ar sl/min	
5***	$0.0019 \pm .0001$	410 ± 20 0.034 $\pm 10\%$	210 ± 10 0.018 $\pm 10\%$	238 ± 12	.028
6	$0.0052 \pm .0003$	140 ± 6 0.012 $\pm 10\%$	210 ± 10 0.018 $\pm 10\%$	238 ± 12	.217

*These conditions are the average values and maximum uncertainty of quantities that were recorded as each case was repeated for the separate probe laser, overtone emission, IR emission and F atom titration measurements.

** F_2 feed to mass heater + F_2 feed bypassing mass heater

***Reduce HF($v=1$) from $\Delta v = 1$ spectra. Since F_2 hot and cold feeds were each about 5 percent too high. Hence F_2H_2 product was 10 percent too high for that data.

TABLE 4. ARGON FEED DISTRIBUTION TO FLOW TUBE

<u>Location</u>	<u>Rate</u> (calibrated Rotometers) std liters/min
1 Mass Heater Inlet	3
2 F ₂ Dilution Injector	68 ± 3
3 H ₂ Injector	146 ± 5
4 Purge between mass heater and F ₂ dilution stage	3
5 Steady purge of HF(HCl) Injector	5 ± 3
6 Total viewpoint purge	<u>13 ± 1</u> 238 ± 12

zero reference. Such purge flow could not be much higher than the HF (and probably HCl) flow rates in order to achieve steady and accurate HF absorption signals due to the additive; this condition is probably indicative of an unstable chemical wall effect in the copper feed lines at high dilution. (6) Purge to each set of viewports was controlled separately with needle valves. The total flow to all eight sets is given in Table 4. The purge flow through each port into the flow tube represents a 0.0036 fraction of the total flow passing by the slot inside the flow tube; a small disturbance to the velocity profile. Such small purge proved adequate, however, to remove ground state HF from the window volume and establish stable levels of absorption insensitive to changes in purge flow about this value.

Reactive Gases and Additives

Gases F_2 , HF and HCl were metered with monel mass flow transducers obtained from Matheson. These flow transducers were calibrated and checked on a regular basis using a standard volume in the feed system, isolation valves, a pressure gauge and a stopwatch. For H_2 (UHP grade) a rotometer gave reliable calibration results at the feed pressure employed and was preferred over the slow responding mass flow transducer. Commercial F_2 was used directly from 1A cylinders with a UTRC safety enclosure system; an in-line sodium bifluoride trap was used to remove HF from F_2 . Distilled HF was obtained in a monel cylinder from Ozark Mahoning and was cooled with LN_2 and pumped on prior to use; HCl was used directly from a #3 cylinder of technical purity.

Pressure Distribution in Flow Tube

The pressure data shown in Figure 4 include repeatability obtained from tests on separate days. Data were obtained with a wafer fluid scanner and a pressure transducer. Reactants have only a small effect on the flow pressure for these very dilute cases. As discussed above, the pressure in the mass heater is maintained at a level above the value in the F_2 dilution section. A small pressure rise $\Delta p \sim 1$ torr occurs across the H_2 injector which indicates that a very small ejector effect exists with this angled injector (Fig. 2). The pressure in the reaction zone is relatively flat with an average value of about 20.0 torr. (Calibration of pressure was with a Wallace and Tiernen gauge.)

Velocity Profiles Along Flow Tube, Check on Velocity Results With Metered Argon Flow

Velocity profiles at several stations along the flow tube were measured with a 1/16 in. diameter pitot probe and a MKS Baratron differential transducer.

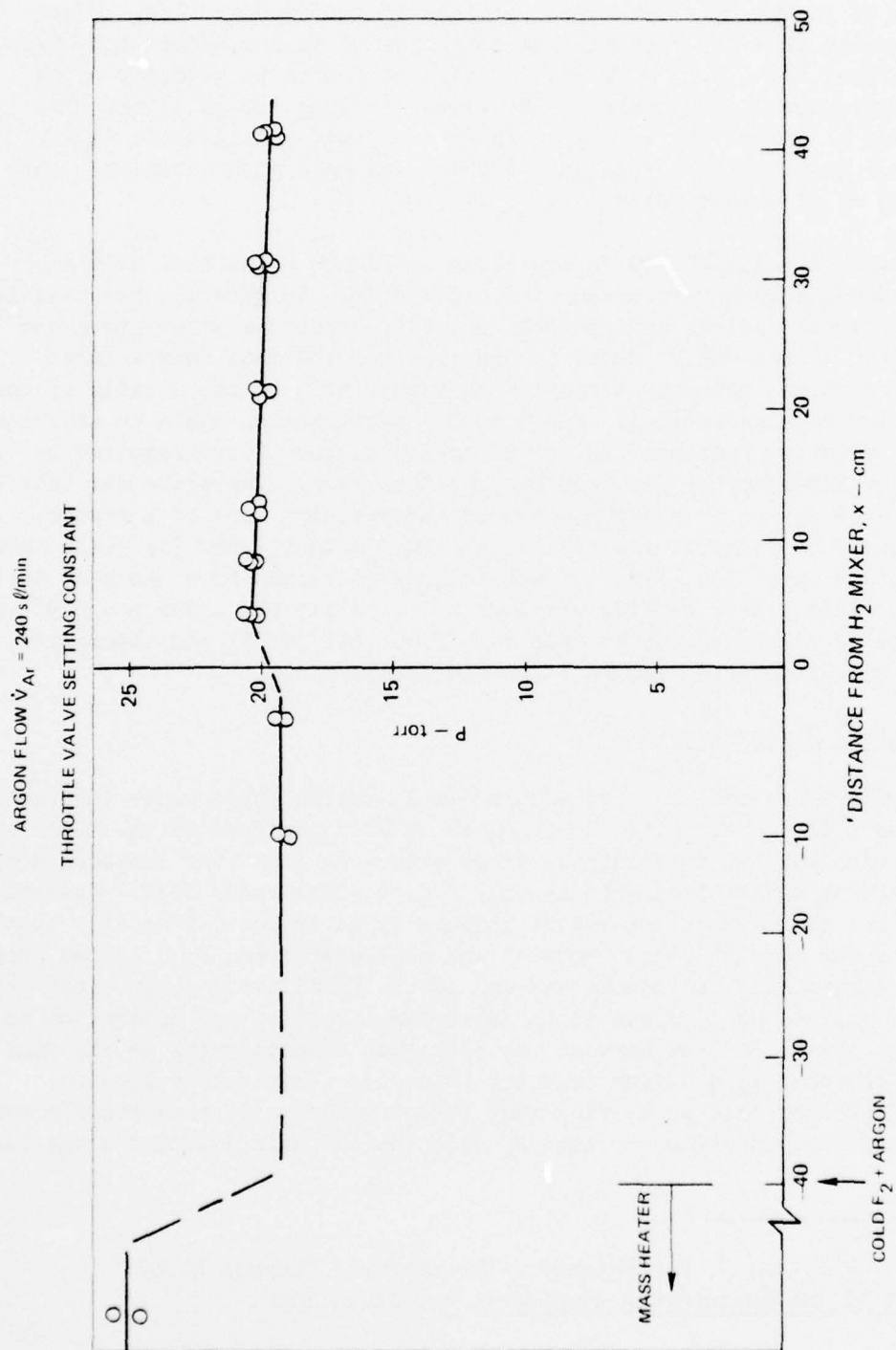


FIGURE 4 PRESSURE DISTRIBUTION ALONG FLOW TUBE

A radial traverse assembly was used as shown in Figure 5 that could be installed at each set of viewports. Data were obtained in nonreactive flow. Pitot pressure results $\Delta p \sim 1.5$ torr maximum corresponded to a subsonic core Mach number in argon, $M \sim 0.3$. Probe results were converted to velocity using standard compressible flow tables. The probe was long enough in the flow direction and alignment was accurate enough such that little probe correction is needed and none has been applied. A check was made with argon feed rate for one case as discussed below.

Results at $x = 11, 20, 40$ cm are shown in Figure 6 and at $x = 76$ cm, Figure 7. Results were very steady and repeatable. In general, the profiles were as uniform as desired and steepest velocity gradients were within one probe diameter of the wall. Close to the injector the data show a local peaking in velocity, probably a complex characteristic of the details of the mixer and flow tube geometries. Since such a perturbation could be accounted for by incorporating this profile in the analysis, the effort required to correct it by altering the geometry has not been made. The probe was subsequently located at $x = 76$ cm downstream of the reaction zone of interest, but where the tube diameter was still $D = 5$ cm. Velocity results still show a large uniform core flow. The average velocity obtained by a ten step integration over this radial profile was 0.88×10^4 cm/sec which for $p = 1.96$ torr, the pressure at $x = 76$ cm corresponds to a flow rate of 253 std liters/min, very close to the metered flow rate 240 std liters/min.

Gas Temperature Uniformity

Gas temperature was measured with a simple thermocouple probe inserted through a port in the transition section about 4 cm upstream of the H_2 injector (Fig. 1). With the aid of relations in Reference 6, the error introduced by probe conduction was estimated to be only 2°C , a small value here. Operational experience has shown that temperature uniformity is influenced greatly by the flow purging the annular region between the mass heater and F_2 dilution stage. This purge enters near the downstream end of the F_2 dilution stage where the mass heater wall is cold, flows in the upstream direction and enters the main flow through the small gaps between the seven hot exhaust ports in the mass heater and the cold F_2 dilution injector (Fig. 1). Temperature studies, Figure 8, show that this purge flow must be low in order to preserve the temperature uniformity provided by high F_2 dilution and cold dilution stage liner walls.

-
6. Rizika, J. W. and W. M. Rohsenow, "Thermocouple Thermal Error," Industrial and Engineering Chemistry, 44, 1168, 1952.

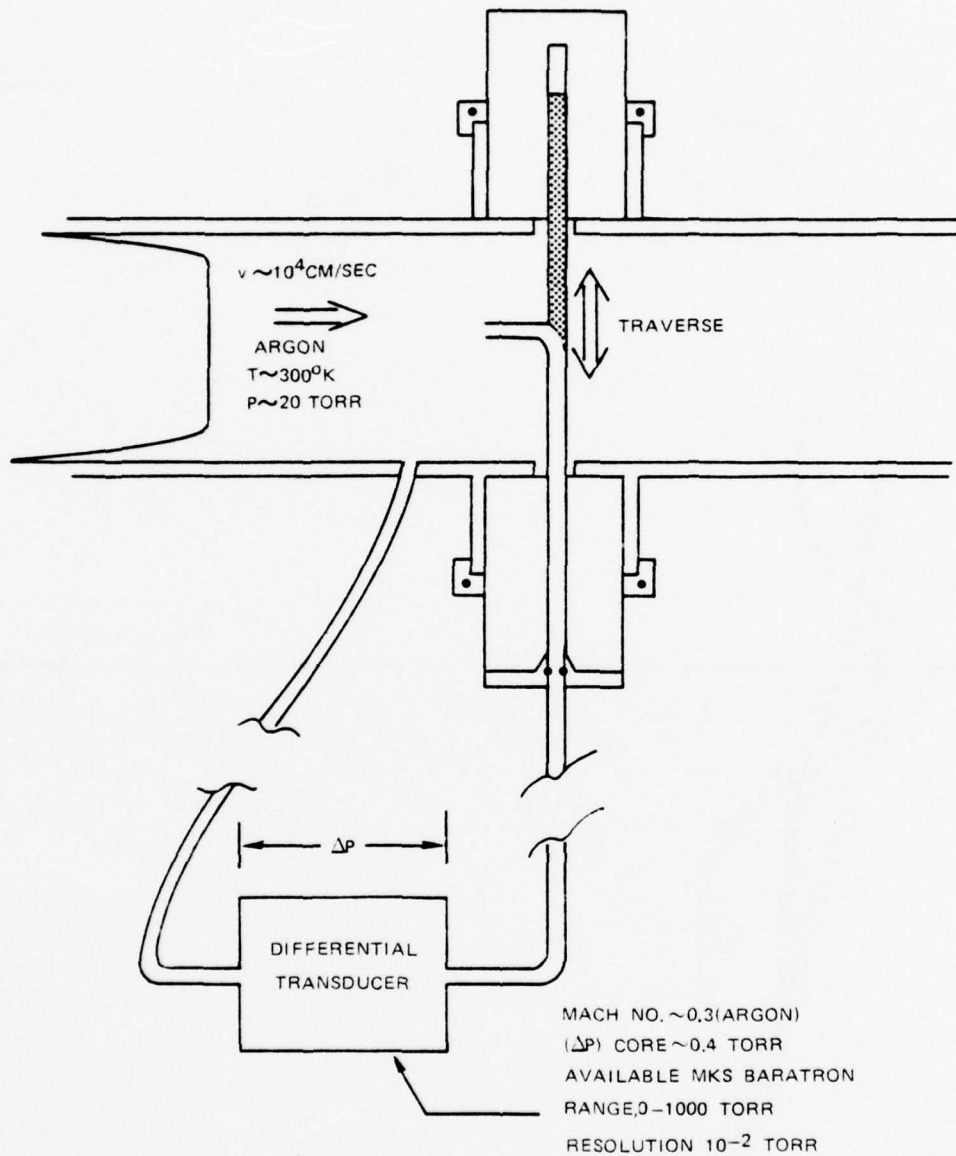


FIGURE 5 VELOCITY PROFILE MEASUREMENT

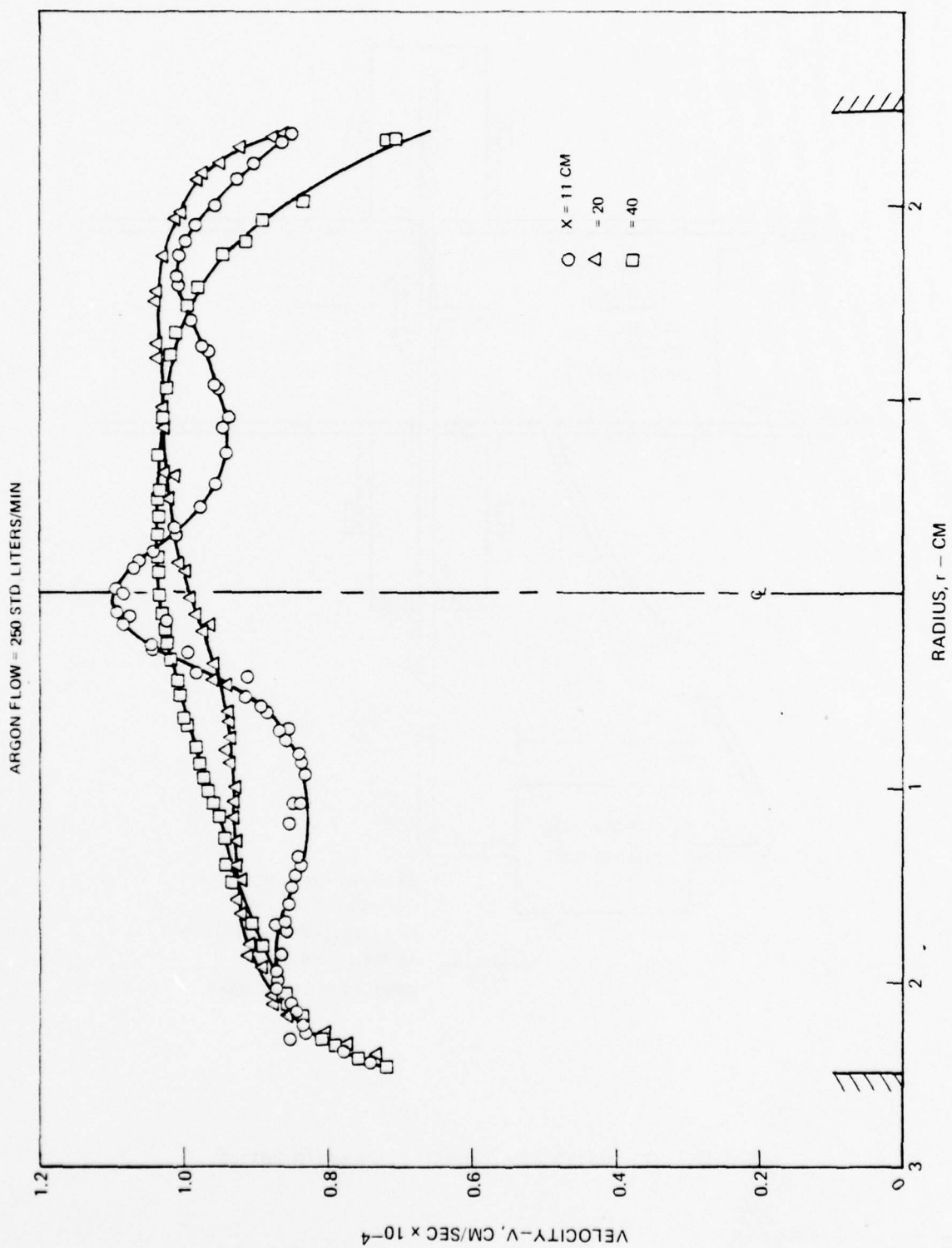


FIGURE 6 FLOW TUBE VELOCITY DISTRIBUTION DATA

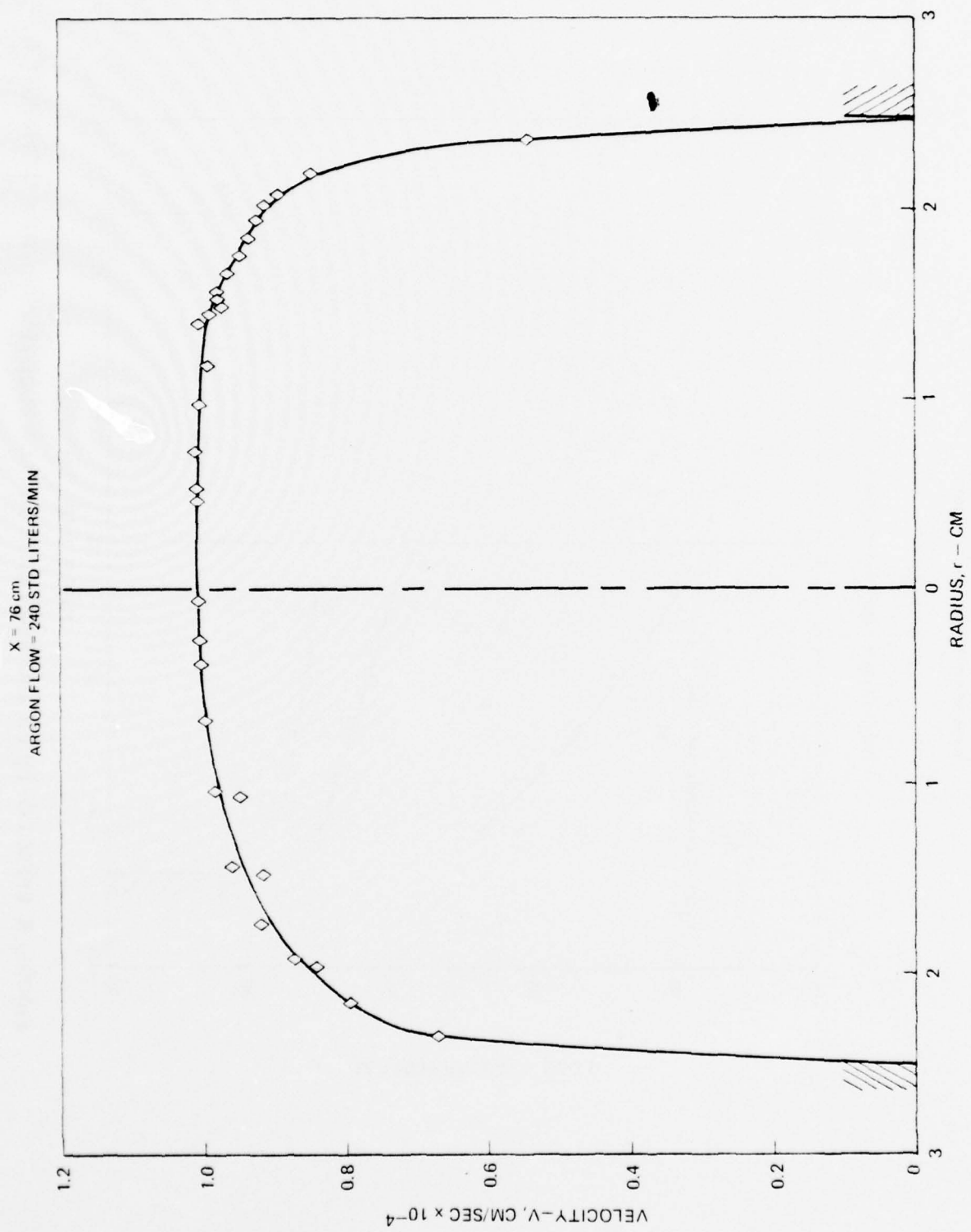


FIGURE 7 FLOW TUBE VELOCITY DISTRIBUTION DATA

MASS HEATER SET TEMP, $T_S = 630^\circ\text{C}$

$P = 20$ TORR

TOTAL FLOW $V = 250$ STD LITERS/MIN

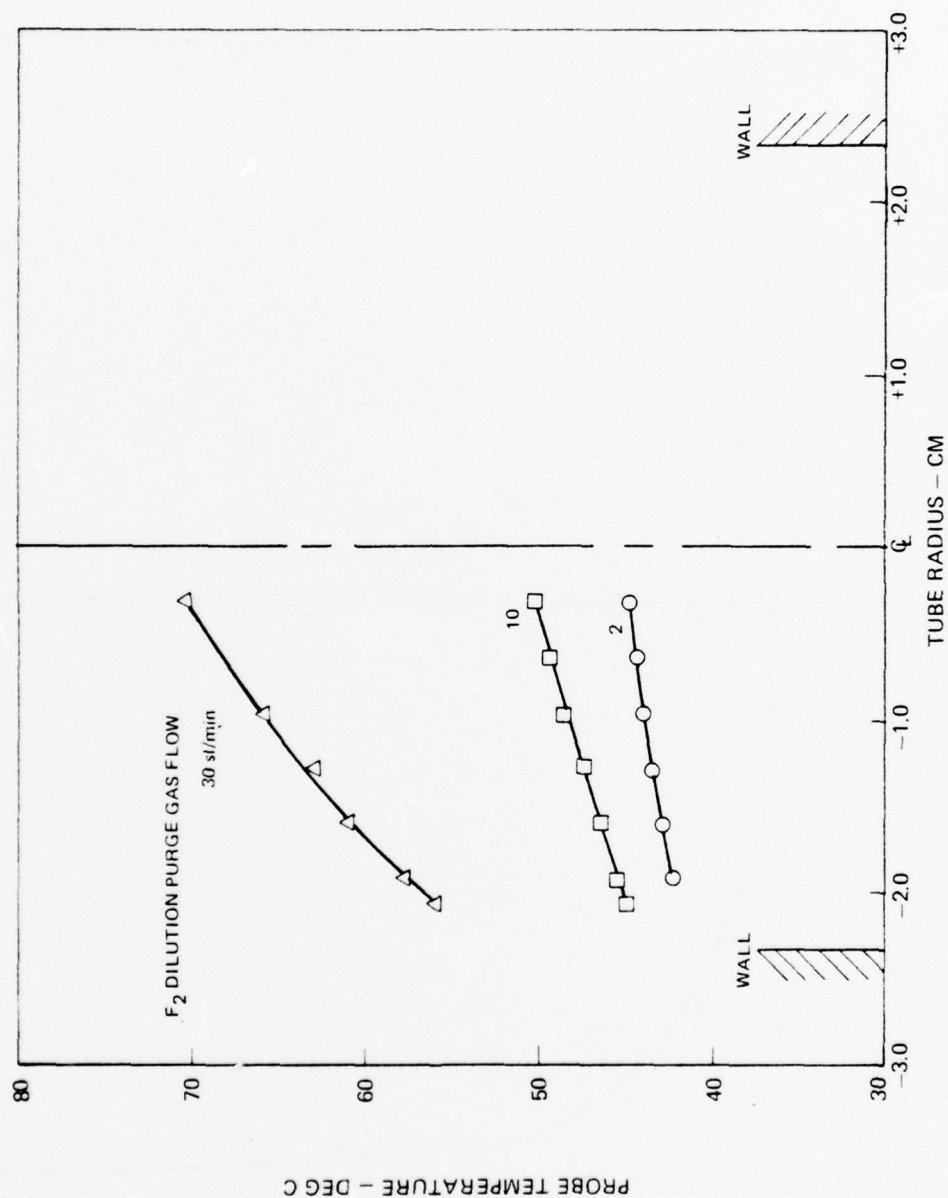


FIGURE 8 EFFECT OF PURGE GAS FLOW RATE ON FLOW TUBE TEMPERATURE DISTRIBUTION

With the dilution purge flow set at a low value the effect of the mass heater flow on the gas temperature distribution was investigated by turning the mass heater flow on using argon instead of F_2 . Results (Fig. 9) show a relatively uniform increase of $2^{\circ}C$ across the flow tube due to the mass heater which indicates reasonably uniform mixing has occurred. For actual conditions Tables 2, 3, and 4, this gas temperature measurement rose to about $62^{\circ}C$ ($335^{\circ}K$) and uniformity while not checked was probably $\pm 4^{\circ}C$. When mixed with room temperature argon in the H_2 injector, the flow tube initial temperature is estimated to be $T = 308 \pm 3^{\circ}K$.

HF Probe Laser Absorption

Measurement Technique

An HF probe laser absorption diagnostic (Fig. 10) was assembled under the present program employing a CW HF single mode probe laser similar to the one described in Reference 7. The probe laser was mounted on an optical table isolated with an air suspension system with well regulated table height. The sensitive, stable, double beam, single detector arrangement of Figure 10 was selected based on the expected requirements for the F atom titration measurement. A large area room temperature PbS detector coupled with a 5 cm diameter aluminum sphere provided adequate signal and was relatively insensitive to small angular perturbations in beam position. The overall arrangement of components on the 4 ft. x 12 ft. optical table is shown in Figure 3. When driving the PZT stack on the laser cavity with a ramp, a stable power profile over the doppler broadened gain region was achieved as viewed on the PbS detector (Fig. 11). A Lamb dip is clearly evident, further indication of a stable single longitudinal mode. In general for absorption measurements here, the cavity PZT voltage was set manually near line center; the output frequency would remain within the Lamb dip region for periods of minutes without active feedback. Generally, frequency was stable to ± 30 MHz, sufficient for about 3 percent accuracy in absorption (Ref. 7).

The operational characteristics of this dual beam absorption technique with a single detector are shown in Figures 12 and 13. Note in Figure 13 that stability of better than 1 percent of full scale was achieved for 1-minute periods (typically stability was 0.4 percent). Such stability allowed measurement of F atom titration signals to about 10 percent accuracy for the lowest F_2 feedrates of interest into the mass heater, ~ 30 sec/min (Fig. 13). Note also that the window purge flow was on and set as discussed in the section on gas flow rates.

-
7. Hinchey, J. J., "Determination of Vibration-Rotation Line Strengths for HF and DF by Use of an HF/DF CW Laser," J. Opt. Soc. Am., 64, 9, 1974.

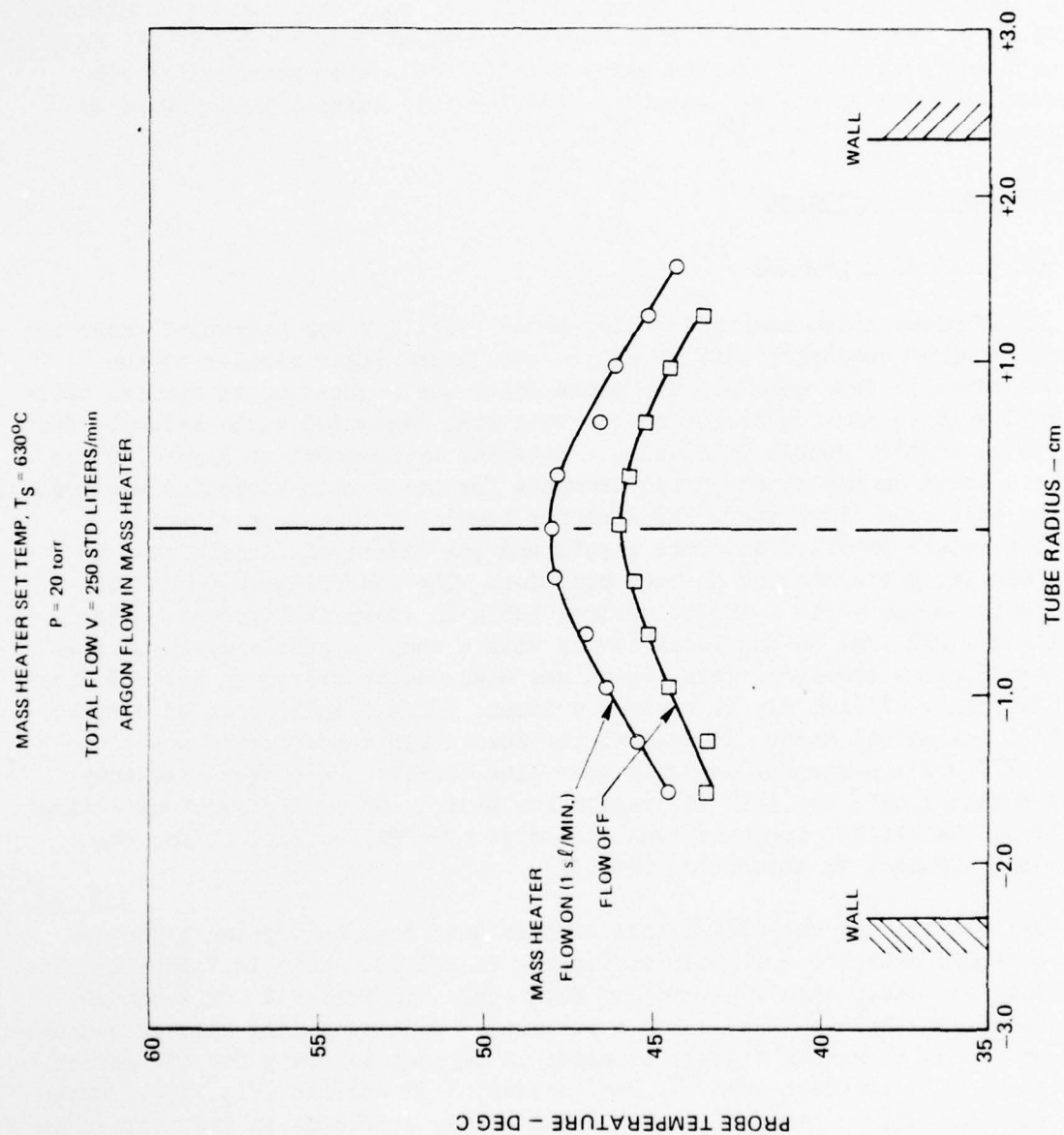


FIGURE EFFECT OF MASS HEATER ON FLOW TUBE TEMPERATURE DISTRIBUTION

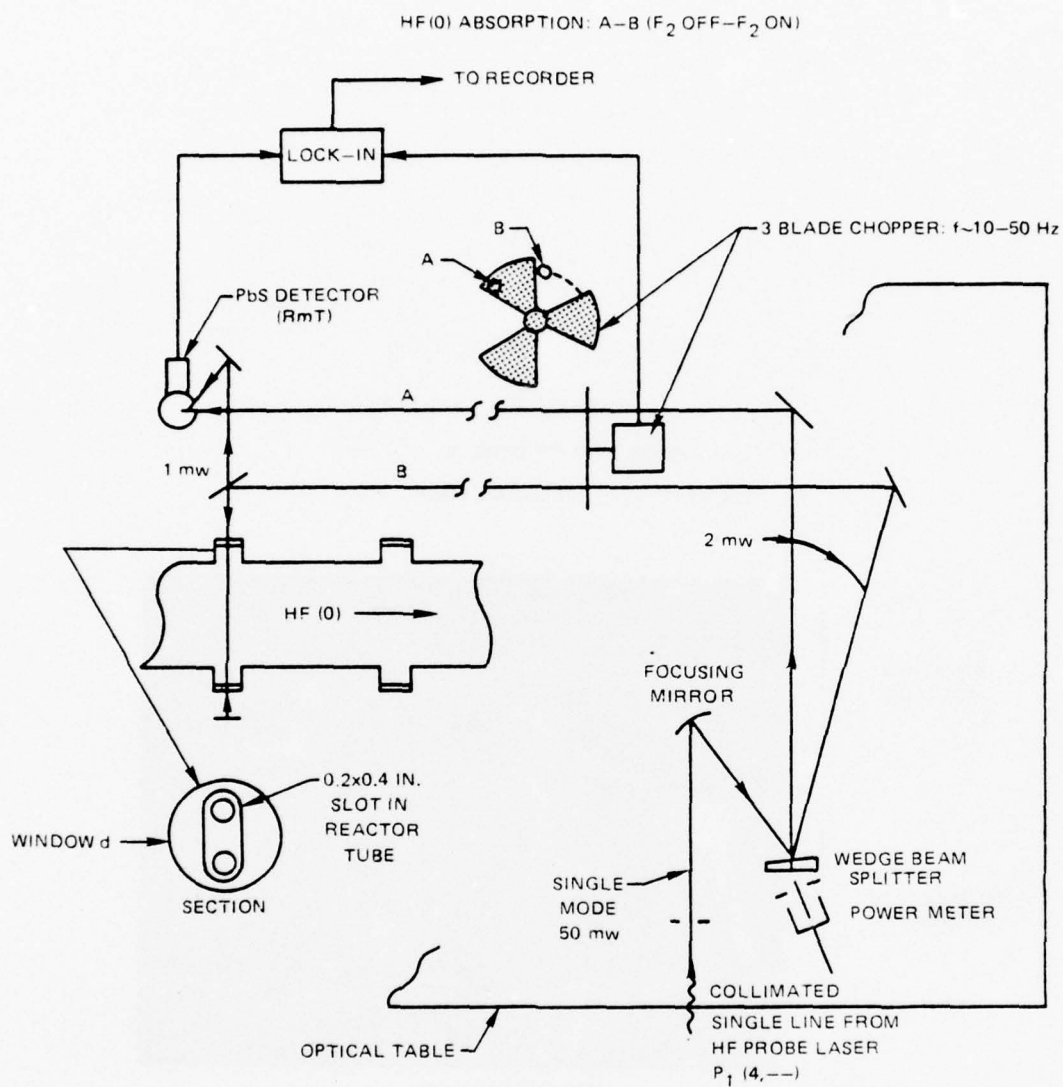


FIGURE 10 HF PROBE LASER ABSORPTION DIAGNOSTIC

P_1 (4) TRANSITION
VARIABLE CAVITY LENGTH
CHOPPER OFF, REF. BEAM ONLY

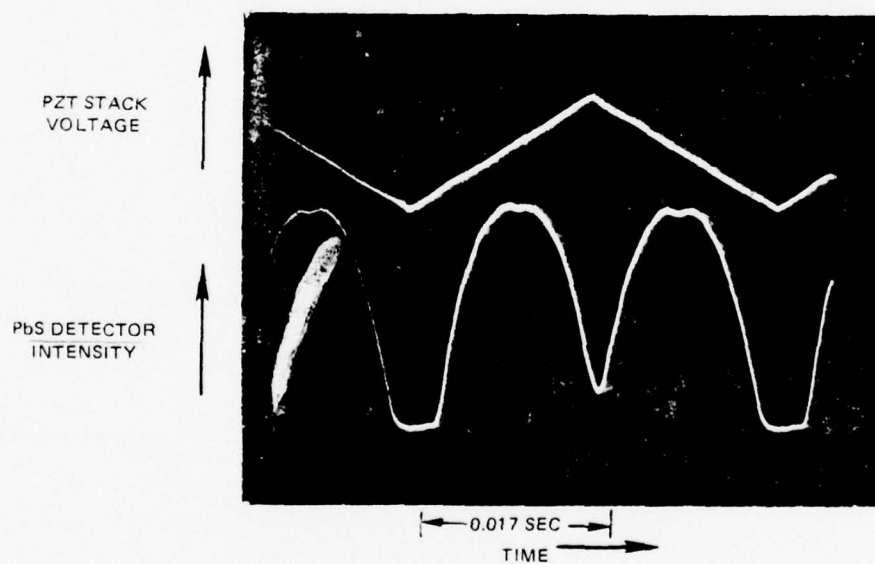
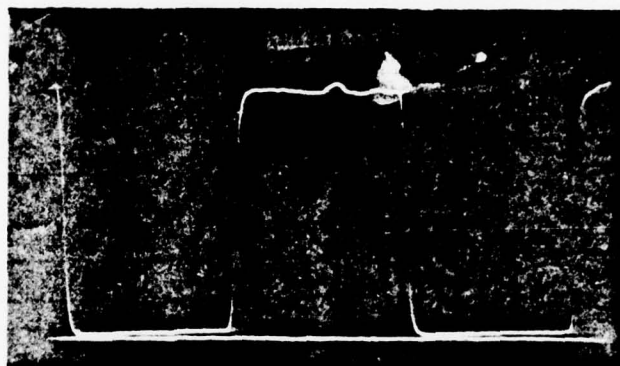


FIGURE 11 PROBE LASER ABSORPTION SIGNAL

P_1 (4) TRANSITION
 FIXED CAVITY LENGTH
 CHOPPER ON (10-50 Hz TYPICAL)

PbS DETECTOR
 INTENSITY
 (UPPER BEAM)

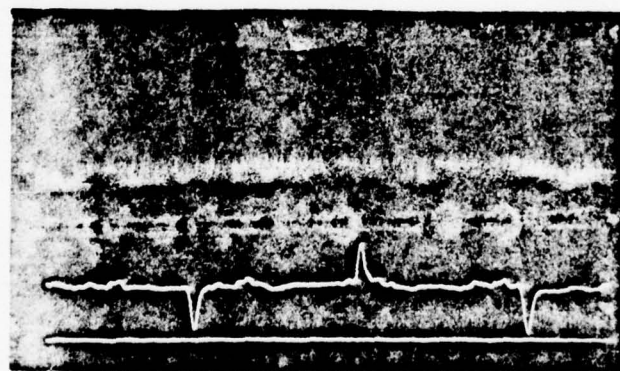
PZT STACK
 VOLTAGE
 (LOWER BEAM)



a) REFERENCE BEAM ONLY

PbS DETECTOR
 INTENSITY
 (UPPER BEAM)

PZT STACK
 VOLTAGE
 (LOWER BEAM)



b) REFERENCE AND PROBE BEAM

TIME →

0.01
 SEC TYPICAL

FIGURE 12 PROBE LASER ABSORPTION SIGNAL

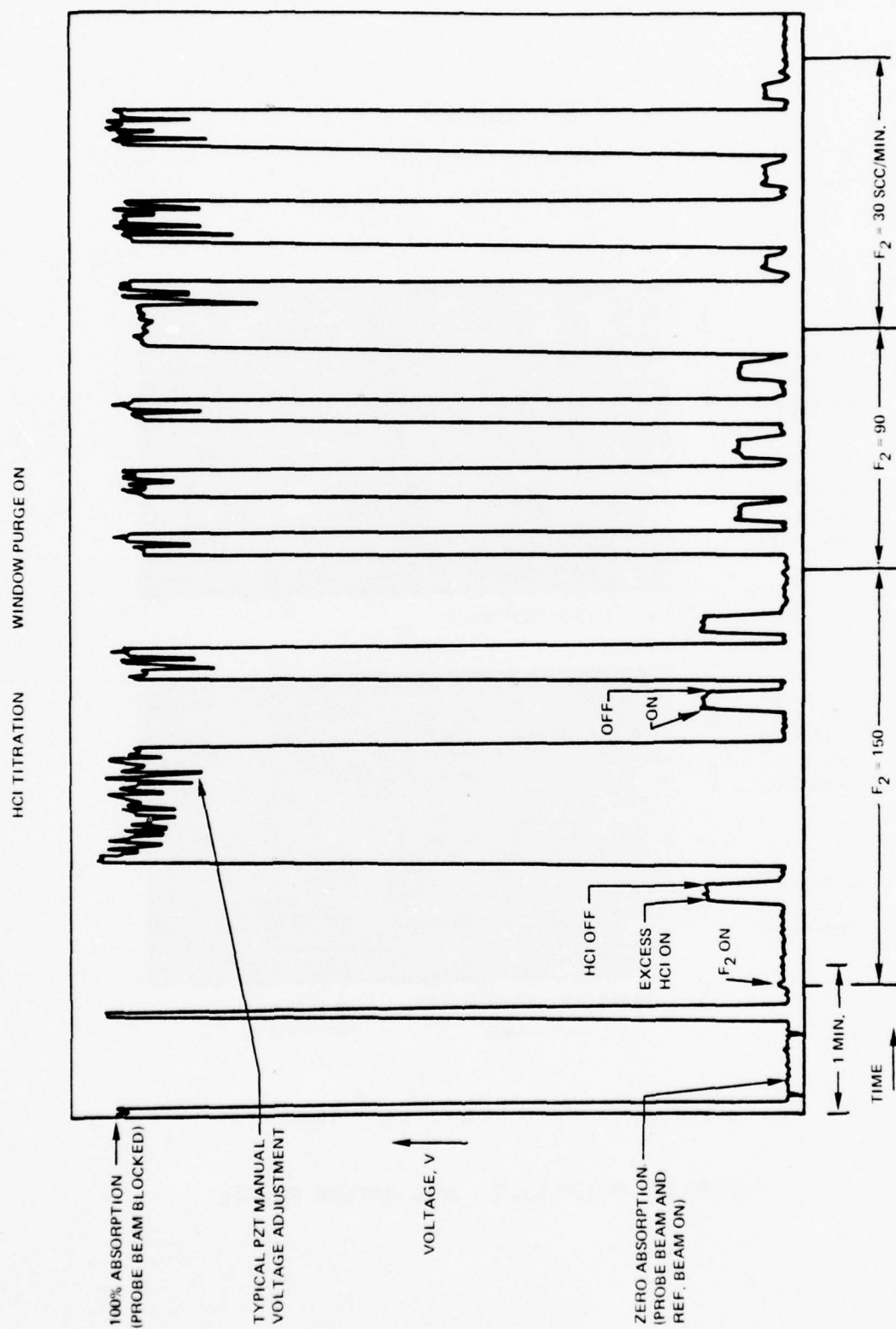


FIGURE 13 PROBE LASER ABSORPTION DATA ACQUISITION

Calibration Check With Direct HF Addition

Results of tests in which HF was added to the flow tube through a separate injector ring (Fig. 1) are shown in Figure 14. These measurements are pretty much in the linear range of the absorption and agree very well with calculations using Hinchey's data for doppler broadened line center absorption coefficient (Ref. 7) with the 10 cm total absorption length in this double pass arrangement (Fig. 10). Pressure broadening due to Ar does not seem to be a factor here at $p = 20$ torr and based on results of pulsed experiments, Section III, would be at most a 5 percent effect. Such data (Fig. 14) suggest also that there is little loss of ground state HF to the walls between the HF injector and observation point $x = 41$ cm. HF diffusion would be slower than H and even for total disappearance at the wall would probably be limited to a 5 to 10 percent effect.

Titration for F Atoms

The HCl titration technique for F atoms was checked out with ESR tests as part of this program (See Section V). This technique was applied in the flow tube studies by detecting the appearance of HF with the probe laser as HCl was added. At first excess HCl (> 1000 scc/min) was added to the argon flowing to the H_2 injector with $H_2 = 0$ (Fig. 13). A saturation level of HF formed was noted well downstream and checked for repeatability for each run. This absorption saturation level varied with F_2 feed to the mass heater as expected (Fig. 13) and at the expected levels. Very little interaction of this saturation level with cold F_2 flow was noted with excess HCl, consistent with the slow $Cl + F_2$ reaction rate at room temperature (see Section V).

Since some slight changes in the excess HCl titration result ($\lesssim 10$ percent) were noted periodically with cold F_2 , an attempt was made to check the stoichiometry of the titration reaction with metered HCl addition. In order to accomplish this, the HCl was added through the injector ring that had been used for HF (Fig. 1) since the concentration of HCl in the feed lines to this ring could be kept high to avoid having difficulties with spurious loss of HCl to the feed line walls, as seemed to be a concern in HF additive studies. Results (Figs. 15 and 16) show that at first a 1:1 HF:HCl correspondence does exist until a relatively sharp departure occurs from such a linear response curve and p_{HF} rises only very slowly with HCl flow rate thereafter. This slow rise is likely related to the $Cl + F_2$ reaction. This system has not been modeled for these tests as yet, but for now it has seemed reasonable to extrapolate the slowly rising curve back to its intercept with the linear response curve to define the level of F atoms. This point for cases 1 through 4 of Table 2 is shown in Figure 15 while F levels, cases 5 and 6 of Table III, are shown in Figure 16. An overall calibration of the mass heater from such intercepts is given in Figure 17.

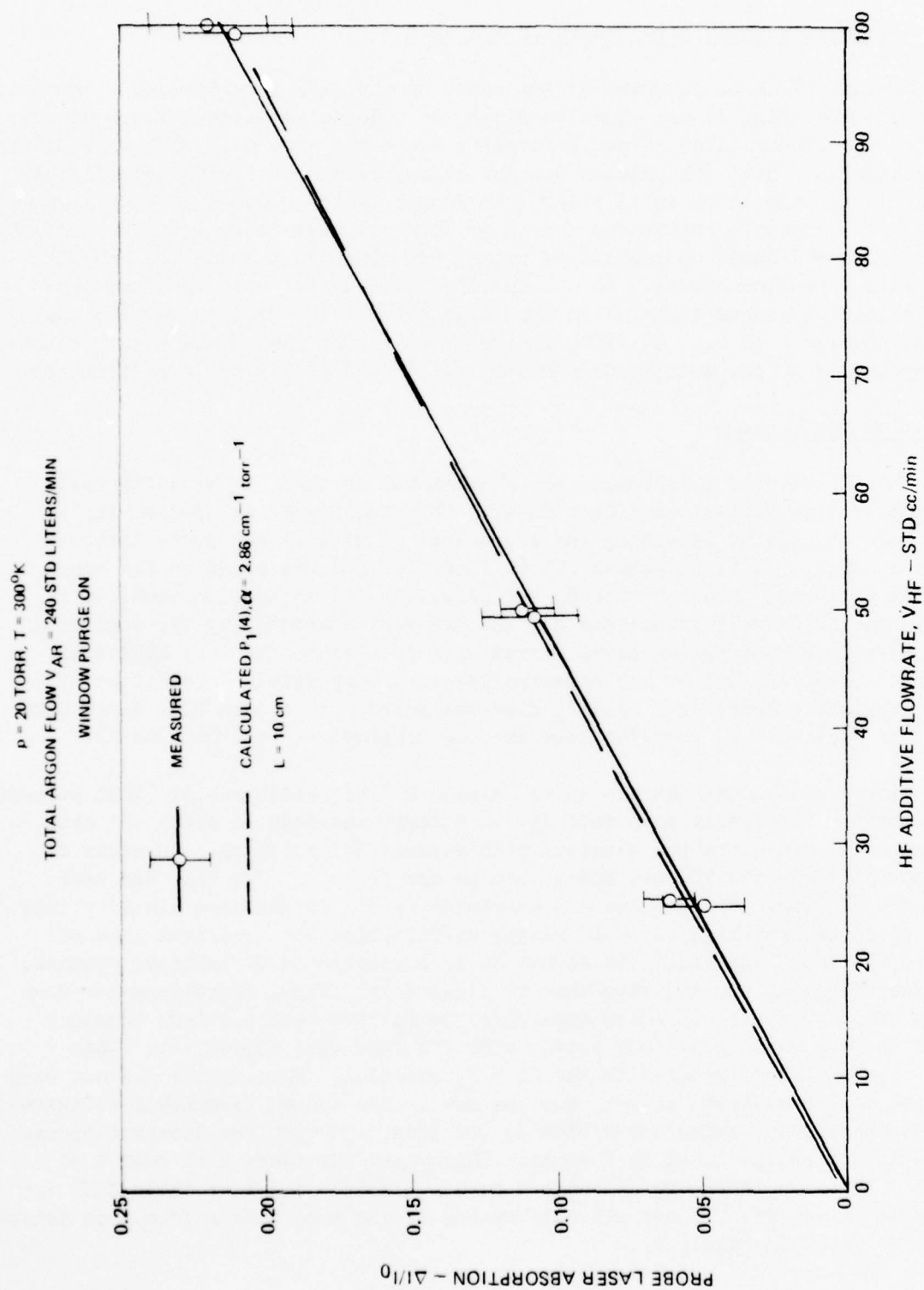


FIGURE 14 PROBE LASER ABSORPTION CALIBRATION CHECK BY HF ADDITION

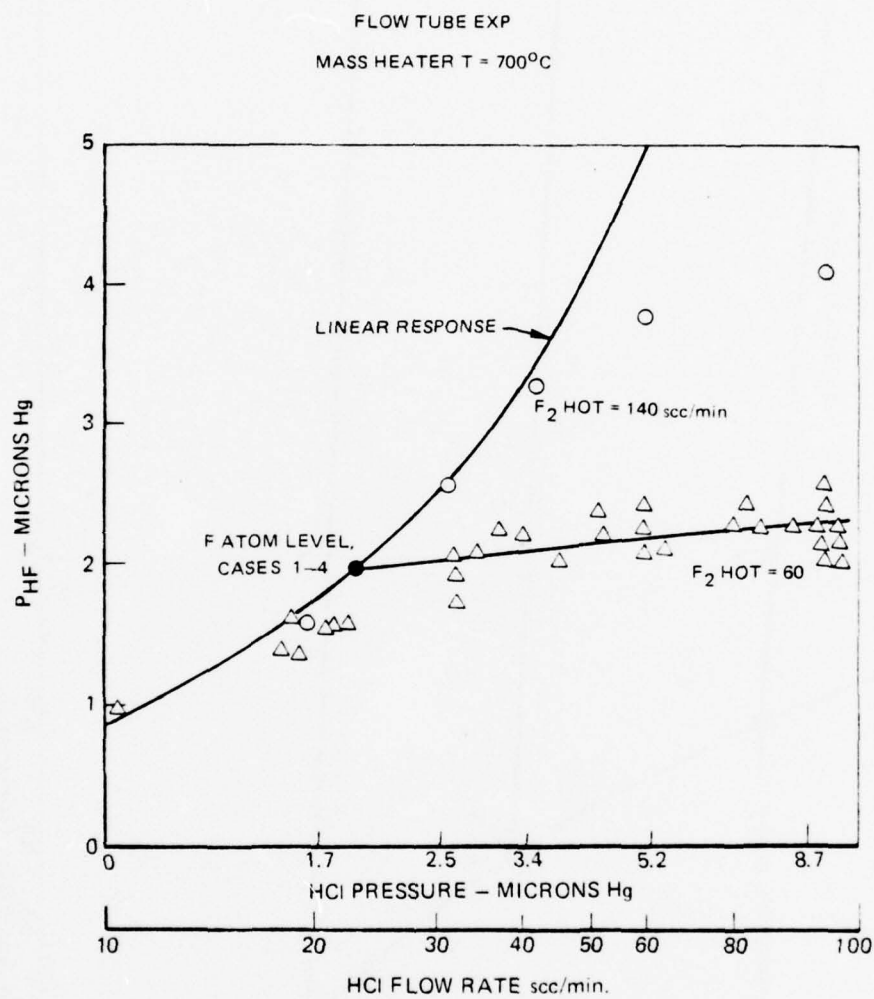


FIGURE 15 HCl TITRATION FOR F

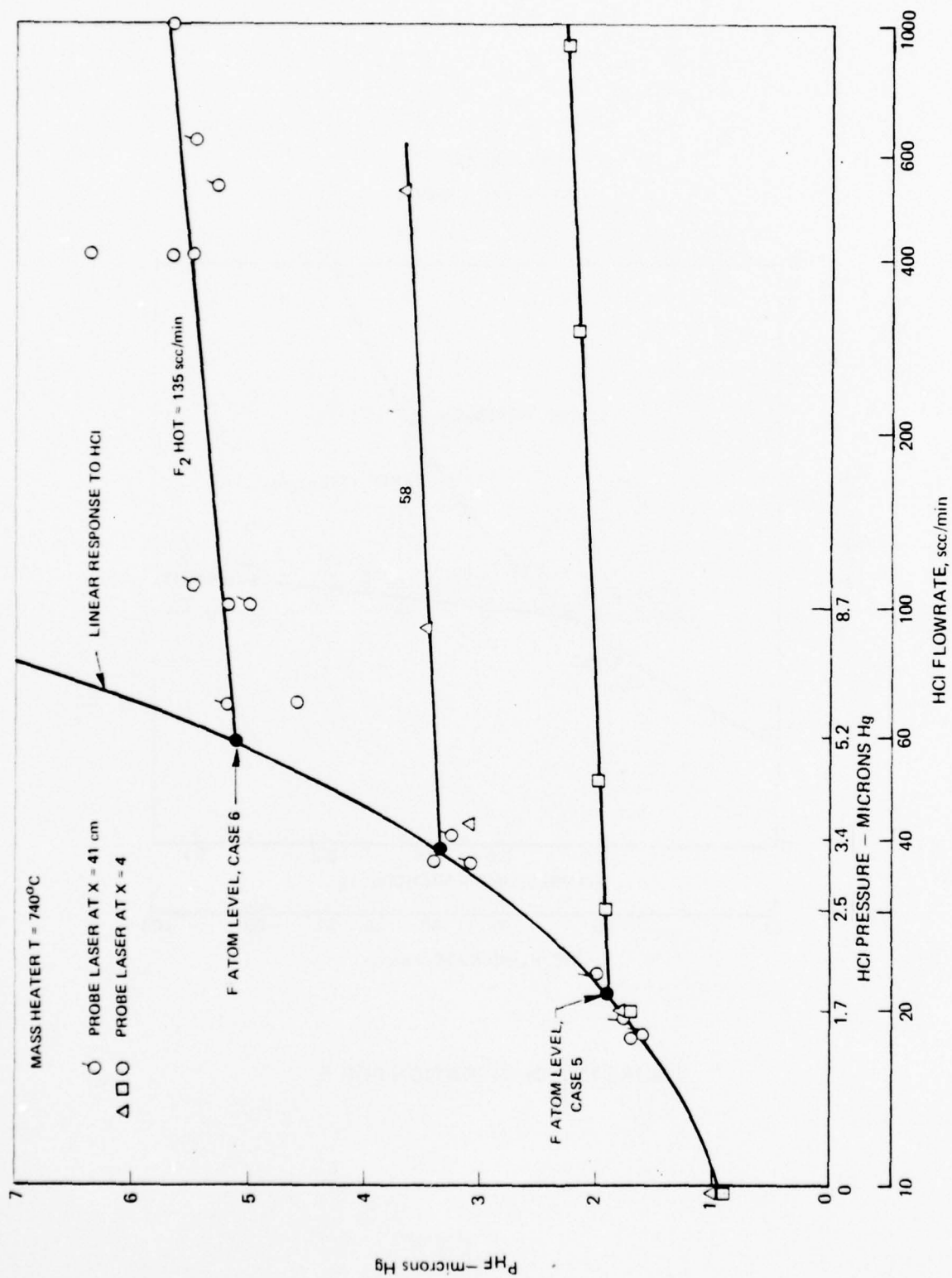


FIGURE 16 HCl TITRATION FOR F

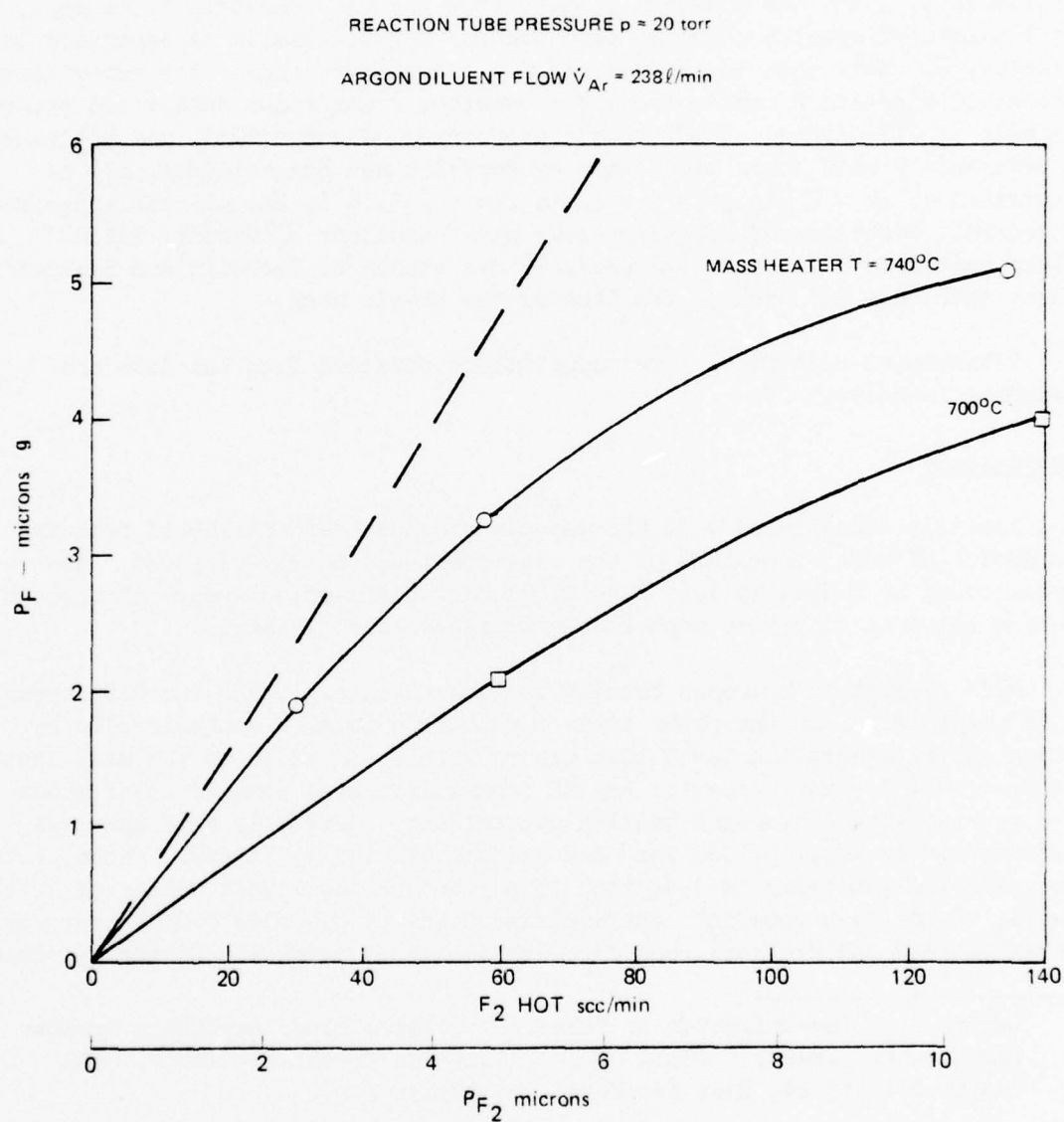


FIGURE 17 INITIAL F ATOM CONCENTRATION FROM HCl TITRATION

Emission Spectroscopy Measurements

The emission spectroscopy instrumentation is discussed extensively in References 1, 3 and the addendum to Reference 1. The same principles apply to the fundamental spectra obtained here and further discussion is contained in Reference 8. Note that in general, it was planned to compare the experimentally determined Einstein A coefficients for overtone transitions determined experimentally by Sileo in his Ph.D. thesis at Cornell, January 1975, and published in Reference 9 with those calculated by Herbelin and Emanuel (Ref. 10) by comparison of $\Delta v = 1$ and $\Delta v = 3$ results for $v = 3, 4$ in the present experiment. In general, Herbelin and Emanuel values gave excellent agreement, while values quoted by Sileo and Cool (Ref. 5) are closer to Herbelin and Emanuel's values than they had been at the time of the thesis work.

Vibrational-rotational level populations obtained from the data are presented in Section IV.

Contaminants

Possible contamination of the gas mixture has been considered from the standpoint of total leak rate of the experiment and purity of gases. The system could be pumped to less than 0.001 torr blank-off pressure through an in-line LN_2 trap to reduce condensable pressure even further.

With respect to hydrogen bearing contaminants, e.g., H_2O and C_xH_y types it is possible to use the probe laser to estimate total H contamination by noting the HF absorption level that occurs when F_2 is added to the mass heater but H_2 or HCl are not present. Any HF formed indicates some of the F atoms have reacted with a hydrogen bearing contaminant. Generally such spurious HF formation is below 0.0003 torr and was checked for all tests. Hence, such contamination generally is less than 15 percent of the lowest values of initial F used. Total leak rate into the experiment was at or below 0.0004 torr for operating flow and pressure, and since this leak is primarily N_2 the spurious

8. Lynds, L., "Investigation of Master Oscillator Power Amplifier Systems for Chemical Lasers," Final Report, Contract F29601-73-C-0072, UTRC Report N911653-24, East Hartford, CT, August 1974.
9. Sileo, R. N. and T. A. Cool, "Overtone Emission Spectroscopy of HF and DF: Vibrational Matrix Elements and Dipole Moment Function," J. Chem. Phys., **65**, 117, 1976.
10. Herbelin, J. M. and G. Emanuel, "Einstein Coefficients for Diatomic Molecules," J. Chem. Phys., **60**, 689, 1974.

level of HF is likely related to contaminants in the argon for these highly dilute experiments. The argon used was obtained from standard UTRC sources and the purity is about equivalent to a high purity or prepurified grade so the total contaminant level of the argon at 20 torr would be between 0.0004 and 0.0010 torr, with some fraction H_2O or CH_4 . The hot F_2 probe laser contaminant test can identify cylinders of argon which obviously have hydrogen bearing contamination levels much higher than typical values. On one such occasion spurious HF signals were of the order of the F_2 pressure and were related to the argon by systematically turning off sections of the multi-cylinder argon tank farm that supplies the experiment; in this case two of the ten 1A cylinders in the farm were found which when shut off caused the high spurious HF signal to go away and these were discarded.

In summary, contaminants OH, CH and spurious HF are ≤ 0.0003 torr for this experiment while N_2 is probably ≤ 0.0004 torr. (Smaller amounts of O_2 are likely present.) Due to the fast nature of HF:HF and HF:H interactions, the fast formation of initial HF levels of the order of F ($\geq .002$ torr) it is not likely that these contaminants levels will have a significant effect on interpretation of present experimental results.

Discussion and Recommendations

The mode of data acquisition here has required that the conditions for each case be repeated at least three times in order to acquire the three types of experimental information that are basic to determination of the production of HF and the individual vibrational level populations up to $v = 6$; (1) probe laser absorption, (2) absolute IR emission spectroscopy, (3) absolute overtone emission spectroscopy for $\Delta v = 3$. In the present program the application of HCl titration to determination of F atom level was evaluated and improvements made during the course of the program such that the final determination of F atom partial pressure with metered HCl was made by repeating each case a fourth time. Such a mode of data acquisition requires that great care be taken in the calibration and application of all instrumentation used to define conditions and that cross checks be made periodically among the types of measurements. Such care and cross checks were made to the extent possible with a manual method of data acquisition. For example, all flowmeters were calibrated with known volumes, accurate pressure gauges and a stopwatch and were checked periodically during the course of data acquisition. Calibration of the emission spectrometer with a standard source was possible at any location of the spectrometer system along the flow tube and such calibration checks were performed before and after each set of data. Also, when one type of measurement was being made, say IR emission, then the probe laser was placed at a downstream location and the level of absorption noted. The velocity probe was placed at a downstream location and the center line pitot pressure noted for each run. In addition where possible

within the scope of this program sets of data were repeated, principally here the probe laser absorption for cases 1 through 4 of Table 2. Some emission spectra for cases 1 through 4 were repeated during the course of HF additive tests since the zero HF additive condition was referenced again. Results gave reasonable agreement with prior data. Repeat data for the H atom cases, 5 and 6, were not acquired.

Nevertheless, the above procedures are difficult to follow in order to arrive at a set of experimental results with the degree of internal consistency required to evaluate both production and vibrational level population at various stages of the development of the chain along the flow tube in analytical terms as related to the conditions of the experiment. Such a procedure was followed here because it was justified relative to the level of analytical understanding of H_2/F_2 chain reaction kinetics at the time and was consistent with the experimental stage of the art for the thermally initiated flow tube.

In terms of the methods employed to acquire the data, the experimental state-of-the-art and the scope of the program, the results obtained here and from data analysis, Section IV, are very encouraging. Of particular significance for absolute measurement interpretations are the good calibration check of the probe laser with known HF addition (Fig. 14), the near 1:1 correspondence between HF formed and HCl added during the metered titration tests (Figs. 15 and 16), and the agreement between ultimate HF levels predicted from measured conditions with measured ultimate levels of HF using the probe laser (Figs. 43 and 47 for case 1). Absolute emission measurements have been checked several times and the agreement between $\Delta v = 1$ and $\Delta v = 3$ for $v = 3, 4$ is encouraging since the present understanding of transition probabilities (Refs. 9 and 10) seems to have narrowed the discrepancies a great deal. For the present cases a large fraction of the total production of HF early in the flow tube close to the H_2 injector is in vibrationally excited levels $v = 1, 2$; hence, the accuracy of emission data is important in determining total production as well as the accuracy of probe laser data. At the end of the reaction zone ground state HF is dominant and the probe laser is of greatest significance. In between, both measurements are relevant. Further work could be done to scale cases such as 3 and 4 with pressure and velocity to obtain chemical rate information based more extensively on probe laser data only. Probe laser studies with the HF additive at one downstream station showed a simple sum relation and such measurements at earlier stations should show enhanced reliance on probe laser data for HF production because of enhanced deactivation to the ground state. Data at various levels of initial F should be extended as a simple check on HF production results. In this regard, case 6 results need to be repeated and an experimental check made on the ultimate HF level.

Present results give a good indication of the detailed type of physical behavior of HF:HF interaction that is occurring and do indicate a chemical rate of HF formation. In light of the present state of experimental results for cases 5 and 6 (Table 3), however, and the need for some revisions to HF:HF modeling, the identification of an overall role for H atoms in the chain is incomplete at this time.

For the future, further analytical work is needed to compare with present experimental results. When defining future experiments of this type certain changes are more or less obvious, particularly the HF level very close to the H_2 injector must be examined to document the level of HF that may be present early in the chain due to small recirculation patterns in the wake of the injector bars. In this regard slight modification of the H_2 injector should be possible to purge such recirculation zones. It would also be desirable to speed up the data acquisition, take all types of measurements during the same run and to automate the data acquisition. In addition, scaling of results with diluent pressure would be desirable. However, beyond this it is likely that further progress will be linked to the ability to provide better knowledge and control of overall conditions on close to an instantaneous basis; progress of this type as well as automated data acquisition could best be done by linking the experiment to a small computer in the laboratory.

Summary and Conclusions

A CW flow tube H_2/F_2 chain reaction experiment was conducted with thermal initiation to measure population distribution in the various V and J levels and the ground state of HF over a range of conditions for which results likely could provide rate information for the overall reaction and molecular energy transfer processes that were uncertain.

Hot, partially dissociated F_2 from a mass heater is adjusted to room temperature by mixing with argon rapidly enough to preserve F. Additional cold F_2 is added to adjust overall F_2 dissociation. Hydrogen and additional diluent are injected through a fine scale mixer and the chain reaction proceeds under dilute, near isothermal conditions typically 99.7 percent argon with $\Delta T < 20^\circ C$. The flow tube diameter is $D = 5$ cm, $P = 20$ torr and velocity $v \sim 10^4$ cm/sec. Relatively uniform conditions prevail over the reaction lengths observed $L = 50$ cm; diffusion of HF and H to the walls are estimated to be about 8 percent and 25 percent effects by $x = 50$ cm and $HF(v)$ and H loss to the walls are inhibited further by coating the walls with Teflon. The reaction was observed at seven viewports along the reaction length: each viewport was a narrow slot in the tube coupled to a side port sealed with a sapphire window. Metered purge gas was added to each port.

Initial F pressure was measured with metered HCl titration and HF probe laser absorption. Ground state HF was measured with probe laser absorption. Vibrational levels in HF $v = 1, 2, 3, 4$ were measured with absolute IR, $\Delta v = 1$, emission spectroscopy. Vibrational levels $v = 3, 4, 5, 6$ were measured with overtone emission spectroscopy using $\Delta v = 3$. Temperature profiles were measured with a thermocouple probe. Velocity profiles were measured with a pitot probe and results incorporated in the analysis. Partial pressures of reactants F_2 and H_2 were calculated from measurements of total pressure and F_2 and H_2 , and argon flowrates using calibrated mass flow transducers and rotometers. Pressure distribution along the flow tube was measured with a transducer and wafer scanner.

The objectives of the flow tube experiment were sought in two series of tests: (1) operation over a wide range of F_2/H_2 with fixed F and HF addition to obtain reaction rate and HF:HF interaction information and (2) setting of higher F maintaining constant H_2 and nearly constant HF production to enhance the effect of H:HF collisions.

The desired conditions and data accuracy were obtained to a large extent except within the remaining uncertainty in modeling of HF:HF interaction the HF production was not close enough for the two cases selected in (2) to draw any definite conclusions about H:HF interaction at this time.

Results as analyzed give a good indication of the detailed type of physical behavior of HF:HF interaction that is occurring on both a short and long time scale in the development of the chain and allow a conclusion to be reached about the type of modeling that must be employed. For chemical rates results give a strong indication of a lower limit to the hot reaction rate of about $1/2$ the present value at room temperature. Further investigation to clear up a small uncertainty about initial HF levels very close to the injector and some extension of the conditions investigated could narrow the chemical rate uncertainty even further.

SECTION III. PULSED REACTION EXPERIMENTS

Pulsed reaction experiments were used to study the chain reaction in premixed H_2 and F_2 . The reaction is initiated by producing fluorine atoms in the mixture by dissociating F_2 with pulsed UV radiation from a doubled frequency ruby laser. Three types of experiments were performed: First, a study was made of the temporal development of populations in vibrational states of HF produced from the reaction. Fluorescence measurements were used to track excited state populations and absorption of cw radiation to follow ground state formation. Second, small signal gain was determined for $v(1-0)$ and $v(2-1)$ transitions by use of a gain probe. Third, pulsed laser radiation from the reacting mixture was studied using a laser configuration.

The rationale for these experiments is that they would serve as an experimental check on the laser computer program as modified by results from flow-tube experiments and other available data. Pulsed experiments were chosen as being relatively simple in that the problems attendant with mixing and flow are not present, the reaction is initiated over the total volume in a short time period and changes in temperature and pressure could be monitored in a constant volume cell. The experimental results have been compared with computer calculations of population development as the kinetics were tested with variations in initial F atom concentration and in the H_2/F_2 ratio. These comparisons are presented in Section IV of this report.

Pulsed Fluorescence Experiment

The chain reaction between fluorine and hydrogen was initiated by dissociating a small fraction of the fluorine with radiation from a frequency doubled ruby laser. Diagrams of the experiment are shown in Figures 18 and 19. Fluorescence from the chemically formed and vibrationally excited HF was detected using appropriate band filters with an AuGe detector for $v(1-0)$, an InSb detector for $v(2-0)$ and with a Varian LSE photomultiplier for $v(3-0)$, $v(4-1)$, $v(5-2)$ and $v(6-3)$. Intensity changes were measured to determine population changes in the various levels with time. Ground state HF($v=0$) was determined by absorption measurements using a cw HF probe laser. Data were recorded on scope pictures. Rise times for the detection systems were better than 0.5 μ sec. Pressure and temperature increases during the reaction were measured using a Kistler pressure transducer in a constant

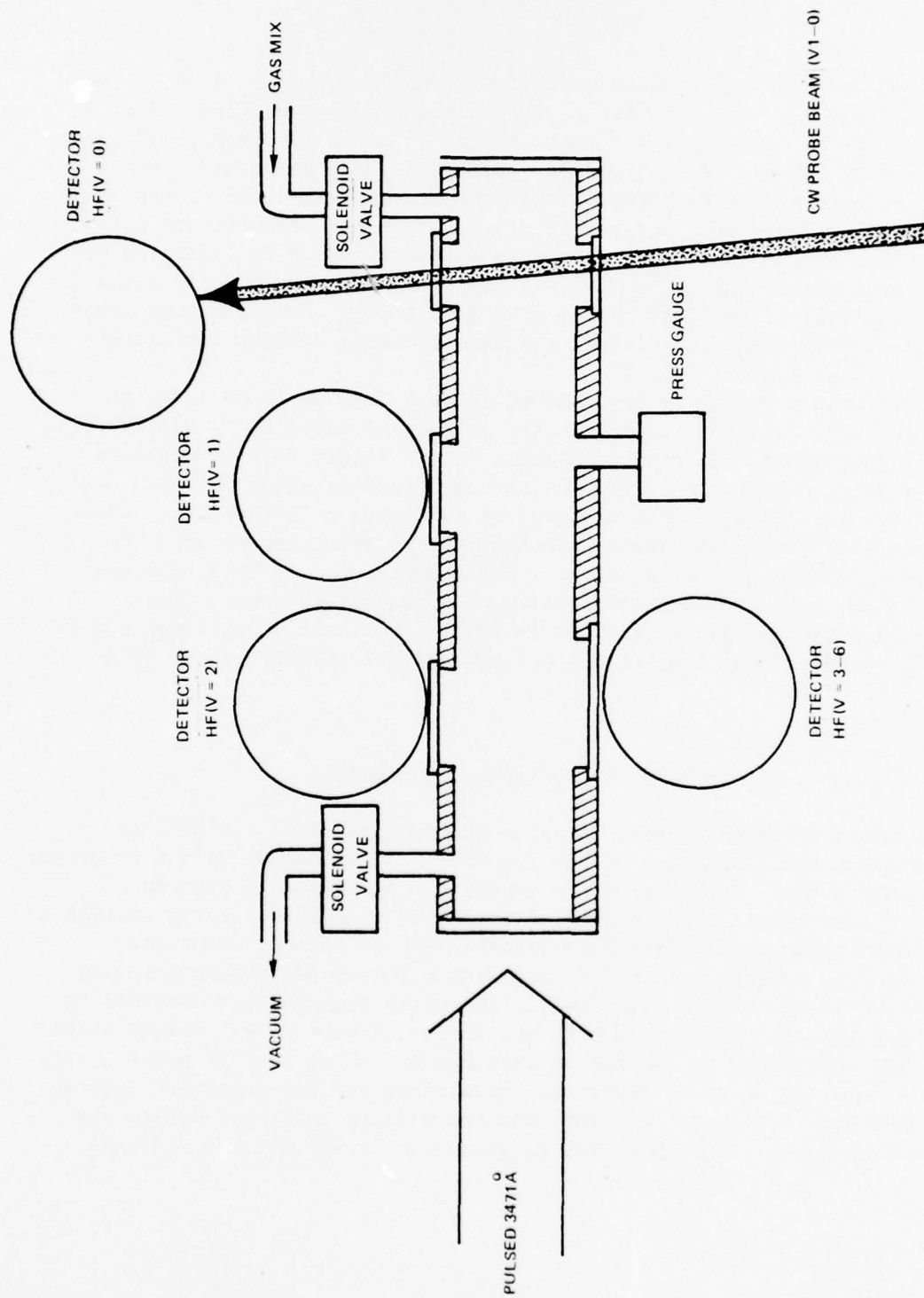


FIGURE 18 FLUORESCENCE EXPERIMENT

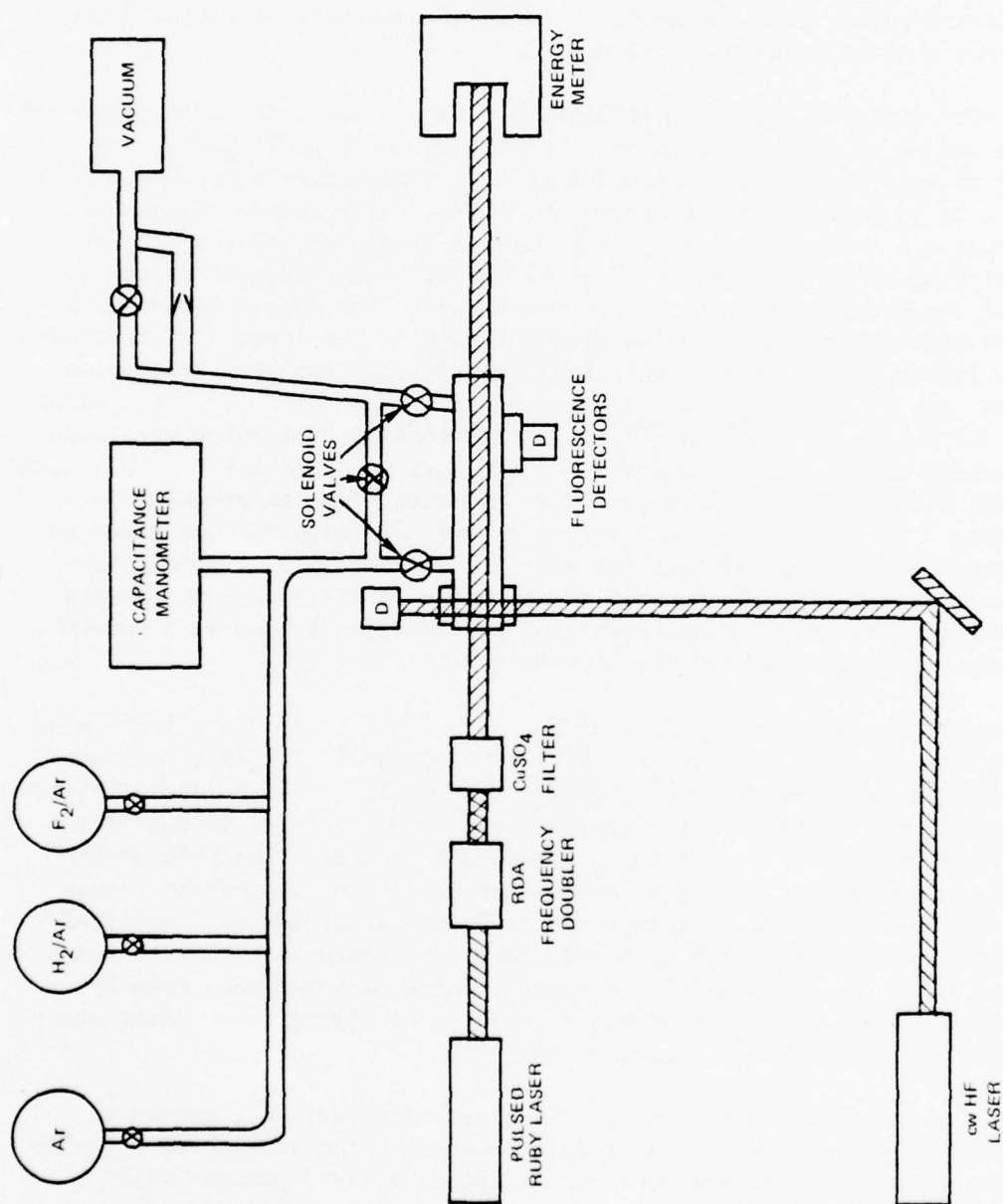


FIGURE 19 FLUORESCENCE EXPERIMENT

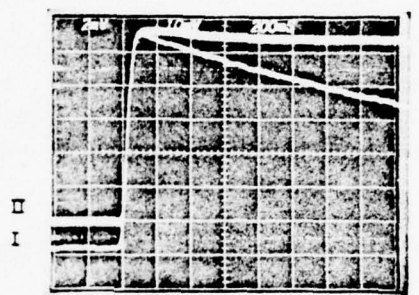
volume cell momentarily closed off with solenoid valves. The cell, made of Kel-F, was 15.2 cm long, 1.2 cm in diameter, and was fitted with sapphire windows. The Kistler gauge was calibrated against a capacitance manometer using pressure pulses over the pressure range of interest. A sample trace of the gauge outputs is shown in Figure 20.

Fluorine dissociation was accomplished using a ruby laser that delivered up to 0.6 Joules of pulsed radiation at 6942\AA within 50 to 70 nsec. The frequency of this radiation was doubled using a temperature tuned RDA crystal to provide up to 0.18 Joules of energy at 3471\AA . Pulse energy was measured with a Scientech energy meter calibrated with a blackbody using a shutter. The pulsed beam had a diameter of 10 to 11 mm which closely matches the cell ID (12 mm) for excitation of the whole gas volume. The concentration of F atoms produced was determined by carefully measuring the energy (with corrections for window losses) and calculating dissociation using the absorption coefficient for F_2 determined by Steunenberg and Vogel (Ref. 11). The value for α at 3471\AA is 1.21×10^{-4} at 273°K ; corrections to this value were made for the actual experimental temperature. Attempts to determine F atom content by reaction with HCl and measurement of HF produced from the reaction were unsuccessful. In a Kel-F cell the degree of reaction with HCl was found to be variable. In an aluminum cell the reaction did not go. Although this method was successfully demonstrated as described in Section V, it appears to be not suited to small volume - static flow experiments and wall interactions apparently have a significant effect.

Gas mixtures were made by flowing H_2 , F_2 , and He or Ar first through a mixing section consisting of three meters of aluminum tubing in the form of a coil, next through the fluorescence cell fitted with Kel-F solenoid valves with a by-pass valve and finally through a calibrated orifice to the vacuum pumps. The fluorine was passed through NaF to remove HF. Analysis of the F_2 by gas chromatography showed O_2 content of less than 0.1 percent. Gas pressure was measured with a capacitance manometer which had been calibrated with a mercury manometer. The best defined fluorescence data were obtained using premixed F_2 in argon and H_2 in argon. These mixtures were made by adding argon to 14.7 psi F_2 for a total pressure of 300 psi and adding argon to 14.7 psi H_2 for a total pressure of 500 psi.

In a flowing system where one gas is added after another, pressure measurements do not give a true measure of concentration because of a change in throat area of the exit aperture as the boundary layer changes with increasing pressure. The flow system was calibrated for this effect by

11. Steunenberg, R. K., and R. C. Vogel, "The Absorption Spectrum of Fluorine," J. Am. Chem. Soc., 78, 901, 1956.



PRESSURE PULSE-5.2 TORR
TRACE I-KISTLER GAUGE
TRACE II-CAPACITANCE MANOMETER

FIGURE 20 CALIBRATION-KISTLER GAUGE VS CAPACITANCE MANOMETER

introducing argon through two valves in sequence, turning the valves off in the opposite sequence while reading pressures. The dependence of flow rate on pressure was obtained in the following way:

Let p = test cell static pressure
 A = exit valve effective throat area
 f = molar flow rate

Now for choked flow through the valve

$$f/A = C_p$$

where C is a proportionality factor depending on the properties of the gas. If the gas properties remain essentially the same, this factor will remain constant. Similarly, the effective throat area (dependent on boundary layer thickness) will then depend only on the pressure. To find $A = A(p)$ consider the following:

Add a gas mixture (say $\text{Ar} + \text{F}_2$) to a known pressure p . Then we have

$$f = C_p A$$

Suppose another valve is opened to allow another mixture ($\text{Ar} + \text{H}_2$), raising the pressure to p' . Then

$$f' = C_p A'$$

Now f and f' are not known absolutely but the ratio f/f' may be found. Suppose f_1 is the flow rate of the first gas added to the cell and f_2 that of the second. Then

$$f = f_1$$

$$f' = f_1 + f_2$$

Also let p_1 and p_2 be the partial pressures of the two gases in the final mixture. Now

$$\frac{f}{f'} = \frac{f_1}{f_1 + f_2} = \frac{pA'}{p'A}$$

and

$$\frac{f_1}{f_2} = \frac{p_1}{p_2}$$

$$\frac{f_1/f_2}{1 + f_1/f_2} = \frac{pA}{p'A'} = \frac{p_1/p_2}{1 + p_1/p_2}$$

or

$$\frac{A}{A'} = \frac{p_1}{p_1 + p_2} \frac{p'}{p} = \frac{p_1 (p_1 + p_2)}{(p_1 + p_2) p}$$

$$\frac{A}{A'} = \frac{p_1}{p}$$

Thus if the partial pressure of the first gas in the final mixture is known, the change in effective area is known. A series of tests over various pressures were run to obtain $A = A(p)$ and the values were used to construct the correction curve shown in Figure 21.

The partial pressure of gas 1 can be found by closing off the test cell and initiating the reaction of $F_2 + H_2$. The resultant HF formed can then be related to p_{F_2} or p_{H_2} , whichever is smaller. Knowledge of the relative makeup of gas 1 and gas 2 will then yield p_1 .

Absorption by HF of radiation from a small cw probe laser was used to check the actual F_2 and H_2 concentrations by determining the amount of HF produced in F_2 rich and in H_2 rich mixtures. This radiation was also used in the pulsed experiments for following the kinetics of ground state HF production. A small cw HF probe laser was developed for these purposes which has excellent amplitude and frequency stability (Ref. 12). The laser radiation is single mode and can be tuned over the doppler broadened power curve of about 300 MHz. The capability of tuning to line center is necessary because absorption measurements made at frequencies removed from line center will significantly err (Ref. 7). This was especially so in mixtures containing 100 torr of argon which caused pressure broadening and line shift in the HF absorption curve. In order to evaluate this effect, absorption measurements were made for pure

12. Hinchey, J., "Operation of a Small Single-Mode Stable cw Hydrogen Fluoride Laser", J. Appl. Phys., 15, 4, April 1974.

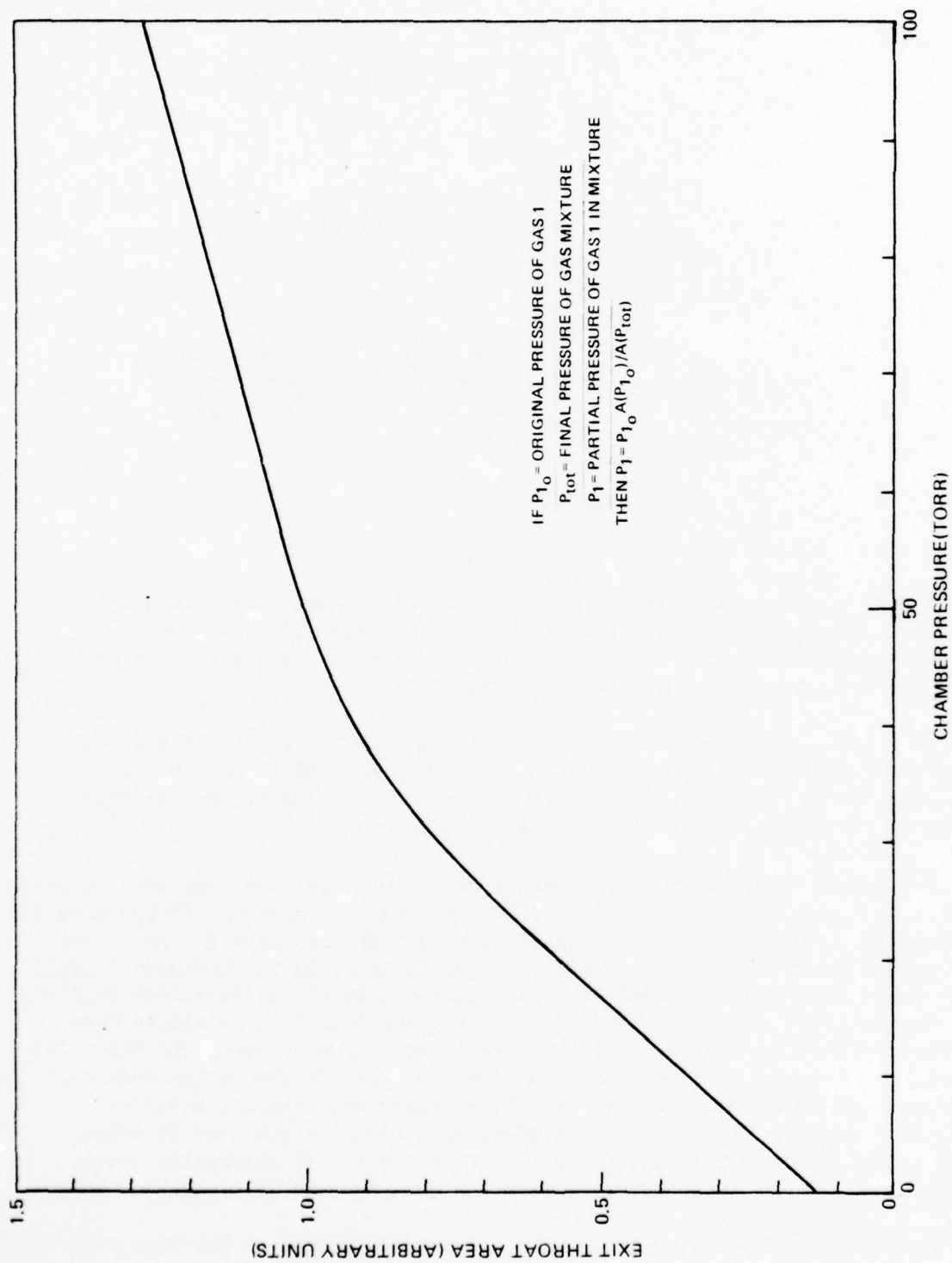


FIGURE 21 VARIATION OF EXIT THROAT AREA WITH CHAMBER PRESSURE

HF and HF diluted with 100 torr Ar as the laser frequency varied over its linewidth. A sample measurement of I and I_0 for 0.33 torr HF is shown in Figure 22. Similar measurements for HF at 0.43 torr in Figure 23 show that for pure HF a plot of $\ln I/I_0$ vs. frequency produces an absorption curve centered at the laser ν_0 , whereas for the sample containing 100 torr of argon there is a frequency shift 65 MHz from ν_0 and considerable pressure broadening. These results are in agreement with previous measurements of line shifts and broadening (Ref. 13). In the latter case, measurement of absorption at the laser line center results in a value over 50 percent lower than the value for pure HF. By making many such measurements for laser lines 1P4 and 1P6 the plot shown in Figure 24 was constructed and used to interpret absorption measurements. Using these corrections to the absorption measurements, the HF produced by a cw arc lamp from H_2 rich and F_2 rich mixtures with 100 torr Ar was determined. In an aluminum cell only 50 to 60 percent of the expected HF was found, indicating that the aluminum walls inhibited the reaction. Up to 95 percent of the expected HF was found in a Kel-F cell, and this cell was chosen for the pulsed fluorescence studies.

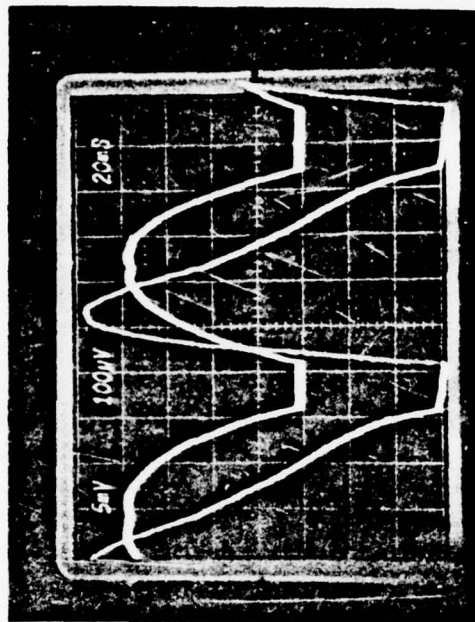
Pulsed Fluorescence Data

The data for the fluorescence experiment were obtained as scope traces of outputs from the detectors for pressure (Kistler gauge), fluorescence from HF levels $v = 1$, $v = 2$, and $v \geq 3$, and for intensity of transmitted cw laser radiation (for $v = 0$). An example of these traces, which were recorded simultaneously, is shown in Figure 25 for a gas mix containing 0.2 torr H_2 , 1.0 torr F_2 and 100 torr Ar. The formation of HF ($v = 0$) is evidenced as a decrease in intensity of transmitted probe laser radiation which occurs over a relatively long time of milliseconds. Immediately after the initiating pulse a small gain can be seen in this trace. Also the formation and deactivation of HF ($v = 1$) and the change in pressure due to temperature increase from the reaction are on this long time scale. However, the formation and decay of HF ($v = 2$) and HF ($v \geq 3$) occurs in a much shorter time. In Figure 26, fluorescence traces for the individual vibrational transitions $v(6-3)$, $v(5-2)$, $v(4-1)$ are shown. These pictures which were taken in three individual pulse experiments using the same pulse energy demonstrate the extremely fast formation of HF in levels above ($v = 2$) and the very fast relaxation of these levels.

Attempts were made to measure the absolute intensity of fluorescence in order to determine absolute populations in each level. Because the detectors needed to be placed right against the cell windows for adequate signal, it was not possible to define the source distance and aperture needed for

13. Jaffe, J., et al., "Pressure Induced Shifts of Hydrogen Fluoride Lines Due to Noble Gases," J. Chem. Phys., 43, 1525, 1965.

HF 0.33 torr - Ar 100 torr



HF (0.33 torr)

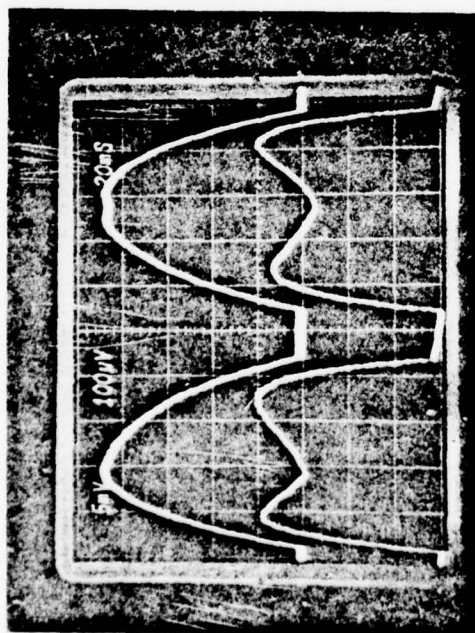


FIGURE 22 ABSORPTION OF 1P4 RADIATION BY HF AND HF IN ARGON

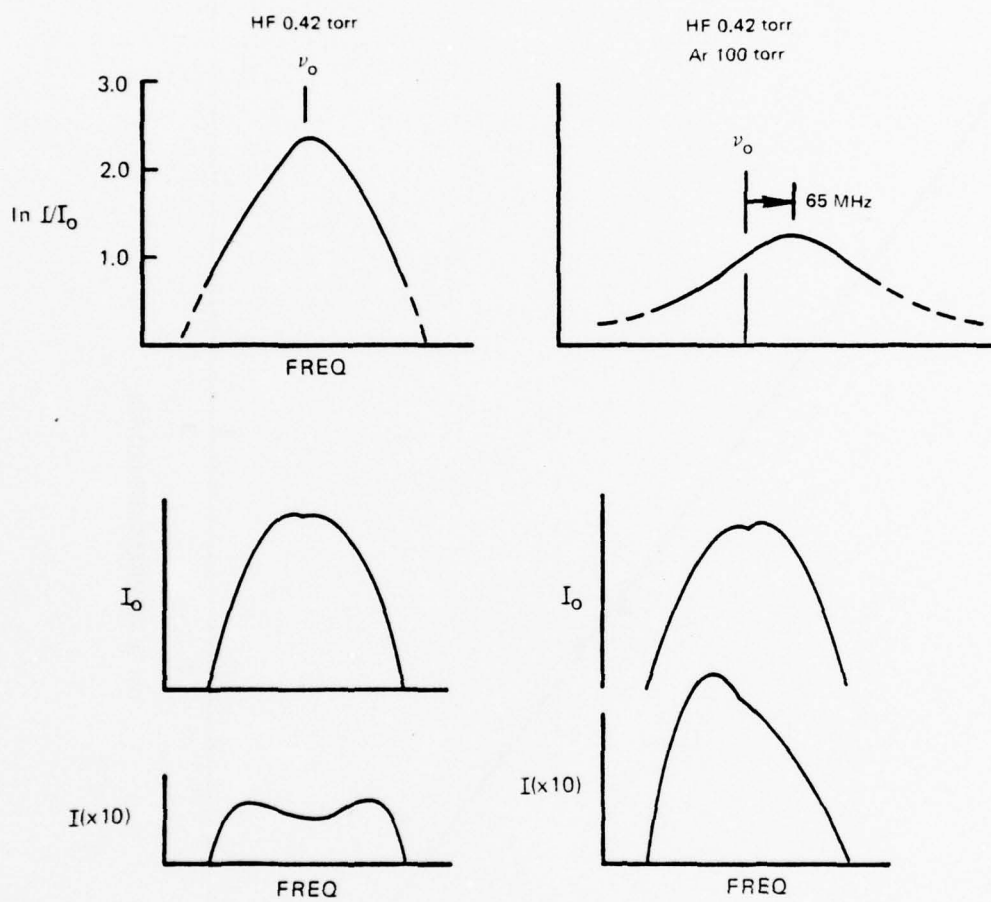


FIGURE 23 EFFECT OF ARGON ON HF LINEWIDTH

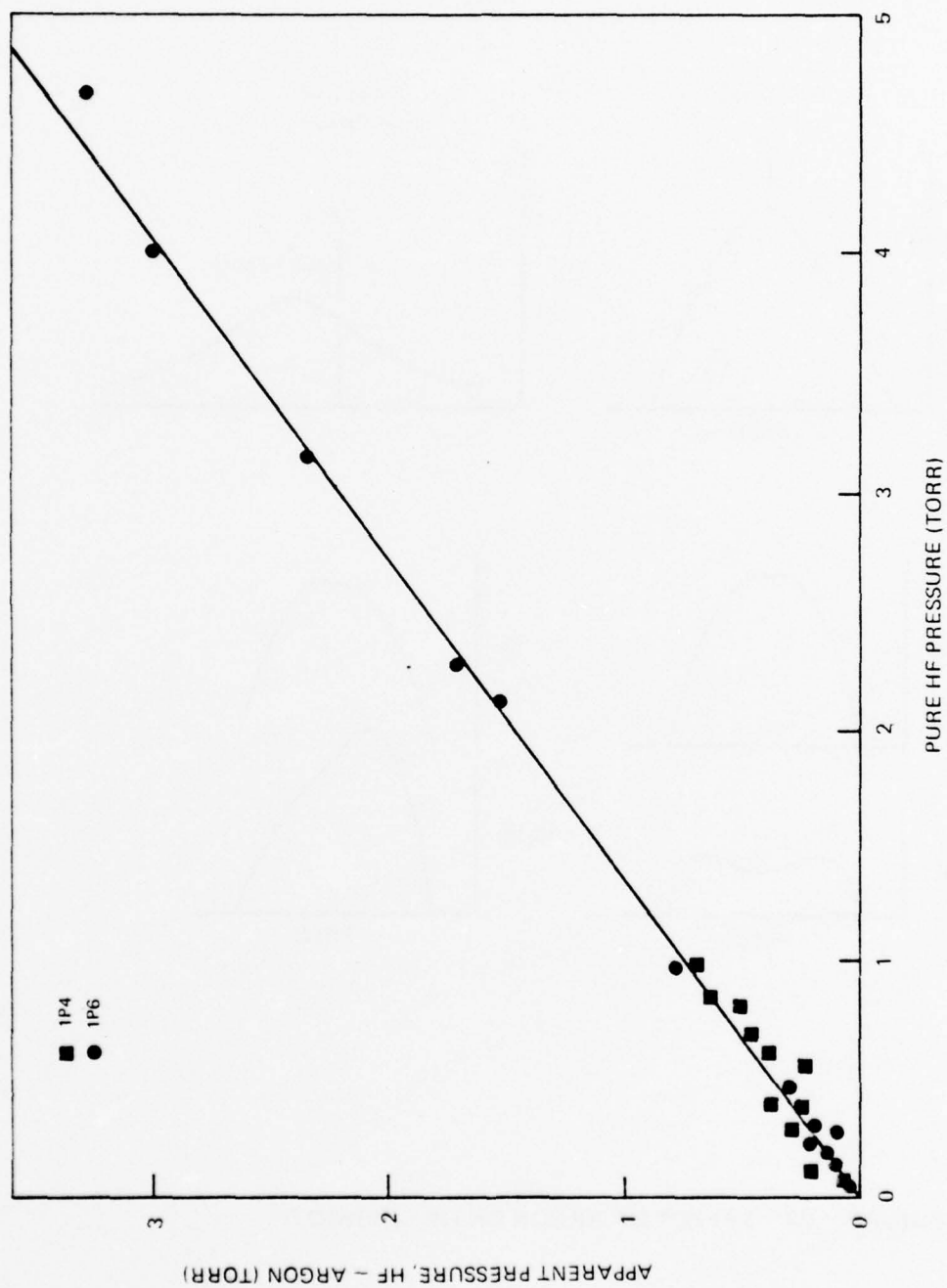
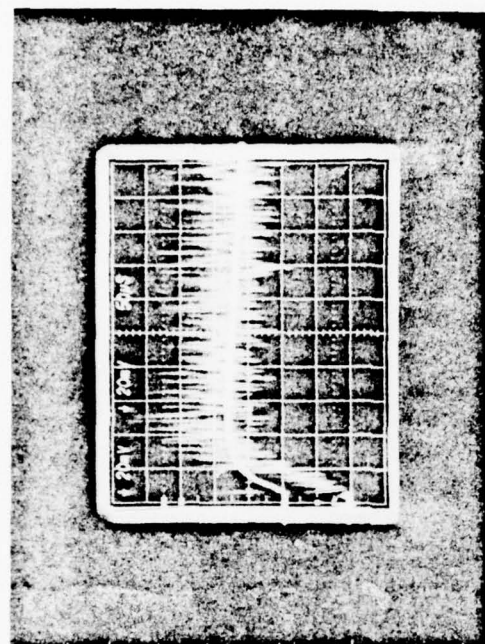
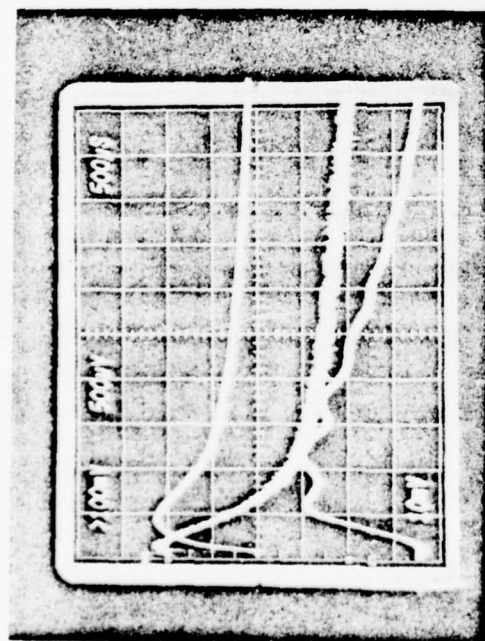


FIGURE 24 EFFECT OF 100 TORR Ar ON APPARENT HF PRESSURE

H_2 0.2 torr F_2 1.0 torr Ar 100 torr
 0.067 JOULES AT 3471\AA



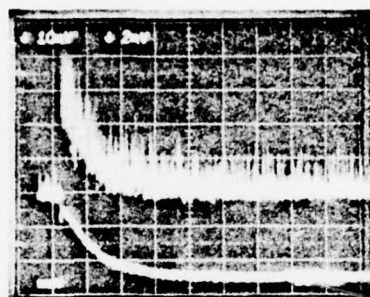
HF (V = 2) —
 HF (V > 3) —



HF (V = 0) —
 HF (V = 1) —

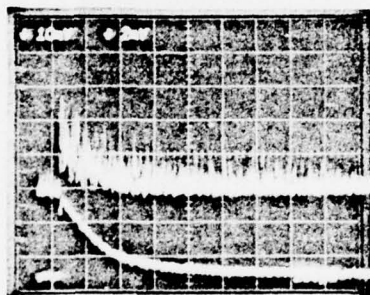
PRESSURE

FIGURE 25 FLUORESCENCE TRACES



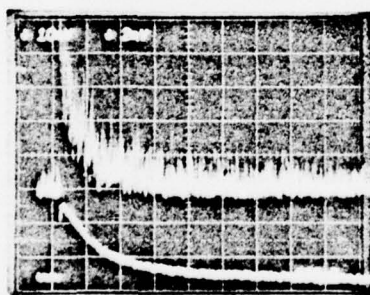
v(4-1)

v(2-0)



v(5-2)

v(2-0)



v(6-3)

v(2-0)

MIXTURE 0.2 TORR H_2 , 1.0 TORR F_2 , 98.8 TORR Ar
PULSE ENERGY—0.17 JOULES 200 μ SEC/CM

FIGURE 26 FLOURESCENCE TRACES

calibration. Also attempts to measure fluorescence through a 1/4 meter spectrometer were not successful because of inadequate fluorescence strength.

Fluorescence experiments were run with four kinds of mixtures: (1) mixtures of H_2 and F_2 , (2) mixtures of H_2 and F_2 with He added, (3) mixtures of H_2 and F_2 with argon added, and (4) mixtures of premixed H_2 and Ar with premixed F_2 and Ar. For the experimental cases with the premixed gases, the gas mixture composition was accurately known and the dilution was sufficient to keep the temperature increase within moderate limits of 40 to 90°C. These two criteria were not met for the first three mixtures. For this reason the data for the premixed gases will be presented here and are the ones compared with the computer model. The other mixtures will be discussed below.

Variations were made in H_2 and F_2 content using mixtures containing (A) 0.2 torr H_2 , 1.0 torr F_2 , 98.8 torr Ar; (B) 2.0 torr H_2 , 1.0 torr F_2 , 97 torr Ar; (C) 0.5 torr H_2 , 1.0 torr F_2 , 98.5 torr Ar; (D) 0.5 torr H_2 , 0.5 torr F_2 , 99 torr Ar; (E) 1.0 torr H_2 , 0.5 torr F_2 , 98.5 torr Ar. For each of these mixtures variations were made in the initial F atom concentrations by modifying the exciting pulse energy.

An example for each of these mixtures of the HF ($v = 0$) number density and gas temperature time dependence is shown in Figures 27, 28, 29, 30, 31 and 32. These graphs derive from scope traces such as Figure 25 where temperature is calculated from measured pressure rise, and absorption of the cw beam is used to calculate number density with corrections for line broadening and temperature dependence of the absorption coefficient. Generally, it is found that the temperature peaks at or before the maximum HF production. For mixtures A, B and C, the HF produced reasonably approximates that of the maximum amount possible through complete reaction. For cases D, E and F, the HF amount is somewhat less. It was found that for each mixture the amount of HF produced was dependent on initial F atom content (pulse energy) and tended to produce the theoretical maximum at high F atom content. This effect is discussed in the Data Analysis section and is apparent in Figures 57 through 62. A complete listing is contained in Table 5 of all the experiments for which data were obtained using the mixtures A, B, C, D, E and F. These data are further discussed in the Data Analysis section.

Table 6 contains a summary of the experiments that were run for the other kinds of mixtures excluding premixed gas mixtures. The first experiments (Table 6-A) were with undiluted H_2 and F_2 . Examples of fluorescence traces obtained with these mixtures are shown in Figures 33 and 34. Many of these runs were analyzed to get rate coefficients; however, because of the extreme temperature rise of up to 100°C, we have little confidence in these analyses and they are not presented here. One curious aspect of these experiments is associated with prereaction which was commonly observed. In cases

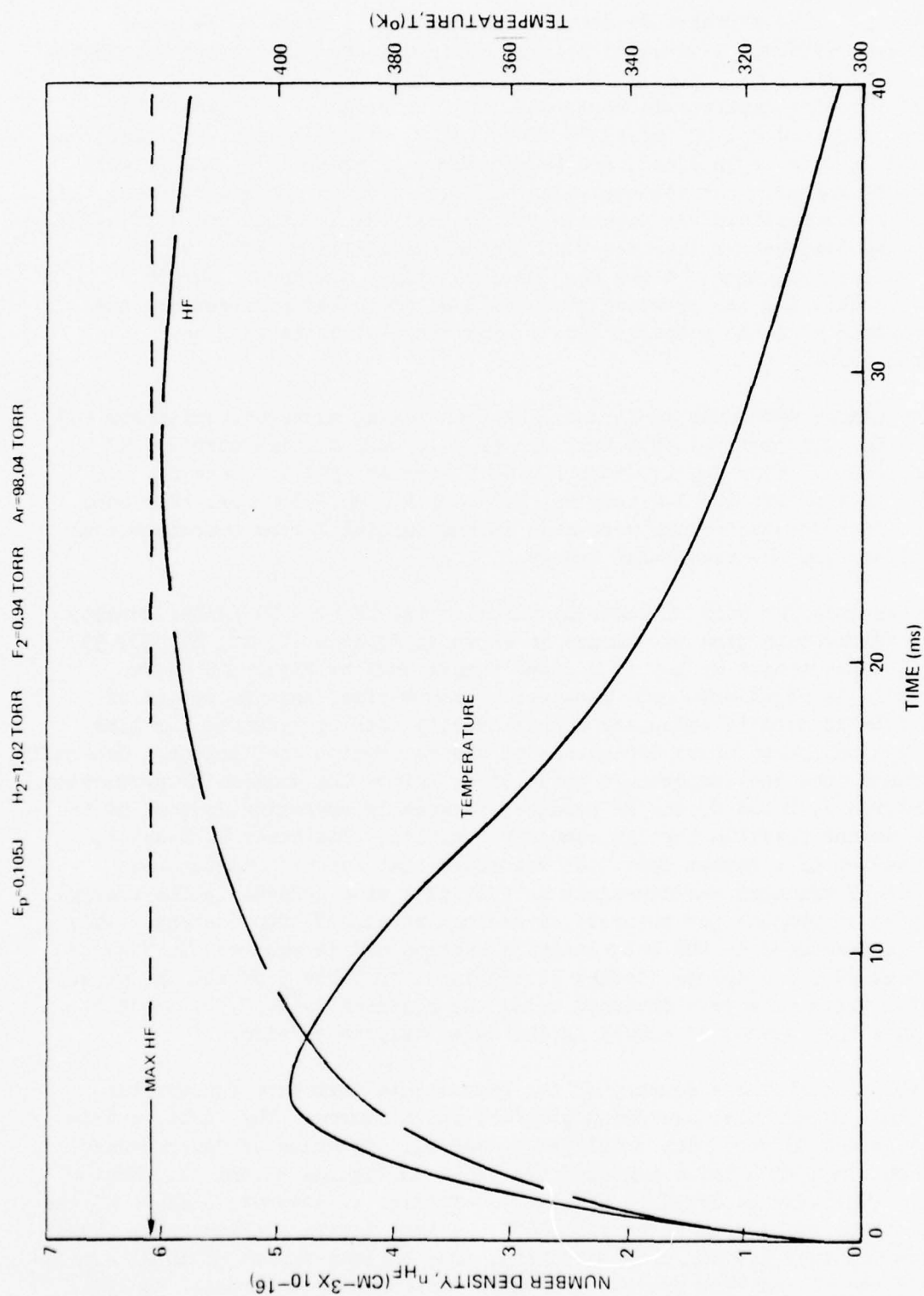


FIGURE 27 HF NUMBER DENSITY AND TEMPERATURE HISTORIES
 PULSED-FLUORESCENCE CASE A10

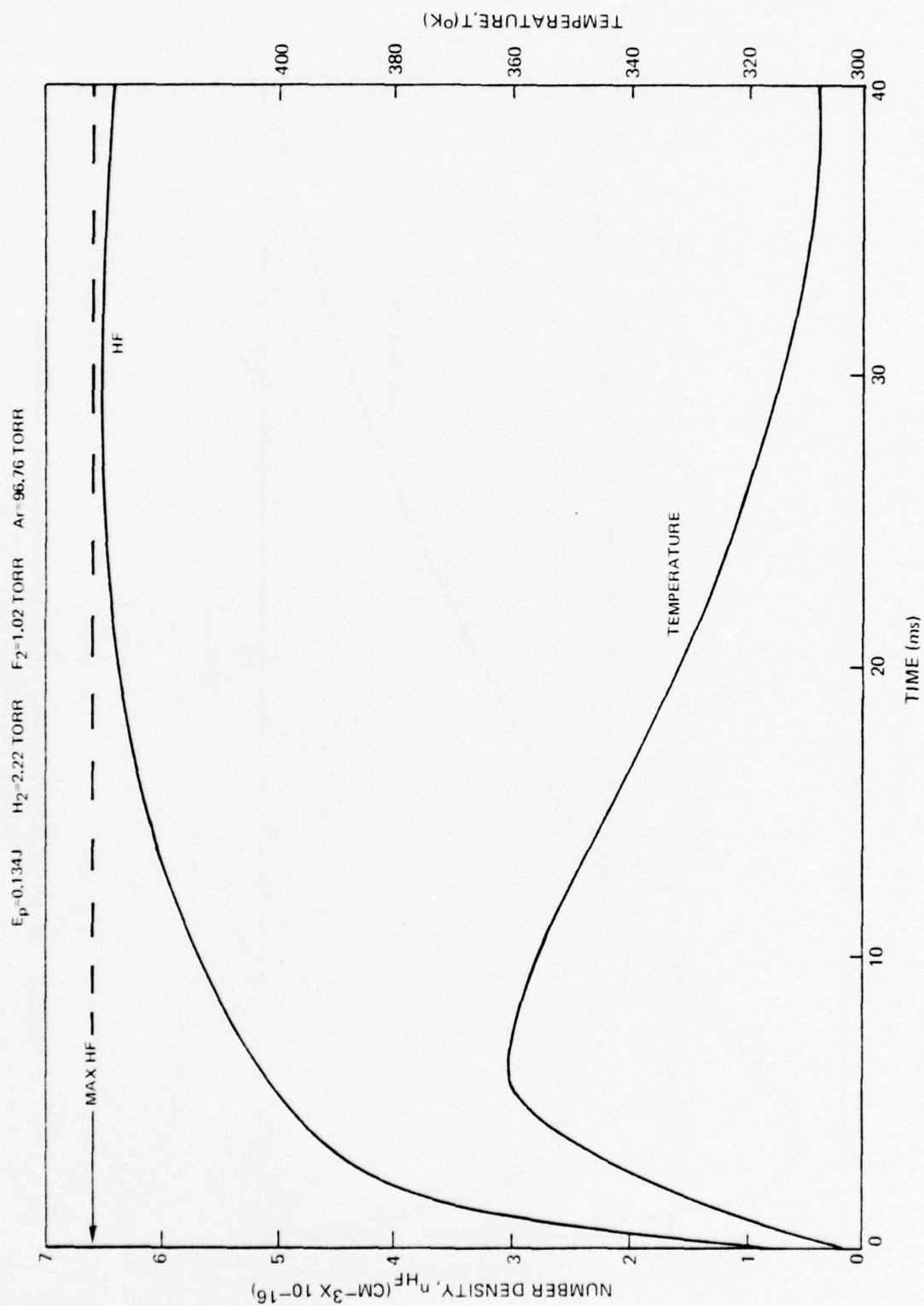


FIGURE 28 HF NUMBER DENSITY AND TEMPERATURE HISTORIES
 PULSED-FLUORESCENCE CASE B4

$E_p = 0.105J$ $H_2 = 0.55 \text{ TORR}$ $F_2 = 0.99 \text{ TORR}$ $Ar = 98.46 \text{ TORR}$

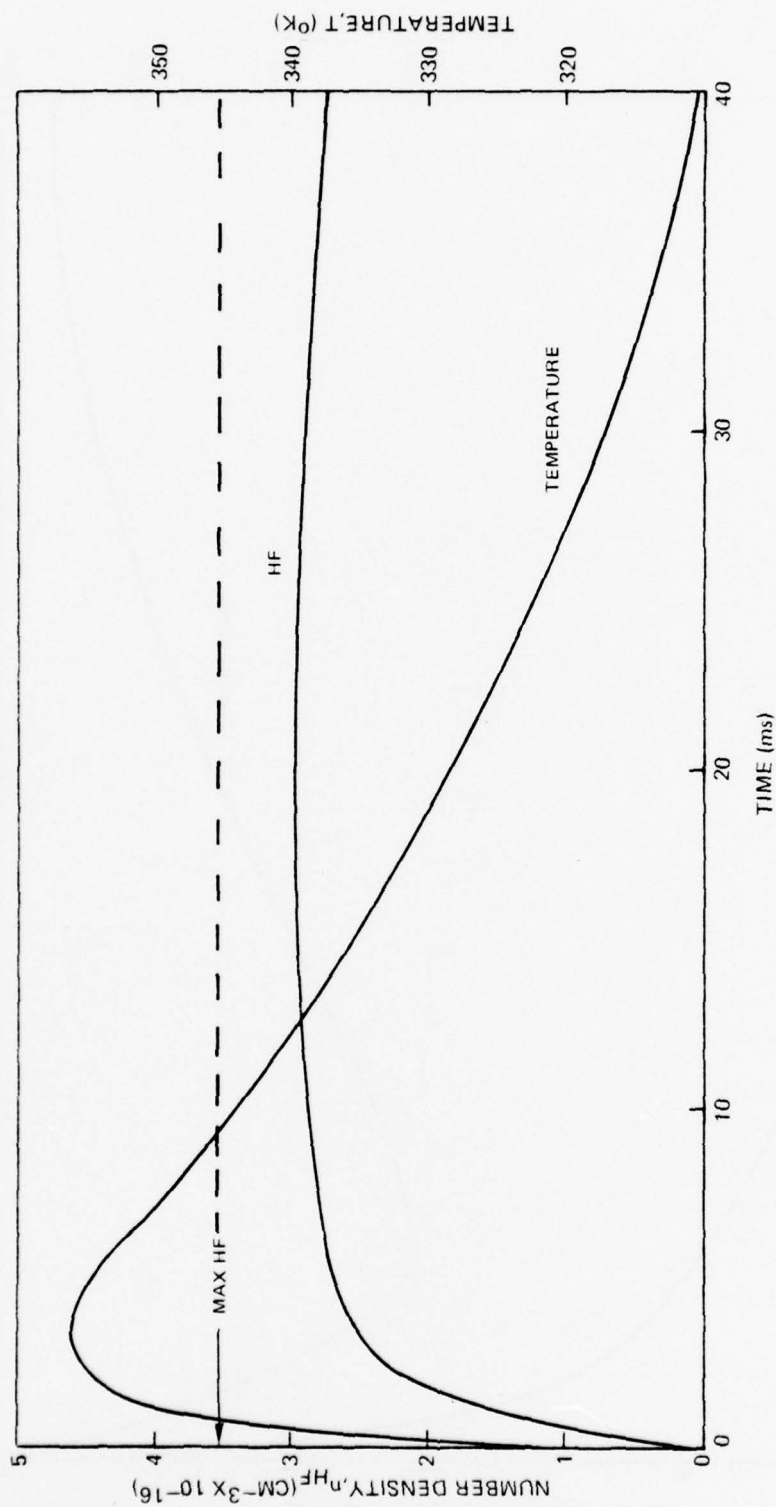


FIGURE 29 HF NUMBER DENSITY AND TEMPERATURE HISTORIES
PULSED-FLUORESCENCE CASE C7

$E_p = 0.11 \text{ J}$ $\text{H}_2 = 0.55 \text{ TORR}$ $\text{F}_2 = 0.49 \text{ TORR}$ $\text{Ar} = 98.96 \text{ TORR}$

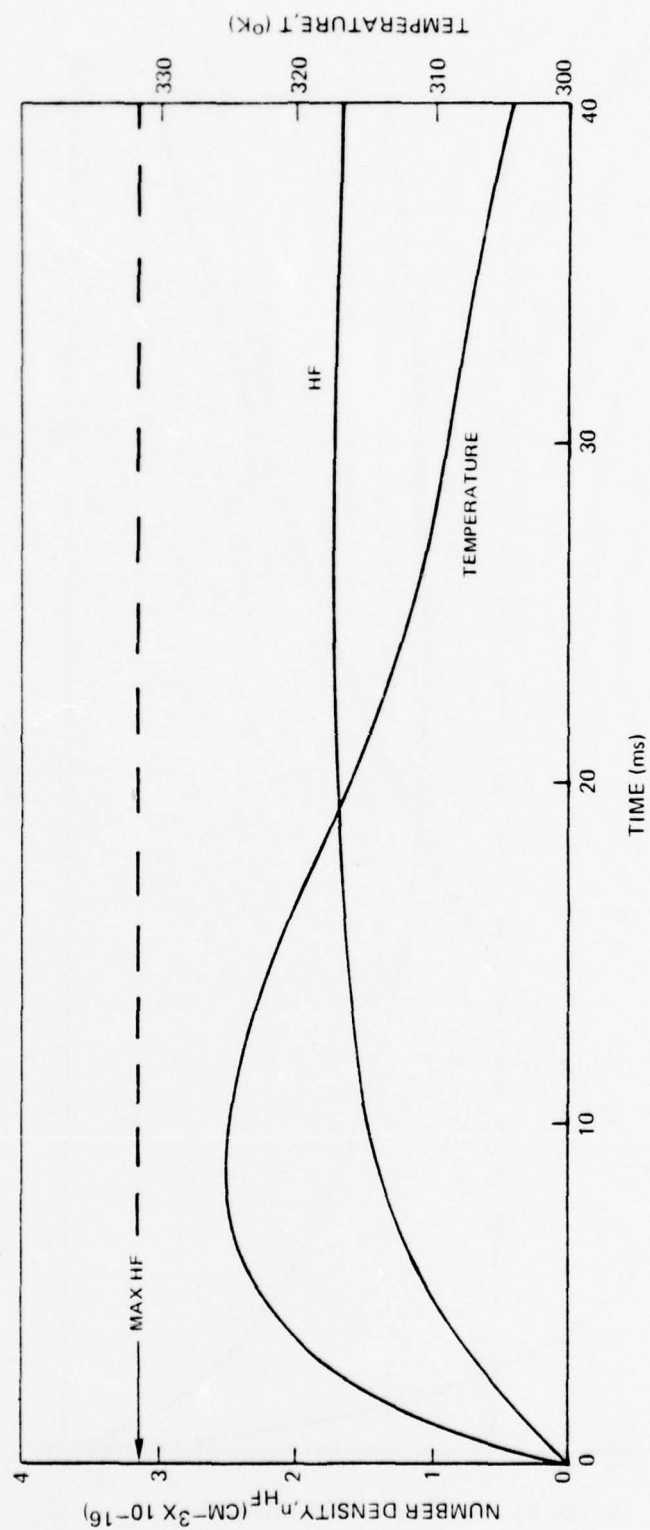


FIGURE 30 HF NUMBER DENSITY AND TEMPERATURE HISTORIES
PULSED-FLUORESCENCE CASE DH4

$E_p = 0.123 \text{ J}$ $H_2 = 1.02 \text{ TORR}$ $F_2 = 0.49 \text{ TORR}$ $Ar = 98.49 \text{ TORR}$

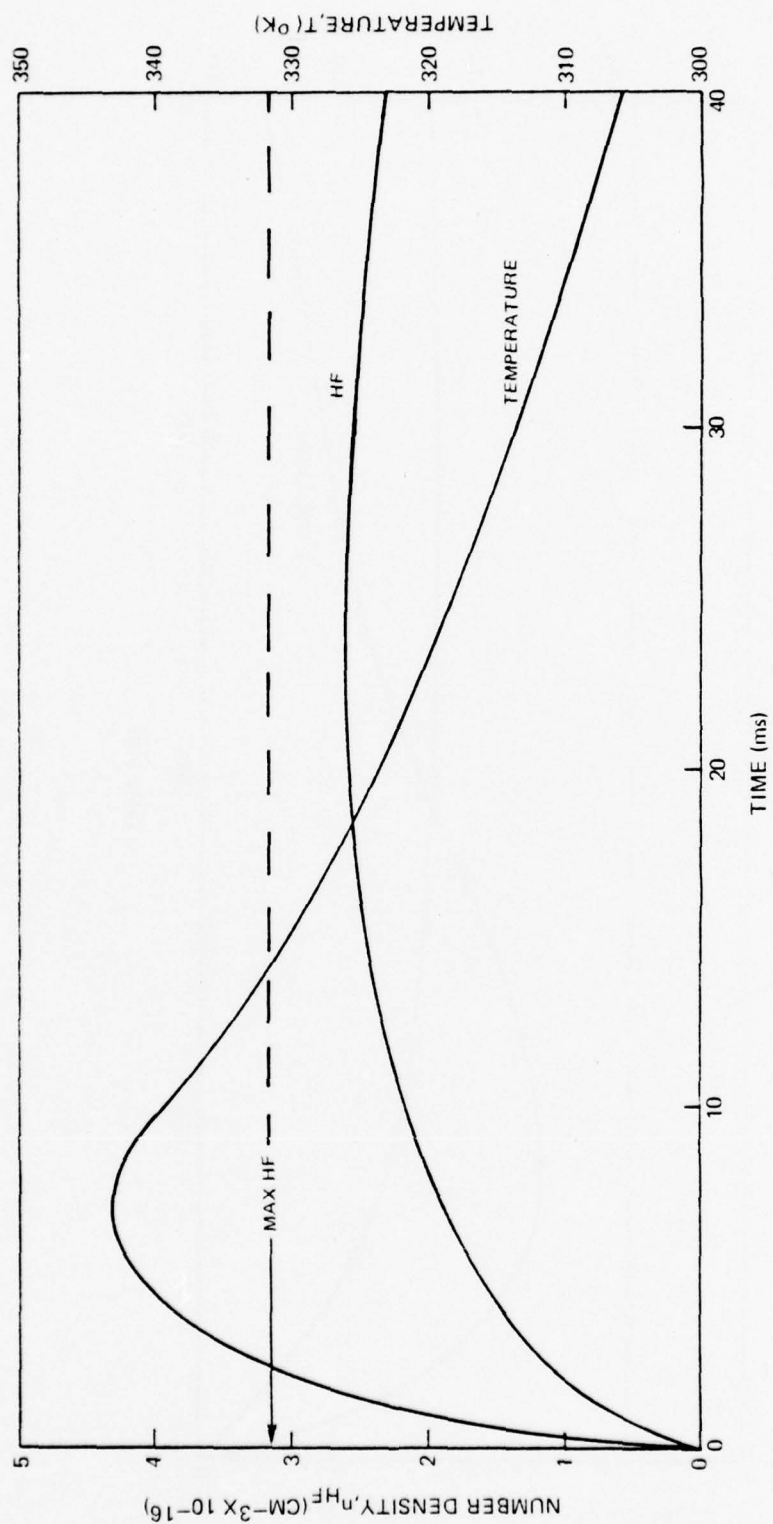


FIGURE 31 HF NUMBER DENSITY AND TEMPERATURE HISTORIES
PULSED-FLUORESCENCE CASE EF2

$E_p = 0.129 \text{ J}$ $\text{H}_2 = 0.24 \text{ TORR}$ $\text{F}_2 = 1.01 \text{ TORR}$ $\text{Ar} = 98.75 \text{ TORR}$

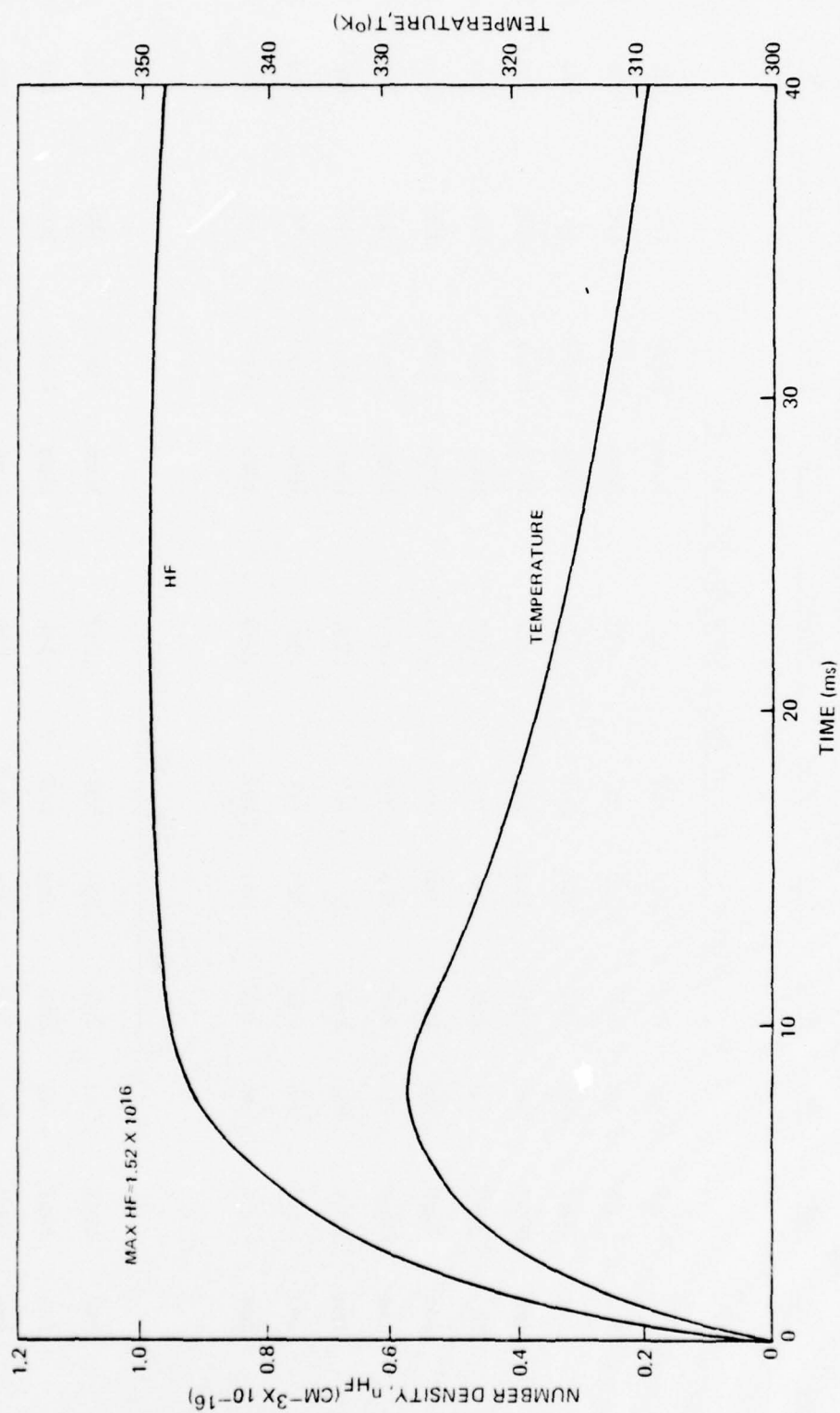


FIGURE 32 HF NUMBER DENSITY AND TEMPERATURE HISTORIES
PULSED-FLUORESCENCE CASE FF2

TABLE 5. PULSED FLDRESCENCE DATA WITH PREMIXED GASES

Run No.	$v = 1$			$v = 2$			$v = 3$			Pulse Energy Joules	Kistler		c.w. Laser		c.w. Laser		
	2.5μ			1.3μ			$.88\mu$				TB	Gain	TB	Line	TB	Line	
	TB	Gain		TB	Gain		TB	Gain									TB
A Mixture - 1 torr H ₂ , 1 torr F ₂ , 98 torr Ar																	
A6	1ms	20 μ V	20 μ s	2mV	20 μ s	1mV	.11	10ms	20mV	1P6	1ms	10ms	1ms	1P6	1ms	10ms	
A7	1ms	20 μ V	20 μ s	2mV	20 μ s	1mV	.073	10ms	20mV	1P6	1ms	10ms	1ms	1P6	1ms	10ms	
A8	1ms	20 μ V	.2ms	2mV	.2ms	1mV	.103	10ms	20mV	1P6	1ms	10ms	1ms	1P6	1ms	10ms	
A9	1ms	20 μ V	.5ms	2mV	.5ms	1mV	.112	10ms	20mV	1P6	1ms	10ms	1ms	1P6	1ms	10ms	
A10	1ms	20 μ V	.5ms	2mV	.5ms	1mV	.105	10ms	20mV	1P6	1ms	10ms	1ms	1P6	1ms	10ms	
A11	1ms	20 μ V	.5ms	2mV	.5ms	1mV	.034	10ms	20mV	1P6	1ms	10ms	1ms	1P6	1ms	10ms	
A12	1ms	20 μ V	.5ms	2mV	.5ms	1mV	.05	10ms	20mV	1P6	1ms	10ms	1ms	1P6	1ms	10ms	
A13	1ms	20 μ V	.5ms	2mV	.5ms	1mV	.134	10ms	20mV	1P6	1ms	10ms	1ms	1P6	1ms	10ms	
A14	1ms	20 μ V	.5ms	2mV	.5ms	1mV	.09	10ms	20mV	1P6	1ms	10ms	1ms	1P6	1ms	10ms	
A15	1ms	20 μ V	.5ms	2mV	.5ms	1mV	.099	10ms	20mV	1P6	1ms	10ms	1ms	1P6	1ms	10ms	
B Mixture - 2H ₂ , 1F ₂ , 100Ar																	
B3	1ms	20 μ V	.5ms	2mV	.5ms	1mV	.067	10ms	20mV	1P6	1ms	10ms	1ms	1P6	1ms	10ms	
B4	1ms	20 μ V	.5ms	2mV	.5ms	1mV	.134	10ms	20mV	1P6	1ms	10ms	1ms	1P6	1ms	10ms	
B5	1ms	10 μ V	.5ms	1mV	.5ms	.5mV	.054	10ms	20mV	1P6	1ms	10ms	1ms	1P6	1ms	10ms	

TABLE 5. PULSED FLUORESCENCE DATA WITH PREMIXED GASES (CONT'D)

Run No.	$V = 1$			$V = 2$			$V = 3$			Pulse Energy Joules	Kistler		c.w. Laser	
	2.5μ			1.3μ			$.88\mu$				TB		Line	
	TB	Gain		TB	Gain		TB	Gain			TB	Gain	TB	
C Mixture - $.5H_2$, $1F_2$, $100Ar$														
C1	1ms	$10\mu V$.5ms	1mV	.5ms	.5mV	.073	10ms	20mV	1P6	1ms	10ms		
C2	1ms	$20\mu V$.5ms	2mV	.5ms	1mV	.063	10ms	20mV	1P6	1ms	10ms		
C3	1ms	$20\mu V$.5ms	2mV	.5ms	1mV	.087	10ms	20mV	1P6	1ms	10ms		
C4	1ms	$20\mu V$.5ms	2mV	.5ms	1mV	.095	10ms	20mV	1P6	1ms	10ms		
C5	1ms	$20\mu V$	$50\mu s$	2mV	$50\mu s$	1mV	.093	10ms	20mV	1P6	1ms	10ms		
C6	1ms	$20\mu V$	$10\mu s$	2mV	$10\mu s$	1mV	.101	10ms	20mV	1P6	1ms	10ms		
C7	1ms	$20\mu V$	$5\mu s$	2mV	$5\mu s$	2mV	.105	10ms	20mV	1P6	1ms	10ms		
C8	1ms	$20\mu V$.5ms	2mV	.5ms	1mV	.164	10ms	20mV	1P6	1ms	10ms		
C9	1ms	$20\mu V$.5ms	2mV	.5ms	1mV	.152	10ms	20mV	1P6	1ms	10ms		
C11	1ms	$20\mu V$.5ms	2mV	.5ms	1mV	.134	10ms	20mV	1P6	1ms	10ms		
C12	1ms	$20\mu V$.5ms	2mV	.5ms	1mV	.134	10ms	20mV	1P6	1ms	10ms		
D Mixture - $.5H_2$, $.5F_2$, $100Ar$														
D2	1ms	$10\mu V$.5ms	.5mV	.5ms	.5mV	.123	10ms	20mV	1P6	1ms	10ms		
D3	1ms	$10\mu V$.5ms	.5mV	.5ms	.5mV	.156	10ms	20mV	1P4	1ms	10ms		
D5	1ms	$10\mu V$.5ms	1mV	.5ms	1mV	.095	10ms	20mV	1P4	1ms	10ms		

TABLE 5. PULSED FLUORESCENCE DATA WITH PREMIXED GASES (CONT'D)

Run No.	$v = 1$			$v = 2$			$v = 3$			Pulse Energy Joules	Kistler TB	Gain	c.w. Laser Line	c.w. Laser TB
	TB	2.5μ		TB	1.3μ		TB	$.88\mu$						
		Gain			Gain			Gain						
D Mixture - $.5H_2$, $.5F_2$, $100Ar$ (Cont'd)														
D6	1ms	$10\mu V$.5ms	1mV	.5ms	1mV	.097	10ms	20mV	1P4	1ms	10ms		
D7	1ms	$10\mu V$.5ms	1mV	.5ms	1mV	.09	10ms	20mV	1P4	1ms	10ms		
D8	1ms	$10\mu V$.5ms	1mV	.5ms	1mV	.084	5ms	20mV	1P4	1ms	5ms		
D9	1ms	$10\mu V$.5ms	1mV	.5ms	1mV	.142	5ms	20mV	1P4	1ms	5ms		
D10	1ms	$10\mu V$.5ms	1mV	.5ms	1mV	.141	5ms	20mV	1P4	1ms	5ms		
DH1	1ms	$20\mu V$.159	5ms	20mV	1P6	1ms	5ms		
DH2	1ms	$20\mu V$.152	5ms	20mV	1P6	1ms	5ms		
DH3	1ms	$20\mu V$.134	5ms	20mV	1P6	1ms	5ms		
DH4	1ms	$20\mu V$.109	5ms	20mV	1P6	5ms	5ms		
DH5	1ms	$20\mu V$.045	5ms	20mV	1P6	5ms	5ms		
DH6	1ms	$20\mu V$.101	5ms	20mV	1P6	5ms	5ms		
DH7	1ms	$20\mu V$.106	5ms	20mV	1P6	5ms	5ms		
DH8	1ms	$20\mu V$.097	5ms	20mV	1P6	10ms	5ms		
DH9	1ms	$20\mu V$.069	5ms	20mV	1P6	10ms	5ms		

TABLE 5. PULSED FLUORESCENCE DATA WITH PREMIXED GASES (CONT'D)

Run No.	$v = 1$			$v = 2$			$v = 3$			Pulse Energy Joules	Kistler		c.w. Laser	
	2.5μ			1.3μ			$.88\mu$							
	TB	Gain		TB	Gain		TB	Gain					TB	Gain
EF Mixture - $.5H_2, 1F_2$														
EF1	1ms	20 μ V							.134	5ms	20mV	1P6	1ms	5ms
EF2	1ms	20 μ V							.123	5ms	20mV	1P6	1ms	5ms
EF3	1ms	20 μ V							.127	5ms	20mV	1P6	1ms	5ms
EF4	1ms	20 μ V							.157	5ms	20mV	1P6	1ms	5ms
EF5	1ms	20 μ V							.160	5ms	20mV	1P6	1ms	5ms
EF6	1ms	20 μ V							.140	5ms	20mV	1P6	1ms	5ms
EF7	1ms	20 μ V							.140	5ms	20mV	1P6	1ms	5ms
EF8	1ms	20 μ V							.054	5ms	20mV	1P6	1ms	5ms
EF9	1ms	20 μ V							.108	5ms	20mV	1P6	1ms	5ms
EF10	1ms	20 μ V							.041	5ms	20mV	1P6	1ms	5ms
EF11	1ms	20 μ V							.076	5ms	20mV	1P6	1ms	5ms
EF12	1ms	20 μ V							.046	5ms	20mV	1P6	1ms	5ms
F Mixture - $.2H_2, 1F_2, 100Ar$														
F1	2ms	10 μ V		1ms	2mV		1ms	1mV	.028	10ms	20mV	1P6	2ms	10ms
F3	1ms	10 μ V		.5ms	2mV		.5ms	1mV	.050	5ms	20mV	1P6	1ms	5ms

TABLE 5. PULSED FLUORESCENCE DATA WITH PREMIXED GASES (CONT'D)

Run No.	$v = 1$		$v = 2$		$v = 3$		Pulse Energy Joules	Kistler		c.w. Laser		c.w. Laser	
	TB	Gain	TB	Gain	TB	Gain		TB	Gain	Line	TB	TB	Line
F4	1ms	10 μ V	.5ms	2mV	.5ms	1mV	.056	5ms	20mV	1P4	1ms	5ms	1P4
F5	1ms	10 μ V	.5ms	2mV	.5ms	1mV	.077	5ms	10mV	1P4	1ms	5ms	1P4
F6	.5ms	10 μ V	.5ms	2mV	.5ms	1mV	.132	2ms	10mV	1P4	.5ms	2ms	1P4
F7	.5ms	2 μ V	.2ms	5mV	.2ms	2mV	.127	1ms	10mV	1P4	.5ms	1ms	1P4
F9	.5ms	2 μ V	.2ms	5mV	.2ms	2mV	.121	1ms	10mV	1P4	.5ms	1ms	1P4
F10	.5ms	2 μ V	.2ms	5mV	.2ms	2mV	.181	1ms	10mV	1P4	.5ms	1ms	1P4
F11	.1ms	20 μ V	2 μ s	5mV	2 μ s	2mV	.176	1ms	10mV	1P4	.1ms	1ms	1P4
F12	.1ms	20 μ V	2 μ s	5mV	2 μ s	2mV	.159	1ms	10mV	1P4	.1ms	1ms	1P4
FF1	10ms	20 μ V					.050	5ms	20mV	1P6	5ms	10ms	1P6
FF2	10ms	20 μ V					.129	5ms	20mV	1P6	5ms	10ms	1P6
FF3	10ms	20 μ V			$v = (4-1)$.172	5ms	20mV	1P6	5ms	10ms	1P6
G1	.1ms	20 μ V	.2ms	10mV	.2ms	2mV	.192			1P4	.1ms		
G2	.1ms	20 μ V	.2ms	10mV	.2ms	2mV	.181			1P4	.1ms		
G3	.1ms	20 μ V	.2ms	10mV	$v = (6-3)$.159			1P4	.1ms		
G4	.1ms	20 μ V	.2ms	10mV	$v = (5-2)$.171			1P4	.1ms		

TABLE 6. SUMMARY OF PRELIMINARY PULSE EXPERIMENTS

A. Mixtures of H_2 and F_2 (no diluent)

Mix I 1.0 Torr F_2 0.2 Torr H_2

Pulse Energy (Joules):

0.025	0.04	0.08
0.035	0.045	0.08
0.035	0.05	0.08
0.04	0.05	0.09
0.04	0.07	0.097

Mix II 1.0 Torr F_2 .5 Torr H_2

Pulse Energy (Joules):

0.007	0.024	0.043	0.065
0.008	0.024	0.054	0.067
0.010	0.025	0.057	0.068
0.011	0.035	0.058	0.068
0.012	0.037	0.060	0.073
0.012	0.038	0.061	0.035
0.015	0.040	0.061	0.047
0.019	0.040	0.063	0.048
0.020	0.041	0.065	0.059

Mix III 1.0 Torr F_2 0.6 Torr H_2

Pulse Energy (Joules):

0.035	0.06	0.092
0.035	0.06	

Mix IV 1.0 Torr F_2 1.0 Torr H_2

Pulse Energy (Joules):

0.035	0.056	0.074
0.035	0.060	0.087

TABLE 6. SUMMARY OF PRELIMINARY PULSE EXPERIMENTS (CONT'D)

Mix V	1.0 Torr F ₂	1.5 Torr H ₂	
Pulse Energy (Joules):			
	0.028	0.043	0.057
	0.031	0.052	0.093

Mix VI	1.0 Torr F ₂	2.0 Torr H ₂	
Pulse Energy (Joules):			
	0.034		
	0.053		
	0.091		

Mix VII	2.0 Torr F ₂	0.2 Torr H ₂	
Pulse Energy (Joules):			
	0.09		

Mix VIII	8.0 Torr F ₂	8.0 Torr H ₂	80 Torr N ₂
Pulse Energy (Joules):			
	0.063	0.082	
	0.063	0.085	

Mix IX	0.5 Torr F ₂	5.0 Torr H ₂	
Pulse Energy (Joules):			
	0.09		

B. Mixtures with Helium

Mix I	1.0 Torr F ₂	0.2 Torr H ₂	50 Torr He
Pulse Energy (Joules):			
	0.025	0.070	
	0.025	0.081	

TABLE 6. SUMMARY OF PRELIMINARY PULSE EXPERIMENTS (CONT'D)

Mix II	1.0 Torr F ₂	0.2 Torr H ₂	100 Torr He
	Pulse Energy (Joules):		
	0.040	0.045	0.08
	0.044	0.05	0.08
			0.09
Mix III	1.0 Torr F ₂	0.5 Torr H ₂	1.0 Torr N ₂
	Pulse Energy (Joules):		
	0.027	0.033	0.04
	0.03	0.037	
Mix IV	1.0 Torr F ₂	0.6 Torr H ₂	50 Torr He
	Pulse Energy (Joules):		
	0.05	0.065	
	0.06	0.092	
Mix V	1.0 Torr F ₂	1.0 Torr H ₂	50 Torr He
	Pulse Energy (Joules):		
	0.028	0.056	0.087
	0.035	0.060	0.094
			0.097
Mix VI	1.0 Torr F ₂	1.5 Torr H ₂	50 Torr He
	Pulse Energy (Joules):		
	0.031	0.043	0.057
	0.034	0.051	0.075
			0.093
			0.097
Mix VII	1.0 Torr F ₂	2.0 Torr H ₂	50 Torr He
	Pulse Energy (Joules):		
	0.053	0.091	
	0.088		

TABLE 6. SUMMARY OF PRELIMINARY PULSE EXPERIMENTS (CONT'D)

Mix VIII 0.5 Torr F₂ 5.0 Torr H₂ 50 Torr He

Pulse Energy (Joules):

0.091

0.093

Mix IX 8.0 Torr F₂ 8.0 Torr H₂ 80 Torr N₂

Pulse Energy (Joules):

0.025

0.063

0.082

0.028

0.065

0.085

Determination of HF produced from F₂-H₂-He mixtures to determine F₂ concentrations.
Each mixture pulsed 3 times for complete reaction.

Mix I 1.0 Torr F₂ 1.0 Torr H₂ 50 Torr He

Test 1 - pulse energy (joules): 0.11 0.085 0.11

Test 2 0.11 0.11 0.13

Test 3 0.13 0.10 0.11

Mix II .5 Torr F₂ .5 Torr H₂ 50 Torr He

Test 1 - pulse energy (joules): 0.12 0.45 0.11

Test 2 0.107 0.088 0.11

Test 3 0.139 0.142 0.133

Mix III 1.0 Torr F₂ 1.5 Torr H₂ 50 Torr He

Test 1 - pulse energy (joules): 0.105 0.05 0.09

Test 2 0.123 0.1 0.052

Test 3 0.095 0.08 0.098

Mix IV 0.5 Torr F₂ 1.0 Torr H₂ 50 Torr He

Test 1 - pulse energy (joules): 0.055 0.085 0.095

Test 2 0.075 0.085 0.06

Test 3 0.09 0.09 0.1

TABLE 6. SUMMARY OF PRELIMINARY PULSE EXPERIMENTS (CONT'D)

C. Mixtures with Argon

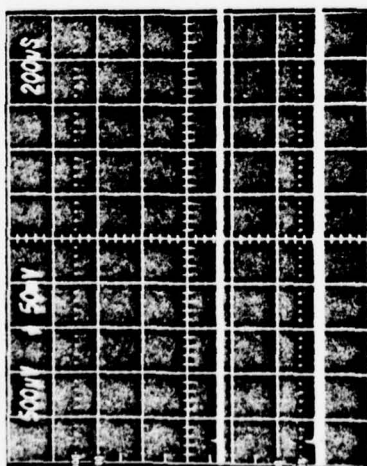
Mix I	100 Torr Ar	1.0 Torr F ₂	0.2 Torr H ₂
Pulse Energy (Joules):			
	0.08	0.047	0.067
	0.017	0.05	0.08
	0.035	0.05	0.086
	0.045	0.055	0.09
			0.098
			0.10
			0.13
			0.17

Check of H₂ content by determination of HF using multiple pulses with above mixture

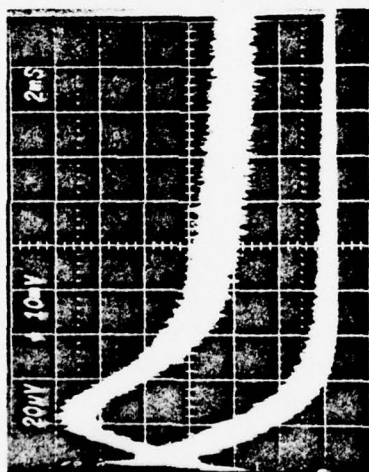
Test 1 - Pulse Energy	0.06	0.08	0.06	HF = 0.29 Torr
Test 2	0.105	0.11	0.12	HF = 0.65 Torr
Test 3	0.075	0.067	0.06	HF = 0.38 Torr
Test 4	0.035	0.113	0.085	HF = 0.55 Torr
Test 5	0.12	0.090	0.096	HF = 1.10 Torr
Test 6	0.05	0.113	0.095	HF = 0.59 Torr
Test 7	0.80	0.65	0.60	HF = 0.61 Torr
Test 8	0.04	0.08	0.06	HF = 0.53 Torr
Test 9	0.098	0.085	0.12	HF = 0.95 Torr
Test 10	0.08	0.08	0.065	HF = 0.55 Torr
Test 11	0.13	0.13	0.12	HF = 0.70 Torr
	0.08	0.09	0.11	HF = 0.64 Torr
Test 12	0.11	0.10	0.11	HF = 0.41 Torr
	0.115	0.02	0.08	HF = 0.53 Torr
Test 13	0.086	0.11	0.080	HF = 0.32 Torr
Test 14	0.085	0.11	0.11	HF = 0.22 Torr
Test 15	0.060	0.080	0.083	HF = 0.32 Torr
Test 16	0.17	0.10		HF = 0.18 Torr

$\text{H}_2(0.5 \text{ TORR}) \text{ F}_2(1.0 \text{ TORR}) \text{ F}(0.0009 \text{ TORR})$

LASER PULSE



FLUORESCENCE $v(1-0)$ AND $\Delta v = 3$



ABSORPTION $P_{1-0}(6)$

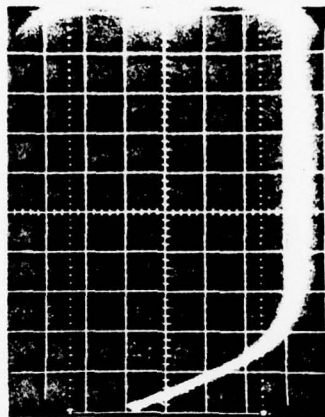
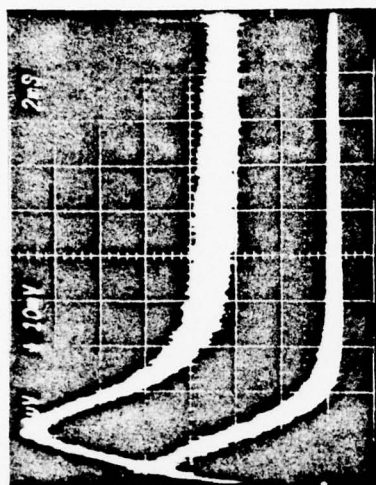
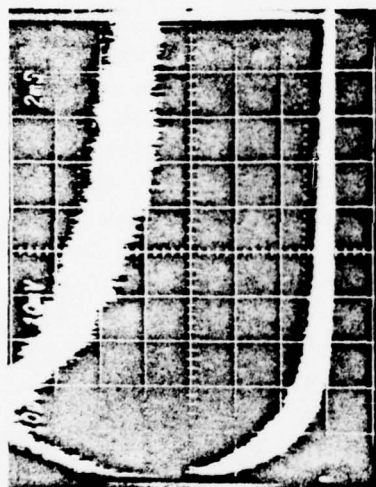


FIGURE 33 REACTION OF AN H_2-F_2 MIXTURE

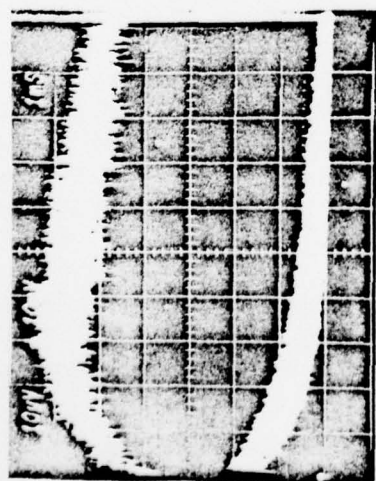
H₂ (0.5 TORR) F₂ (1.0 TORR)



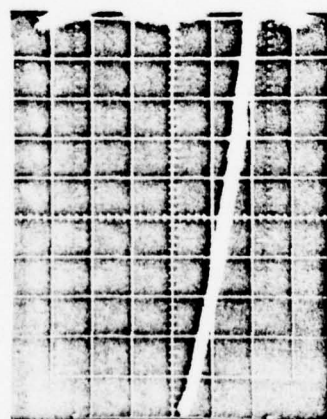
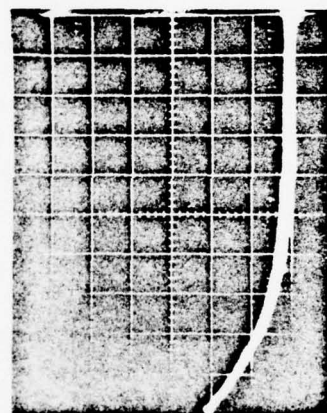
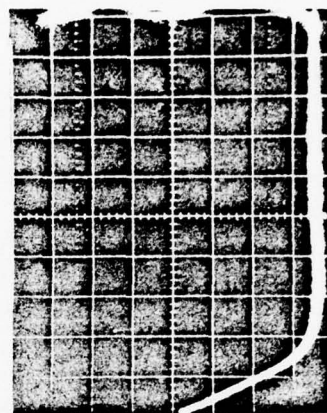
F-ATOM (0.001)



F-ATOM (0.0005)



F-ATOM (0.0004)



ABSORPTION P₁₋₀(6)

FIGURE 34 EFFECT OF INITIAL F-ATOM ON H₂-F₂ REACTIONS

where prereaction produced in excess of 0.02 torr of HF there was a slow build up of HF in $v = 1$ and above immediately after the UV dissociating pulse. After some delay there was a sharp increase in the excited population which was reflected in $v = 0$. The delay time was shorter for increased initial F atom concentration. These effects are illustrated in the scope traces of Figure 35. It would be interesting to look for gain or lasing effects during the spiking. We surmise the spiking behavior is due to inhibition of the chain by HF($v = 0$) with slow buildup of temperature until an explosive reaction occurs.

In another series of experiments (Table 6-B) He was added to the H_2-F_2 mixture to keep the temperature down. Unfortunately the addition of helium disturbs the F_2 concentration because as Bott has pointed out (Ref. 14), the viscosity, average molecular weight and specific heat of the mixture changes so that the initial concentrations were unknown. An attempt was made to back correct the data for these effects. However, testing the mixture by determining HF produced through absorption measurement gave low and inconsistent results. Similar conclusions were reached for the data with Ar as diluent (Table 6-C). For these mixtures there was uncertainty about the H_2 concentration. Because of the high temperature or uncertainty about starting concentrations, data from the experimental runs listed in Table 6 were not analyzed in detail and were not used to evaluate kinetics.

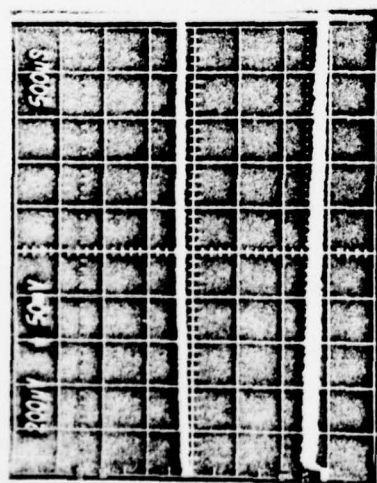
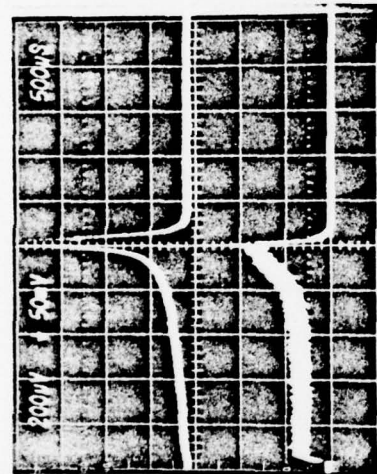
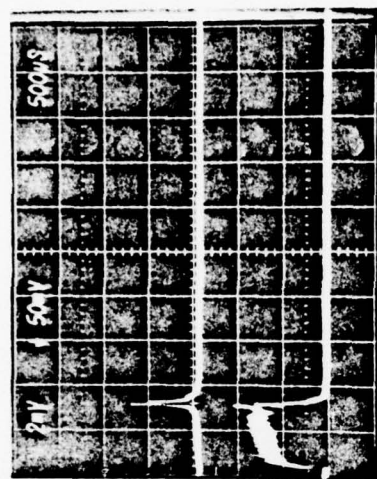
Pulsed Gain Measurements

Gain measurements were made for pulsed chain reactions in mixtures made with premixed F_2/Ar and H_2/Ar . The fluorescence apparatus illustrated in Figures 18 and 19 was used except the cw probe beam traversed the length of the cell (15.2 cm) at a slight angle off the axis of the doubled ruby beam. Intensity of the cw beam was monitored with a AuGe detector and scope pictures were used to record data. Two such gain traces are presented in Figure 36 for a 1P3 and 2P3 laser line with peak gains found at 1.3 and 1.4 percent/cm respectively. A very important aspect of these traces is that the gain typically lasts for 10 to 20 μ sec after the double ruby pulse while the reaction producing HF goes on for milliseconds; that is, most of the reaction energy does not result in laser gain.

For a mixture containing 0.2 torr H_2 , 1.0 torr F_2 , and 98.8 torr Ar, gain measurements were made for the lines 1P2, 1P3, 1P4, 1P6, 1P7, 2P3, 2P4, 2P5 and 2P6 with variations in the initial F atom concentration (pulse

-
14. Bott, J. F., "Gas Dynamic Corrections Applied to Laser Induced Fluorescence Measurements of HF($v=1$) and DF($V=1$) Deactivation," J. Chem. Phys., 61, 3414, 1974.

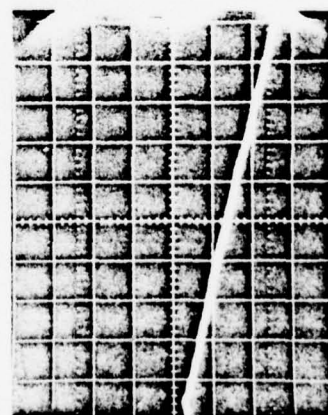
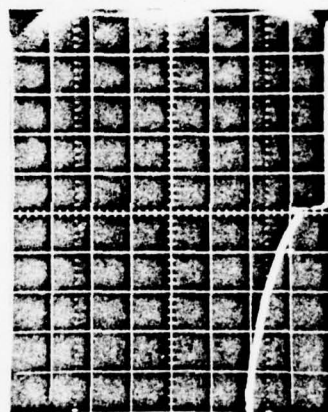
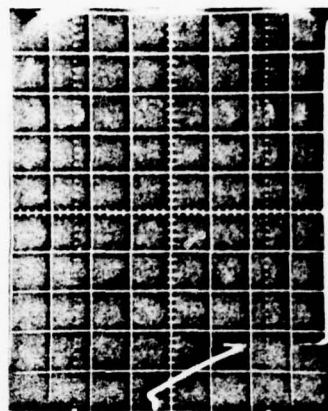
H₂ (0.5 TORR) F₂ (1.0 TORR)



F-ATOM (0.0002 TORR)

F-ATOM (0.0004 TORR)

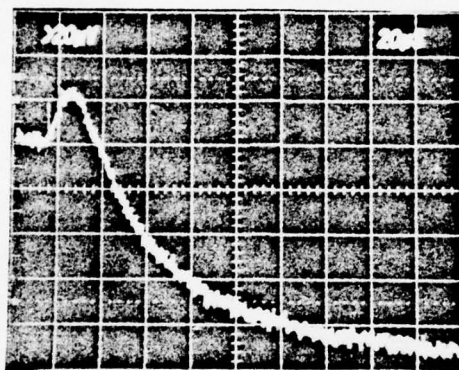
F-ATOM (0.0007 TORR)



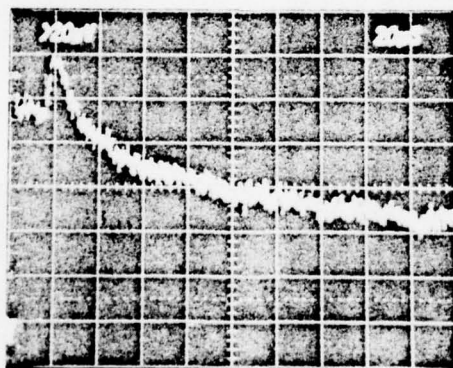
ABSORPTION F₁₋₀ (5)

FIGURE 35 EFFECT OF INITIAL F-ATOM ON REACTION - 0.02 TORR HF PRESENT

0.2 TORR H₂, 1.0 TORR F₂, 98.8 TORR Ar



1P3 GAIN 1.4%/CM
PULSE ENERGY 0.17 JOULES



2P3 GAIN 1.3%/CM
PULSE ENERGY 0.19 JOULES

FIGURE 36 GAIN TRACES

energy). These data are listed in Table 7. In Figure 37 the gain on various lines is shown for experiments using 0.12 joule and 0.17 joule dissociation pulses. Over the range of lines studied the gain is seen to peak at 1P⁴ and at 2P³. The gain on any particular line was found to monotonically increase with increasing pulse energy as shown in Figure 38.

For the mixtures studied, gain at constant pulse energy of the 1P⁴ line was found highest for 0.5 torr H₂, 1.0 torr F₂ and 98.5 torr Ar. The data with various mixtures are listed in Table 7 and plotted in Figure 39. An analysis of these data and comparison with the computer model is presented in Section IV.

Pulsed Laser Tests

Laser tests were made using the mixtures of premixed H₂/Ar and F₂/Ar employed for fluorescence and gain measurements. Frequency doubled radiation from the ruby laser was used to dissociate the fluorine and initiate the chain reaction. The laser configuration closely followed the design of Nichols, et al (Ref. 15).

Previous studies of pulsed lasing on H₂-F₂ mixtures include the work of Basov and coworkers (Ref. 16) who demonstrated pulsed lasing using flash-lamp initiation of the chain reaction from levels up to v, 6-5, in 1969. In these experiments lasing on transitions from v = 4 showed less power than from other levels leading to the conclusion that chain branching by HF(v=4) + F₂ → HF + 2F was an important contributor. These experiments also suggested that HF(v=1) excitation was transferred to H₂ because the 1-0 transition was not observed. Subsequent workers generally did not observe lasing from transitions higher than v = 4 → 3. Careful studies of pulsed lasing were reported by Nichols and coworkers (Ref. 15). In this work a frequency doubled pulsed ruby laser was used to start the F₂-H₂ reaction and laser-emission was found on v = 3 → 2, 2 → 1, 1 → 0. The time history of ten lines was measured simultaneously and ground state HF was determined with a pulsed probe laser and F atom concentration was calculated from known cross sections for photodissociation. The temporal behavior of lasing from individual lines from a pulsed F₂-H₂ laser initiated by doubled pulsed ruby has been reported by

-
15. Nichols, D. B., K. H. Wrolstad, and J. Doyle McClure, "Time-Resolved Spectroscopy of a Pulsed H₂-F₂ Laser with Well-Defined Initial Conditions," J. of Appl. Phys., 45, 12, December 1974.
 16. Basov, N. G., L. V. Kulakov, E. P. Markin, A. I. Mikitin, A. N. Uraevskii, and P. N. Lebedev, "Emission Spectrum of a Chemical Laser Using an H₂ + F₂ Mixture," JETP Lett. 9, 375, 1969.

TABLE 7. DATA FROM GAIN MEASUREMENTS

I. Line Variation (Mixture 0.2H_2 1.0F_2 98.8Ar)

<u>Code</u>	<u>Line</u>	<u>Gain</u> <u>%/cm</u>	<u>Pulse</u> <u>Energy</u>	<u>Code</u>	<u>Line</u>	<u>Gain</u> <u>%/cm</u>	<u>Pulse</u> <u>Energy</u>
M4	1P2	1.22	.153	Q1	1P7	.39	.16
M3		.98	.137	Q3		.39	.15
M2		.90	.115	Q2		.11	.12
M1		.86	.10				
L1	1P3	1.35	.17	N5	2P3	1.3	.19
L2		.79	.15	N4		1.2	.13
L3		.78	.13	N3		1.3	.19
H4	1P4	1.49	.165	N2		1.1	.10
H2		1.01	.12	N1		1.0	.09
H1		.76	.10	K1	2P4	1.09	.16
H3		.82	.10	K2		.66	.12
I1	1P6	.80	.16	O1	2P5	.80	.19
I2		.54	.14	O2		.48	.11
I3		.55	.12	P3	2P6	.80	.19
J2	1P7	.39	.16	P1		.49	.14
J1				P2		.49	.12
J3		.26	.11				

II. Mixture Variation (Line 1P4)

<u>Code</u>	<u>Mixture</u>	<u>Gain</u> <u>%/cm</u>	<u>Pulse</u> <u>Energy</u>	<u>Code</u>	<u>Mixture</u>	<u>Gain</u> <u>%/cm</u>	<u>Pulse</u> <u>Energy</u>
H4	0.2H_2 1F_2 98.8Ar	1.49	.165	S2	$.5\text{H}_2$ 1F_2 98.5Ar	2.32	.15
H2		1.01	.12	S1		1.40	.11
H1		.76	.10				
H3		.82	.10	T3	1H_2 0.5F_2 98.5Ar	.15	.133
				T1		.14	.127
R1	$.5\text{H}_2$ $.5\text{F}_2$ 99Ar	.94	.15	T2		.09	.082
R2		.54	.11				
				O1	2H_2 1F_2 97Ar	no gain, pre-reaction complete absorption of 1P4 line	

0.2 TORR H₂ 1.0 TORR F₂ 98.8 TORR Ar

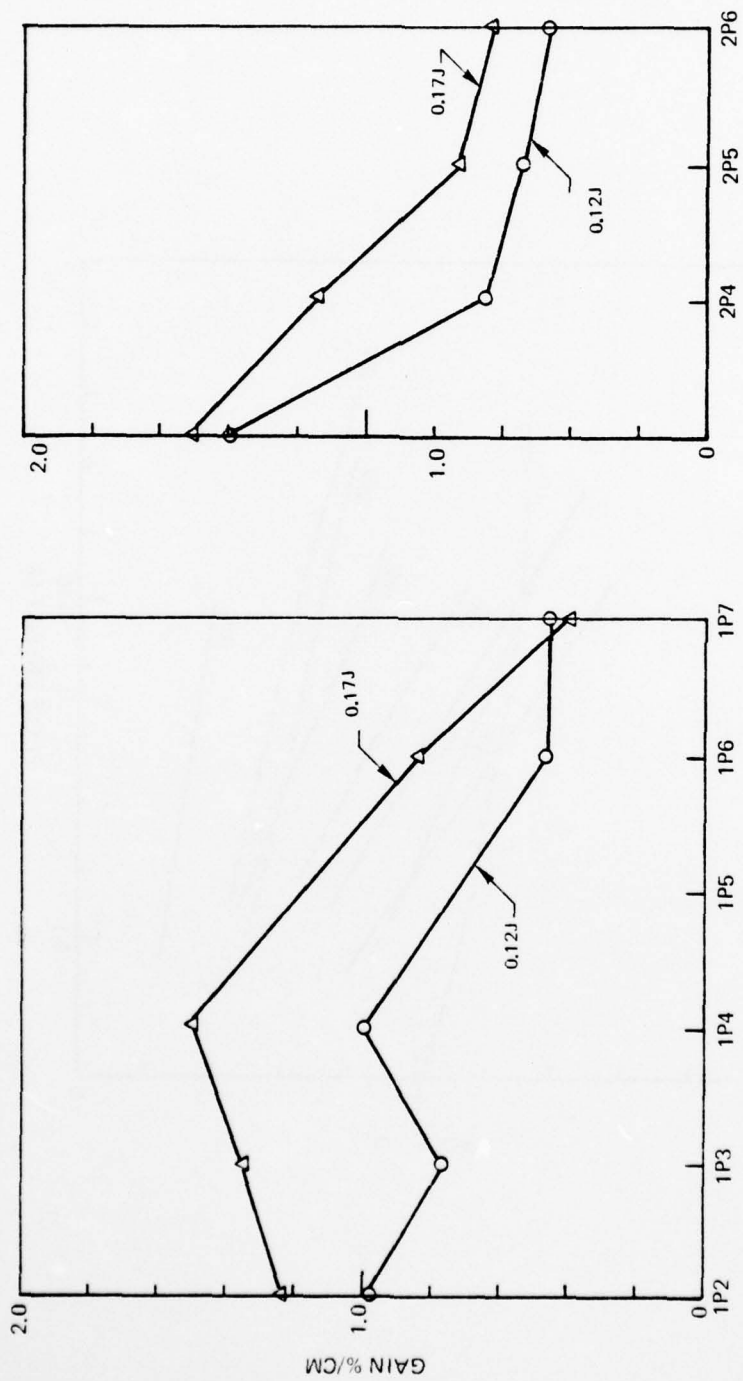


FIGURE 37 GAIN VS LASER TRANSITION

0.2 TORR H_2 1.0 TORR F_2 98.8 TORR Ar

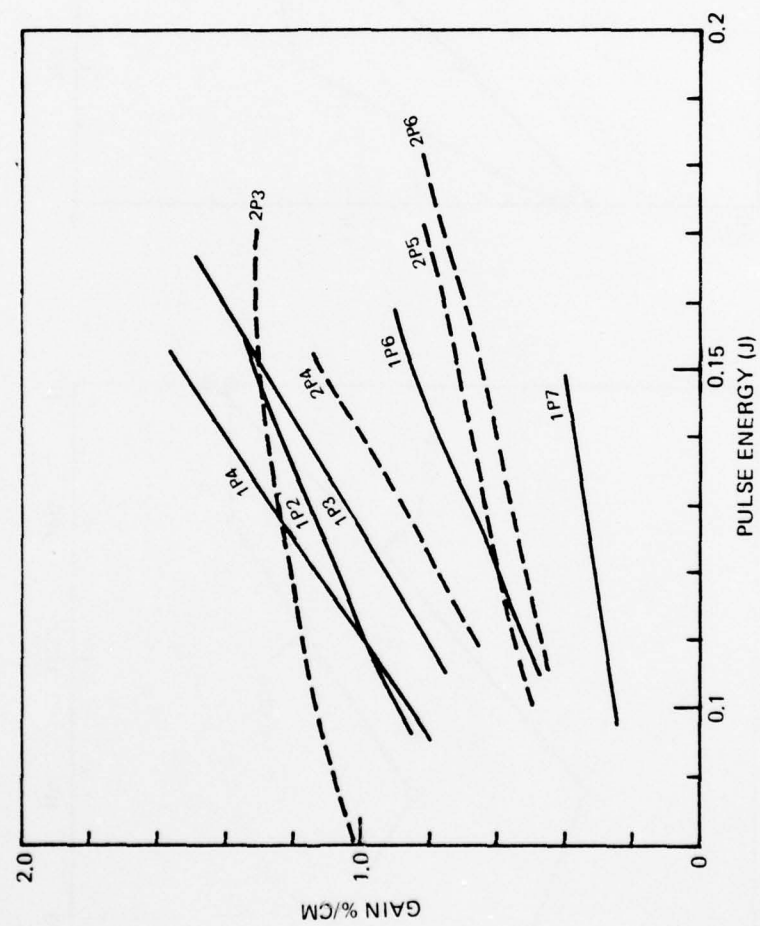


FIGURE 38 GAIN VS PULSE ENERGY

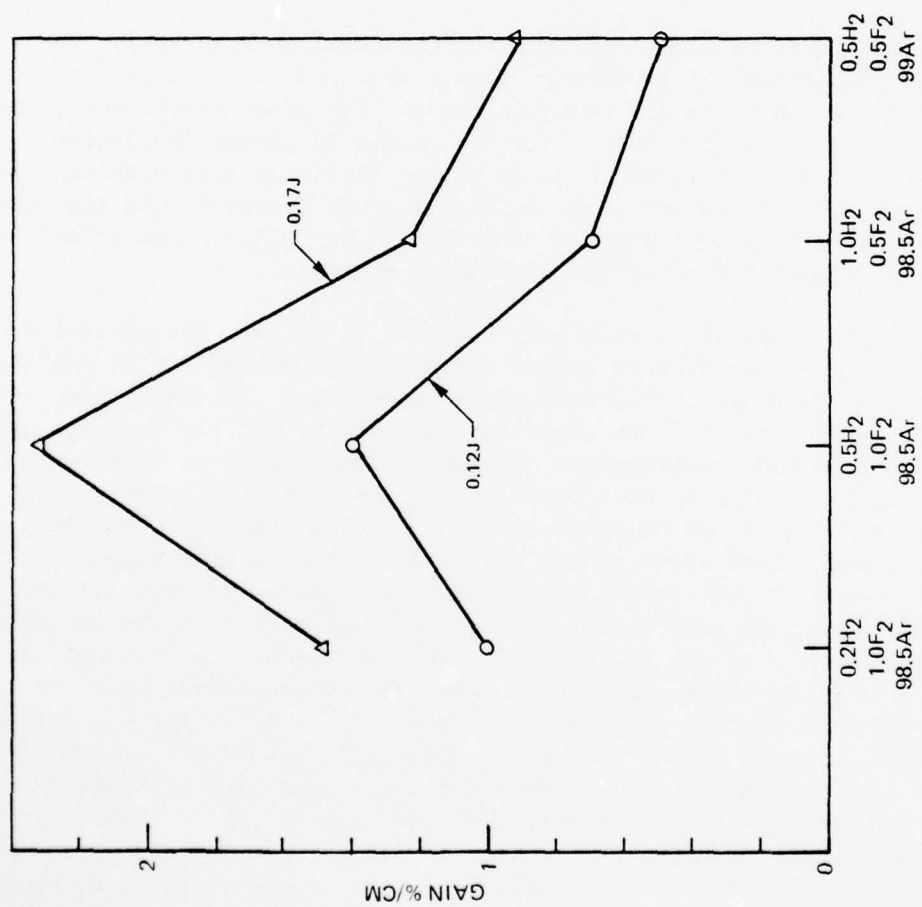


FIGURE 39 GAIN 1P4-VARIOUS MIXTURES

AD-A041 204

UNITED TECHNOLOGIES RESEARCH CENTER EAST HARTFORD CONN

F/G 20/5

LONG RANGE CHAIN LASER STUDIES, PHASE I STUDIES. (U)

JUN 77 L R BOEDEKER, P A BONZYK, J J HINCHEN

F29601-75-C-0139

UNCLASSIFIED

UTRC/R77-952198-58

AFWL-TR-77-43

NL

2 OF 4
AD
A041204



Dolgov (Ref. 17). The laser was found to emit on transitions $v = 5 \rightarrow 4$, $4 \rightarrow 3$, $3 \rightarrow 2$, $2 \rightarrow 1$, and detailed graphs of intensity of each line versus time were determined. Pulsed lasing from the F_2-H_2 chain reaction was also reported by Suchard (Ref. 18) using flashlamp initiation and with time resolved spectroscopy. Lasing from transition up to $v = 6-5$ was observed using a high "Q" optical cavity with 10 percent output coupling. In an earlier study, Suchard (Ref. 19) concluded that only ~ 7 percent of the total laser radiation is on transitions above $v(4-3)$.

A schematic of the laser configuration is shown in Figure 40. Pre-mixed gases continuously flow through a gain cell made from Kel-F with dimensions of length 61 cm and diameter 12 cm. The laser cavity was formed with a flat total reflector and a 10 meter radius 92 percent reflector separated by 96 cm. The second surface of the partially transmitting mirror was AR coated for 2.7 microns. The 3471\AA pulse was injected into the laser cavity by reflection from a sapphire flat coated to reflect S polarized 3471 radiation and transmit P polarized 2.7 micron radiation.

Two sets of laser tests were run. For the first set, the optical components shown in Figure 40 were used. Sapphire windows held at 91° to the laser axis were attached to the ends of the gain cell. Initially, sapphire windows AR coated with MgO were used, but the coating quickly degraded and optical losses became unacceptable. Sapphire windows held at Brewster's angle were also tried in an attempt to cut optical losses. However, this arrangement rejected about 50 percent of the doubled ruby radiation even though the polarization of this beam was oriented for optimum passage by the window. A germanium flat at Brewster's angle was placed between the cell and the totally reflecting mirror to reflect 3471\AA radiation from the optical train and prevent feedback to the RDA crystal with possible crystal damage. Radiation from a cw probe laser was used to align the optical components and measure individual losses. Values found were: 3471\AA reflector - 5 percent, gas cell - 24 percent, germanium flat - 16 percent, transmitting mirror - 8 percent. The optical components were further aligned for peak laser output by flowing a SF_6-H_2 mixture through the cell and by repetitively

17. Dolgov-Savel'ev, G. G., V. F. Zharov, Yu. S. Neganov, and G. M. Chumak, "Vibrational-Rotational Transitions in an H_2+F_2 Chemical Laser," JETP 34, 34, 1972.
18. Suchard, S. N., "Lasing From the Upper Vibrational Levels of a Flash-Initiated H_2-F_2 Laser," Appl. Phys. Lett., 23, 2, 15 July 1973.
19. Suchard, S. N., R. W. Gross and J. S. Whittier, "Time Resolved Spectroscopy of an Initiated H_2-F_2 Laser," Appl. Phys. Lett., 19, 411, 1971.

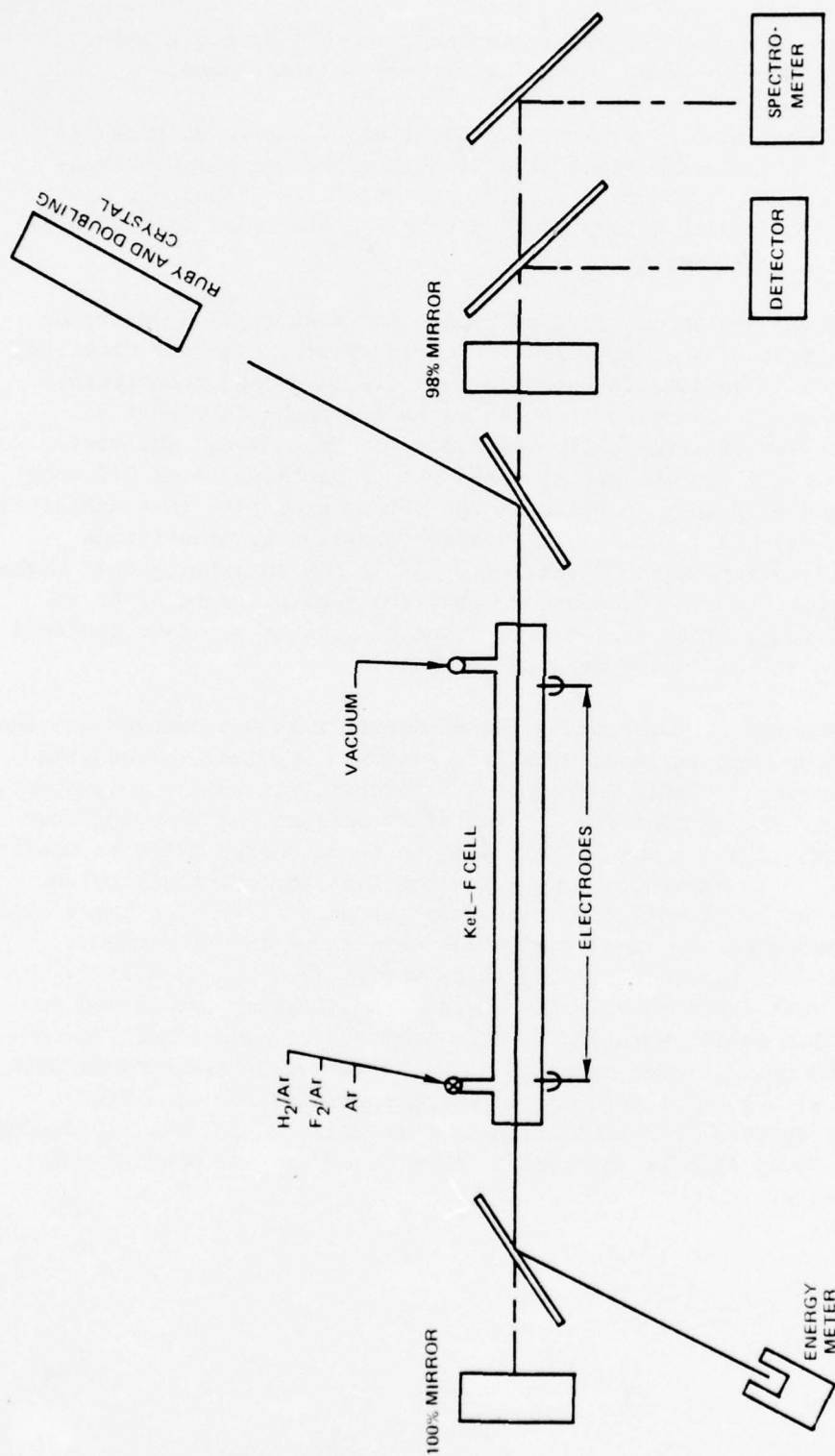


FIGURE 40 LASER EXPERIMENT

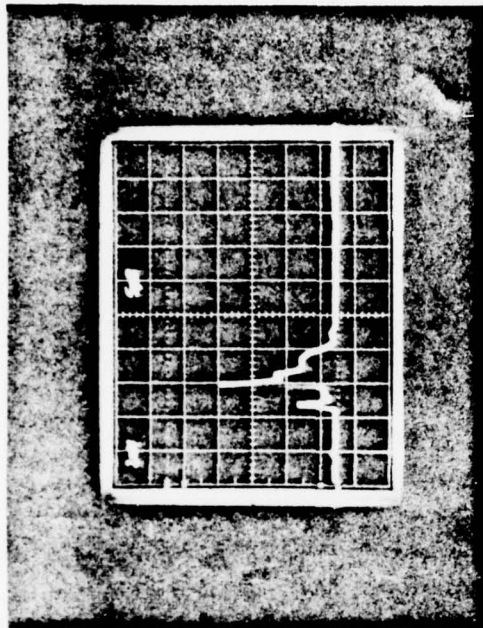
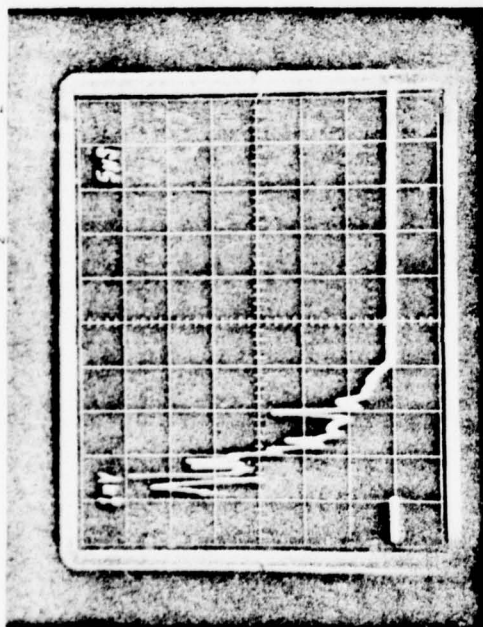
pulsing the mixture with an electrical discharge to achieve rapid laser pulsing. Two pins were inserted in the Kel-F tube as electrodes.

Measurements were made of relative intensities of the total pulse of HF laser radiation and of each spectral component using gas mixtures containing (a) 0.2 torr H_2 , 1.0 torr F_2 , 98.8 torr Ar; (b) 0.5 torr H_2 , 1.0 torr F_2 , 98.5 torr Ar;² (c) 1.0 torr H_2 , 0.5 torr F_2 , 98.5 torr Ar;² (d) 0.5 torr H_2 , 0.5 torr F_2 , 99 torr Ar.

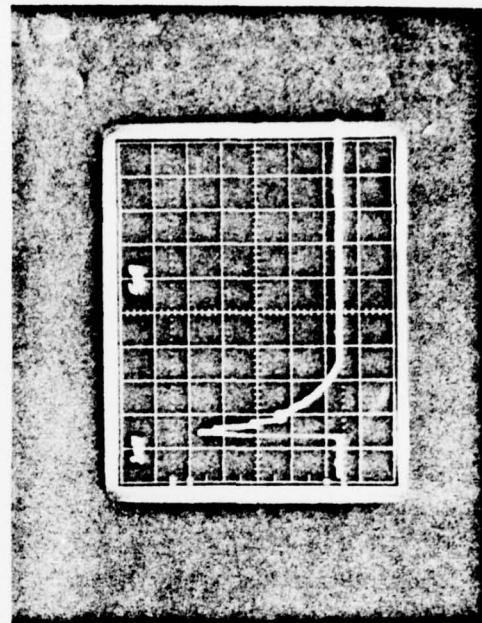
An InSb detector monitored the total pulse and a AuGe (77°K) detector was used at the output of a Jarrell Ash 1/2 meter spectrometer for measuring spectral components. The detector signals were displayed and photographed as oscilloscope traces. Examples of such traces are shown in Figure 41. Data for the first set of laser tests are listed in Table 8-A. The most energetic lasing at 2.5 microns was obtained with a gas mixture of 0.5 torr H_2 , 1.0 torr F_2 and 98.5 torr Ar which is the same composition that exhibited the largest gain (see Table 7). Lasing was not observed on transitions higher than $v(2-1)$ in any tests of this set. It is not surprising that higher transitions were not observed considering that for a gain length of 61 cm the gain for individual lines varied from about 60 percent per pass downward and optical losses in the cavity were 53 percent.

For the second set of laser tests the germanium flat was removed and the 90° sapphire windows were replaced with BaF windows. Optical losses with this configuration were: 3471Å reflector - 25 percent, gas cell - 13 percent, transmitting mirror - 8 percent for a total of 26 percent. A beam splitter diverted 10 percent of the input 3471Å radiation to an energy meter to monitor the dissociation. With removal of the germanium flat approximately twice the former amount of 3471Å radiation traverses the gain cell. The laser pulse energy at 2.5 microns was measured and values were found in the range of 0.001 to 0.002 J as the doubled ruby pulse varied from 0.2 to 0.25 J. Laser lines that were observed with the second configuration are listed in Table 8-B along with relative values for the strength of each line. In contrast to the first tests, laser oscillation was observed on transitions from $v(1-0)$ to $v(5-4)$ with a major part of the energy accounted for by a few $v(1-0)$ lines. It appears from these results that additional lines, including those of $v(6-5)$, would also be observed if more energy in the doubled ruby pulse were available.

H₂ (0.5 TORR) F₂ (1.0 TORR) Ar (100 TORR) PULSE ENERGY 0.14 JOULES

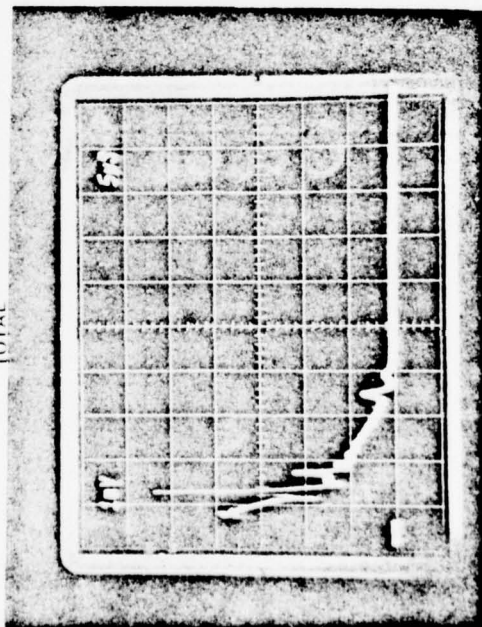


1P4



2P4

TOTAL



TOTAL

FIGURE 41 PULSED LASER OUTPUT

TABLE 8. PULSED LASER TEST DATA

A. Tests with Germanium Mirror

<u>Code</u>	<u>Pulse Energy</u>	<u>Line</u>	<u>Observed</u>	<u>Relative Signal Strength</u>
Laser Run #1 Mix .5 torr H ₂ , 1.0 torr F ₂ , 98.5 torr Ar				
AA	.071	1P ⁴	*	1.9
BB	?	1P ₃	*	6.4
CC	.075	1P ₂		
DD	.070	1P ₅		
EE	.077	1P ₆		
FF1	.068	2P ₃	*	5.0
FF2	.075	2P ₃	*	6.5
GG	.075	2P ₄	*	3.0
HH	.075	2P ₅		
II	.068	2P ₆		
JJ	.080	2P ₇		
KK	.075	2P ₂		
Laser Run #2 Mix 1.0 torr H ₂ , .5 torr F ₂ , 98.5 torr Ar				
AA1	.07	1P ₃		
BB1	.079	1P ⁴		
CC1	.076	2P ₃	*	1.5
DD1	.080	2P ₄		
EE1	.076	1P ₃	*	.9
Laser Run #3 Mix .5 torr H ₂ , .5 torr F ₂ , 99 torr Ar				
AA2	.083	1P ₃	*	.5
BB2	.077	2P ₃	*	.45
CC2	.079	1P ⁴		
DD2	.076	2P ₄		

TABLE 8. PULSED LASER TEST DATA (CONT'D)

<u>Code</u>	<u>Pulse Energy</u>	<u>Line</u>	<u>Observed</u>	<u>Relative Signal Strength</u>
Laser Run #4 Mix .2 torr H ₂ , 1.0 torr F ₂ , 98.8 torr Ar				
AA3	.075	1P3	*	2.0
BB3	.077	1P2		
CC3	.086	1P4	*	1.75
DD3	.075	1P5		
EE3	.074	2P3	*	6.5
FF3	.075	2P4	*	1.25
GG3	.077	2P5		
HH3	.075	1P2		
AA4	.072	3-2 P4		
BB4	.079	3-2 P3		
CC4	.082	3-2 P5		
DD4	.078	3-2 P8		
EE4	.074	4-3 P4		
FF4	.074	4-3 P6		
Laser Run #5 Mix .5 torr H ₂ , 1 torr F ₂ , 98.5 torr Ar				
LA1	.07	1P4	*	.50
LA2	.065	1P5 3-2		
LA3	.068	P4(3-2)		
LA4	.062	P3(3-2)		
LA5	.068	P3(4-3)		
LA6	.065	P4(4-3)		
LA7	.065	P5(4-3)		
LA8	.068	2P3		

TABLE 8. PULSED LASER TEST DATA (CONT'D)

<u>Code</u>	<u>Pulse Energy</u>	<u>Line</u>	<u>Observed</u>	<u>Relative Signal Strength</u>
LA9	.069	P3(2-1)		
LA10	.065	P3(2-1)	*	.75
LA11	.067	P3(2-1)		
LA12	.07	P4(2-1)	*	.65
LA13	.068	P5(2-1)		
LA14	.065	P5(2-1)	*	.52
LA15	.068	P6(2-1)		
LA16	.065	P7(2-1)		
LA17	.063	P3(1-0)		
LA18	.06	P4(1-0)		
LA19	.06	P4(2-1)	*	.35
LA20	.06	P4(1-0)	*	.82
LA21	.06	P4(1-0)	*	1.5
LA22	.06	P5(1-0)		

B. Tests without Germanium Mirror

Gas Mixture 0.5 torr H₂, 1.0 torr F₂, 98.5 torr Ar

<u>Code</u>	<u>Pulse Energy (Joules)</u>	<u>Line</u>	<u>Signal Strength</u>
		v(1-0)	
A1	0.19	P3	400
A2	0.20	P4	500
A3	0.18	P5	
A4	0.15	P6	20

TABLE 8. PULSED LASER TEST DATA (CONT'D)

<u>Code</u>	<u>Pulse Energy (Joules)</u>	<u>Line</u>	<u>Signal Strength</u>
A5	0.18	P7	40
A6	0.20	P8	2
A7	0.21	P9	1
v(2-1)			
B1	0.20	P4	1.0
B2	0.24	P5	0.7
B3	0.20	P6	2.0
B4	0.20	P7	1.5
v(3-2)			
C1	0.19	P5	0.5
C2	0.18	P6	0.3
C3	0.22	P7	---
v(4-3)			
D1	0.22	P2	0.05
D2	0.27	P3	0.1
D3	0.24	P4	0.05
D4	0.18	P5	---
v(5-4)			
E1	0.29	P2	0.02
E2	0.20	P3	---
E3	0.22	P4	---
E4	0.20	P5	---

TABLE 8. PULSED LASER TEST DATA (CONT'D)

<u>Code</u>	<u>Pulse Energy (Joules)</u>	<u>Line</u>	<u>Signal Strength</u>
		v(6-5)	
F1	0.20	P2	---
F2	0.18	P3	---
F3	0.20	P4	---
F4	0.22	P5	---
F5	0.19	P6	---

SECTION IV. DATA ANALYSIS

As data from the flow tube and pulsed-fluorescence experiments became available, an ongoing analysis effort was performed. The purpose was to obtain the best self-consistent set of kinetic rate coefficients that would fit the results from both experiments. Such a rate package would then have application in predicting and optimizing the performance of chain-reaction (and also cold-reaction) HF chemical lasers. The results of this analysis are given below.

Chemical Reactions

At the start of this contractual effort an extensive parameter study was performed to identify the major problem areas related to predicting performance of HF chain reaction lasers. It was concluded that among the possible reaction mechanisms, the key uncertainties were in the forward rates of the pumping reactions ($F + H_2 \rightarrow HF^* + H$, $H + F_2 \rightarrow HF^* + F$). Also of possible importance were wall interactions (at least in the envisioned experiments) and the back cold reaction ($HF(v \geq 3) + H \rightarrow H_2 + F$). Other reaction mechanisms - recombination, chain branching, hot atom effects - were found to be of secondary importance. Furthermore, such effects could not be easily identified in the available experiments.

The findings from the experiments have not contradicted the preliminary conclusions. While it is possible that hot atom effects might influence the pulsed-fluorescence experiments, it appears that the basic hot and cold reaction mechanism is predominant. Some weak evidence of influence from the back cold reaction is present, however, and (for these experiments at least) it seems the influence of the test cell walls cannot be completely ignored.

Flow Tube

Analysis of the flow tube data was first aimed at the evaluation of the hot reaction rate coefficient, which it was thought might be slower than previously reported (see Appendix A for a description of the initial rate package). Four test conditions were considered with varying proportions of F_2 and H_2 (see Table 9). The corresponding HF production is shown in Figure 42.

In the H_2 rich cases the rate determining step is the hot reaction. Thus analytic predictions of the production of HF for such cases will be most sensitive to the value used for the hot-reaction rate coefficient. If one assumes

TABLE 9. INITIAL CONDITIONS

Flow Tube Simulation

Velocity = 10000 cm/sec

Pressure = 20 Torr

Species Concentrations:

<u>Case</u>	<u>X_F</u>	<u>X_{F₂}</u>	<u>X_{H₂}</u>	<u>X_{Ar}</u>
1	0.0001	0.00435	0.00055	0.995
2	0.0001	0.00245	0.000775	0.99675
3	0.0001	0.00095	0.00155	0.9974
4	0.0001	0.00025	0.00310	0.99655
5	0.0001	0.00172	0.00088	0.99731
6	0.00026	0.00059	0.00088	0.99827

FLOW TUBE EXPERIMENT

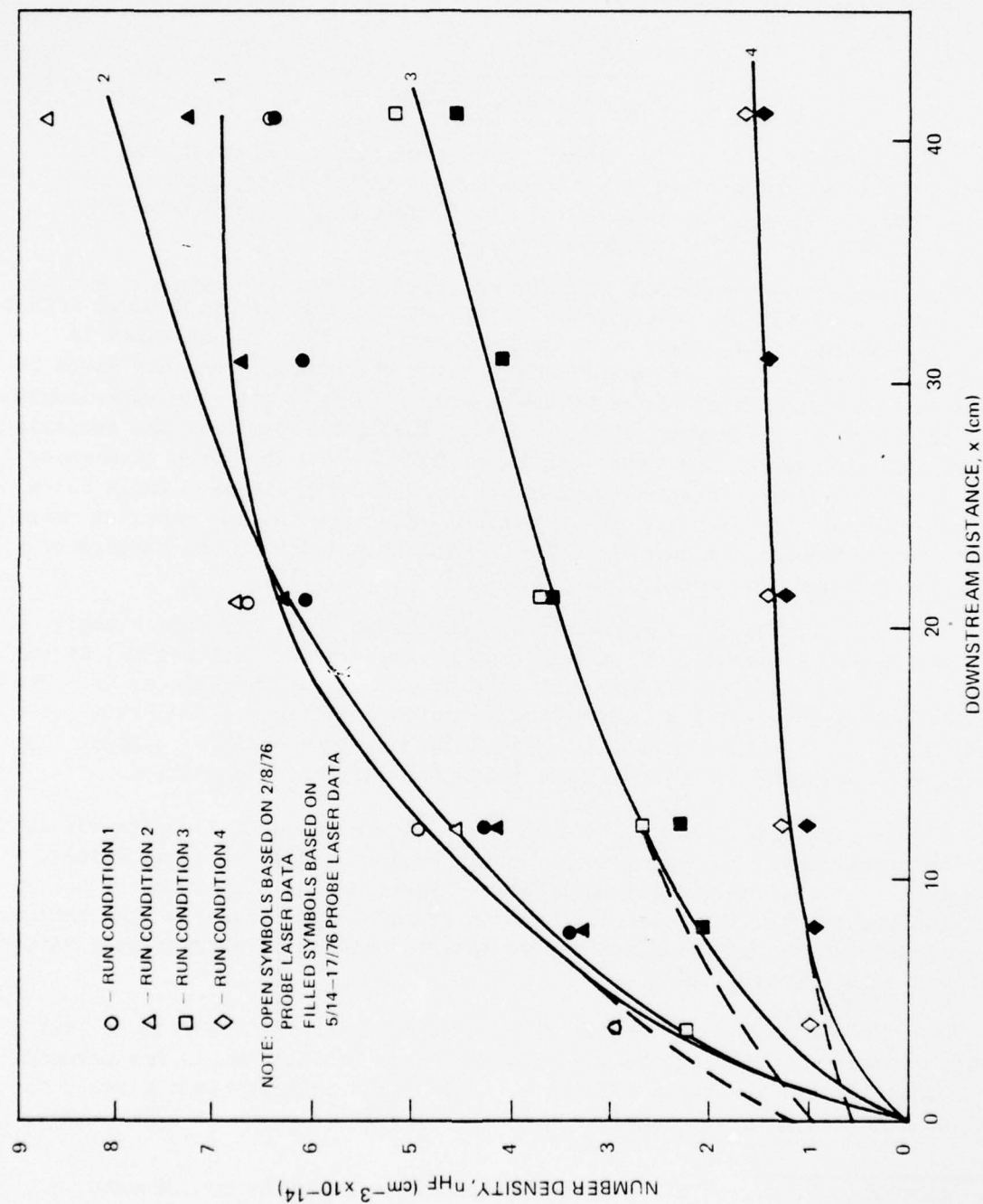


FIGURE 42 VARIATION OF TOTAL HF

that wall interactions and the back cold reaction are unimportant, a preliminary value for the hot reaction rate coefficient can be obtained by measuring dn_{HF}/dt for the H_2 rich cases (3 and 4) and using the formula (see Appendix B).

$$k_h = \frac{k_c \frac{dn_{HF}}{dt} \frac{n_{H_2}}{n_{F_2}}}{2(n_F)_0 k_c n_{H_2} - \frac{dn_{HF}}{dt}} \quad (1)$$

This is a direct result of the steady state approximation. Using such an approach, the value for the hot reaction rate coefficient is found to be approximately one half the commonly accepted value of Albright (Ref. 20) et. al. (i.e., 1.8×10^{-12} cc/molecule-sec).

The quasi-one-dimensional computer code CHEMLZ was then used to test the validity of such a rate. To account for two dimensional boundary layer effects a correction factor is employed in the calculation. This is described in detail in Appendix C. Initial conditions for the calculations are given in Table 9. A comparison of the model calculations (Fit F) with the experimental results are shown in Figures 43 through 46. It can be seen that the comparison is reasonable for the H_2 rich cases (Conditions 3 and 4), but for the F_2 rich cases (Conditions 1 and 2), the predicted increase of HF with distance falls below the experimental curves. Use of the nominal value for the hot reaction rate coefficient improves the agreement for Conditions 1 and 2 at the expense of the good agreement for Conditions 3 and 4.

Note that in all cases the experimental curves start off more steeply than the model. In drawing the curves through the experimental points, it was assumed that at the start of the flow tube (i.e., $X = 0$) there is no HF. The flow in the vicinity of $X = 0$, however, is quite complicated; recirculation zones might exist. In such a case it would be more appropriate to model the experiments assuming a finite initial value for the HF concentration.

If the constraint that $n_{HF} = 0$ at $X = 0$ were relaxed it is quite reasonable to extrapolate the experimental curves back to nonzero initial values. This is illustrated by the dashed lines on Figure 42. A comparison of these modified curves with the model is shown in Figures 47 through 50. The initial concentrations for the calculations are taken equal to the extrapolated values from the experimental curves.

Now the slopes and magnitudes of the experimental and theoretical (Fit F) curves compare considerably better than when zero initial values are assumed. The poorest fit is for run condition 4. This might indicate that a value for the hot reaction rate even smaller than $1/2$ Albright's value is appropriate.

20. Albright, R. G., et al. "Mass-Spectrometric Determination of Rate Constants for H-Atom Reactions with Cl_2 and F_2 ." J. Chem. Phys., **50**, 3632, 1969.

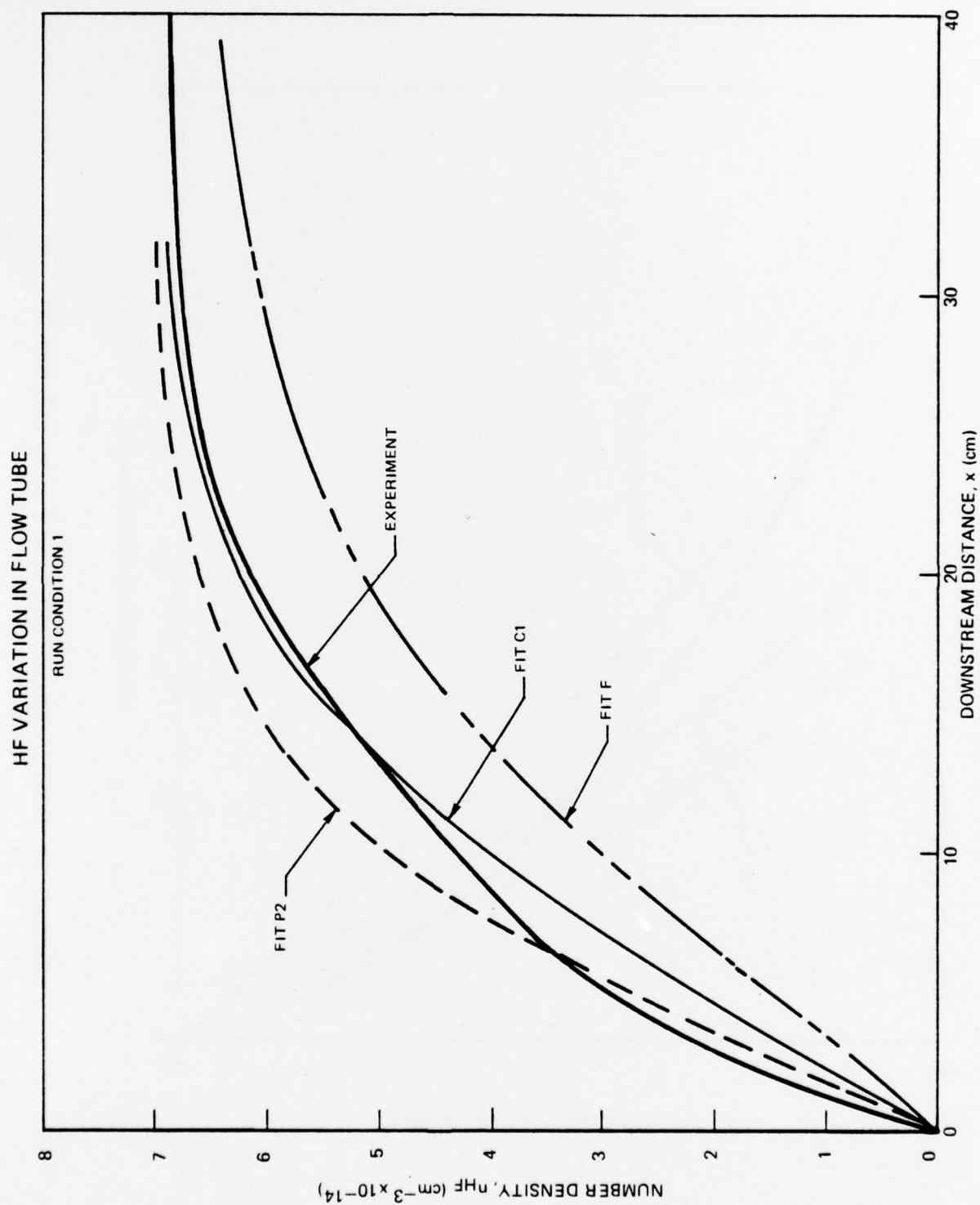


FIGURE 43 COMPARISON BETWEEN MODEL AND EXPERIMENT

HF VARIATION FLOW TUBE
RUN CONDITION 2

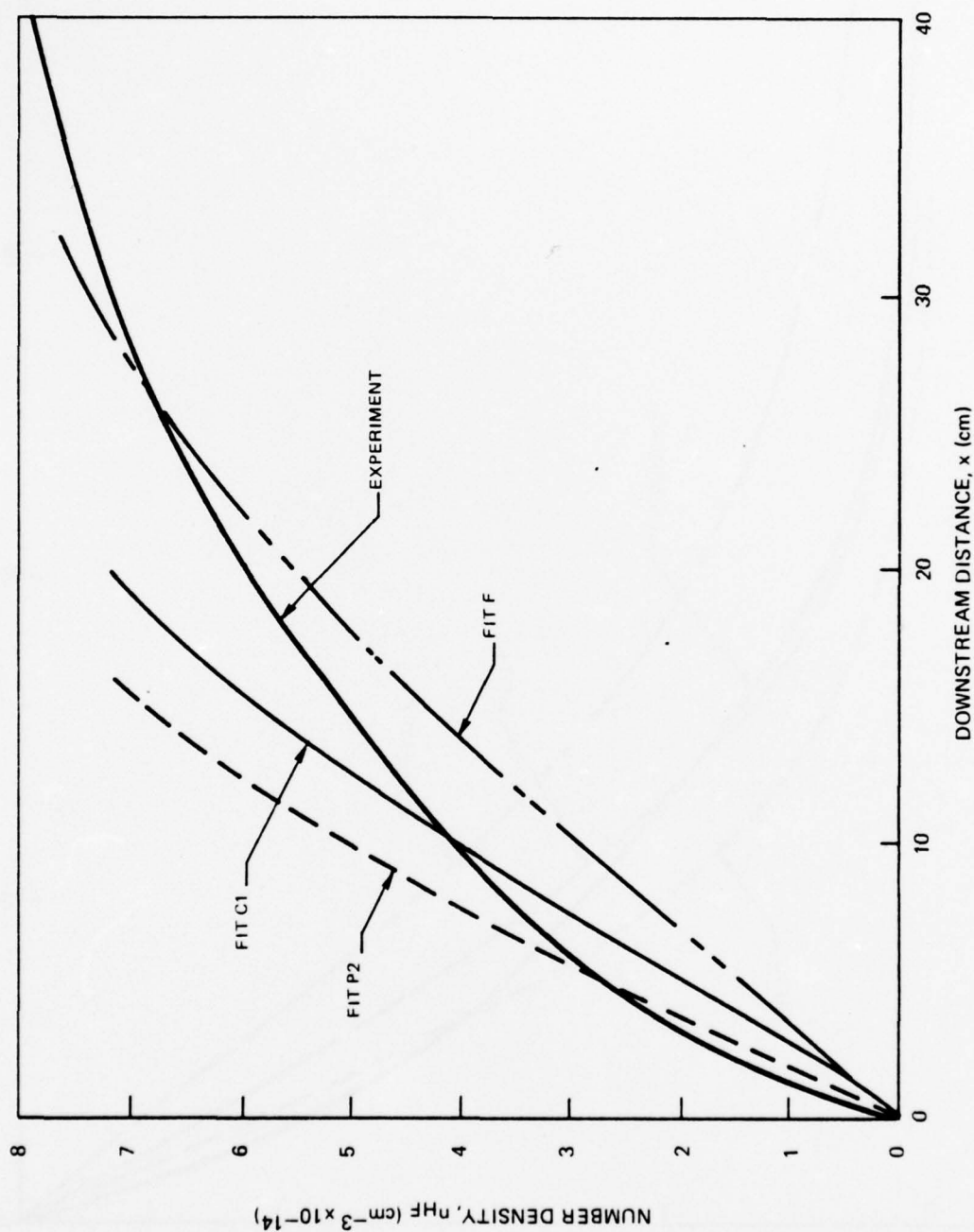


FIGURE 44 COMPARISON BETWEEN MODEL AND EXPERIMENT

HF VARIATION IN FLOW TUBE

RUN CONDITION 3

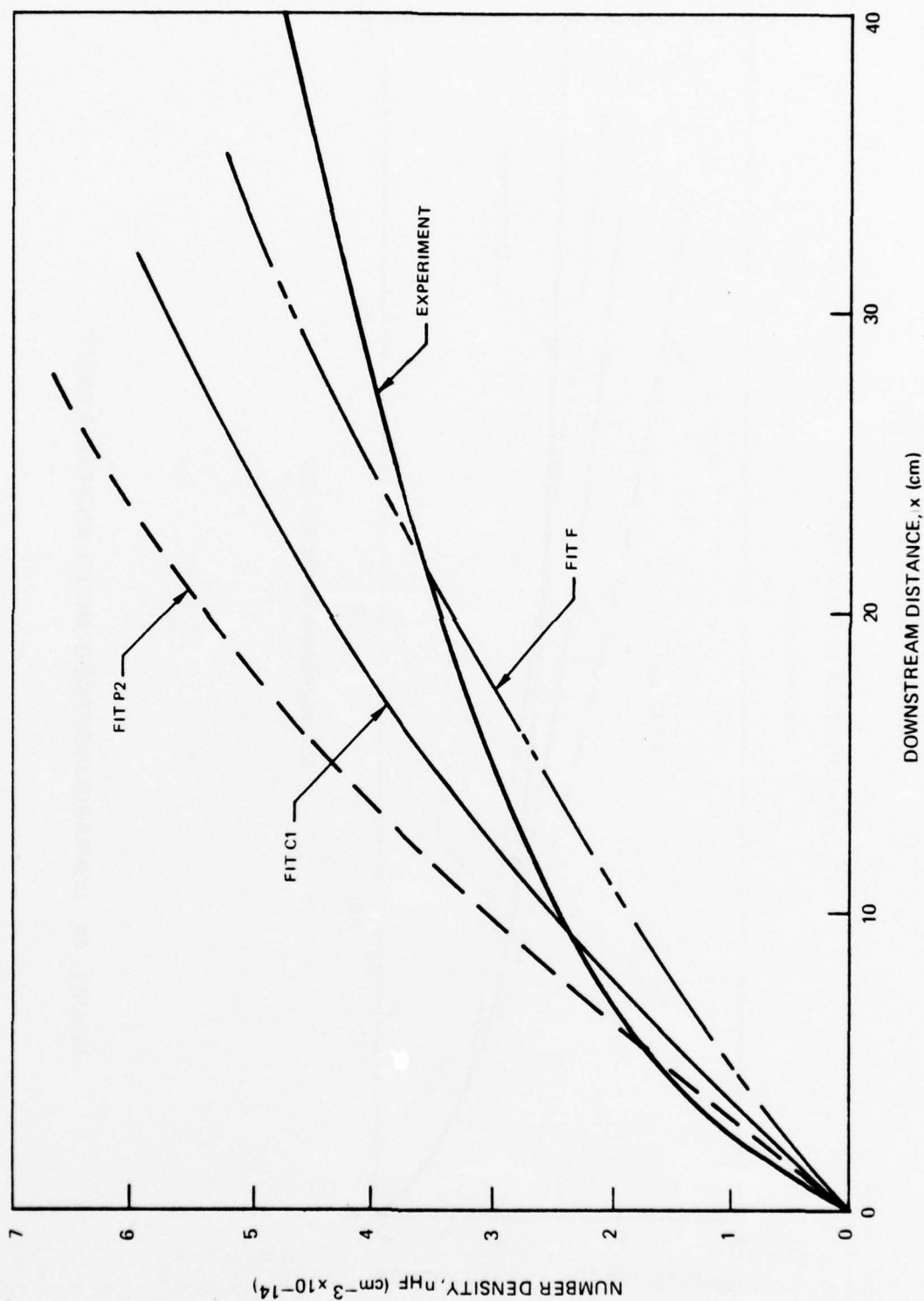


FIGURE 45 COMPARISON BETWEEN MODEL AND EXPERIMENT

HF VARIATION IN FLOW TUBE

RUN CONDITION 4

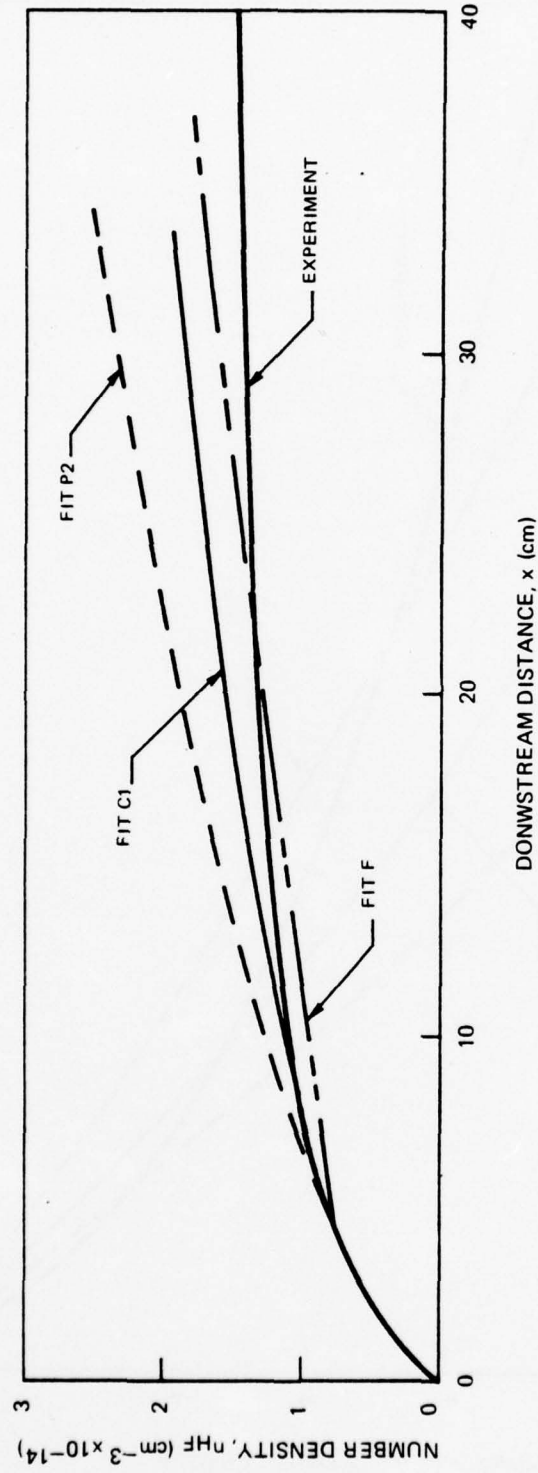


FIGURE 46 COMPARISON BETWEEN MODEL AND EXPERIMENT

HF VARIATION IN FLOW TUBE
RUN CONDITION 1A

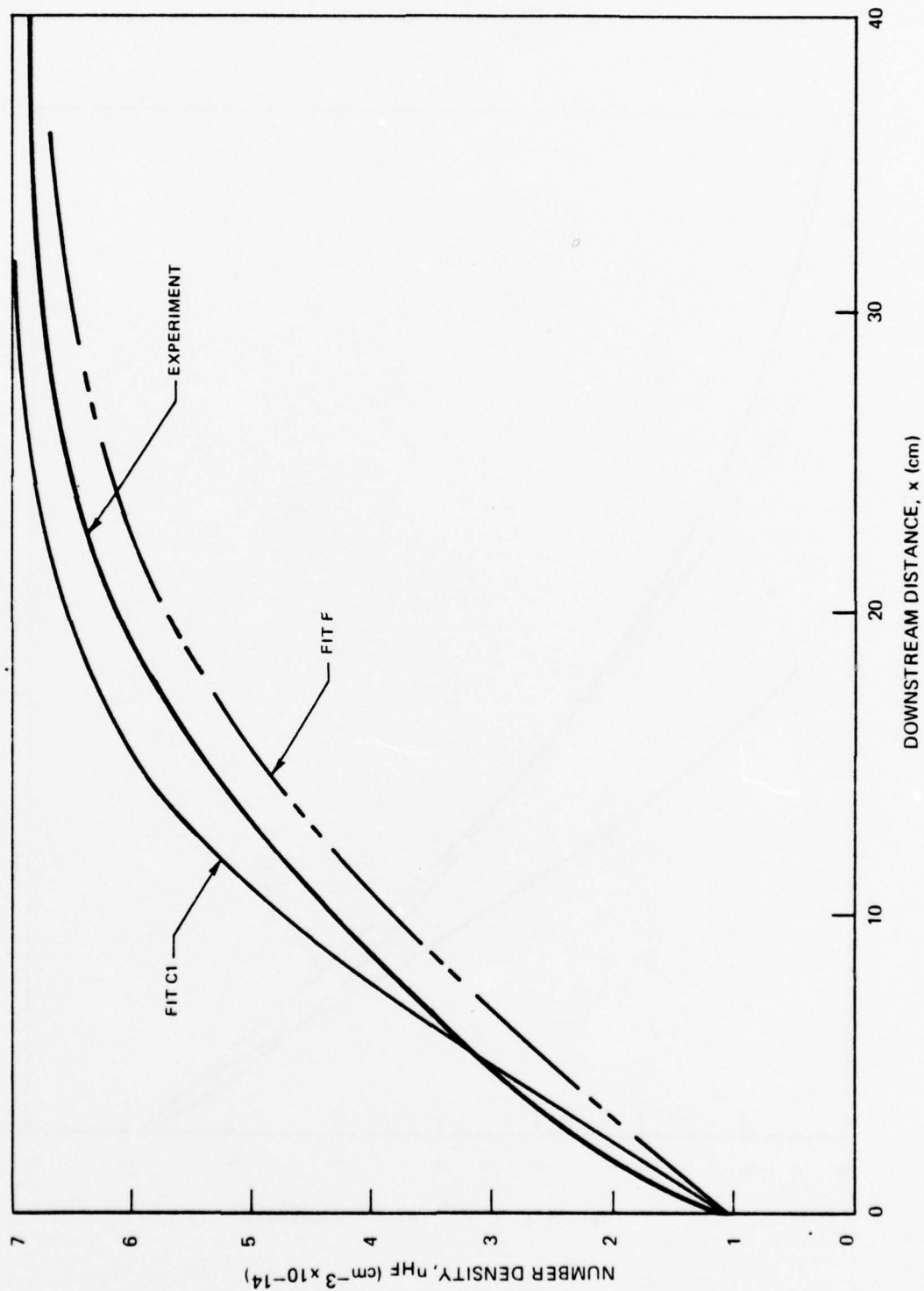


FIGURE 47 COMPARISON BETWEEN MODEL AND EXPERIMENT

HF VARIATION IN FLOW TUBE

RUN CONDITION 2A

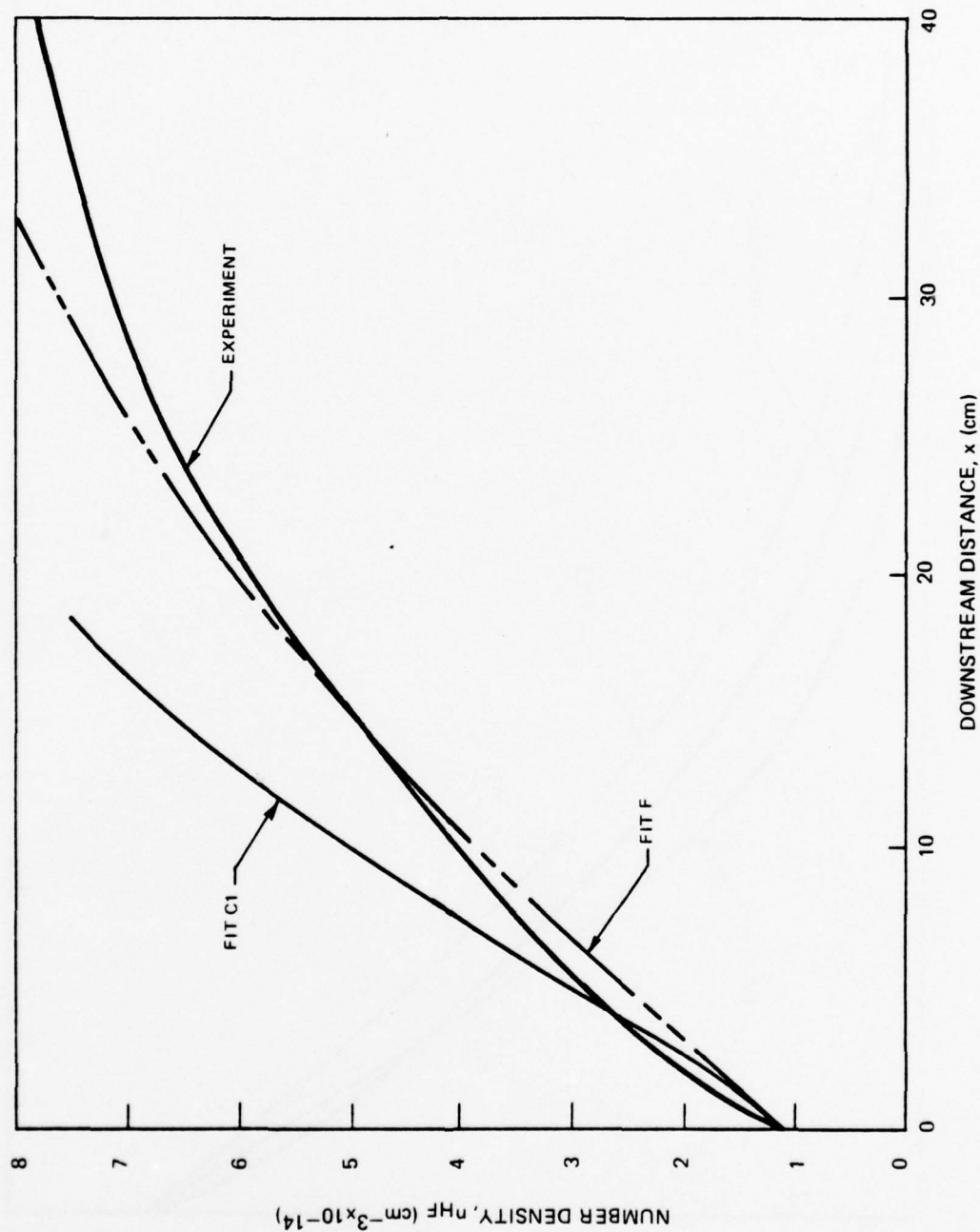


FIGURE 48 COMPARISON BETWEEN MODEL AND EXPERIMENT

HF VARIATION IN FLOW TUBE RUN CONDITION 3A

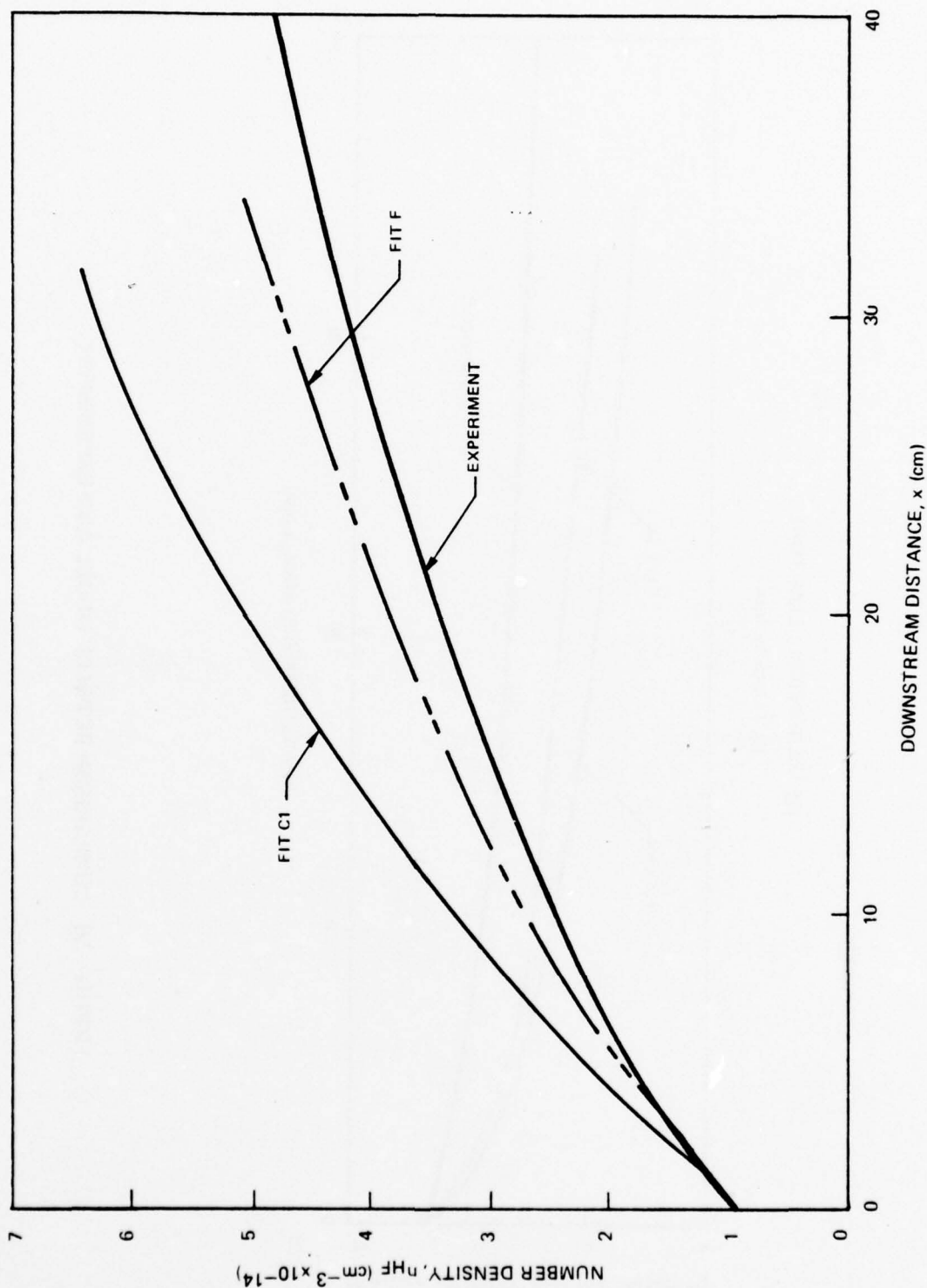


FIGURE 49 COMPARISON BETWEEN MODEL AND EXPERIMENT

HF VARIATION FLOW TUBE
RUN CONDITION 4A

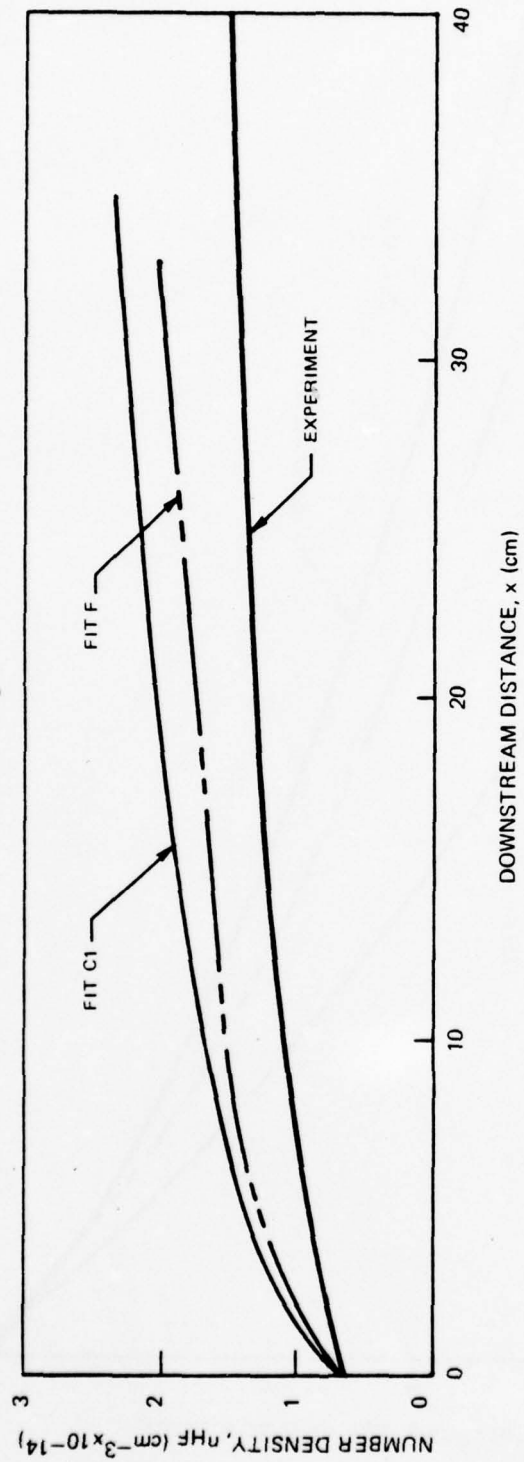


FIGURE 50 COMPARISON BETWEEN MODEL AND EXPERIMENT

On the other hand a better match might also be achieved if the true initial HF concentration were smaller than assumed. While it appears plausible from the above result that some HF is present initially, in the absence of any measurements at $X = 0$ it cannot be conclusively proven.

An alternative explanation to the experimental results might be that the steep initial slopes do indeed represent faster rates for the hot and/or cold reactions, and the shallower slopes later on result from wall interactions (in particular the loss of H or F atoms). Support for such an approach is provided by the pulsed-fluorescence experiments, which indicated faster rate coefficients for both the hot and cold reactions. (This will be described in more detail below.)

The rates that apparently fit the pulsed experiments best are:

$$k_c = 2.0 \times \text{nominal}$$

$$k_h = 1.3 \times \text{nominal}$$

These rates were used in a flow tube calculation in which it was further assumed that all H atoms colliding with the wall were lost (to later recombine to form H_2). This H-atom loss was accounted for approximately, based upon estimates arising from an analysis described in Appendix D. The loss of H atoms was expressed as

$$[\dot{H}]_{\text{walls}} = -[H] e^{-\beta t} \quad (2)$$

with $\beta = 156$. This value was obtained from a fit of the curve in Figure D1. over the time scale of the experiment.

A comparison of this set of rates (Fit P2) is also shown in Figures 43 through 46. As can be seen, even with the inclusion of potential H-atom loss such a set of rates overpredicts the HF population for Conditions 2 through 4 in all but the initial portions of the flow tube.

The final comparison made is for a fit intended to give good general agreement in both experiments. The rates employed for the hot and cold reactions are

$$k_c = 1.5 \times \text{nominal}$$

$$k_h = 0.9 \times \text{nominal}$$

Again the loss of H-atoms to the walls was assumed.* The results of the comparison are shown in Figures 43 through 46 as fit C1. We see that such a fit matches the data reasonably well although the slope of the curves is a bit too shallow at first and too steep later on. Use of such rates in a comparison assuming finite initial HF concentrations is shown in Figures 47 through 50. The fit is a bit poorer and tends in all cases to overestimate the HF populations.

Pulsed-Fluorescence

These experiments were run for six different sets of conditions, which are outlined in Table 10. The time history of the production of HF is available from oscilloscope traces of the absorption of a ($v=1$) \rightarrow ($v=0$) cw laser beam.** Attempts to fit the data using the nominal (Homann) value (Ref. 21) for the cold reaction rate coefficient and half the nominal value (Ref. 20, Albright) for the hot reaction rate coefficient as had been done for the flow tube met with no success. The predicted temporal development of HF fell below the measured values in virtually all cases. The general indication was that faster hot and cold reaction rate coefficients would be required to fit the majority of the data.

In an attempt to facilitate the analysis of the data from each test series, composite plots were made up employing a time normalized to the pulse energy (i.e., $\hat{t} = t \times E_p$). The rationale behind this is that for a quasi-steady-state situation in the absence of any loss mechanisms all the cases would fall along the same curve.

Consider the equation

$$\frac{dn_{HF}}{dt} = \frac{2n_{F_0} k_c k_h n_{F_2} n_{H_2}}{k_c n_{H_2} + k_h n_{F_2}} \quad (3)$$

and also

$$n_{F_0} = CE_p \quad (4)$$

* This had an effect ranging from 0 to 25 percent

** For the conditions of these tests the contribution from upper levels to the total HF population rapidly becomes negligible.

21. Homann, K. H., et al., "Eine Methode Zur Enzengang von Fluorstonier in Inerten Atmosphäre," Ber. Bunse. F. Phys. Chem., 74, 585, 1970.

TABLE 10. INITIAL CONDITIONS

Pulsed Fluorescence Simulation

Pressure = 100 Torr

Species Concentrations:

<u>Species</u>	<u>X_{F₂}</u>	<u>X_{H₂}</u>	<u>X_{Ar}</u>
A	.0094	.0102	.9804
B	.0102	.0222	.9676
C	.0099	.0055	.9846
D	.0049	.0055	.9896
E	.0049	.0102	.9849
F	.0101	.0024	.9875

Thus we may write

$$\frac{dn_{HF}}{dt} = \frac{2C k_c k_h n_{F_2} n_{H_2}}{k_c n_{H_2} + k_h n_{F_2}} \quad (5)$$

Here the right hand side is not explicitly dependent on pulse energy. The presence of heat transfer effects, which will be different for different pulse energies, and of wall interaction effects will cause some deviation in the curves from case to case. However, it is not unreasonable to expect all the results from a given series to start off with essentially the same slopes, with the higher energy cases being perhaps slightly steeper.

The resulting composite plots are shown in Figures 51 through 56. The results for series A, B, and C show relatively little scatter near $t = 0$, although it is difficult to find any correlation between initial slope and the pulse energy. Series D also gives relatively consistent results with the possible exception of DH5 and DH8. On the other hand, the series E and F results show considerable scatter. As a consequence, the results from series A, B, and C have been weighted most heavily and those of E and F least heavily in attempting to find a good overall fit to the data.

A complication that renders data interpretation difficult for the pulsed fluorescence experiments is the apparent adsorption of HF on the test cell walls. It is possible to observe the fall off of HF number density in the latter stages of many tests. Also, the maximum number density produced in any given test tends to fall below the expected maximum based on the initial concentrations of H_2 and F_2 . Furthermore, there is a correlation between the pulse energy of a given test and the maximum HF produced (Figures 57 through 62). It can be seen that higher pulse energies (corresponding to high initial F-atom concentrations and faster reactions) result in high HF concentrations. Such a behavior would occur if there were competition between the walls and the chemical reactions. Finally, an analysis to estimate the worst possible loss of HF to the walls (Appendix D) shows that the amounts that might be lost to the walls are not unreasonable. As a result of these considerations a simple model including the loss of HF to the wall was used to first try to fit some of the experimental data. It was assumed that the adsorption of HF on the walls was proportional to the room available on the walls, $(1 - \frac{n_{HF}|_W}{n_{HF}|_{MAX}})$, where $n_{HF}|_W$ is the equivalent number density of HF already on the walls and $n_{HF}|_{MAX}$ is the maximum allowed. The adsorption is also taken to be proportional to the HF available in the gas phase $n_{HF}|_g$ (Ref. 22). Thus we have

22. Moore, W. J., Physical Chemistry, Prentice-Hall, Englewood Cliffs, NJ, 1955.

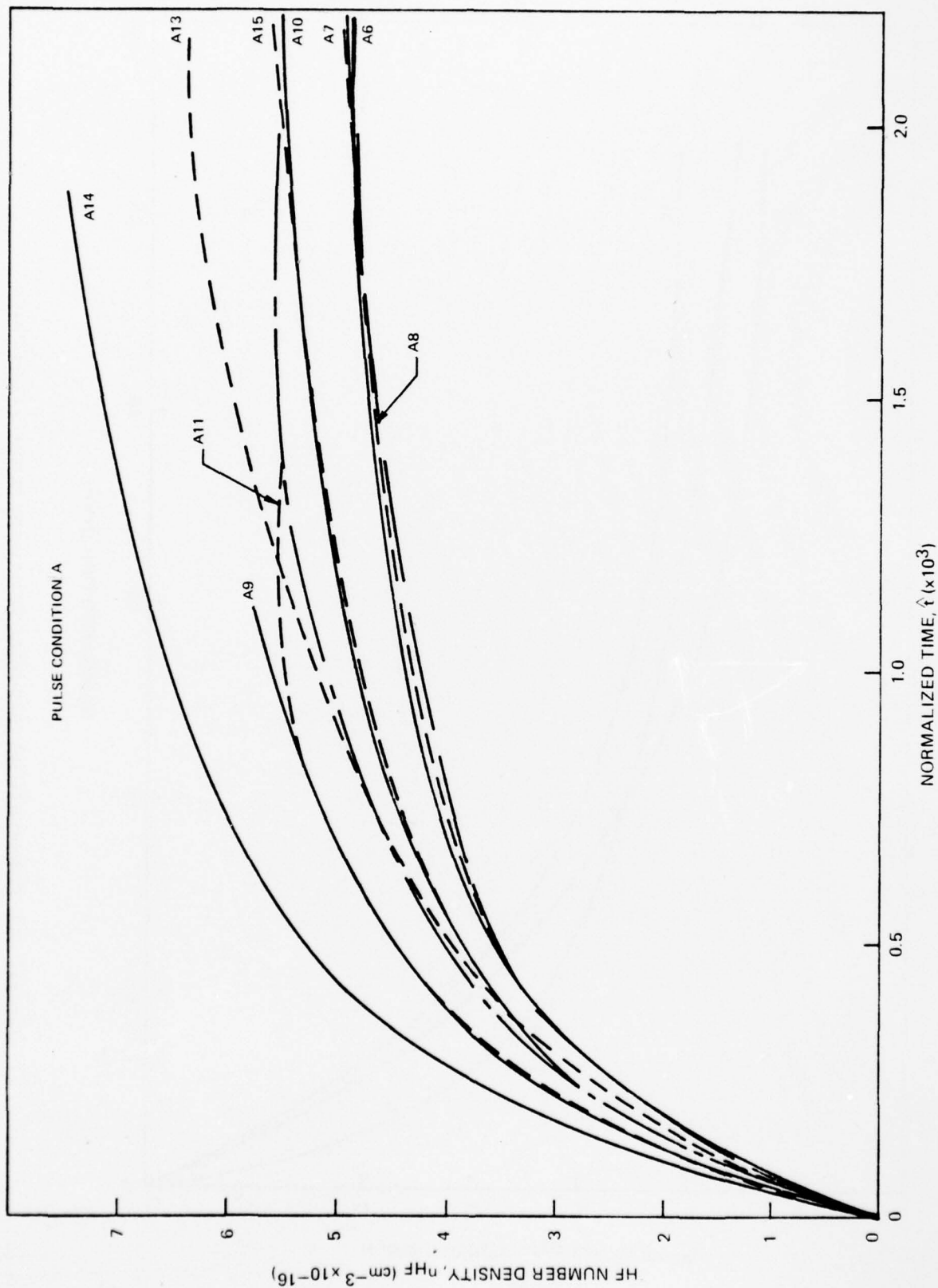


FIGURE 51 COMPOSITE HF TEMPORAL BEHAVIOR NORMALIZED TIME

PULSE CONDITION B

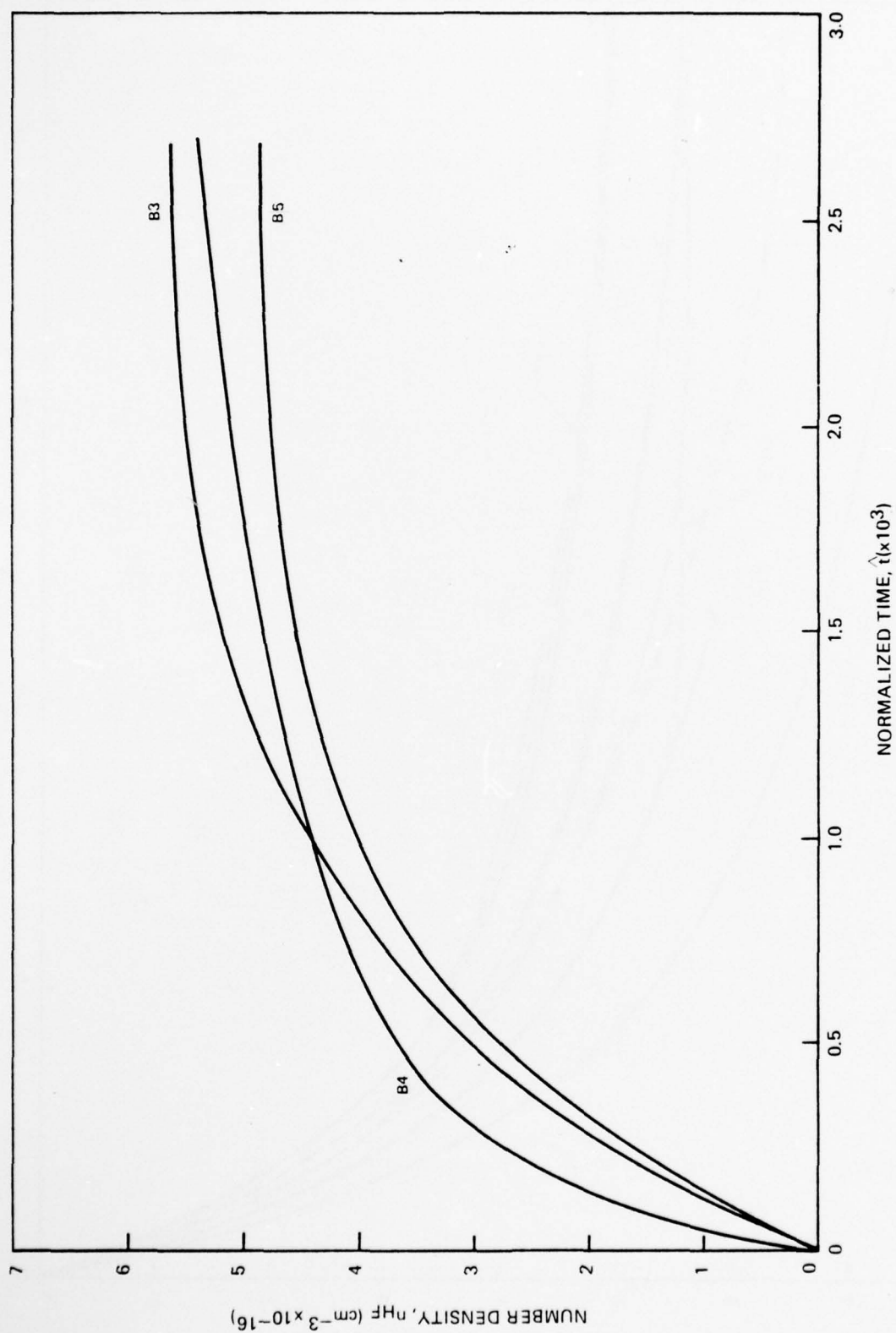


FIGURE 52 COMPOSITE HF TEMPORAL BEHAVIOR NORMALIZED TIME

PULSE CONDITION C

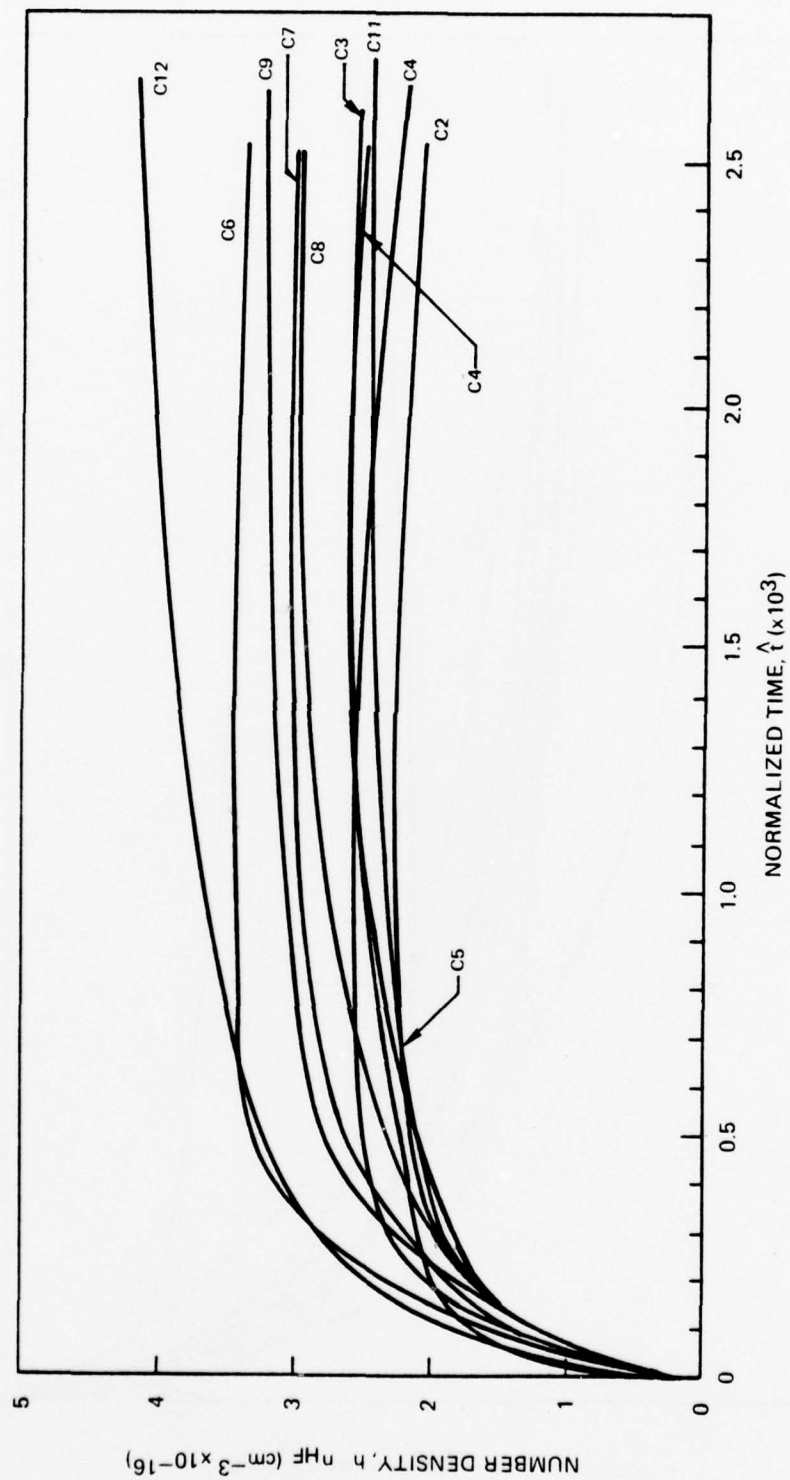


FIGURE 53 COMPOSITE HF TEMPORAL BEHAVIOR

NORMALIZED TIME
PULSE CONDITION D

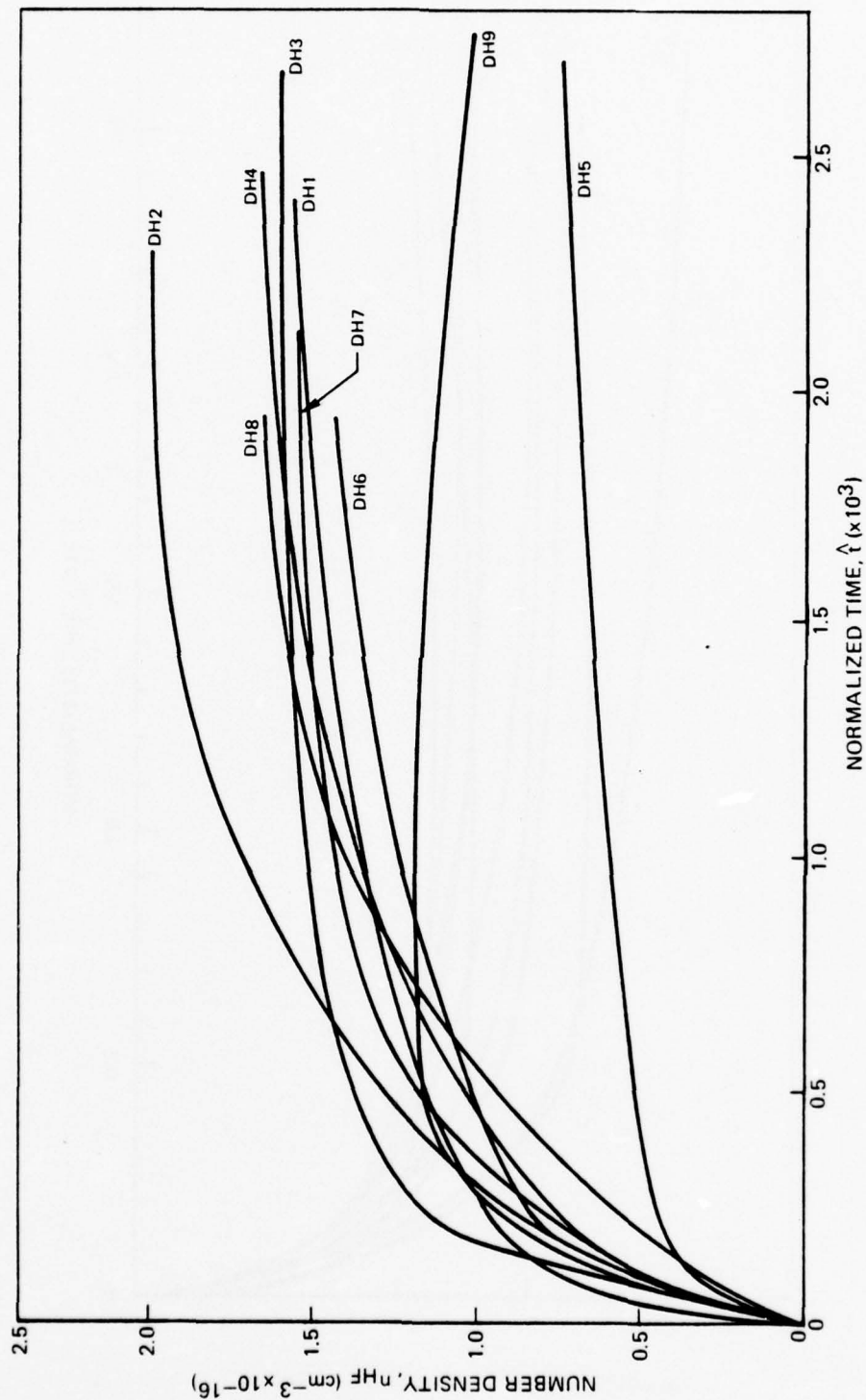


FIGURE 54 COMPOSITE HF TEMPORAL BEHAVIOR

PULSE CONDITION E

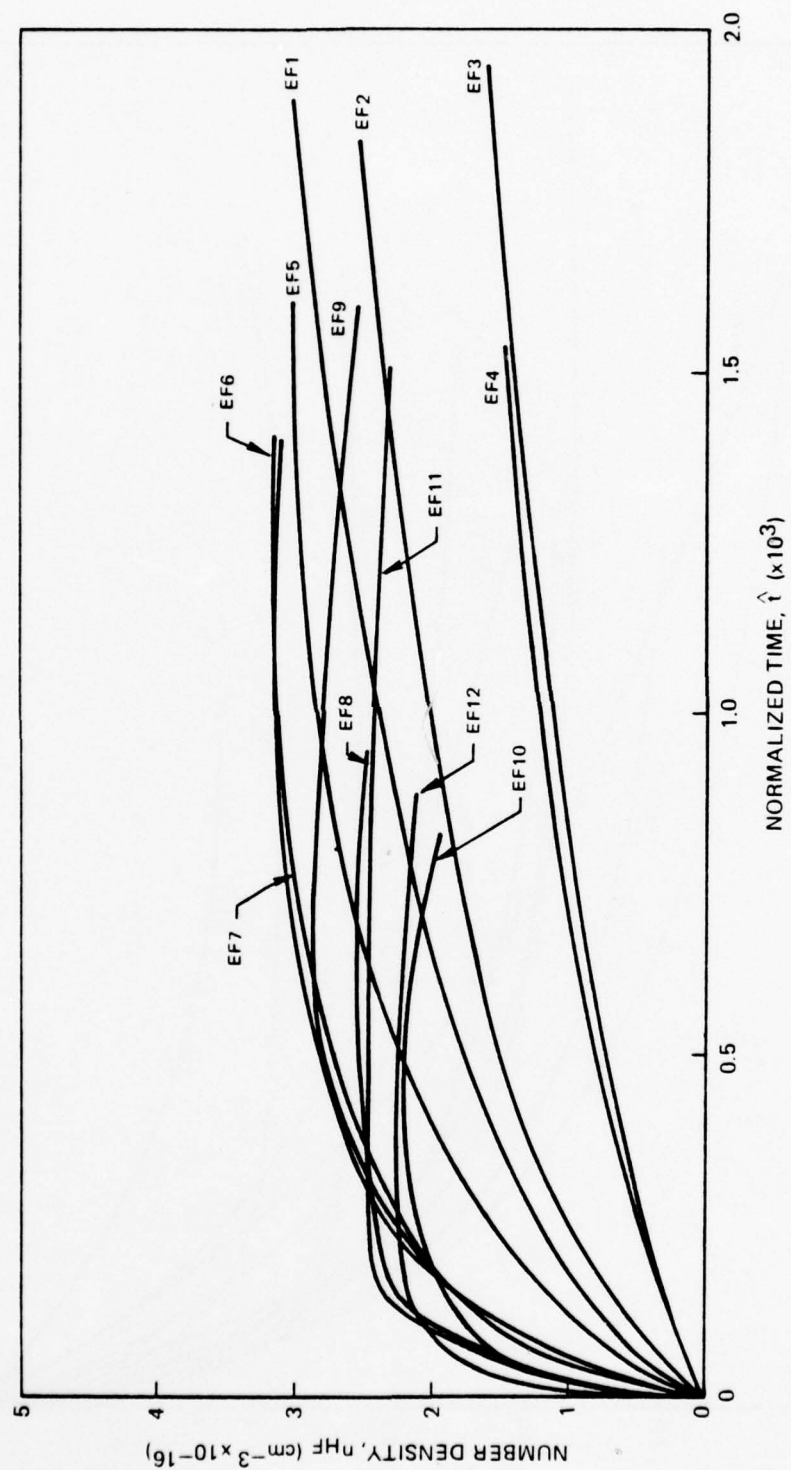


FIGURE 55 COMPOSITE HF TEMPORAL BEHAVIOR
NORMALIZED TIME

PULSE CONDITION F

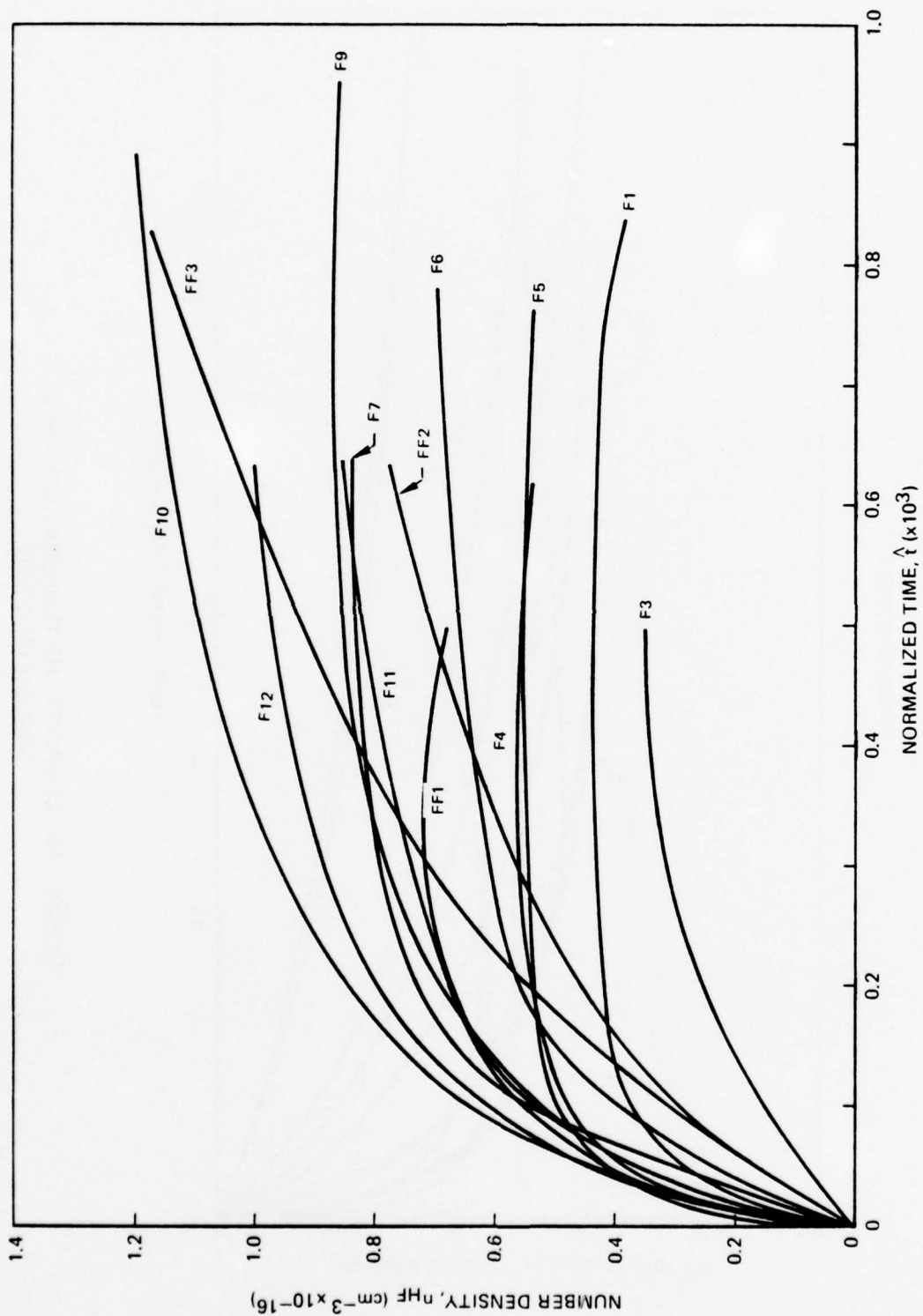


FIGURE 56 COMPOSITE HF TEMPORAL BEHAVIOR
NORMALIZED TIME

TEST SERIES A

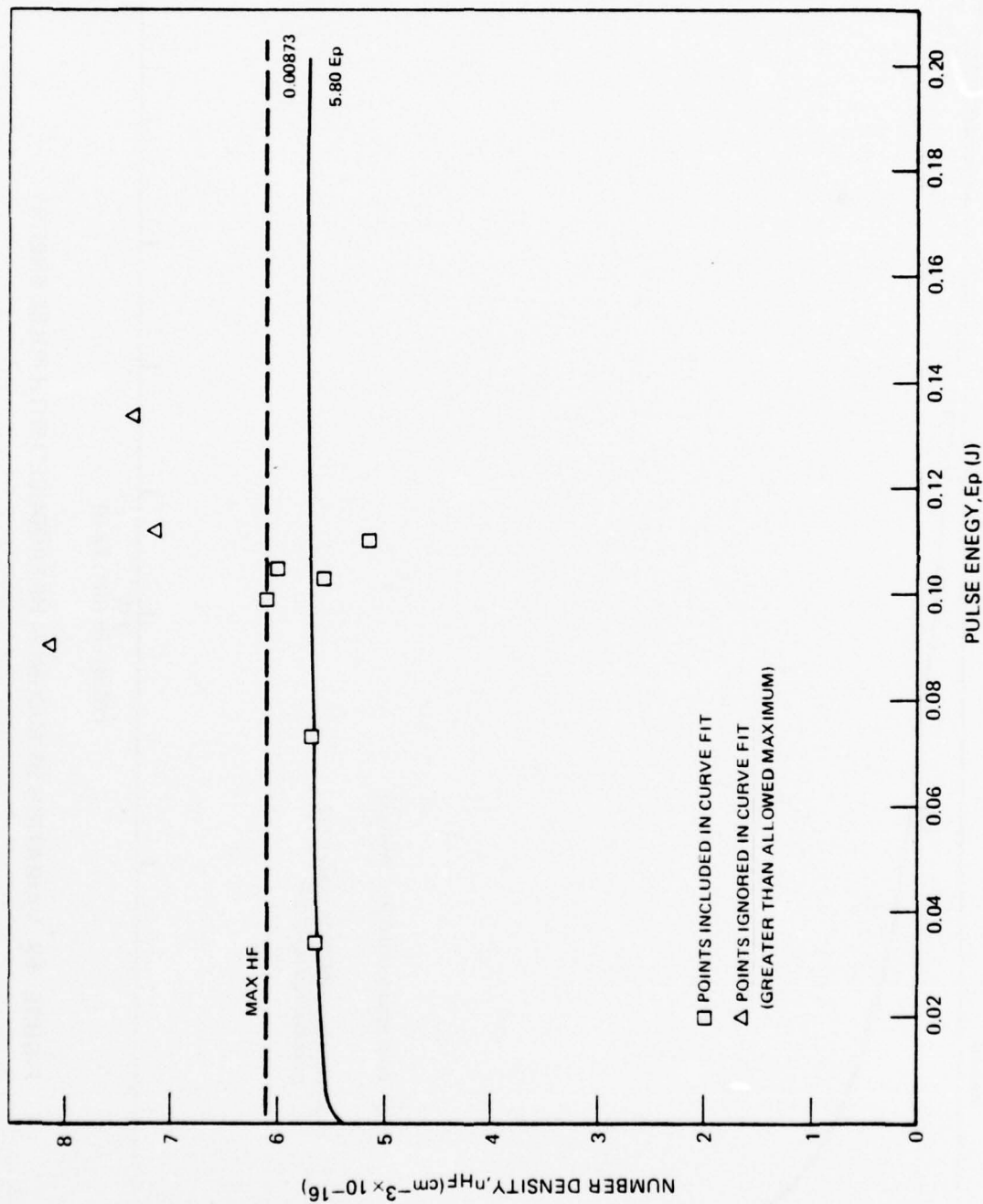


FIGURE 57 VARIATION OF MAXIMUM HF PRODUCED WITH PULSE ENERGY

TEST SERIES B

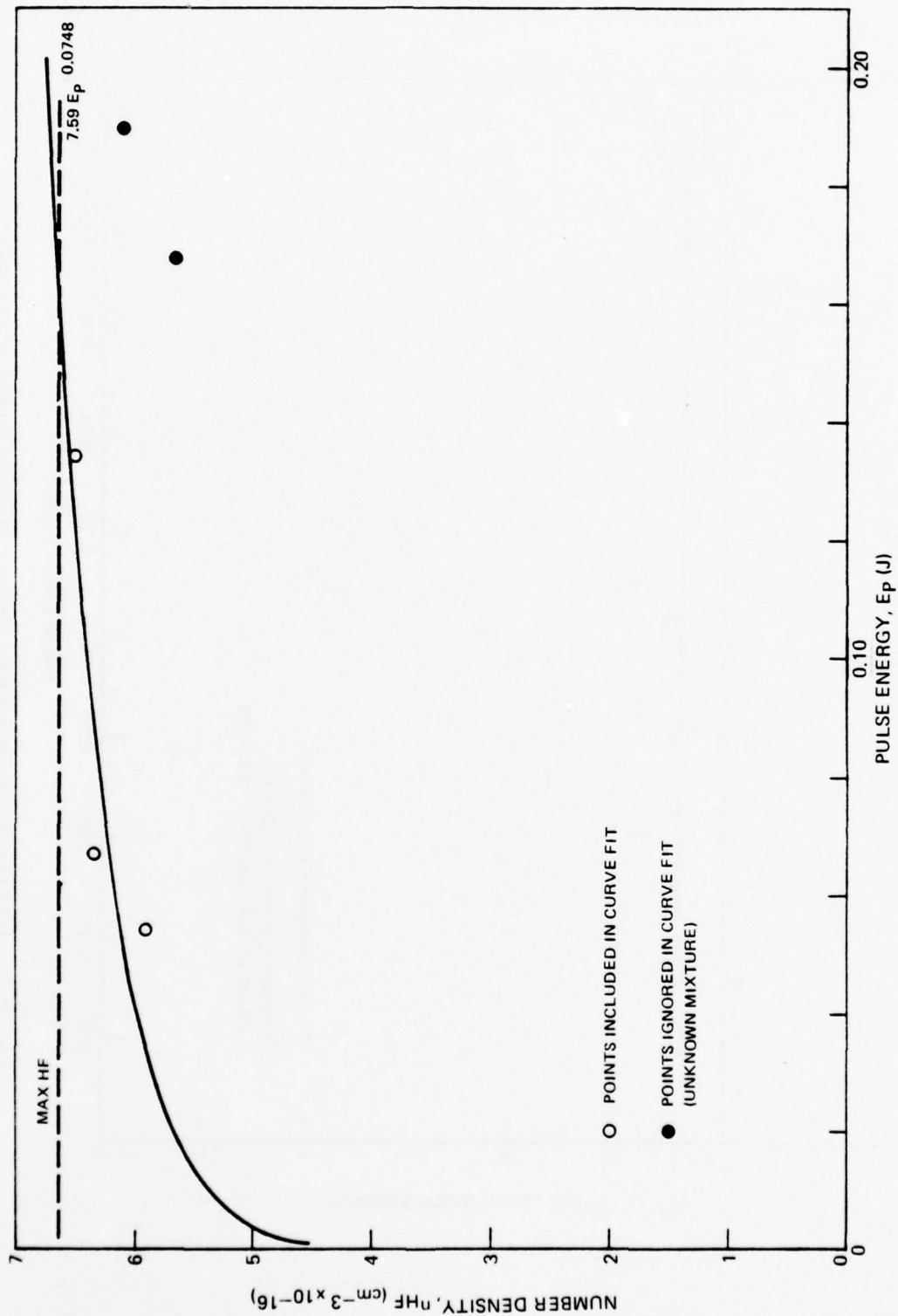


FIGURE 58 VARIATION OF MAXIMUM HF PRODUCED WITH PULSE ENERGY

TEST SERIES C

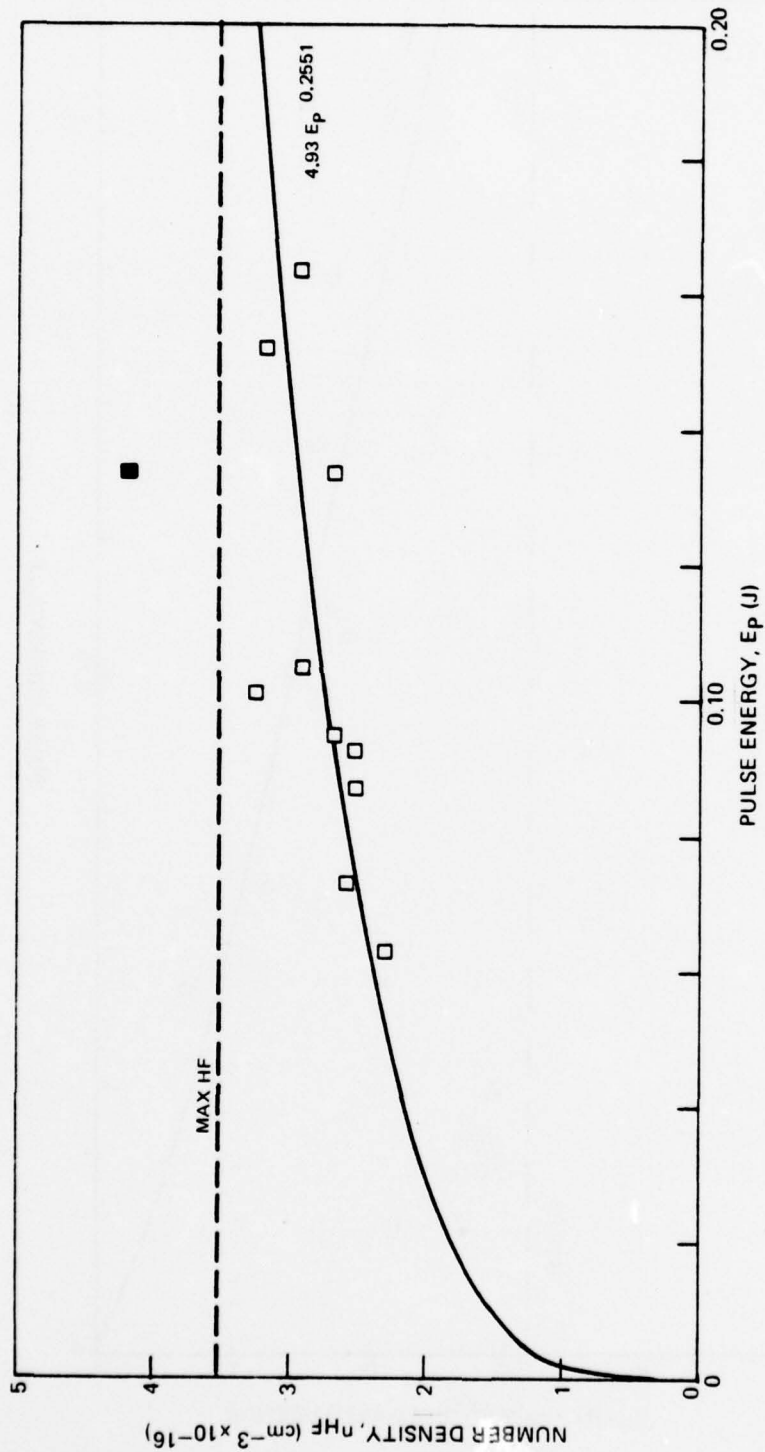


FIGURE 59 VARIATION OF MAXIMUM HF PRODUCED WITH PULSE ENERGY

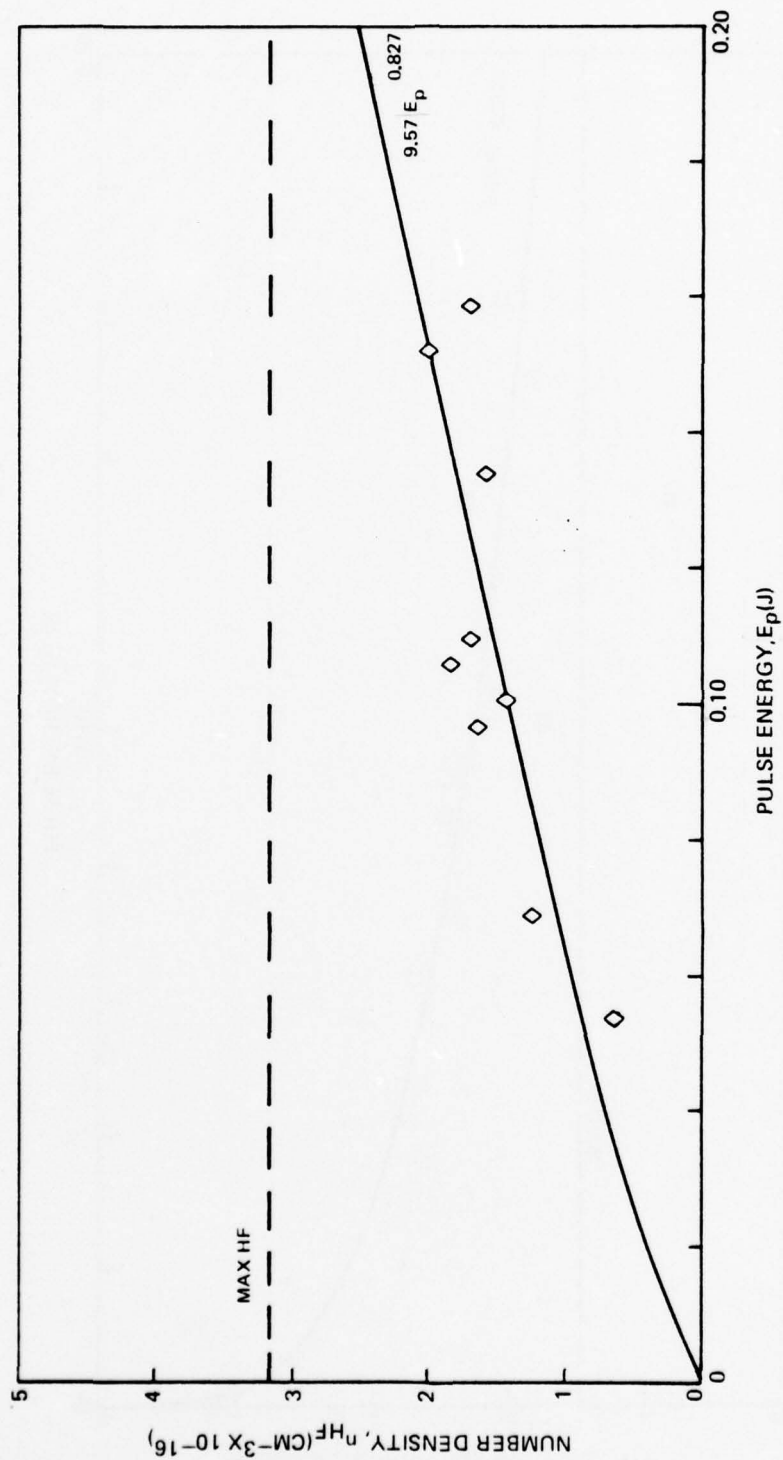


FIGURE 60 VARIATION OF MAXIMUM HF PRODUCED WITH PULSE ENERGY
TEST SERIES DH

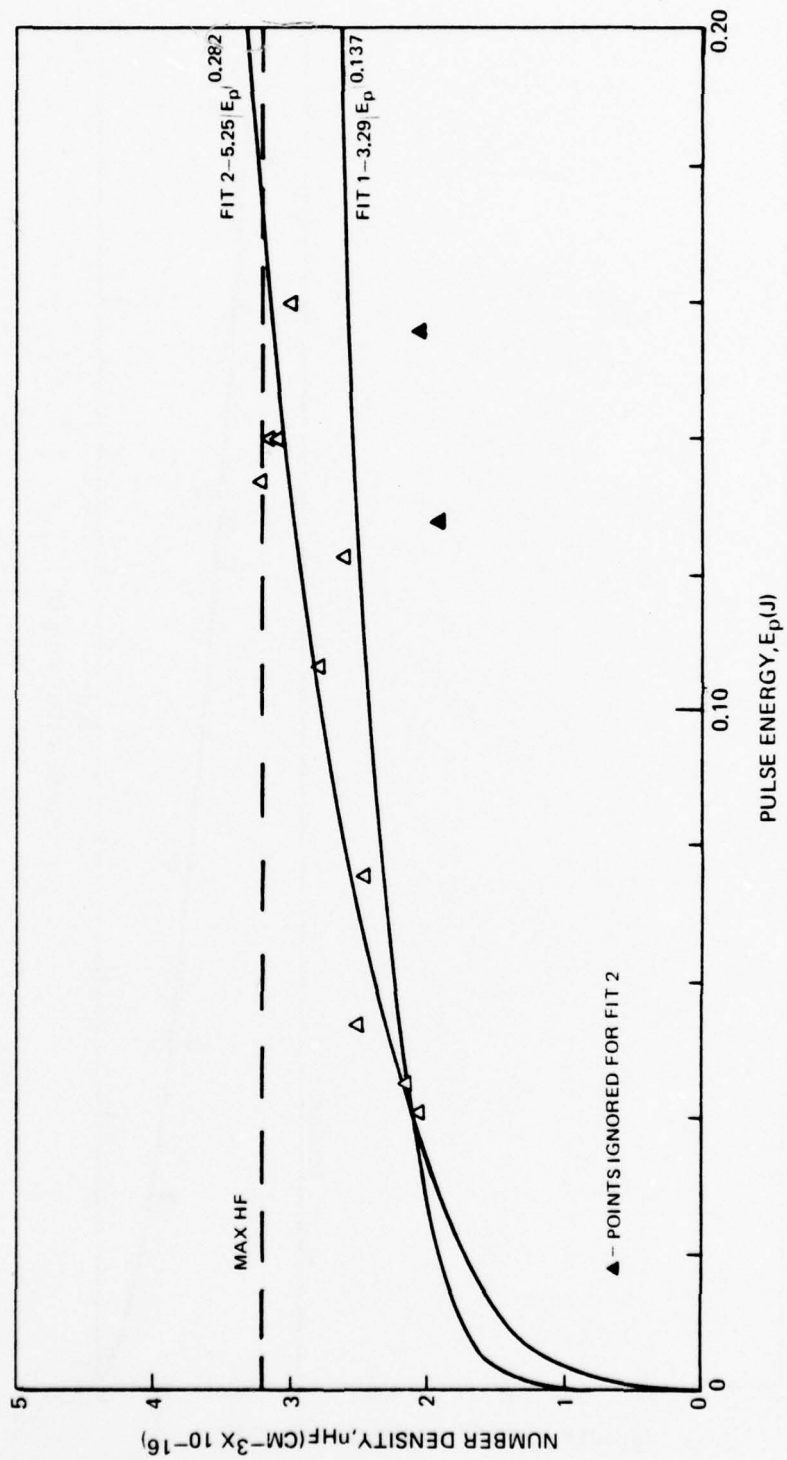


FIGURE 61 VARIATION OF MAXIMUM HF PRODUCED WITH PULSE ENERGY
TEST SERIES EF

TEST SERIES F

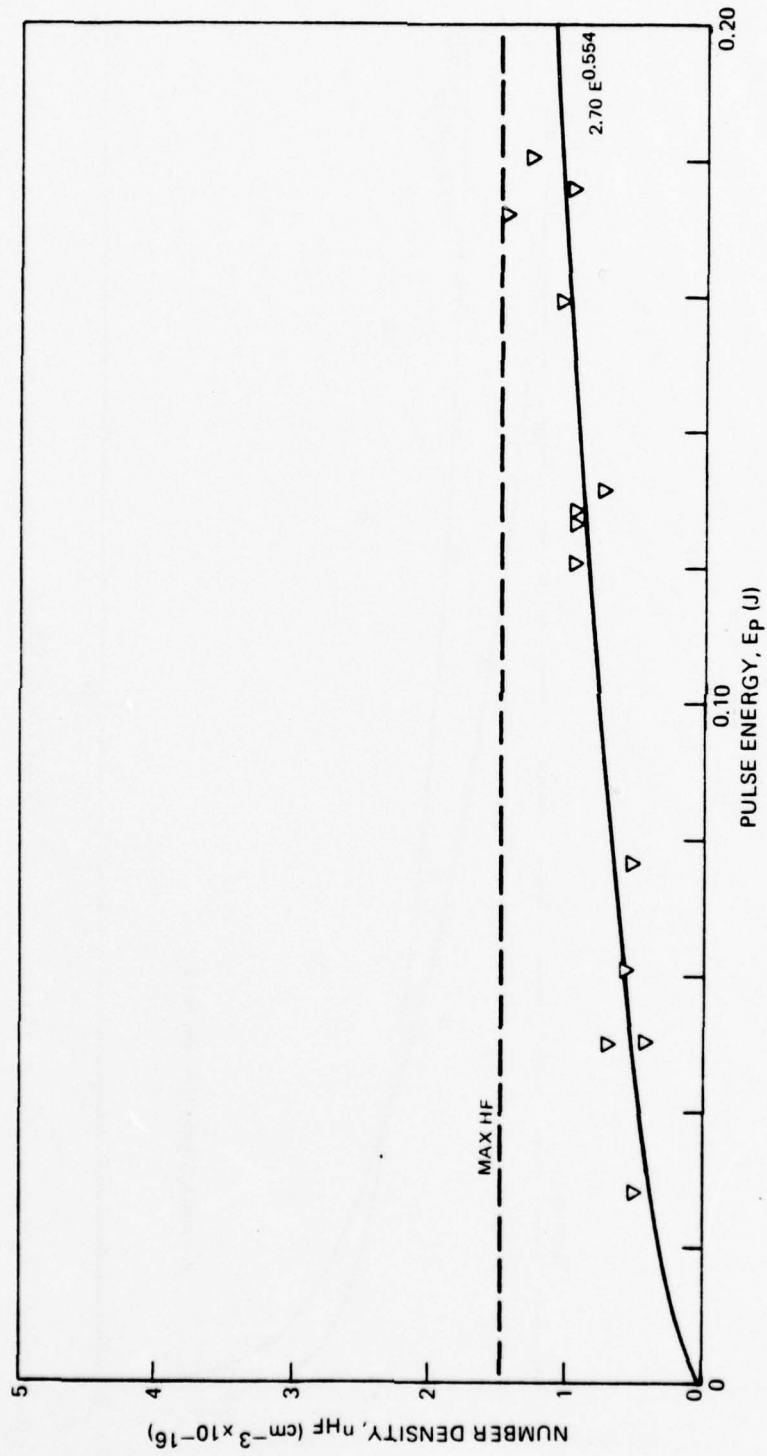


FIGURE 62 VARIATION OF MAXIMUM HF PRODUCED WITH PULSE ENERGY

$$\dot{n}_{\text{HF}|W} = -K_W(n_{\text{HF}}|g)(1 - \frac{n_{\text{HF}}|W}{n_{\text{HF}}|MAX}) \quad (6)$$

The overall production of HF is approximated by the steady state formula

$$\dot{n}_{\text{HF}}|chem = \frac{2(n_F)_0 n_{F_2} n_{H_2} k_h k_c}{k_h n_{F_2} + k_c n_{H_2}} \quad (7)$$

and the net change of HF in the gas phase is then

$$\dot{n}_{\text{HF}}|g = \dot{n}_{\text{HF}}|chem + \dot{n}_{\text{HF}}|W \quad (8)$$

A simple integration of the above equations for several experimental conditions was performed to see if one set of rate parameters could be used to reasonably fit a number of cases (A6-8, B3-5, C6-9, DH1-2). A reasonable fit was obtained for the following set of coefficient values:

$$\begin{aligned} k_h &= 1.3 \times \text{nominal} \\ k_c &= 2.0 \times \text{nominal} \\ k_w &= 200 \text{ sec}^{-1} \\ n_{\text{HF}}|MAX &= 1.5 \times 10^{16} \text{ cm}^{-3} \end{aligned}$$

The results of this exercise are given in the contract test report (Ref. 23). One problem with this fit to the data was that the experimental curves tend to bend over more gradually than the model predicts as the reaction nears completion. A possible explanation for such behavior could be the loss of H atoms to the wall. An examination of that possibility (Appendix D) has indicated a potentially significant effect. Hence the model was modified to account for the loss of H atoms in a manner as described in Appendix B (see Eq. B17). However, the form of k_D is taken to be

$$k_D = A t^{m-1} \quad (9)$$

since we may better fit the analytic curve (Appendix D, Figure D2) for the loss of H atoms to the form

$$n_H = n_{H_0} e^{-A t^m} \quad (10)$$

For complete loss of H atoms the coefficients A and m would have the values 17.325 and 0.608 respectively.

23. Boedeker, L. R., et al., "Long-Range Chain Laser Studies Test Report," for Air Force Contract F29601-75-C-0139, UTRC R76-952198-49, East Hartford, CT, October 1976.

The modified model was then used in extensive comparisons with experiment. Using the composite plots (Figs. 51-56) for guidance, representative cases from each test series were selected for analysis. These cases are listed in Table 11 along with the initial conditions used. The values selected for HF_w are designed to result in a final HF number density near that observed experimentally. The rationale is that the wall may be saturated with HF to different degrees from test to test.

Some of the results of the analysis are summarized in Figures 63 through 74. The curves labeled Fit P is for a fit that gave the best overall fit to the different test series. The values for the various rate coefficients are:

$$\begin{aligned} k_h &= 1.3 \times \text{nominal} \\ k_c &= 2.0 \times \text{nominal} \\ k_w &= 100 \text{ sec}^{-1} \\ n_{HF}|_{MAX} &= 1.5 \times 10^{16} \text{ cm}^{-3} \\ A &= 8.0 \\ m &= 0.608 \end{aligned}$$

The value of 8.0 for A implies an H atom adsorption accommodation coefficient of about 0.5. It is possible to juggle the values of all the wall interaction parameters to obtain somewhat better fits but further effort was not deemed worthwhile.

As can be seen from the curves, the fit is best for series A, B, and C. This is by design since it is felt that those are the most reliable data. The relatively fast rate for the cold reaction is dictated primarily by the initial slope from series C, whereas the somewhat fast hot reaction rate was indicated by series A and B for which the hot reaction is the rate controlling step. Note that even with the inclusion of H atom effects it was not possible to match the observed bending over of the series C curves. Much faster than reasonable wall interaction and chemical rates would be necessary to provide a better fit; and that would be at the expense of good fits for series A and B.

Further note that a single set of rates could not really fit all the series simultaneously. The predictions for series D fall consistently below the experimental curves. This is even more dramatically true for series E. On the other hand, those same rates predict curves well above the measured curves for series F.

The influence of reverse chemical reactions might be invoked as an explanation of this behavior, but inclusion of such effects only showed a strong influence for unreasonably fast rates (greater than gas kinetic) and would imply faster forward rates as well.

TABLE 11. INITIAL CONDITIONS - PULSED FLUORESCENCE EXPERIMENT

Case	F	F ₂	H ₂	HF _g	HF _w
A6	3.51 x 10 ¹³	2.87 x 10 ¹⁶	3.12 x 10 ¹⁶	0.3 x 10 ¹⁶	0.65 x 10 ¹⁶
A7	2.33	2.67	2.92	0.7	1.0
A8	3.28	2.77	3.02	0.5	0.7
A10	3.35	2.85	3.10	0.35	1.1
A15	3.16	2.85	3.10	0.35	1.5
B3	2.32	2.94	6.80	0.70	1.0
B4	4.66	2.99	6.85	0.60	1.2
B5	1.88	2.79	6.65	1.00	0.8
C6	3.38	3.173	1.77	0.0	1.25
C7	3.55	↓	↓	↓	1.0
C8	5.49	↓	↓	↓	0.9
C9	5.09	↓	↓	↓	0.9
DH1	2.66	1.58	1.77	↓	0.0
DH2	2.54	↓	↓	↓	0.19
DH7	1.76	↓	↓	↓	0.4
EF2	2.05	1.58	3.02	↓	1.0
EF5	2.69	↓	↓	↓	1.32
EF6	2.35	↓	↓	↓	1.5
F7	4.35	3.25	0.76	↓	1.0
F10	6.21	↓	↓	↓	1.3
F11	6.04	↓	↓	↓	1.1

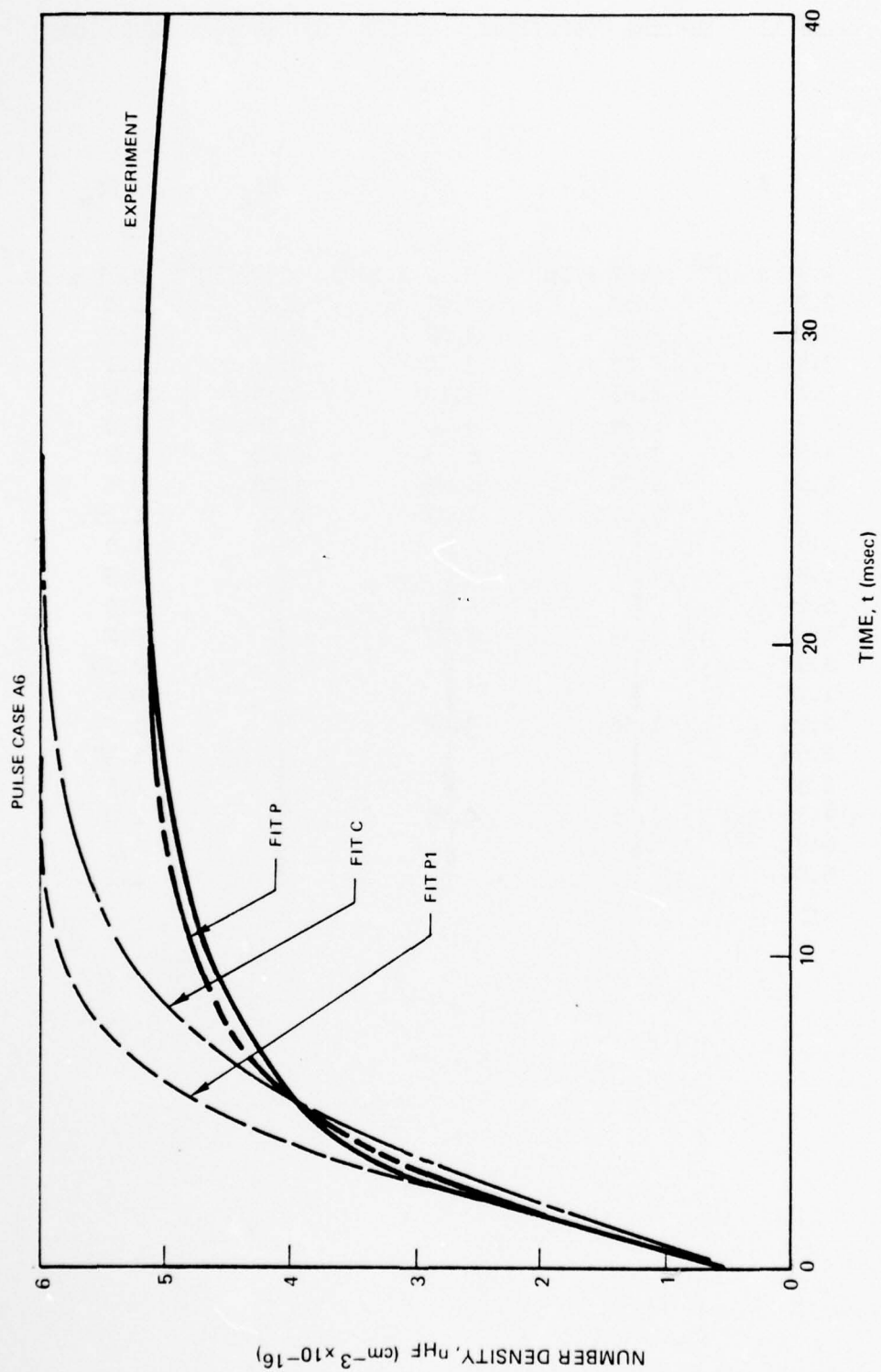


FIGURE 63 COMPARISON OF MODEL WITH EXPERIMENT
OVERALL HF DEVELOPMENT

OVERALL HF DEVELOPMENT
PULSE CASE A15

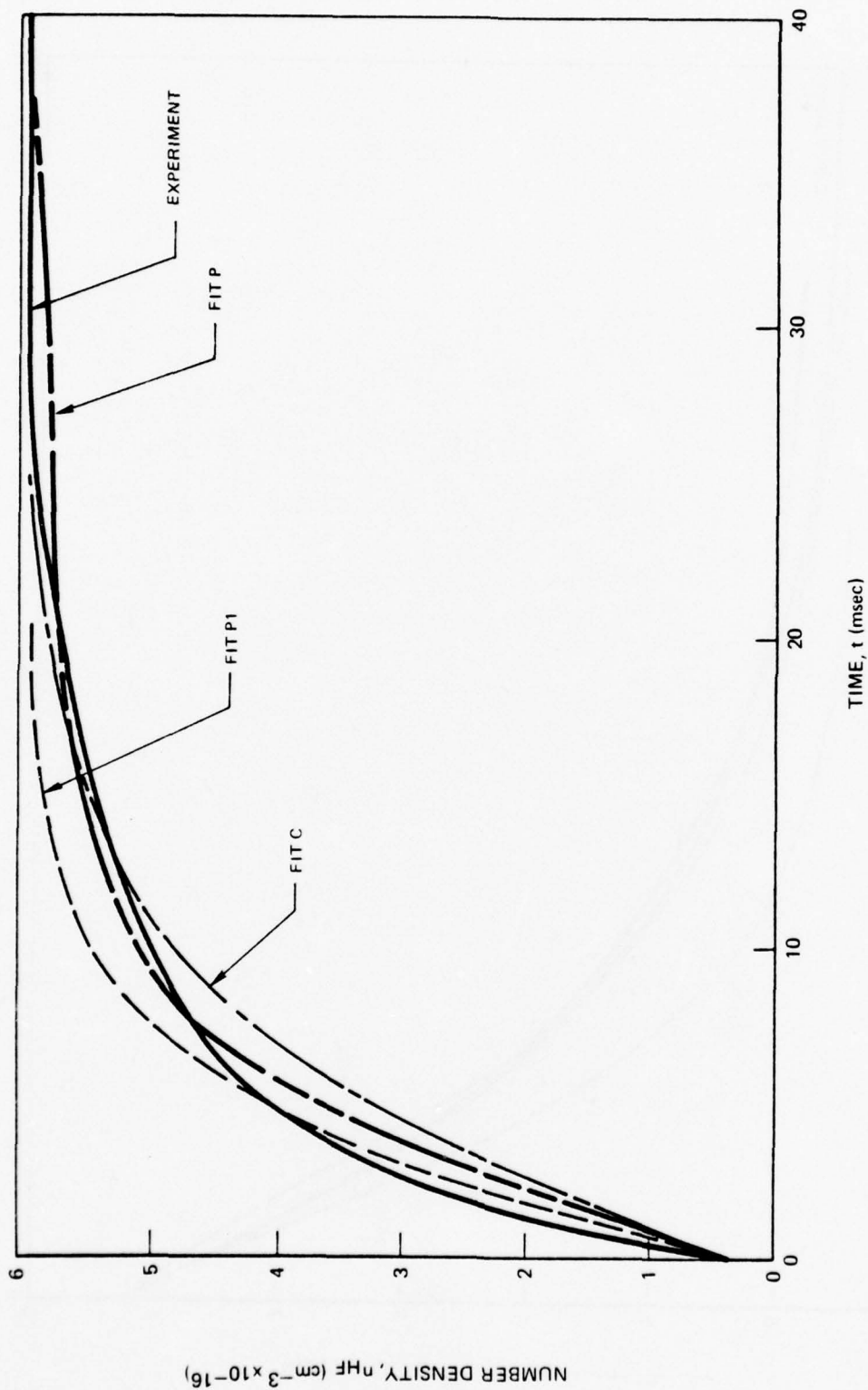


FIGURE 64 COMPARISON OF MODEL WITH EXPERIMENT

PULSE CASE B3

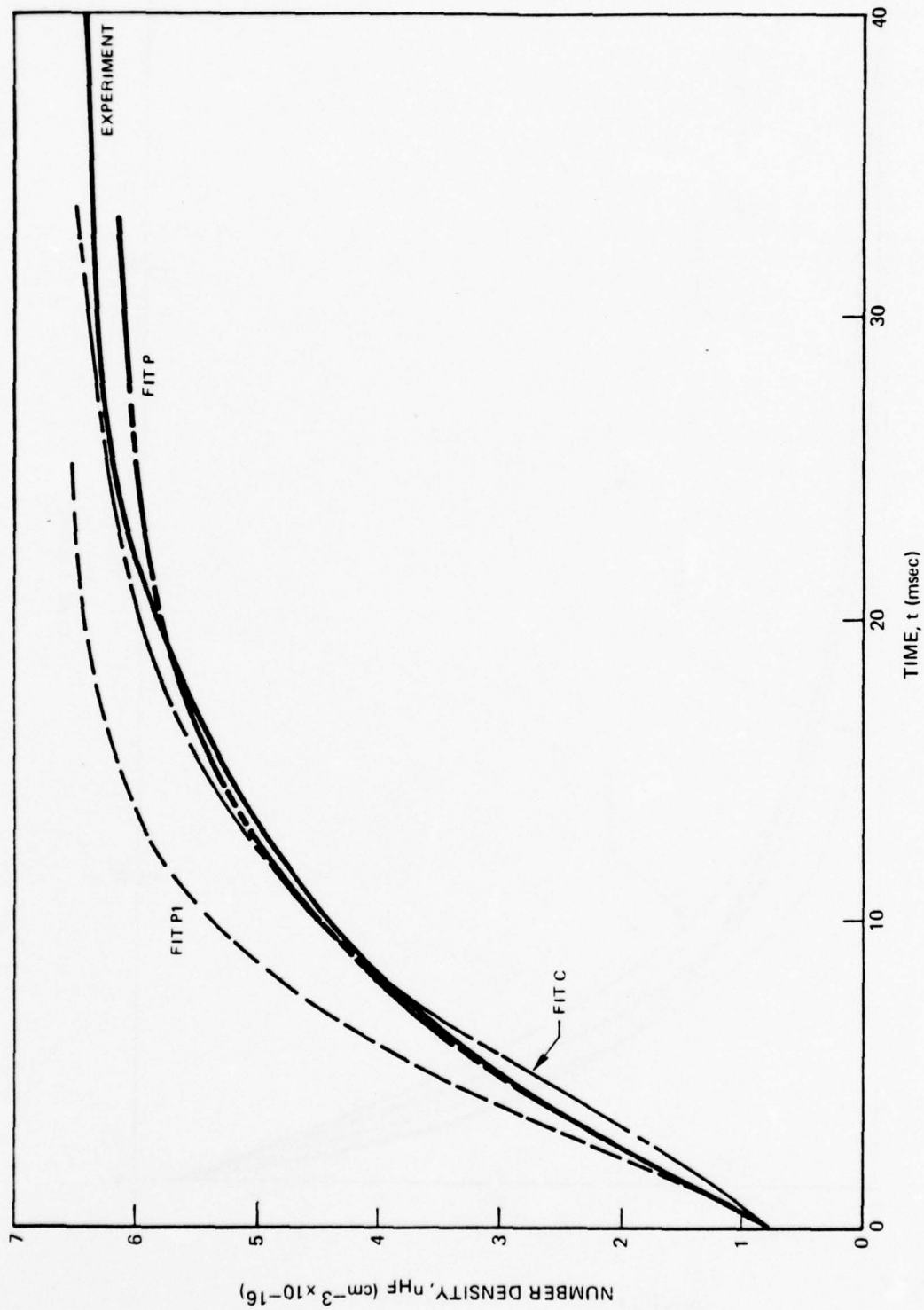


FIGURE 65 COMPARISON OF MODEL WITH EXPERIMENT
OVERALL HF DEVELOPMENT

PULSE CASE B4

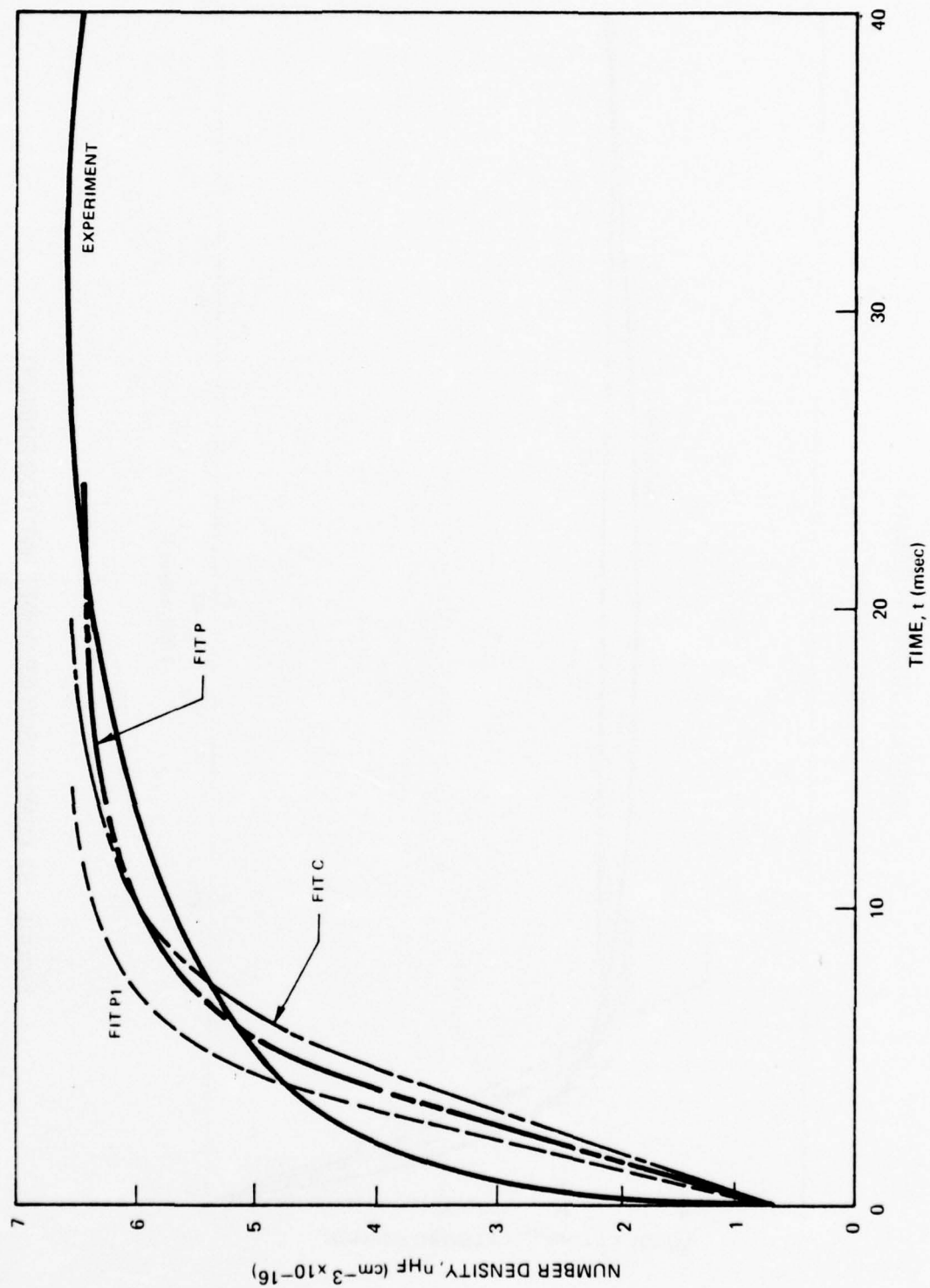


FIGURE 66 COMPARISON OF MODEL WITH EXPERIMENT OVERALL
OVERALL HF DEVELOPMENT

OVERALL HF DEVELOPMENT

PULSE CASE C6

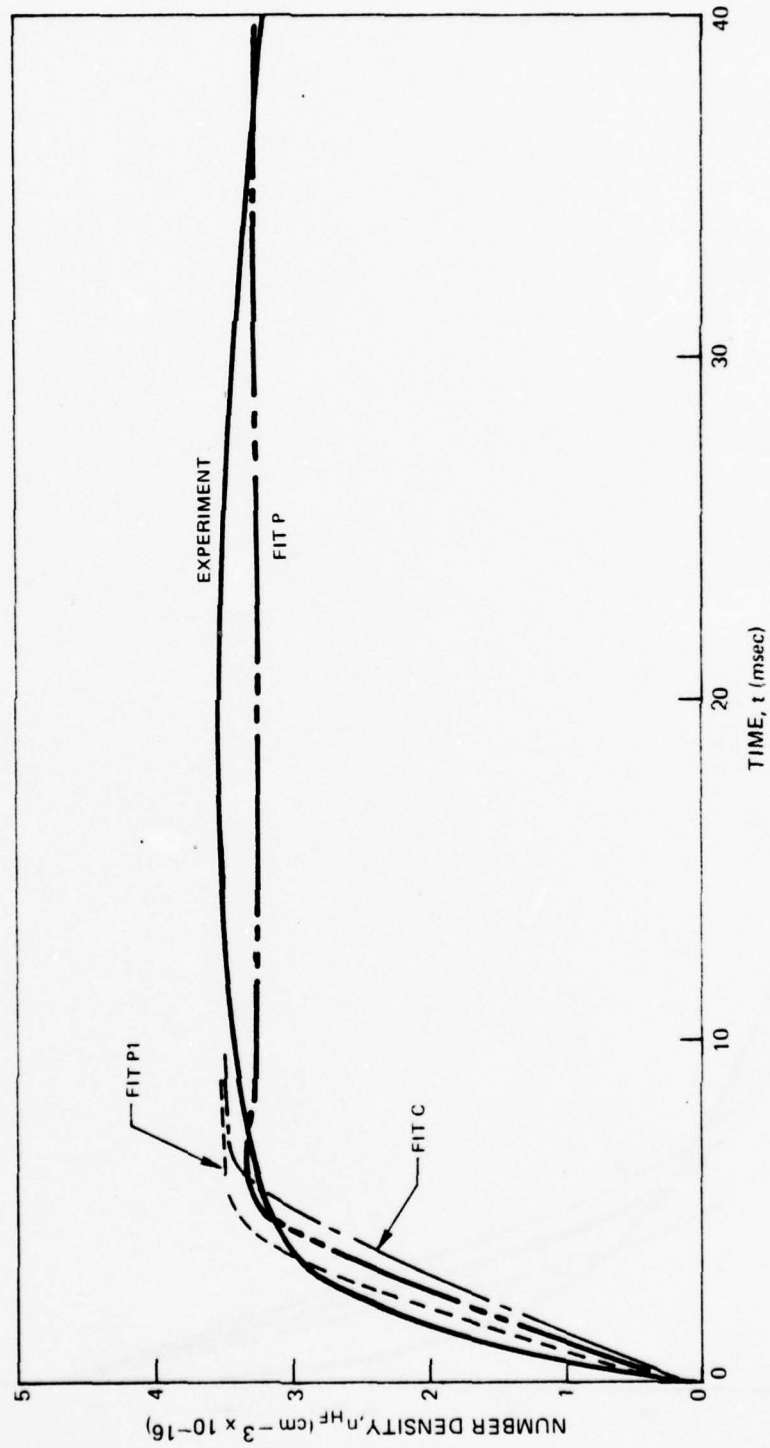


FIGURE 67 COMPARISON OF MODEL WITH EXPERIMENT

OVERALL HF DEVELOPMENT

PULSE CASE C8

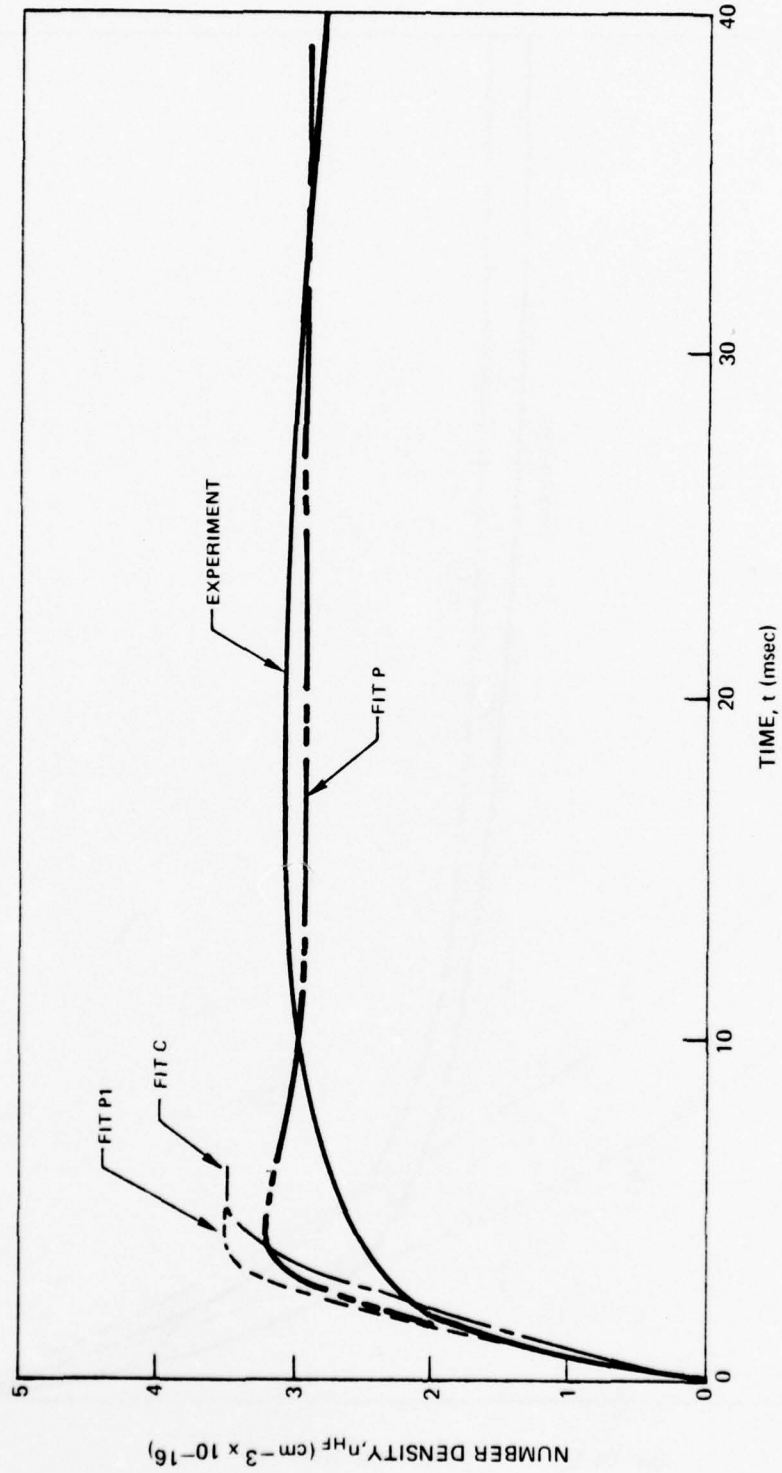


FIGURE 68 COMPARISON OF MODEL WITH EXPERIMENT

OVERALL HF DEVELOPMENT
PLUS CASE DH1

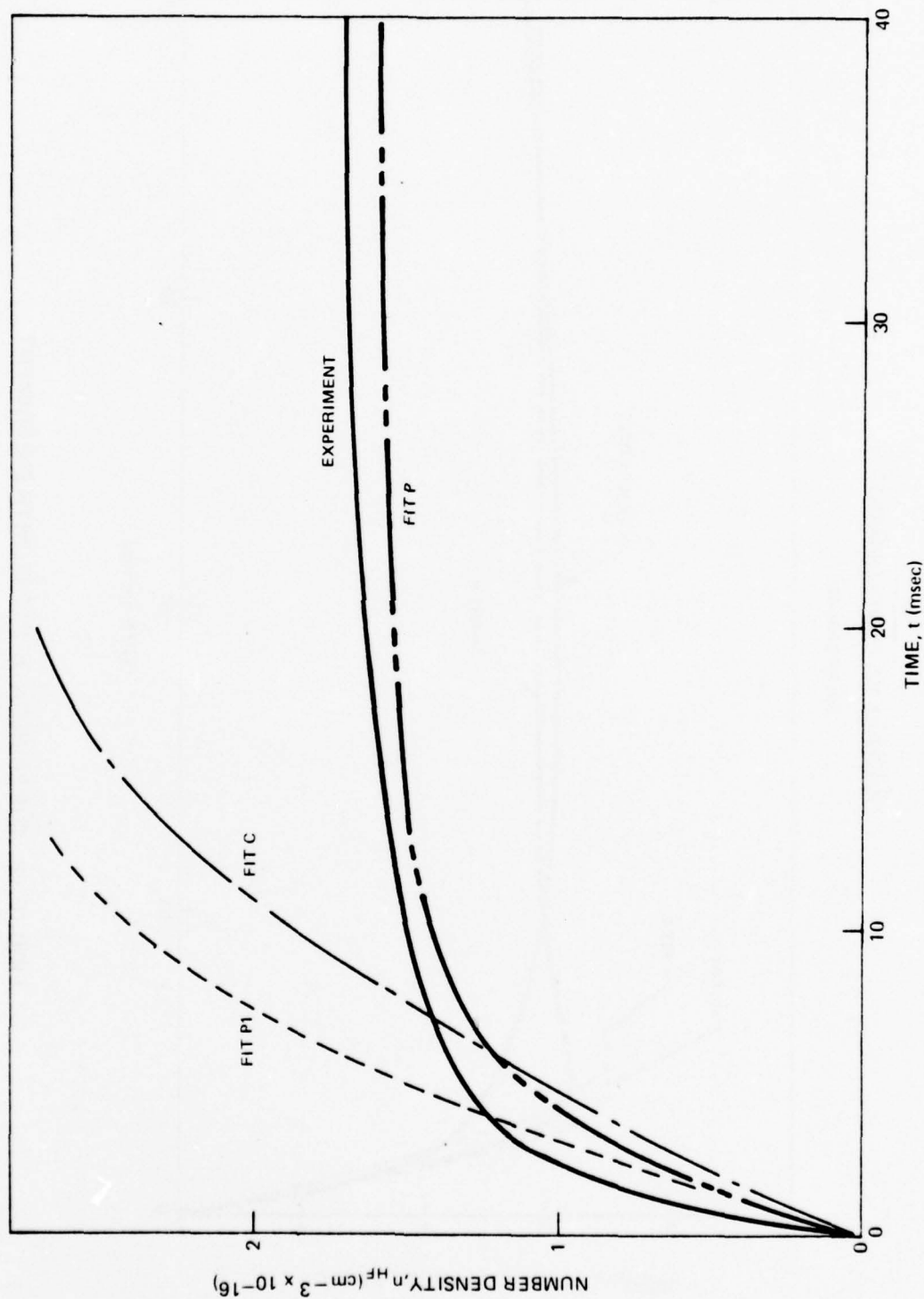


FIGURE 69 COMPARISON OF MODEL WITH EXPERIMENT

OVERALL HF DEVELOPMENT

PULSE CASE DH2

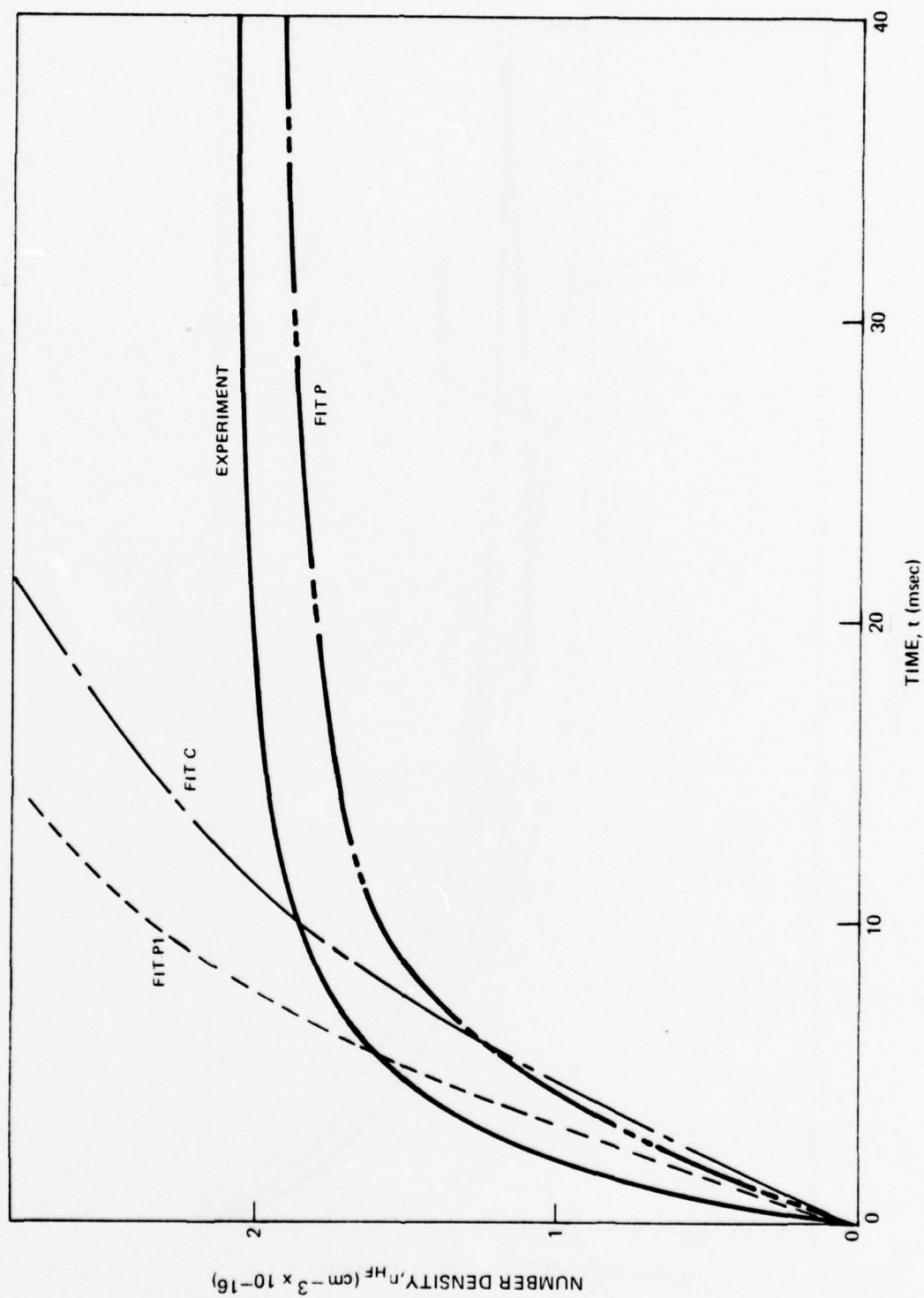


FIGURE 70 COMPARISON OF MODEL WITH EXPERIMENT

OVERALL HF DEVELOPMENT

PULSE CASE EF2

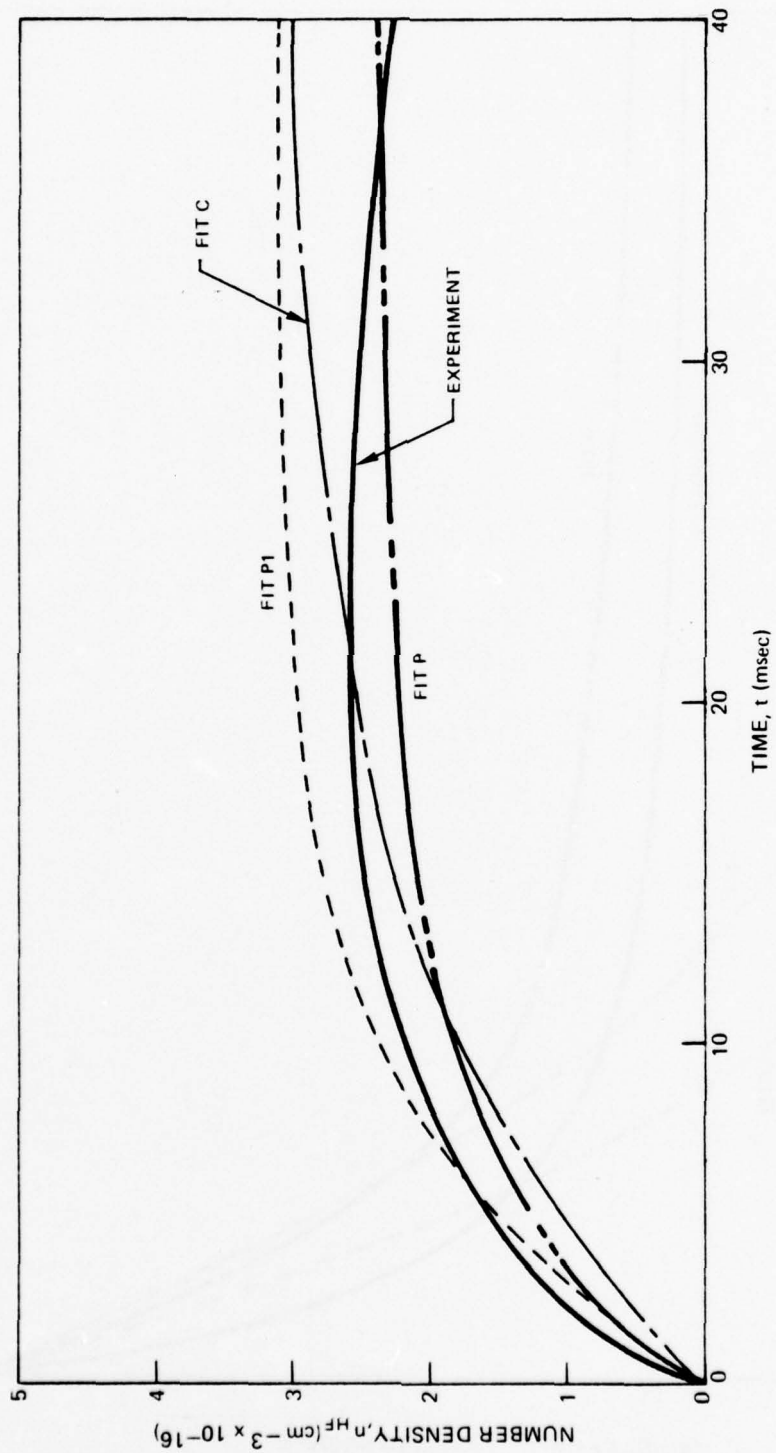


FIGURE 71 COMPARISON OF MODEL WITH EXPERIMENT

OVERALL HF DEVELOPMENT
PULSE CASE EF5

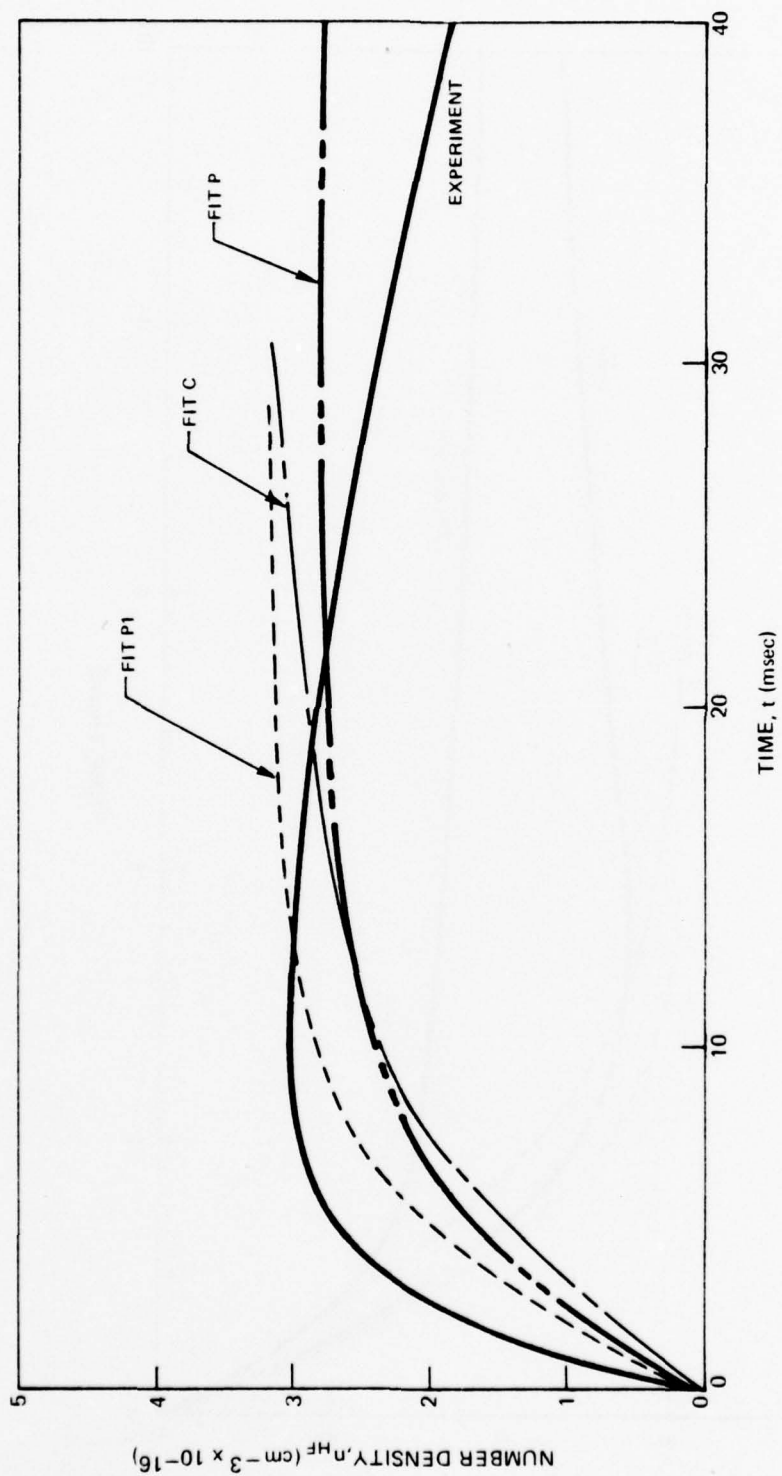


FIGURE 72 COMPARISON OF MODEL WITH EXPERIMENT

PULSE CASE F7

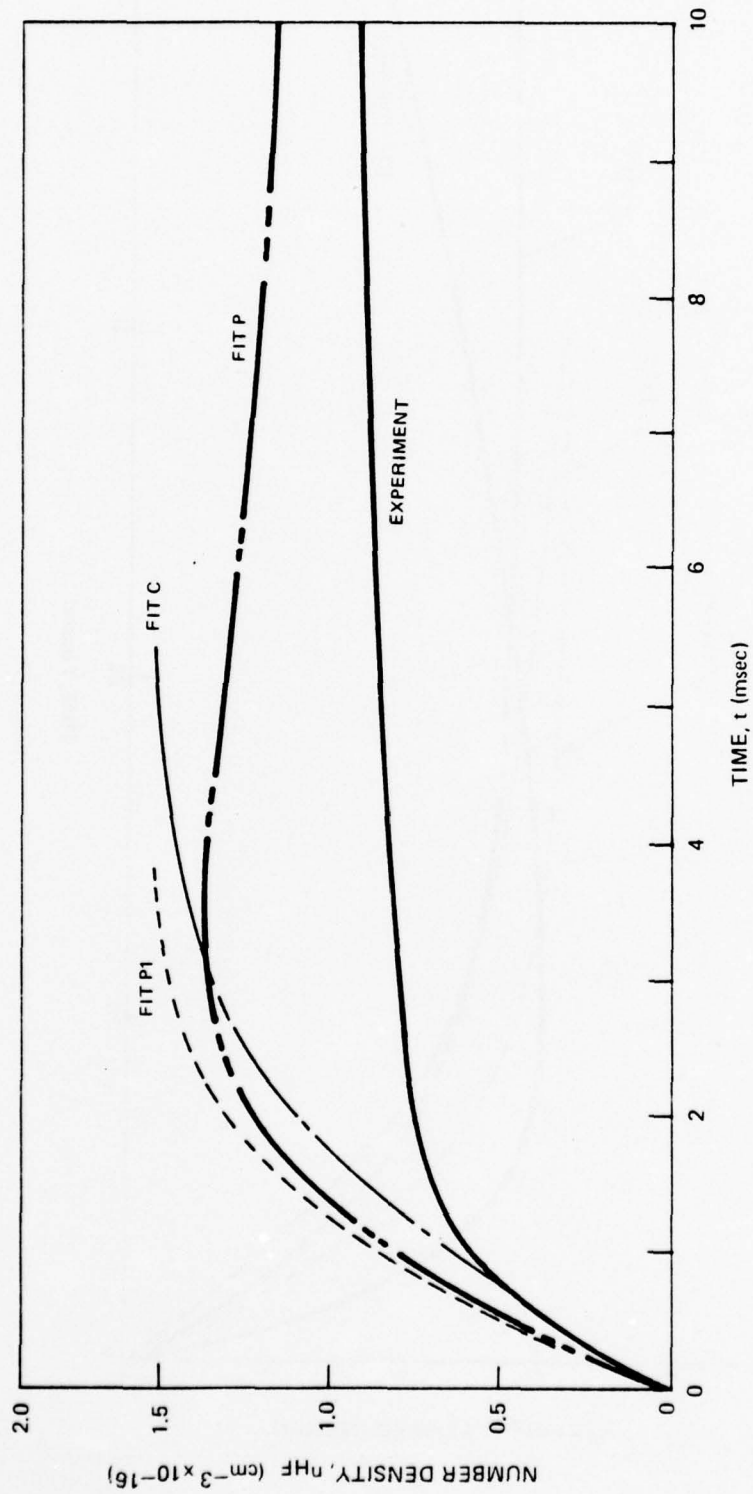


FIGURE 73 COMPARISON OF MODEL WITH EXPERIMENT
OVERALL HF DEVELOPMENT

PULSE CASE F10

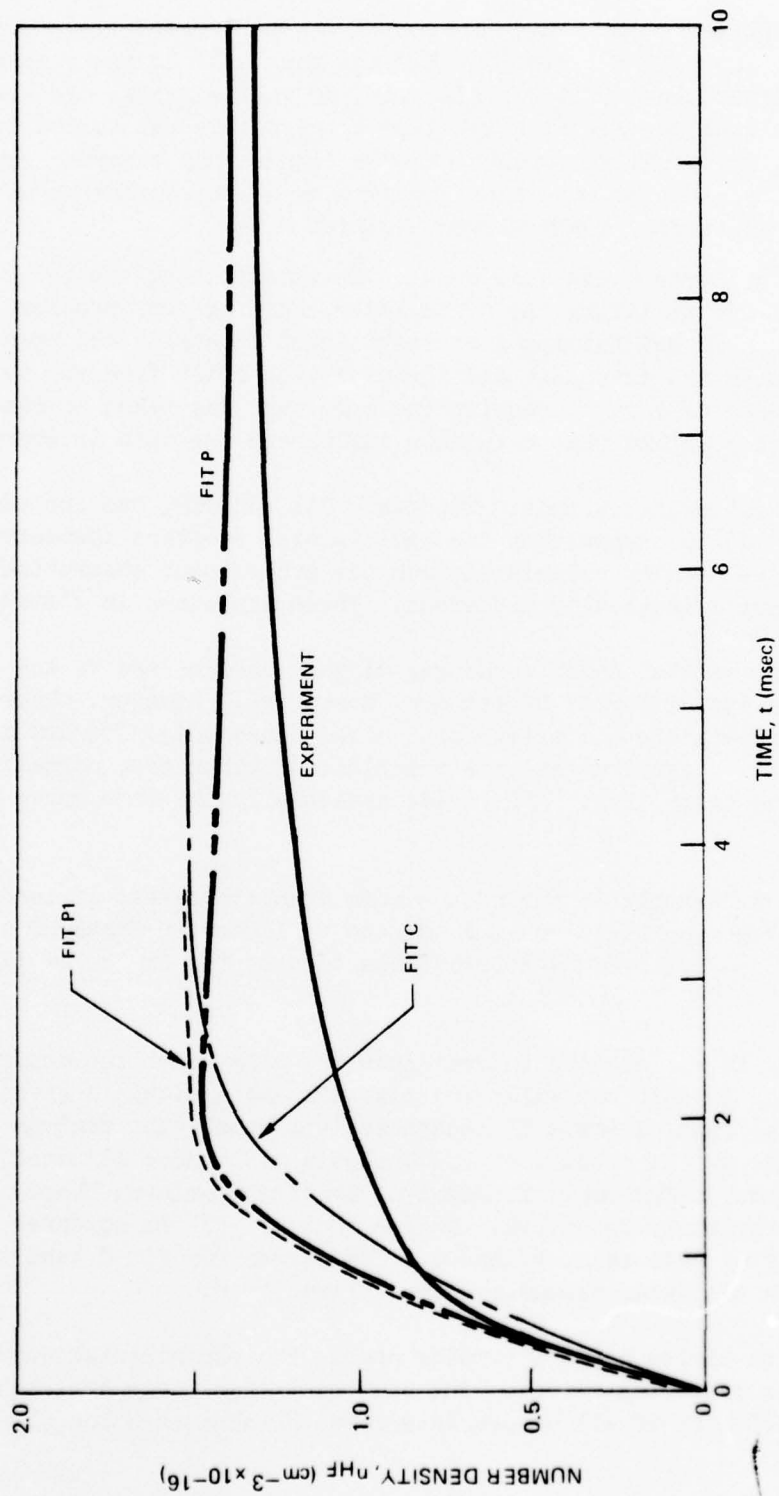


FIGURE 74 COMPARISON OF MODEL WITH EXPERIMENT
OVERALL HF DEVELOPMENT

Also shown in Figures 63 through 74 are curves for the same chemical rates as above, but without any wall effects (Fit P1) and the combined rates meant to fit both sets of experiments (Fit C), also with no wall effects. We see that the initial slopes for Fit P1 still give a reasonable fit to the data, but that naturally the final HF populations are higher than observed experimentally. It is important to note that the absence of the inclusion wall effects does not necessarily imply slower chemical rates.

An alternative approach can also be used in interpreting the pulsed-fluorescence data. In utilizing the probe laser there is some problem with stability, both in maintaining a constant input intensity and remaining on line center. Both the intensity and frequency can drift from run to run, and during the course of a run. Despite the care that was taken to minimize these effects it is possible that they have influenced the data interpretation.

Consider the following example. Two runs, C11 and C12, had the same pulse energy (0.134J) and supposedly the same initial reactant concentrations. The curves of number density calculated from the probe laser absorption traces, however, are dramatically different. These are shown in Figure 75.

One might suppose that somehow the gas mixture changed and we are actually observing two different HF temporal histories. However, observation of the measured temperature histories for the two cases (Fig. 76) implies that we are actually observing the same reaction. Furthermore, normalization of the HF traces to unity (Fig. 77) yields essentially the same curve in both cases.

While the above example is one of the more dramatic cases, it lends strong support to the hypothesis that much of the variation in final HF concentration that has been observed is attributable to drifting in the cw laser signal.

Consequently, it was decided to reanalyze the data under the assumption that no HF was lost to the walls and that all cases within a given series produced the same ultimate HF concentration, namely the maximum allowable. Samples of the results of the analysis with these adjusted HF populations are shown in Figures 78 through 89. Two fits are shown, P1 and C, which have been previously described. Notice that now fit P1 compares well with series F as well as A, B, and C. The curves for fit C tend to be consistently below the data, though perhaps tolerably so.

The match with series D and E remains poor. The experimental curves lie well above the predicted curves. The one thing that these series have in common, to the exclusion of all others, is a lower F_2 concentration (1/2 torr

SERIES C

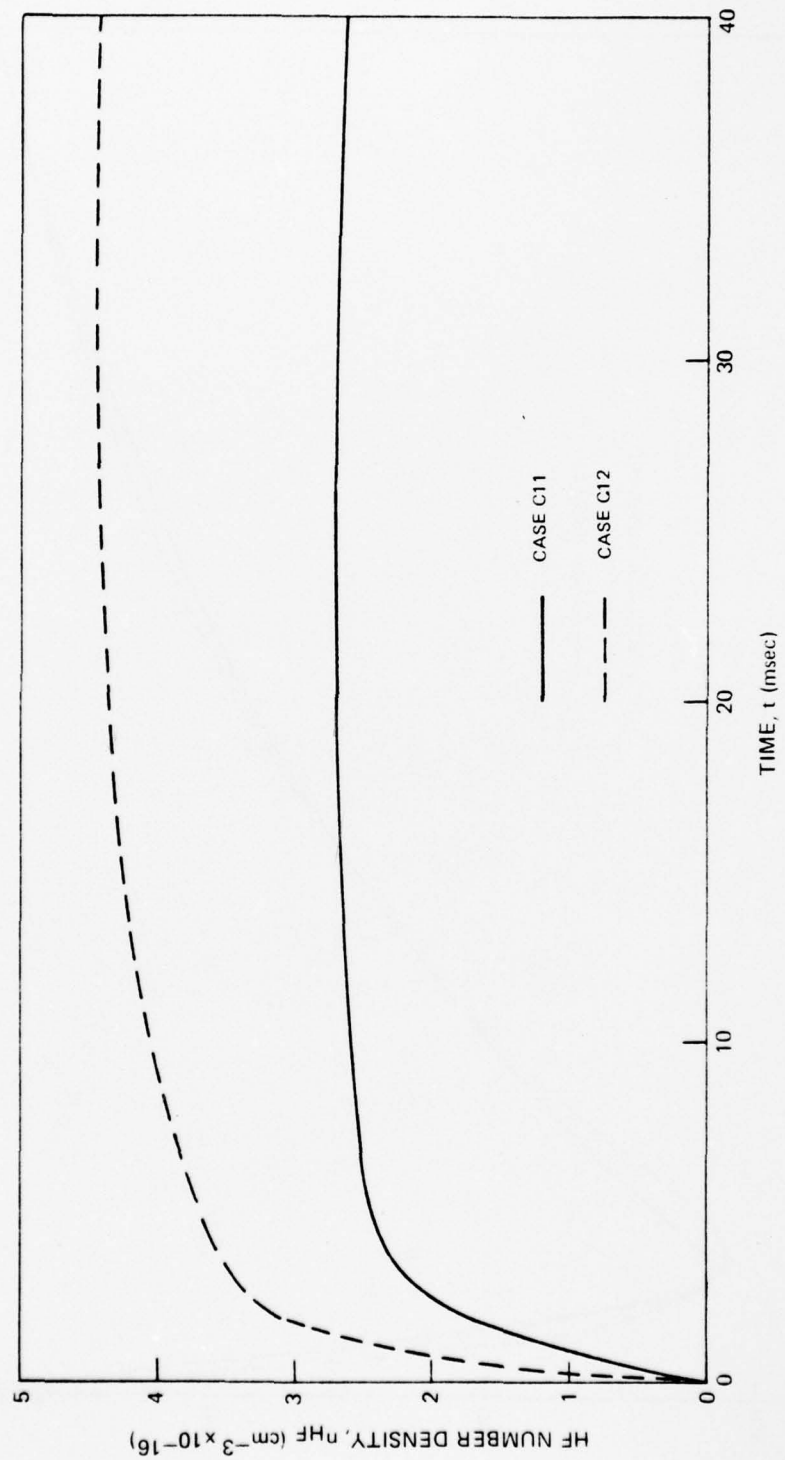


FIGURE 75 COMPARISON OF HF HISTORIES

SERIES C

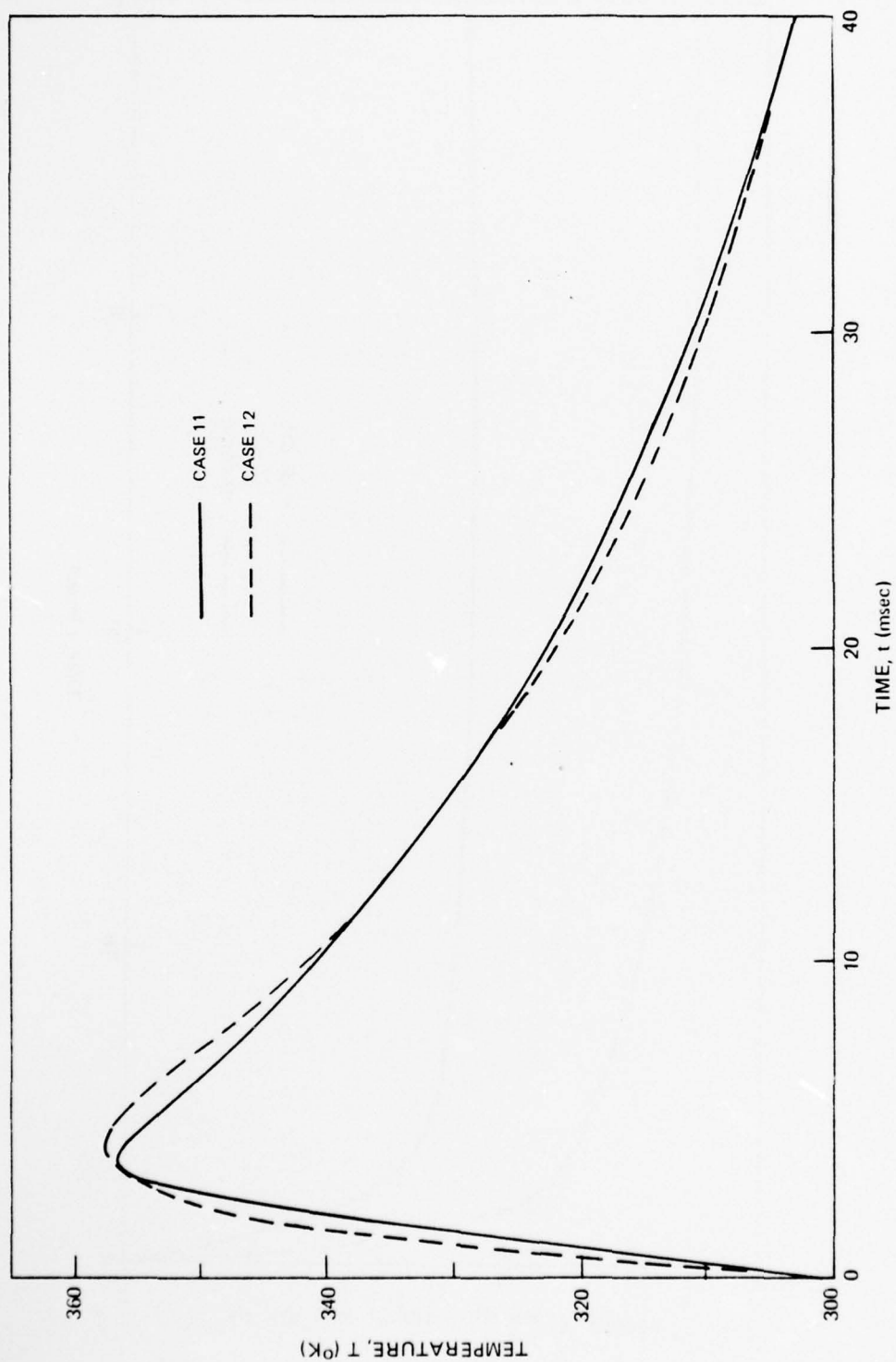


FIGURE 76 COMPARISON OF TEMPERATURE HISTORIES

SERIES C

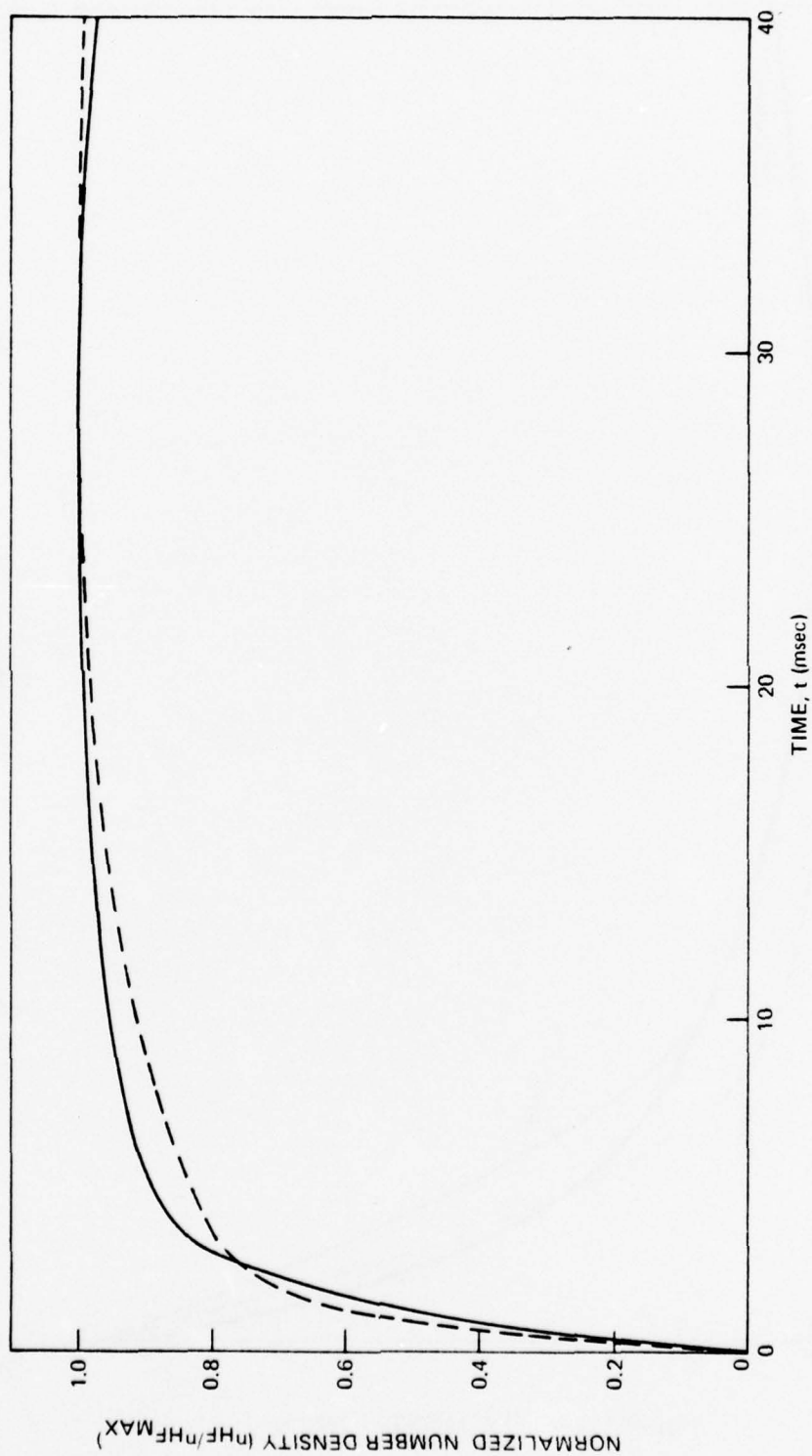


FIGURE 77 COMPARISON OF HF HISTORIES
RELATIVE NUMBER DENSITIES

PULSE CASE A8

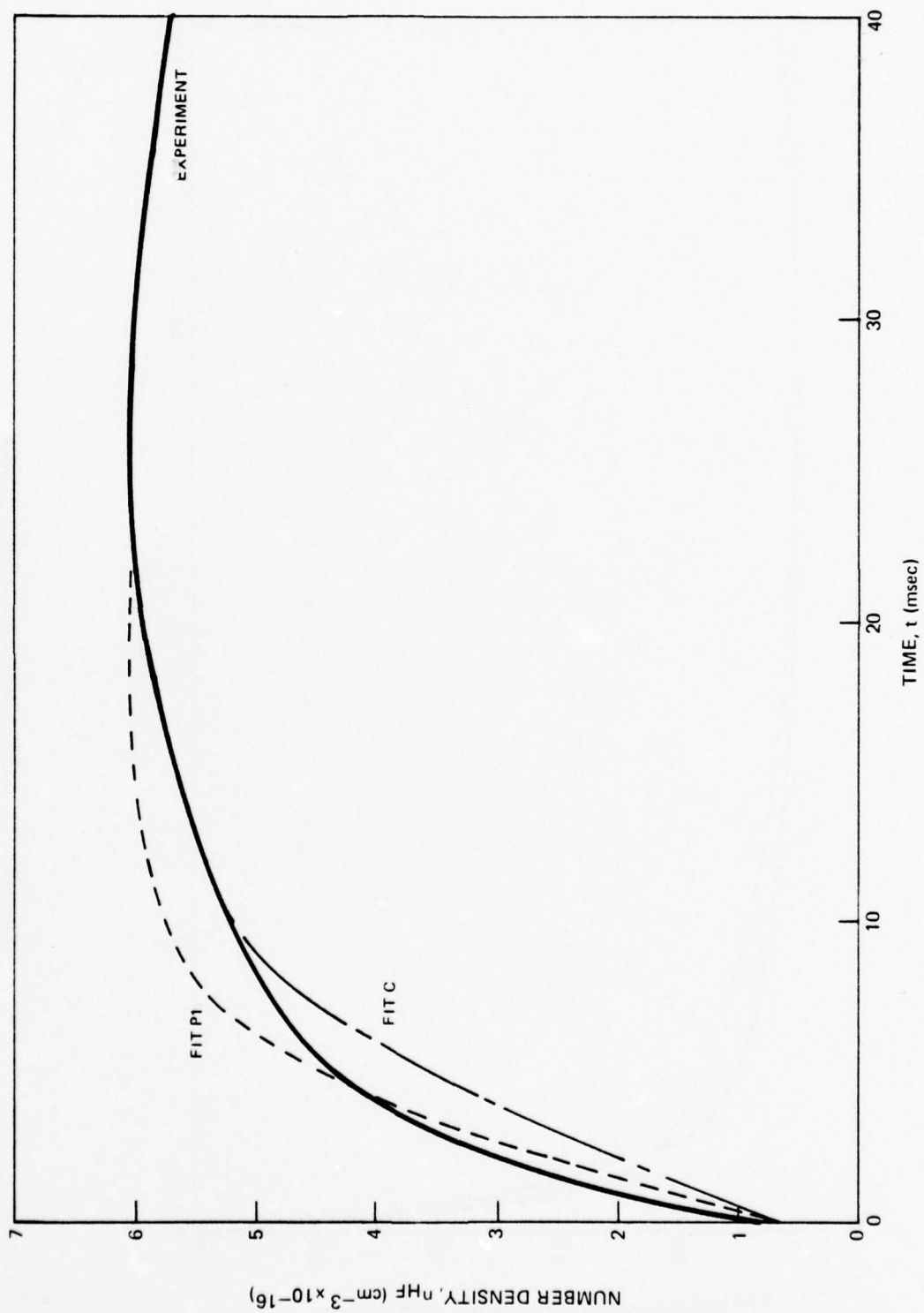


FIGURE 78 COMPARISON OF MODEL WITH EXPERIMENT ADJUSTED HF POPULATIONS

PULSE CASE A10

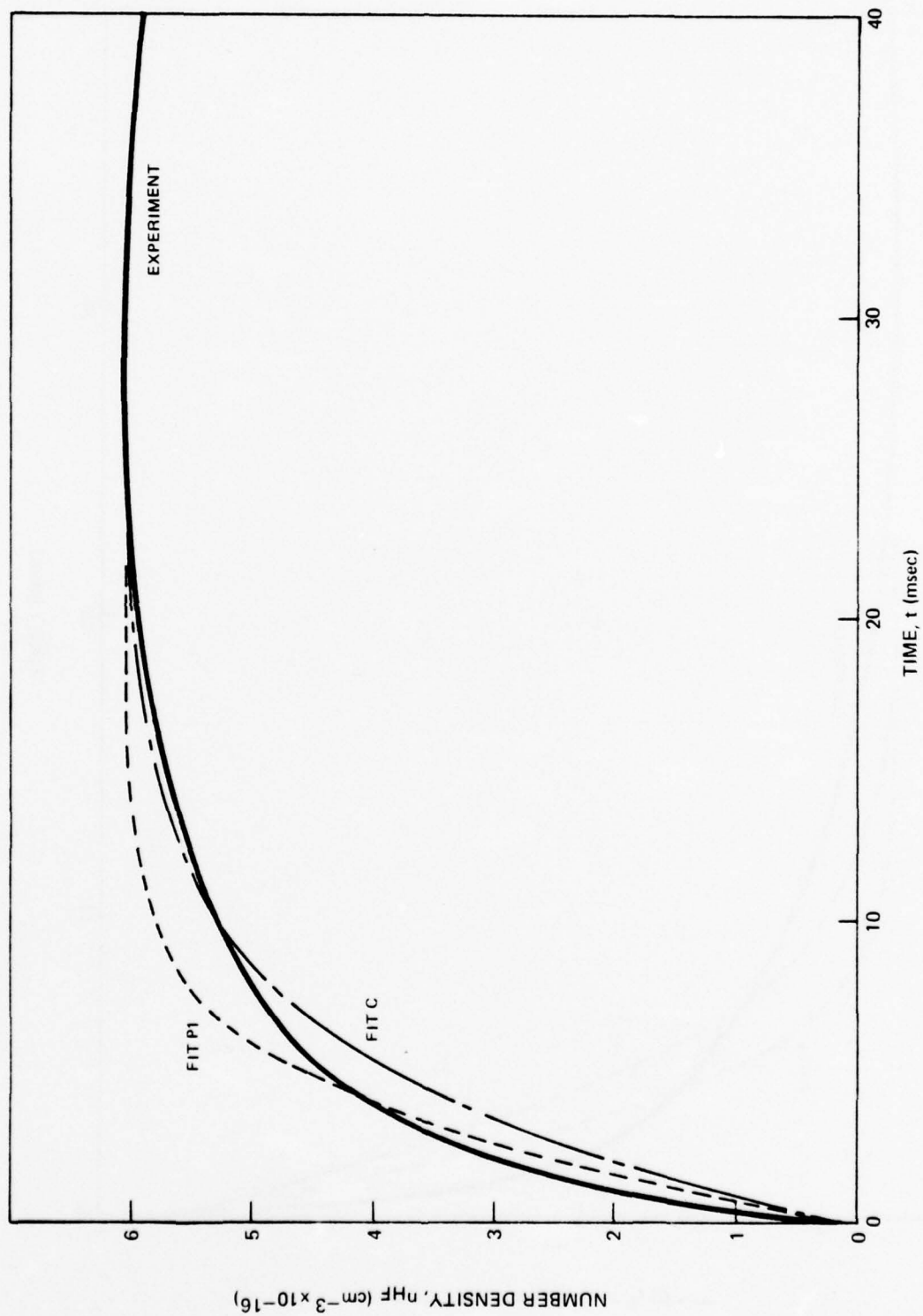


FIGURE 79 COMPARISON OF MODEL WITH EXPERIMENT ADJUSTED HF POPULATIONS

ADJUSTED HF POPULATIONS
PULSE CASE B4

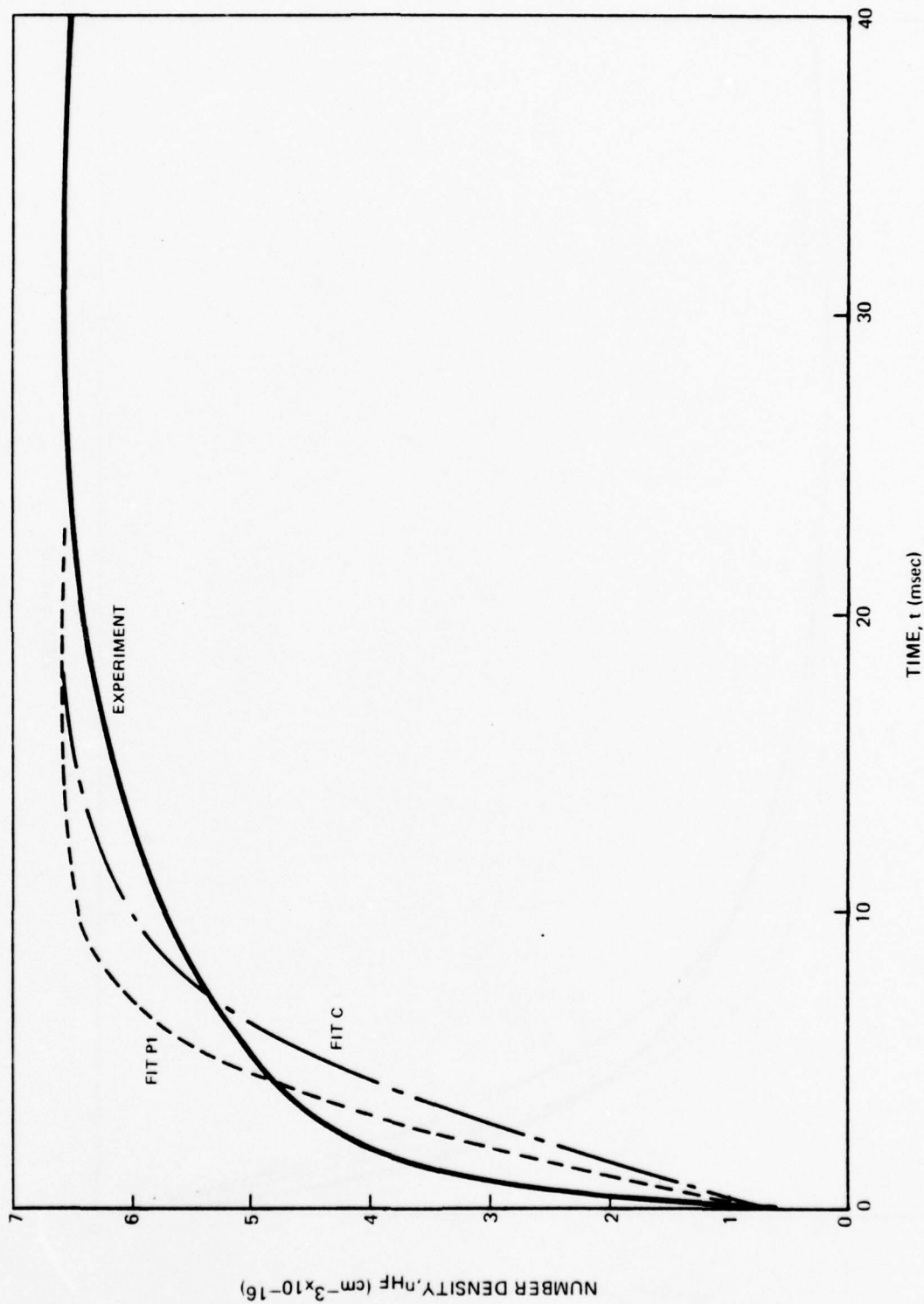


FIGURE 80 COMPARISON OF MODEL WITH EXPERIMENT

ADJUSTED HF POPULATIONS

PULSE CASE B5

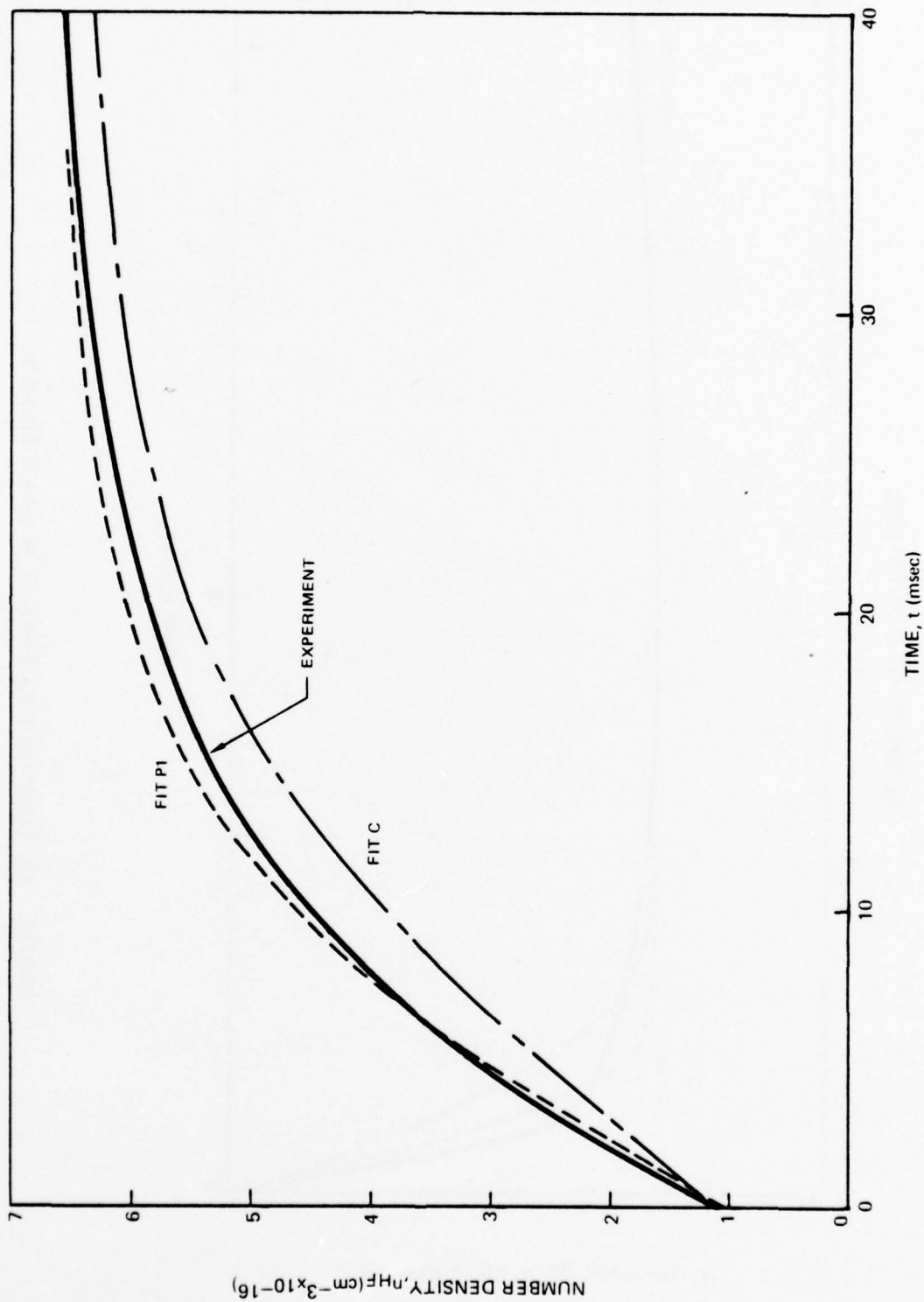


FIGURE 81 COMPARISON OF MODEL WITH EXPERIMENT

ADJUSTED HF POPULATIONS

PULSE CASE C7

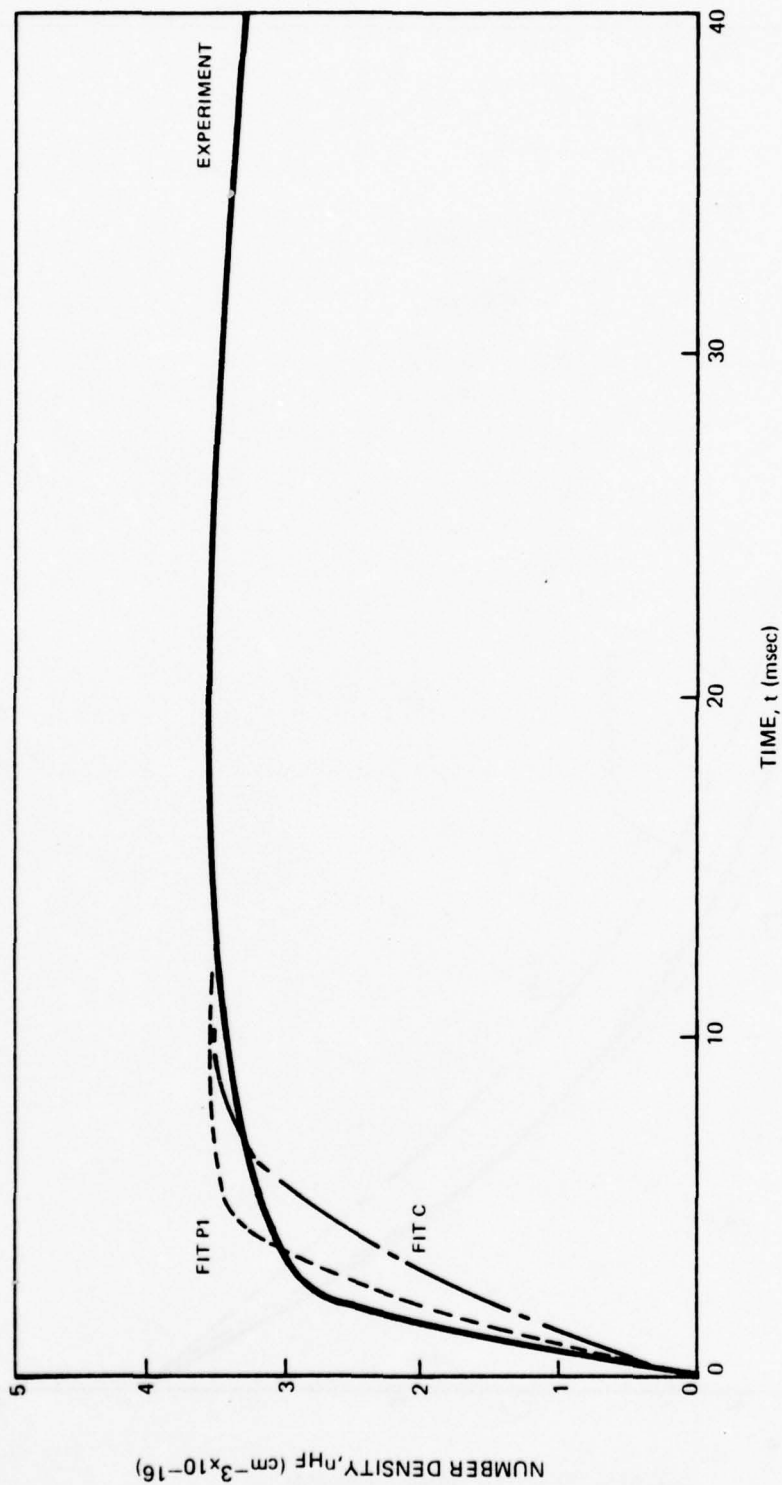


FIGURE 82 COMPARISON OF MODEL WITH EXPERIMENT

ADJUSTED HF POPULATIONS

PULSE CASE C9

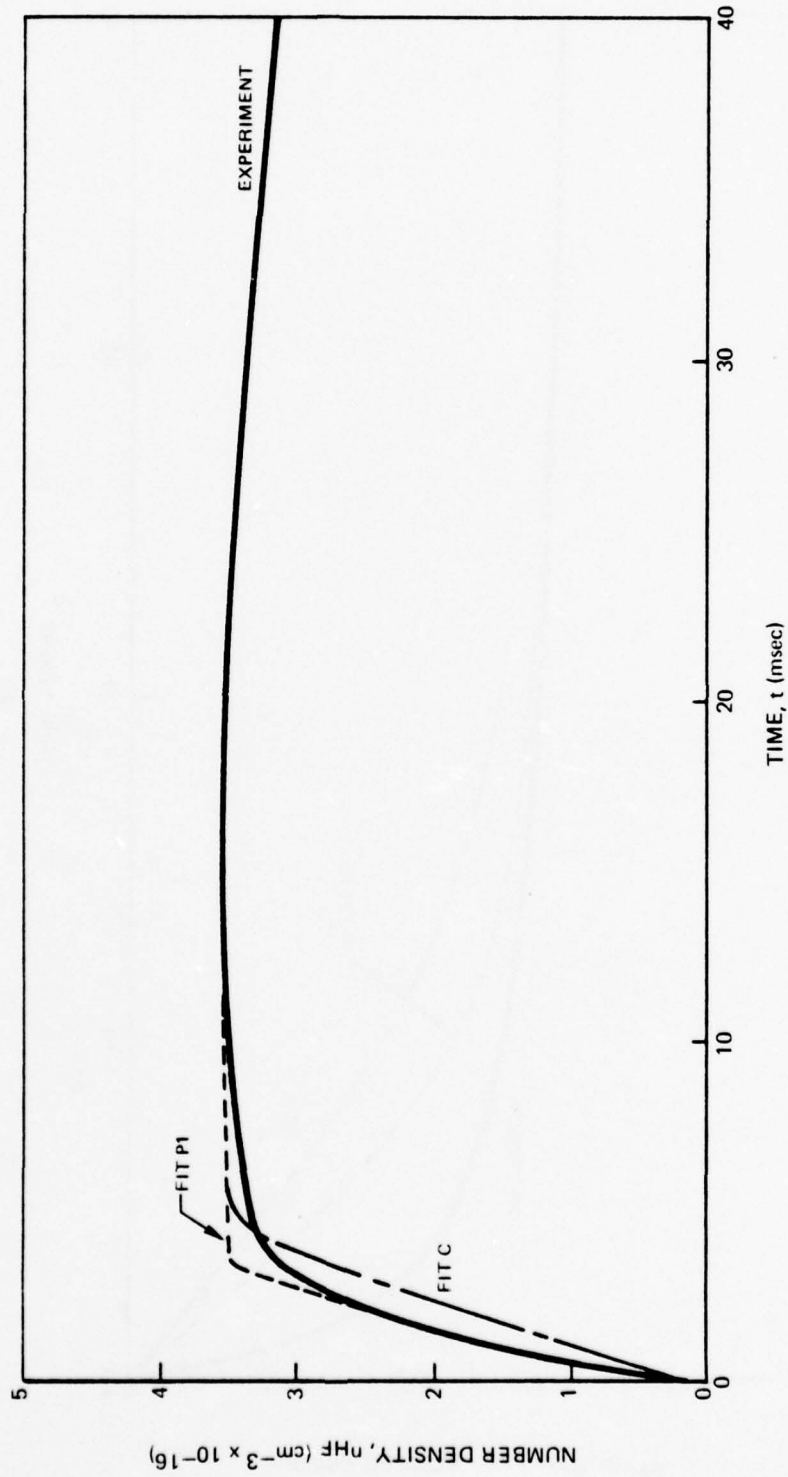


FIGURE 83 COMPARISON OF MODEL WITH EXPERIMENT

ADJUSTED HF POPULATIONS

PULSE CASE DH1

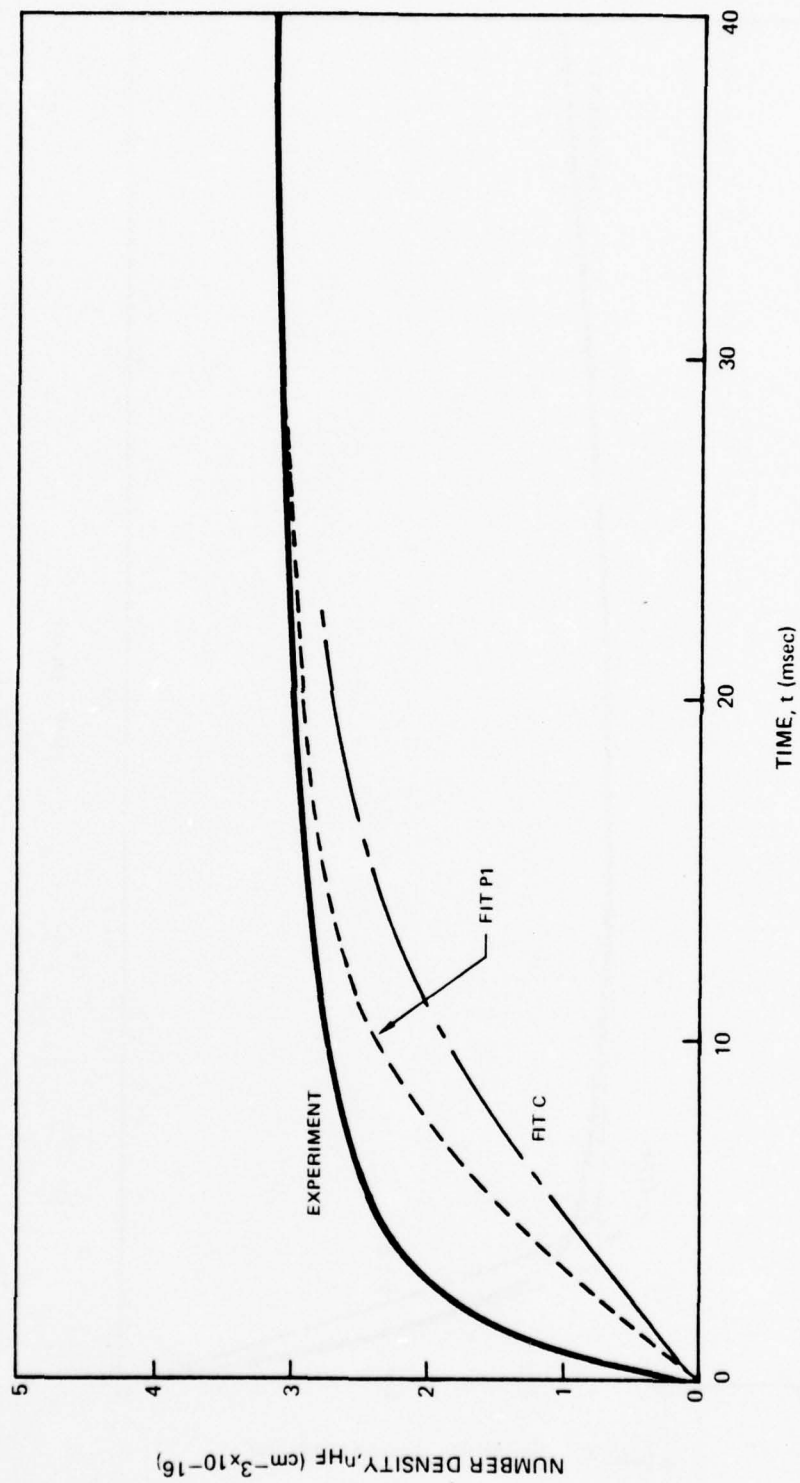


FIGURE 84 COMPARISON OF MODEL WITH EXPERIMENT

ADJUSTED HF POPULATIONS PULSE CASE DH7

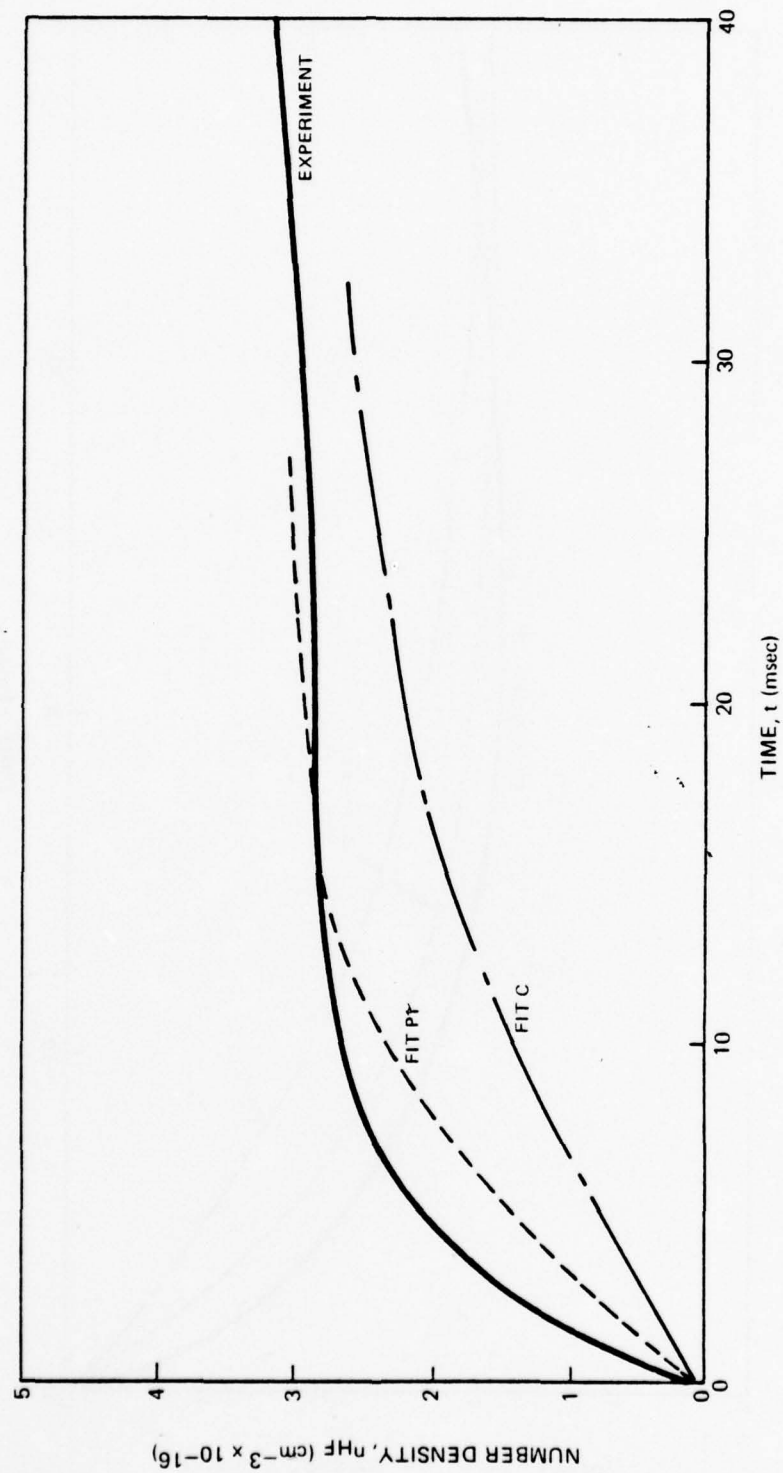


FIGURE 85 COMPARISON OF MODEL WITH EXPERIMENT

ADJUSTED HF POPULATIONS

PULSE CASE EF2

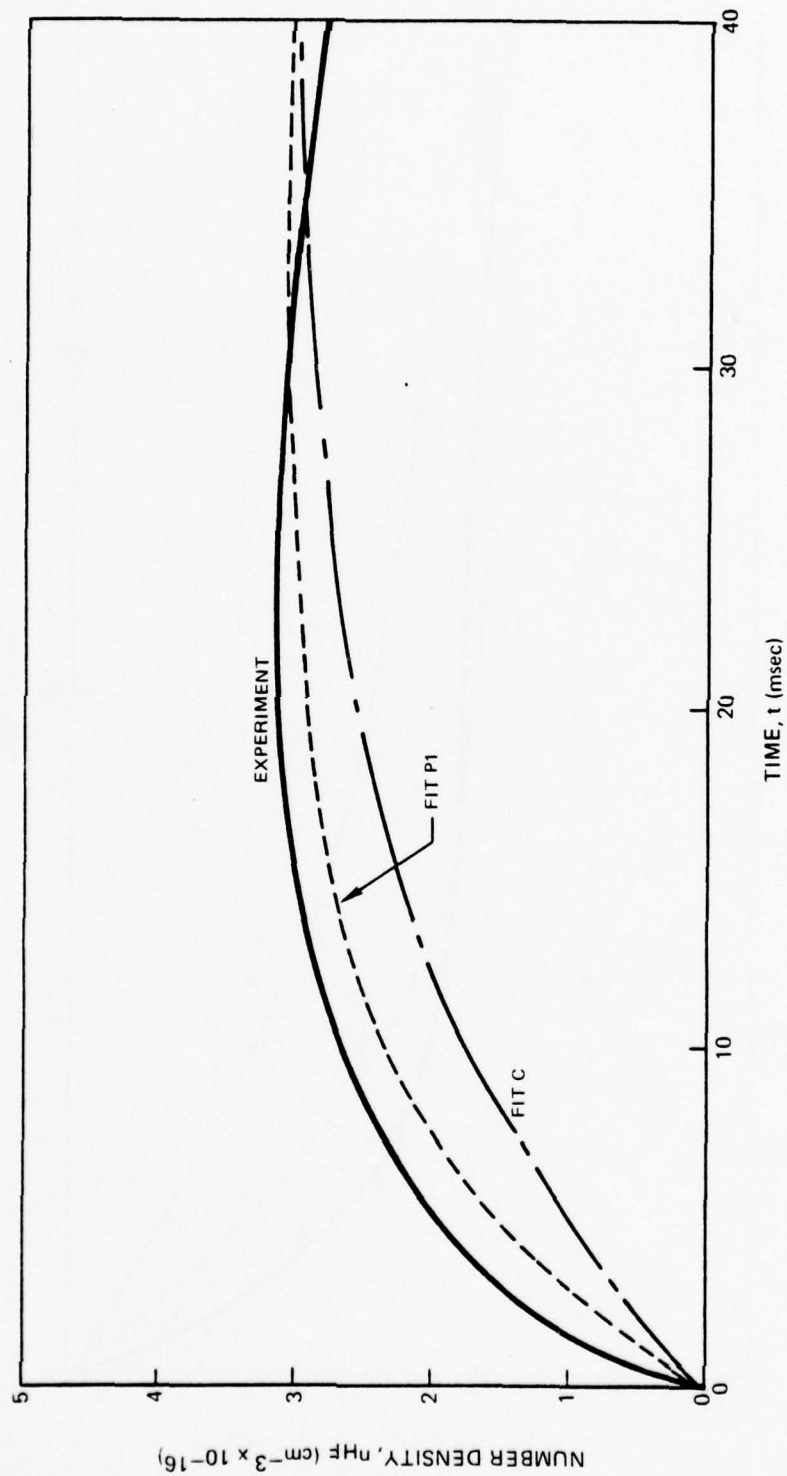


FIGURE 86 COMPARISON OF MODEL WITH EXPERIMENT

ADJUSTED HF POPULATIONS

PULSE CASE EF6

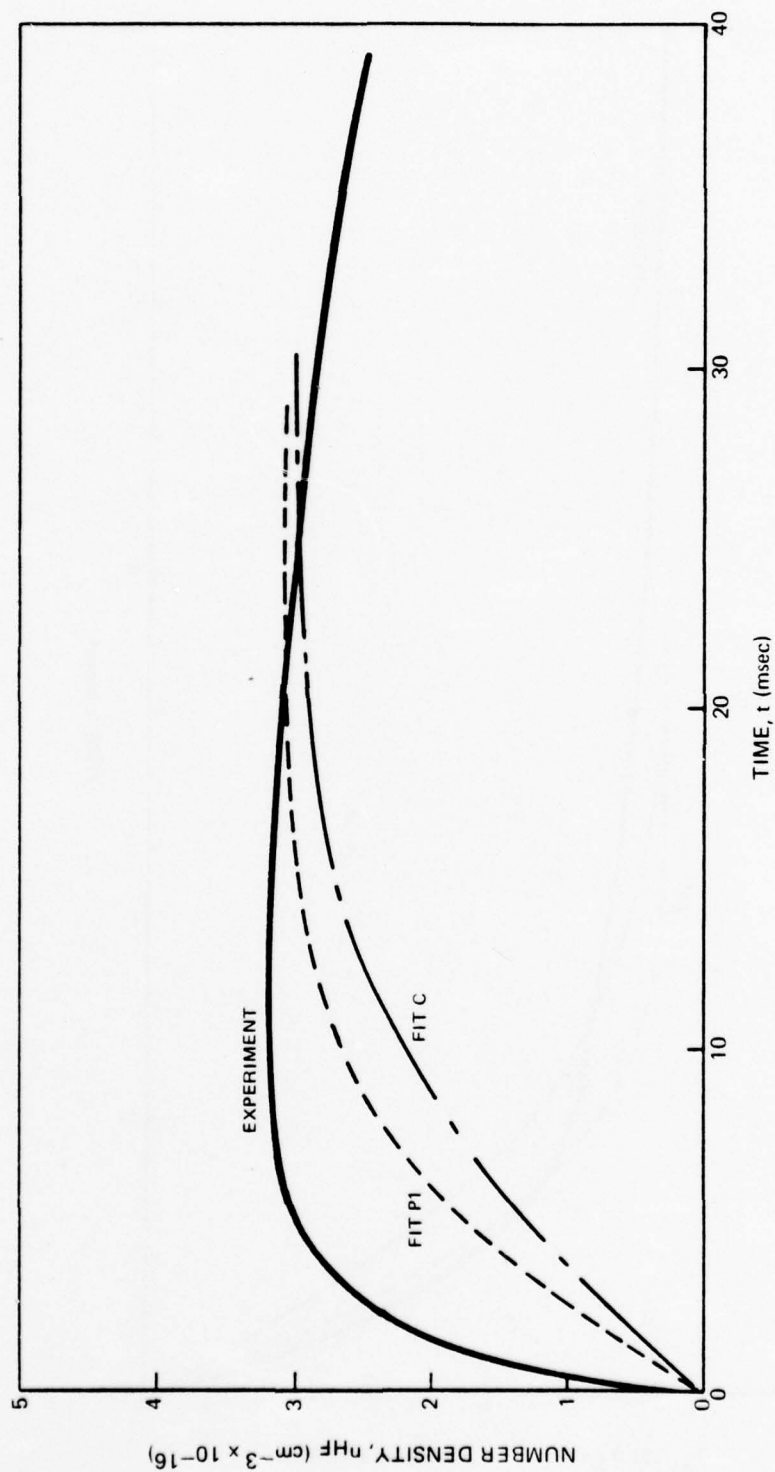


FIGURE 87 COMPARISON OF MODEL WITH EXPERIMENT

ADJUSTED HF POPULATIONS

PULSE CASE F7

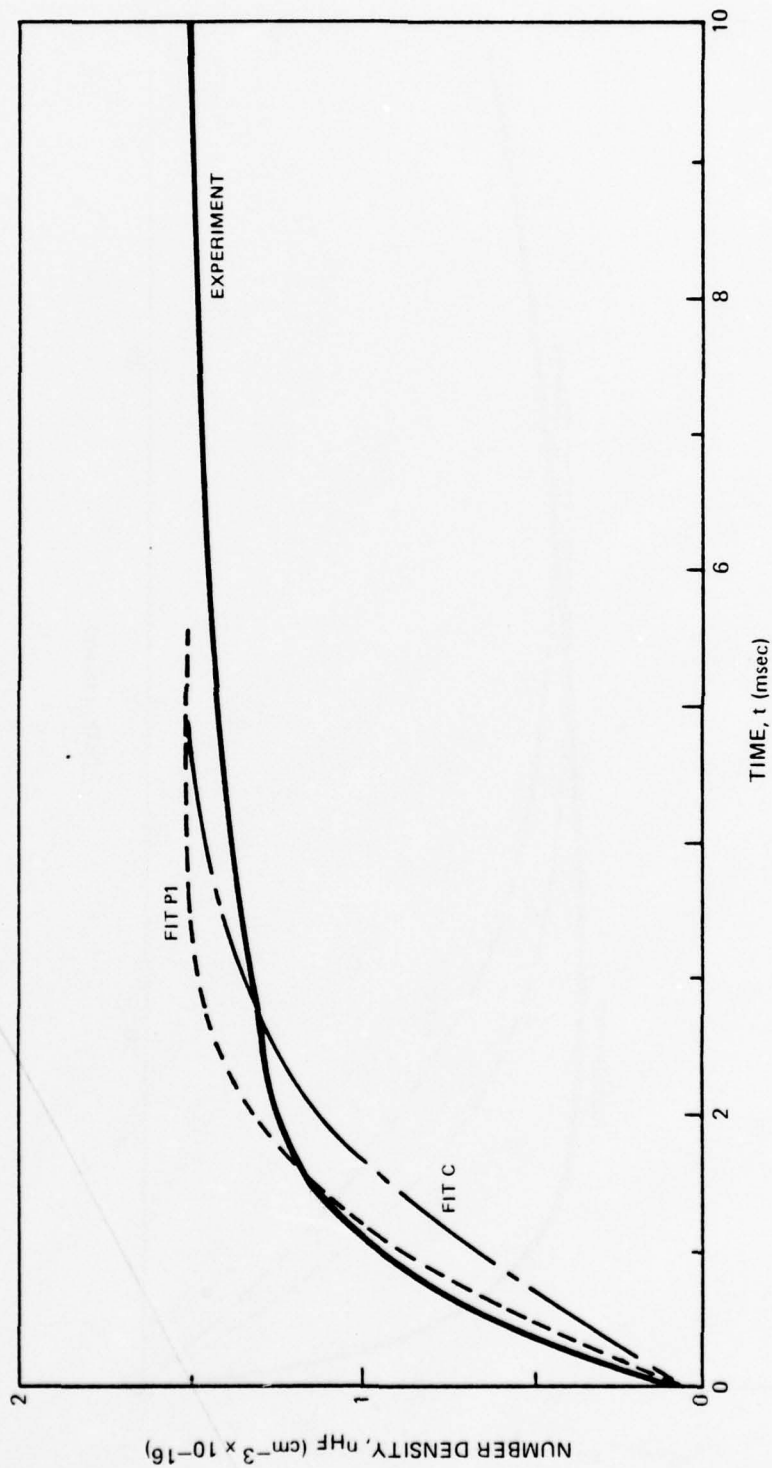


FIGURE 88 COMPARISON OF MODEL WITH EXPERIMENT

ADJUSTED HF POPULATIONS
PULSE CASE F11

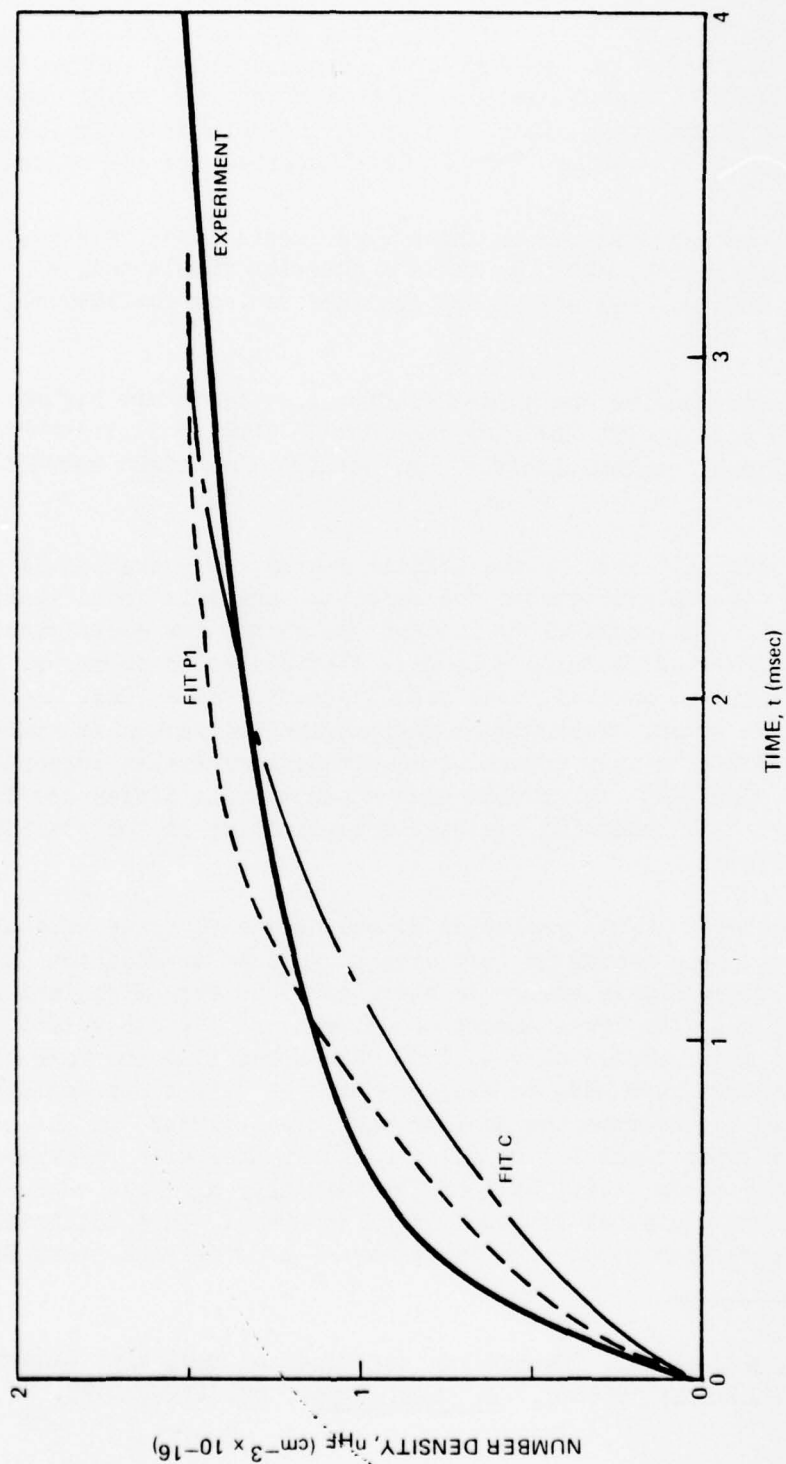


FIGURE 89 COMPARISON OF MODEL WITH EXPERIMENT

vs. 1 torr). If the data are to be believed this implies a nonlinear dependence of the overall HF production rate on F_2 concentration, in fact less than linear. A completely different reaction mechanism than the usual chain would be necessary. For example, F_2 might be playing the role of an inhibitor for some branching or hot atom effect that is less important as its concentration decreases.

There is not enough evidence in these experiments alone to strongly support such possibilities, although it is a question that should be addressed in the future. For now we are inclined to lack confidence in the series D and E data.

The rates indicated for the pulsed fluorescence tests are higher than can be reasonably used to fit the flow tube data. Thus it is instructive to try to find a rational explanation for that finding that might reconcile the difference.

One might infer that perhaps the initial F-atom concentration is somehow in error. If it were underestimated the resultant analysis would yield rates that were too fast. One possibility is that the absorption coefficient used to evaluate the number of fluorine molecules dissociated is in error. There is no reason to believe, however, that the literature value (Ref. 11) would be significantly in error. To invoke a chain branching mechanism would require rate coefficients many orders of magnitude larger than suggested by Sullivan et al. (Ref. 24) to provide even a perceptible difference in the model predictions. The remaining reasonable explanation is the possibility of hot F atom effects.

When one photon of 3471 \AA radiation dissociates a fluorine molecule, 54 percent of the photon energy is left over to go into translation of the fluorine atoms. These highly energetic atoms could be very efficient in dissociating more F_2 . The large amount of diluent, on the other hand, tends to moderate these atoms before they collide with other fluorine molecules. Some calculations have been made to evaluate such an effect approximately, but in a manner likely demonstrate the maximum possible influence on the results. It is assumed that upon dissociation all the excess energy is transferred to one of the fluorine atoms (i.e., half of the initially dissociated F atoms are "hot" with a translational temperature of 15000°K). In a collision of a fluorine molecule F_2 with a hot atom F^* we assume a 50 percent probability

-
24. Sullivan, J. H., et al., "Mechanisms and Types of Explosive Behavior In Hydrogen-Fluoride Systems," J. Chem. Phys., 62, 1714, 1975.

of dissociation. The maximum energy that can be transferred to the internal modes of the F_2 is $(m_{F_2}/(m_F + m_{F_2}))E_F^* = 2/3 (44.4 \text{ kcal/mole}) = 29.6 \text{ kcal/mole}$. This is some 8 kcal/mole below the dissociation energy of F_2 . Thus our assumption of a 50 percent probability per collision is not unreasonable (and likely too great). In competition with the dissociation collisions, the hot atoms are also thermalized by collisions with other molecules, in particular the diluent. The loss rate of F^* is taken to be equal to the collision rate of the F^* divided by the average number of collisions required to thermalize the 15000°K F atom. For He, seven collisions are required to reduce a hot atom's energy by 1/3, and for Ar three collisions are necessary. Fluorine atoms with energies that low would be expected to have quite low probabilities of dissociating F_2 . To be somewhat more conservative we have assumed that 10 collisions are necessary for He to thermalize hot F atoms, and five collisions are necessary for Ar. A calculation was performed for the case 0.2 torr H_2 , 1.0 torr F_2 , 50 torr He, with a pulse energy of 0.8 J. The result was an increase of 11 percent in the net number of atoms, yielding an equivalent increase in the net reaction rate.* Substitution of Ar for the He reduces this effect to virtually negligible, which is the primary reason the final tests were performed using Ar. Furthermore, the diluent pressure in the final tests is nearly 100 torr, thus reducing this hot atom effect still further. It is expected that the influence of highly energetic F atoms on the results of the final series of tests is at worst less than a few percent. Furthermore, any hot F atom effect of this sort would be contrary to the trend implied by the D and E series.

Hence, in the absence of a good new model that would reduce the surprisingly fast rate coefficients deduced, no one set of rates can be found to give a good fit to both the flow tube and pulsed fluorescence experiments. Thus we must assign a range of possible values:

$$\begin{aligned} 0.5 \times \text{nominal} < k_h < 1.3 \times \text{nominal} \\ \text{nominal} < k_c < 2.0 \times \text{nominal} \end{aligned}$$

If we pick values in the middle of these ranges we have

$$\begin{aligned} k_h &\approx .9 \times \text{nominal} \\ k_c &\approx 1.5 \times \text{nominal} \end{aligned}$$

which are the values used in the compromise fit C.

* Results were similar for a pulse energy of 0.4J.

Vibrational Deactivation

Preliminary calculations performed under Task I indicated that the most important deactivation mechanisms in need of study were HF self deactivation (VT and VV) and H-atom deactivation. Support for this emphasis was provided by work at Aerospace Corporation indicating that VT deactivation scales rapidly with vibrational quantum number (Kwok, Ref. 25), and that H atoms are a strong deactivator of HF for $v \geq 3$ (Bott, Ref. 26).

Flow Tube

Use of the original rate package (Appendix A) led to predicted vibrational population distributions far too great for the higher lying levels. Thus it was necessary to revise the vibrational rate package. The computer code CHEMLZ was modified to allow for arbitrary scaling of all V-V and V-T transitions with vibrational quantum number. Provision was also made for multiquanta V-T transitions for all colliding species, and for alternative single quantum V-V models in lieu of that normally in use.

Modifications to the rate package were guided primarily by the findings of Kwok (Ref. 25) and Bott (Ref. 26 and 27). Kwok has found that the rate of disappearance of excited HF scales as $v^{2.3}$. Bott has found that the deactivation of HF by H atoms is slower than our nominal values for $v = 1$ and 2, but considerably faster for $v = 3$.

One rate package tried employed the $v^{2.3}$ scaling on all single quantum V-T transitions. In addition the net deactivation rates by H-atoms for $v = 1, 2$, and 3 were revised to match Bott's values. The temperature dependence and relative probabilities to the various lower levels given by

-
25. Kwok, M., "Studies of the Vibrational Relaxation of Upper Levels of HF ($v \leq 6$) in a Large Diameter, Medium Pressure Flow Tube," presented at the TriService Chemical Laser Symposium, Kirtland AFB, NM, February 1976.
 26. Bott, J. F. and R. F. Heidner III, "A Study of the Vibrational Deactivation of HF ($v = 3$) by H Atoms," presented at the TriService Chemical Laser Symposium, Kirtland AFB, NM, February 1976.
 27. Heidner, R. F. III and J. F. Bott, "Vibrational Deactivation of HF ($v = 1$) and DF ($v = 1$) by H and D Atoms," J. Chem. Phys., 63, 1810, 1975.

Wilkins (Refs. 28 and 29), however, were maintained. This required multiplying the nominal $v = 1$ rate coefficient by 0.049, the $v = 2$ rate coefficients by 0.072, and the $v = 3$ rate coefficients by 3.62. On the assumption that all deactivation above $v = 3$ is rapid, all H-atom rate coefficients for $v > 3$ are also multiplied by 3.62. Similarly, all F atom multiquanta rates were multiplied by 3.3 to bring the 1-0 transition rate into agreement with the value suggested by Cohen (Ref. 30).

Application of these changes to the rate package yielded surprisingly good agreement on the vibrational distributions for the four basic cases (1-4) of the flow tube experiment. Somewhat better agreement was achieved by modifying the V-T formalism slightly. Consider a case in which transitions from a level v are equally probable to all lower levels ($v-1$, $v-2$, ..., 0). Suppose each individual transition scales linearly with v . Then the net rate of disappearance from each level would be proportional to v^2 . The net loss rate of quanta, however, would be considerably greater than for a single quantum process.

Such a multiquanta model was applied to all collision partners except H and F atoms, which already included multiquanta transitions with probabilities apportioned according to the theoretical work of Wilkins. The net rates for the H atom interactions were again revised to reflect Bott's measurements as described above.

To achieve the best fit with the model as formulated in the computer code it was found that the V-V model normally employed could be used if the transitions were scaled with $v^{-1/2}$ rather than v . With such scaling, exothermic transitions of the type $(v, v') \rightarrow (v-1, v'+1)$ are roughly independent of v and diminish slowly with v' . This is a consequence of changes in energy defect for the various transitions. In summary the rate package selected as the best fit to the flow tube data includes the following changes: H atom

-
28. Wilkins, R. L., "Monte Carlo Calculations of Reaction Rates and Energy Distributions Among Reaction Products $H + HF(v) \rightarrow H_2(v') + F$ and $H + HF(v) \rightarrow HF(v') + H$," J. Chem. Phys., **58**, 3038, 1973.
 29. Wilkins, R. L., "Monte Carlo Calculations of Reaction Rates and Energy Distributions Among Reaction Products. IV. $F + HF(v) \rightarrow HF(v') + F$ and $F + DF(v) \rightarrow DF(v') + F$," J. Chem. Phys., **59**, 698, 1973.
 30. Cohen, N. and J. F. Bott, "A Review of Rate Coefficients in the H_2-F_2 Chemical Laser System," SAMSO Report, TR-76-82, Aerospace Corporation, 1976.

rates scaled according to the measurements of Bott; multiquanta V-T transitions individually scaled linearly with v ; and V-V transitions scaled with $v^{-1/2}$. The comparison with experiment for run conditions 1 through 4 are shown in Figures 90 through 109. At first the calculations were performed allowing the model to predict the HF development as well as the vibrational distributions. It was decided, however, that since the actual streamwise HF variation is known from the experimental measurements, and since HF self deactivation is so important, error in fitting the vibrational distribution could be minimized by specifying the measured HF development. The resultant predicted vibrational distributions are also shown in Figures 90 through 109. Indeed the fit to the data is improved. There is, however, a tendency in cases 3 and 4 for the model to over predict deactivation in the latter stages of the flow (Ports 4 and 5).

One shortcoming of the model is its apparent inability to predict the vibrational distribution at early stages of the flow, in particular at the first port location ($x = 4$ cm). In the earlier discussion of chemical reaction rates the possibility of the presence of some HF initially was presented. If we were to consider such a possibility now, the agreement at $x = 4$ improves considerably. This is illustrated in Figure 110 for run condition 3 with an initial mole fraction of 0.00015 of HF (see Figs. 42 and 49). This figure should be compared with Figure 100. The match for vibrational levels 0, 1, and 2 is vastly improved. Similar results hold true for cases 1, 2, and 4. At later ports the vibrational distributions are comparable with those previously predicted.

Thus we see that if recirculation in the mixing region of the flow tube does result in increased concentrations of HF initially the set of vibrational rates selected gives good agreement with experiment at all measurement locations.

An interesting consequence of the changes to the vibrational rate package is that the rapid V-T rates employed render the comparisons of the model with experiment relatively insensitive to the scaling of the single-quantum V-V rates in the model. Previously it had been thought that the long-range V-V model employed in CHEMLZ would have to be drastically changed to avoid the severe anharmonic pumping and total inversions on high vibrational levels that had been predicted in the Task I studies. To avoid this possibility the transition probabilities were scaled differently with v , for example, as $v^{-1/2}$ rather than the typical linear scaling. This reduced upper level transition probabilities bringing them more in line with current thinking

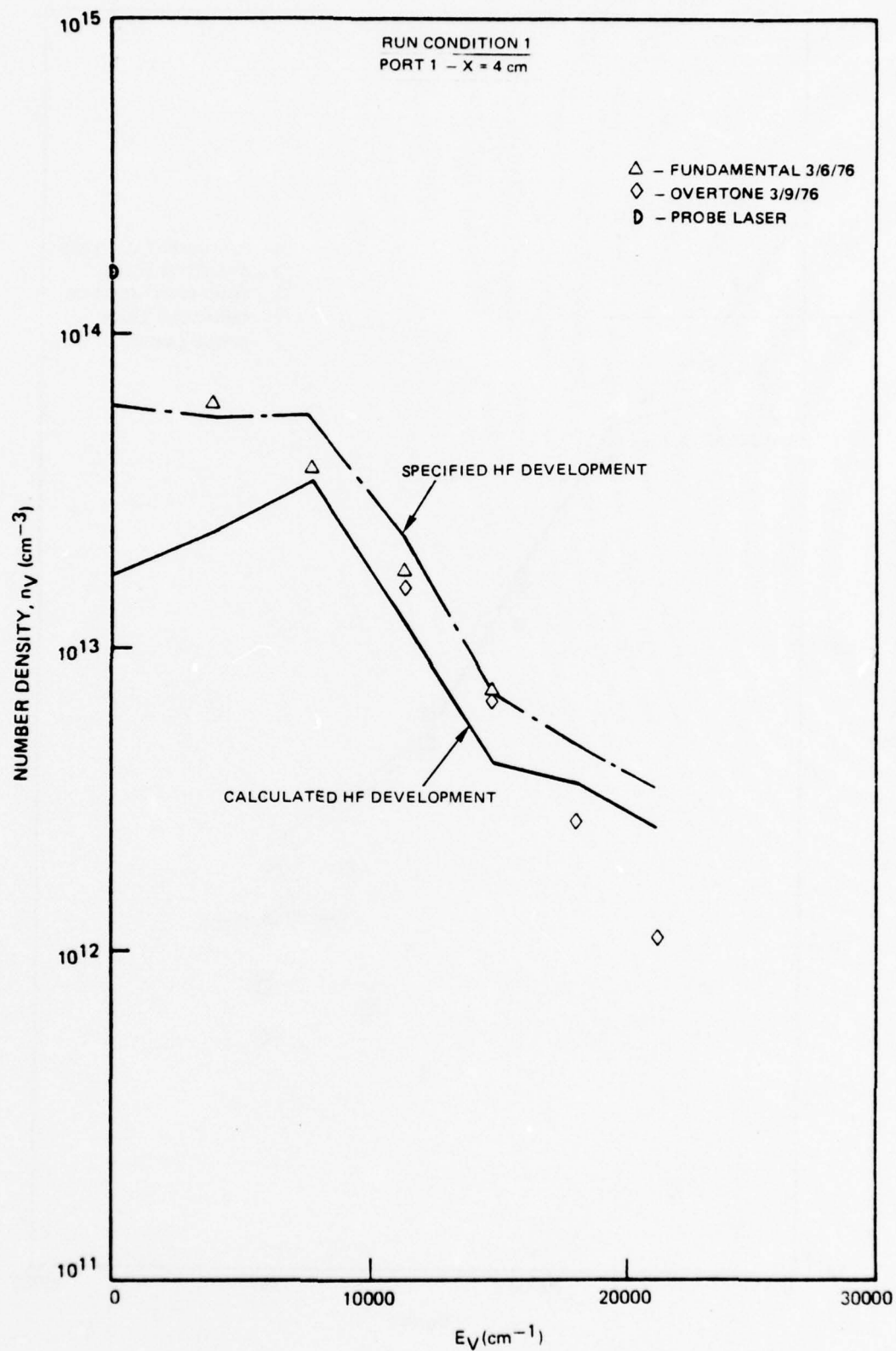


FIGURE 90 COMPARISON WITH MODEL

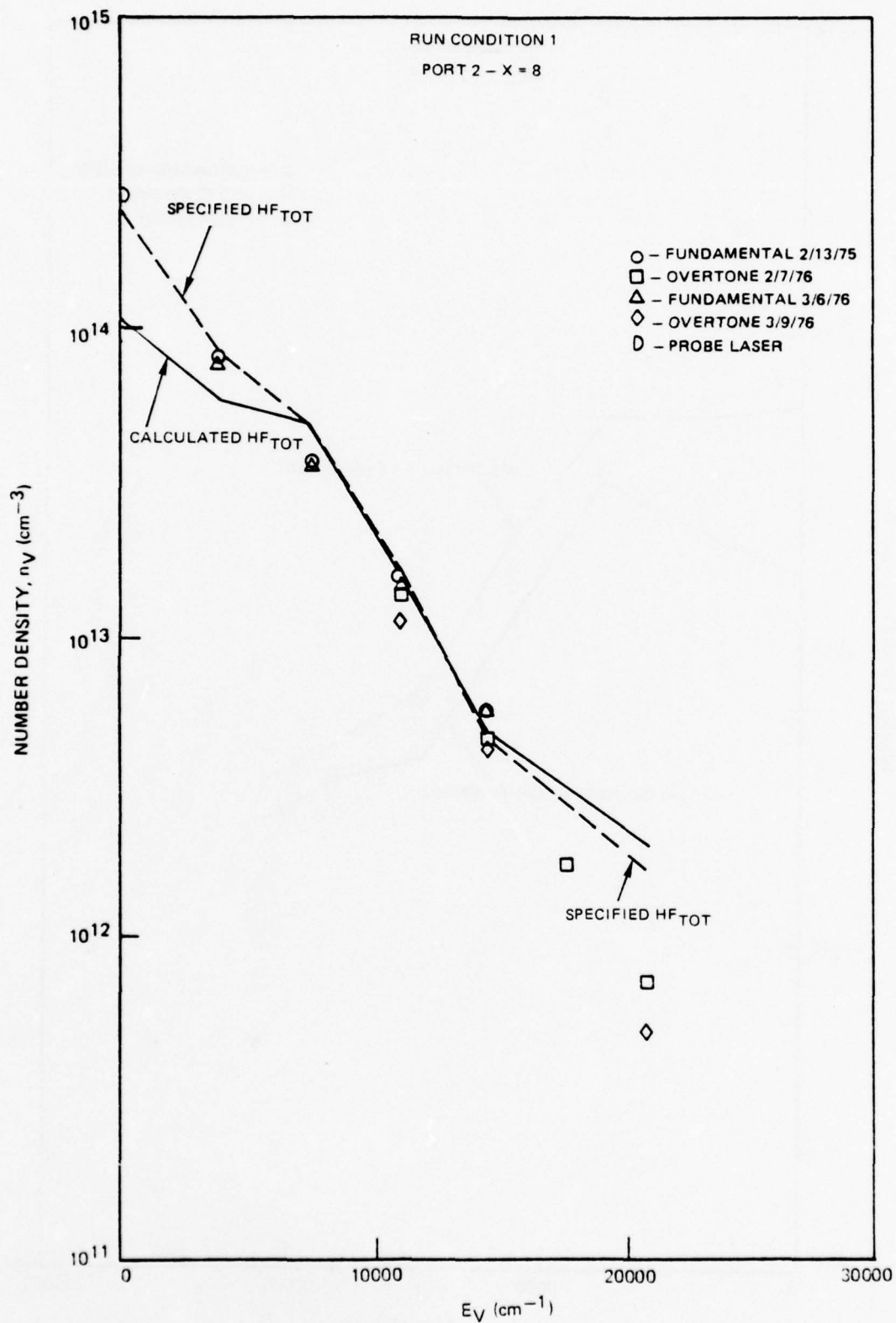


FIGURE 91 COMPARISON WITH MODEL

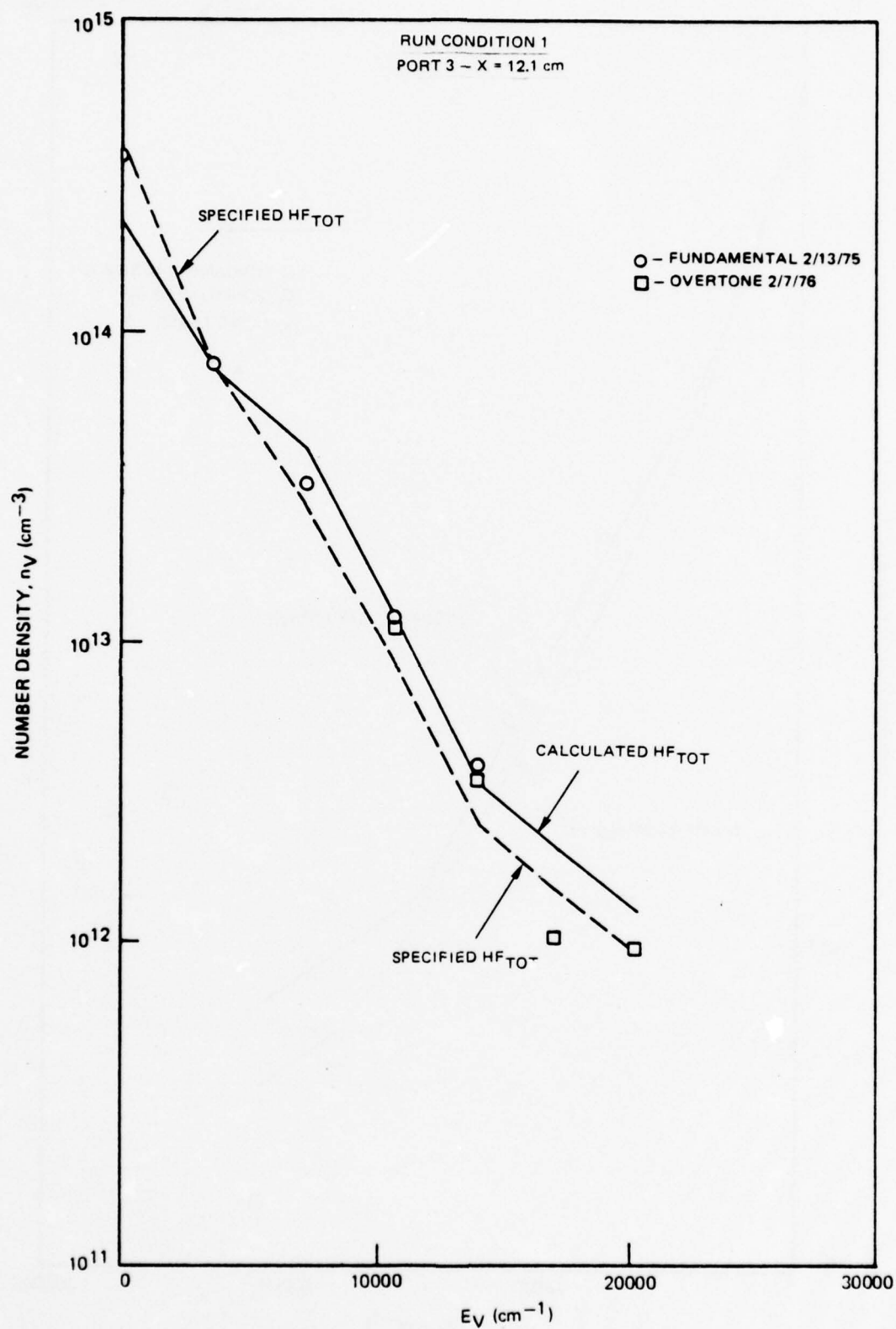


FIGURE 92 COMPARISON WITH MODEL

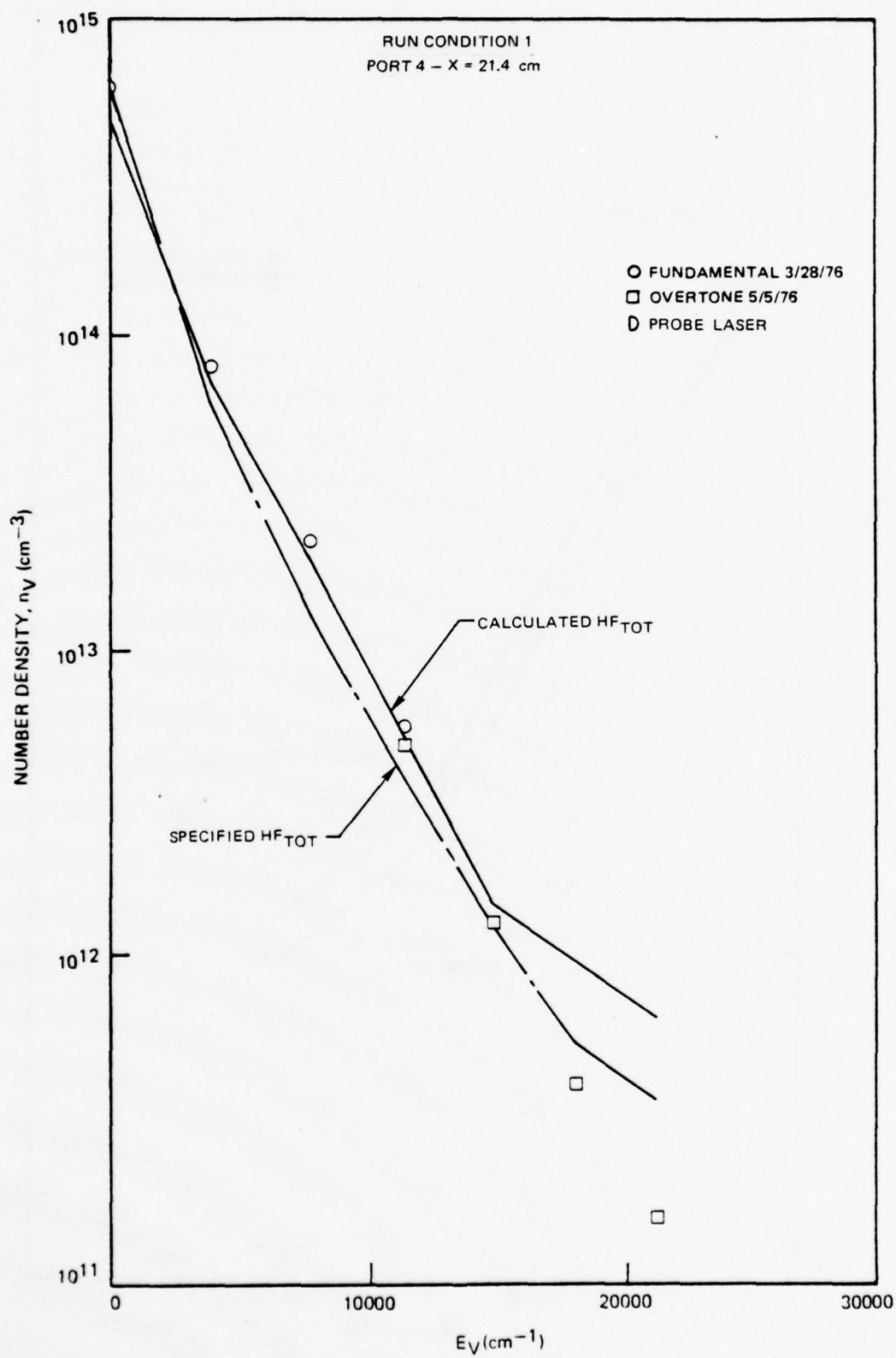


FIGURE 93 COMPARISON WITH MODEL

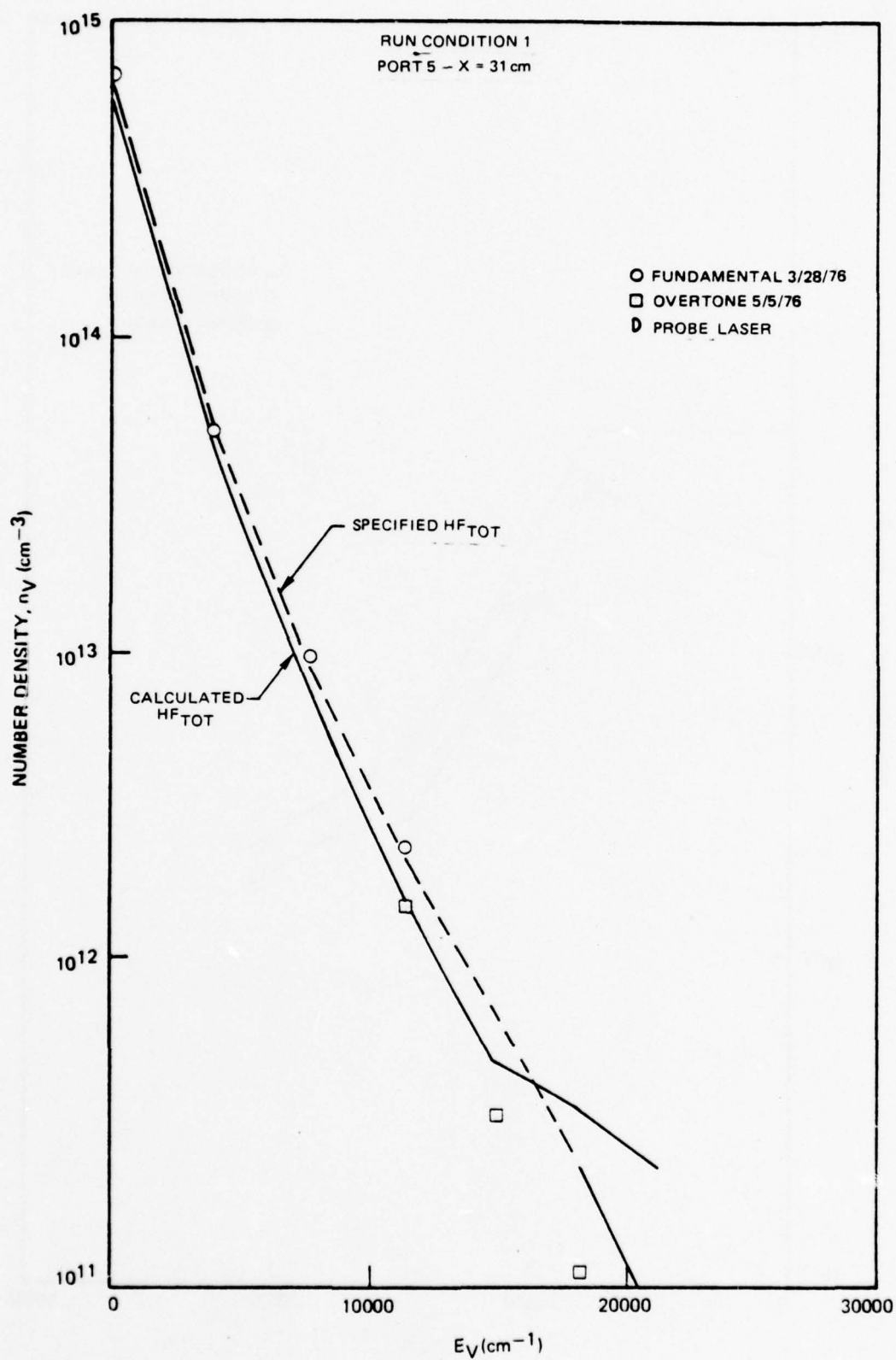


FIGURE 94 COMPARISON WITH MODEL

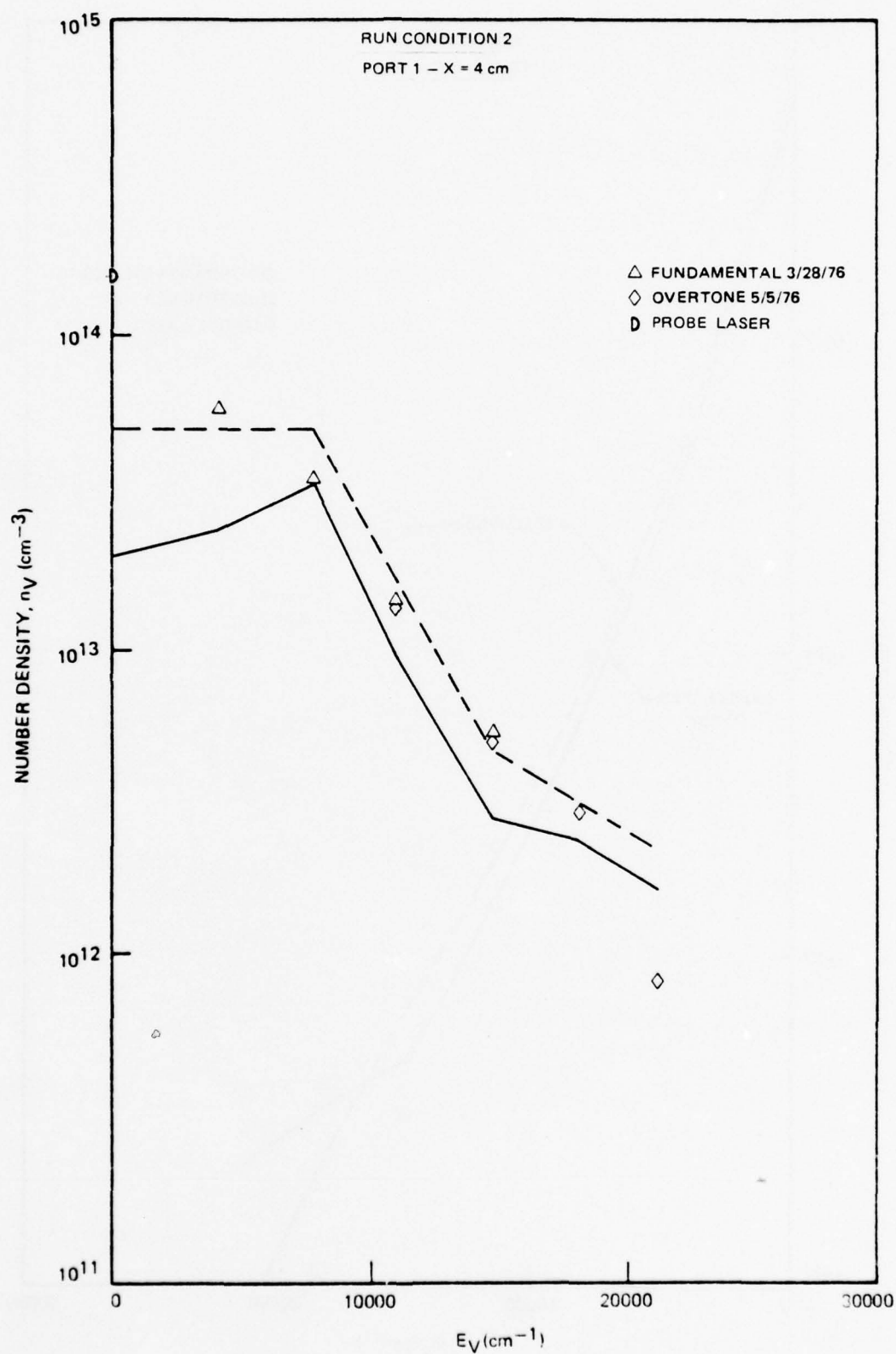


FIGURE 95 COMPARISON WITH MODEL

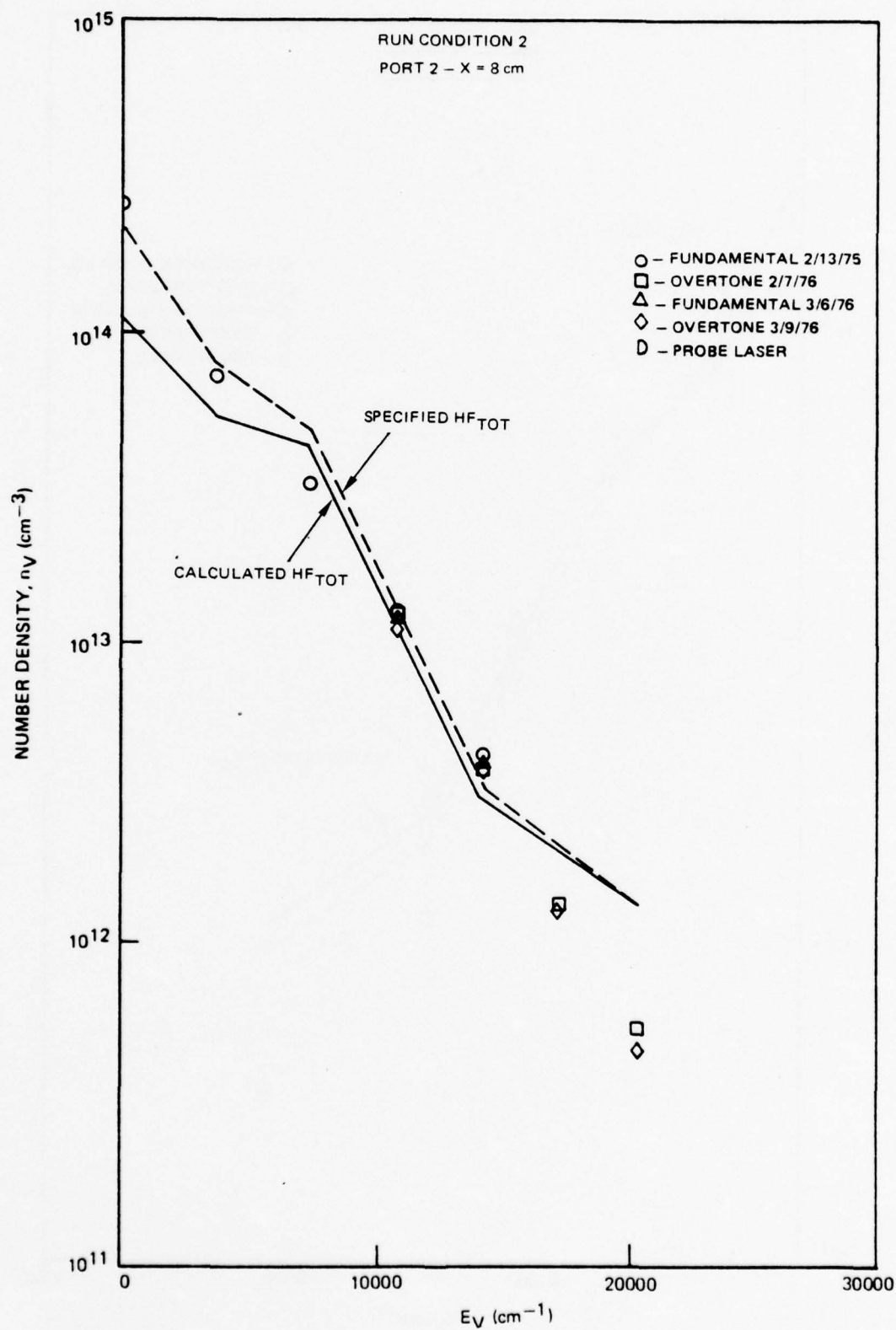


FIGURE 96 COMPARISON WITH MODEL

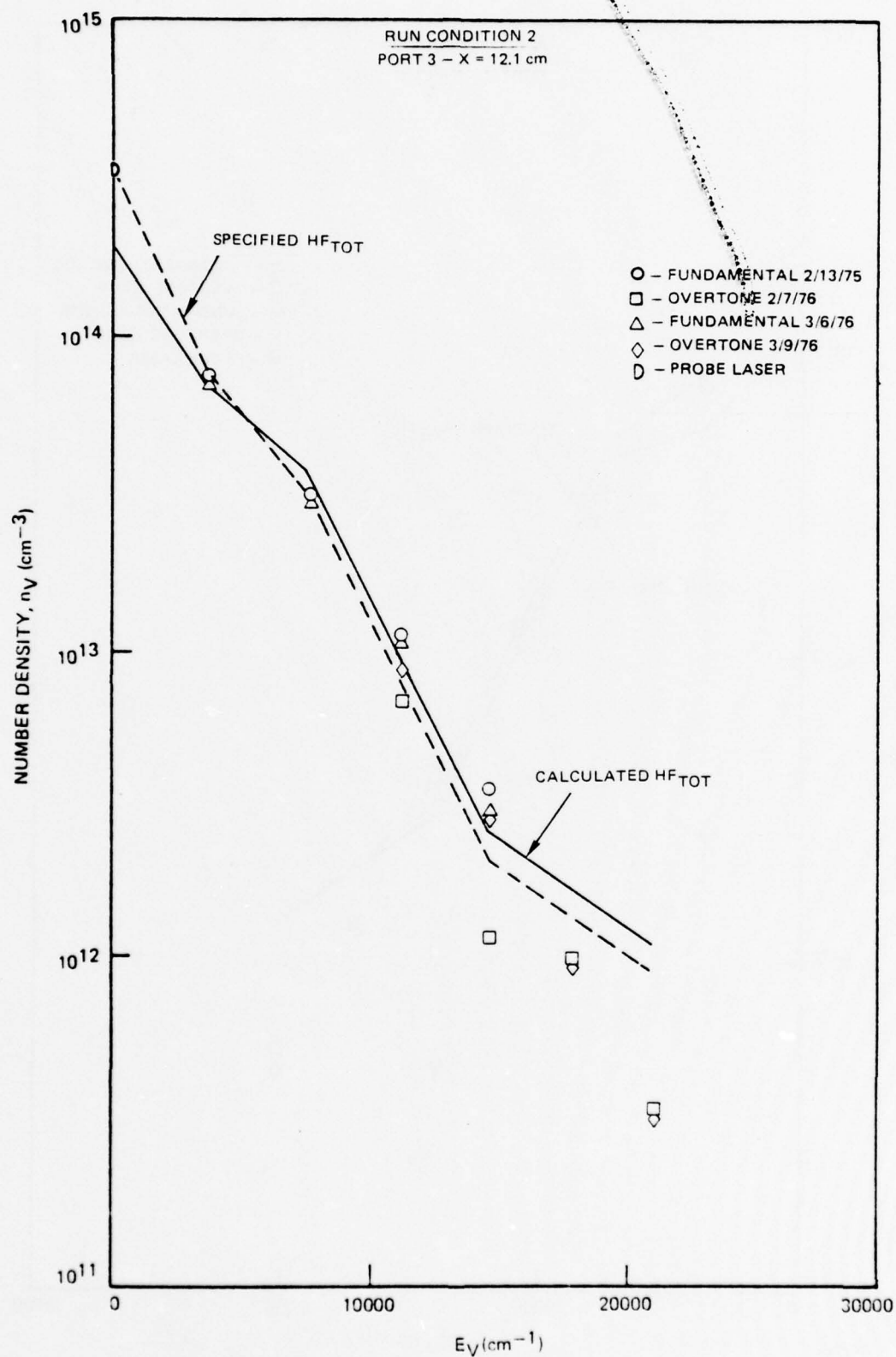


FIGURE 97 COMPARISON WITH MODEL

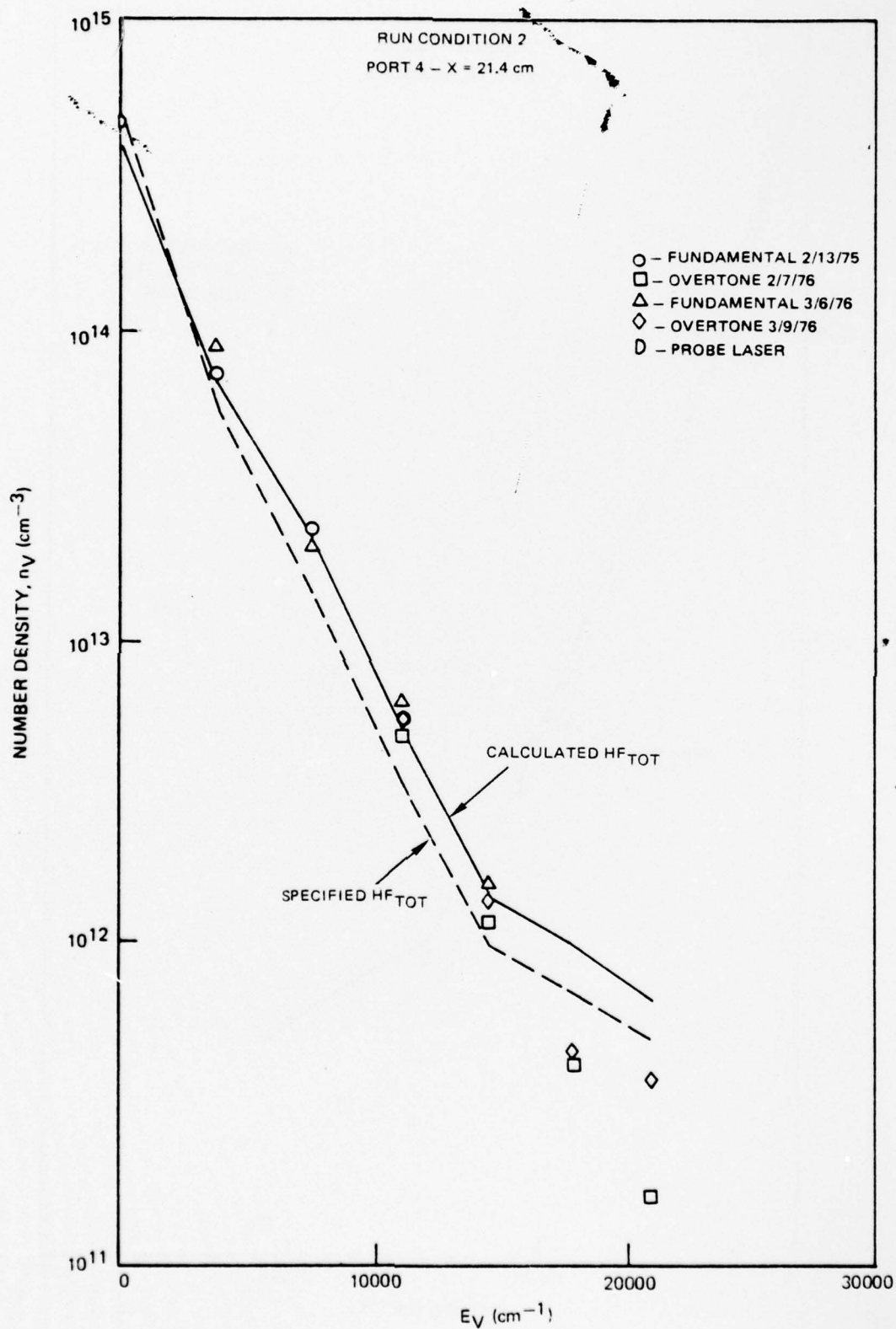


FIGURE 98 COMPARISON WITH MODEL

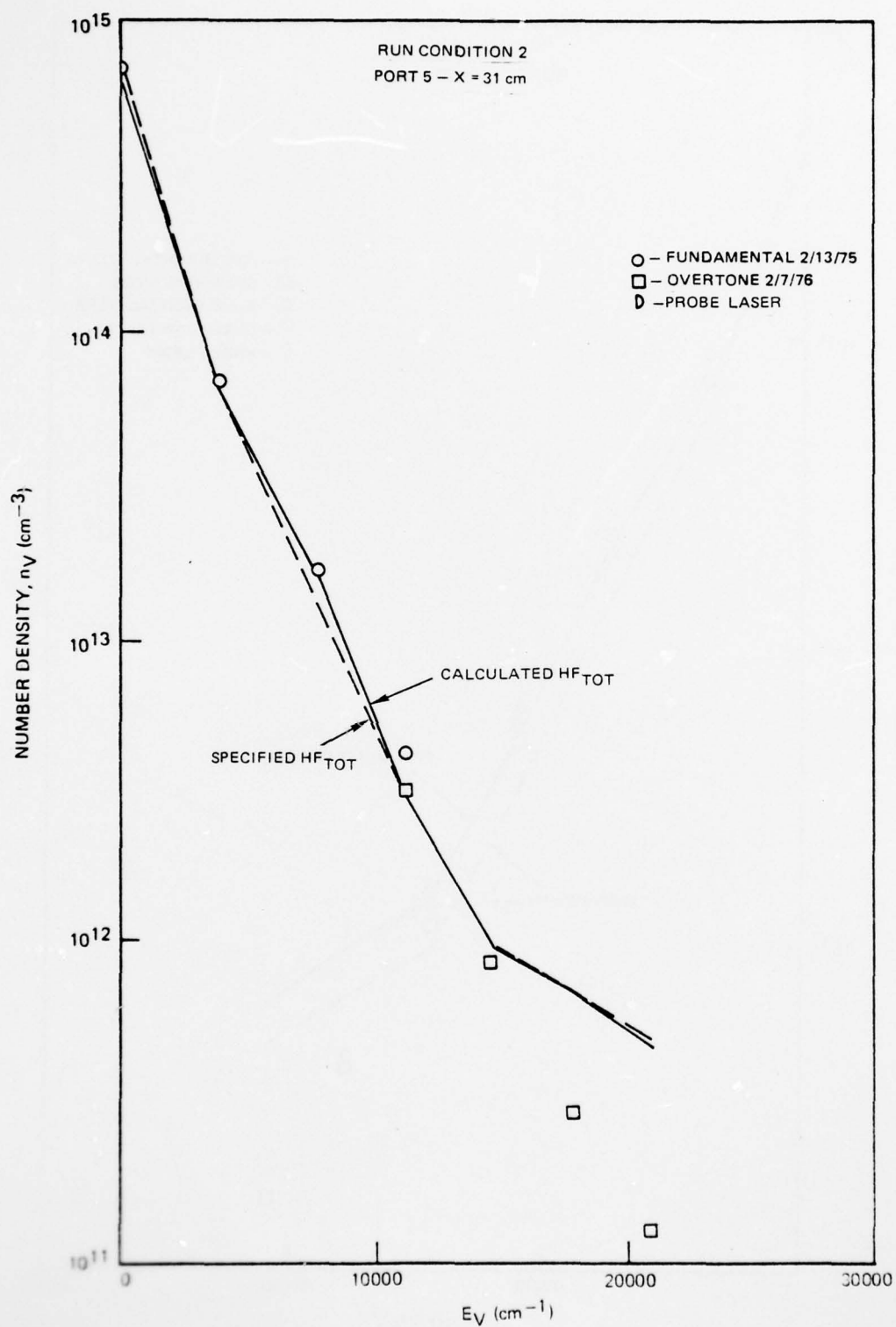


FIGURE 99 COMPARISON WITH MODEL

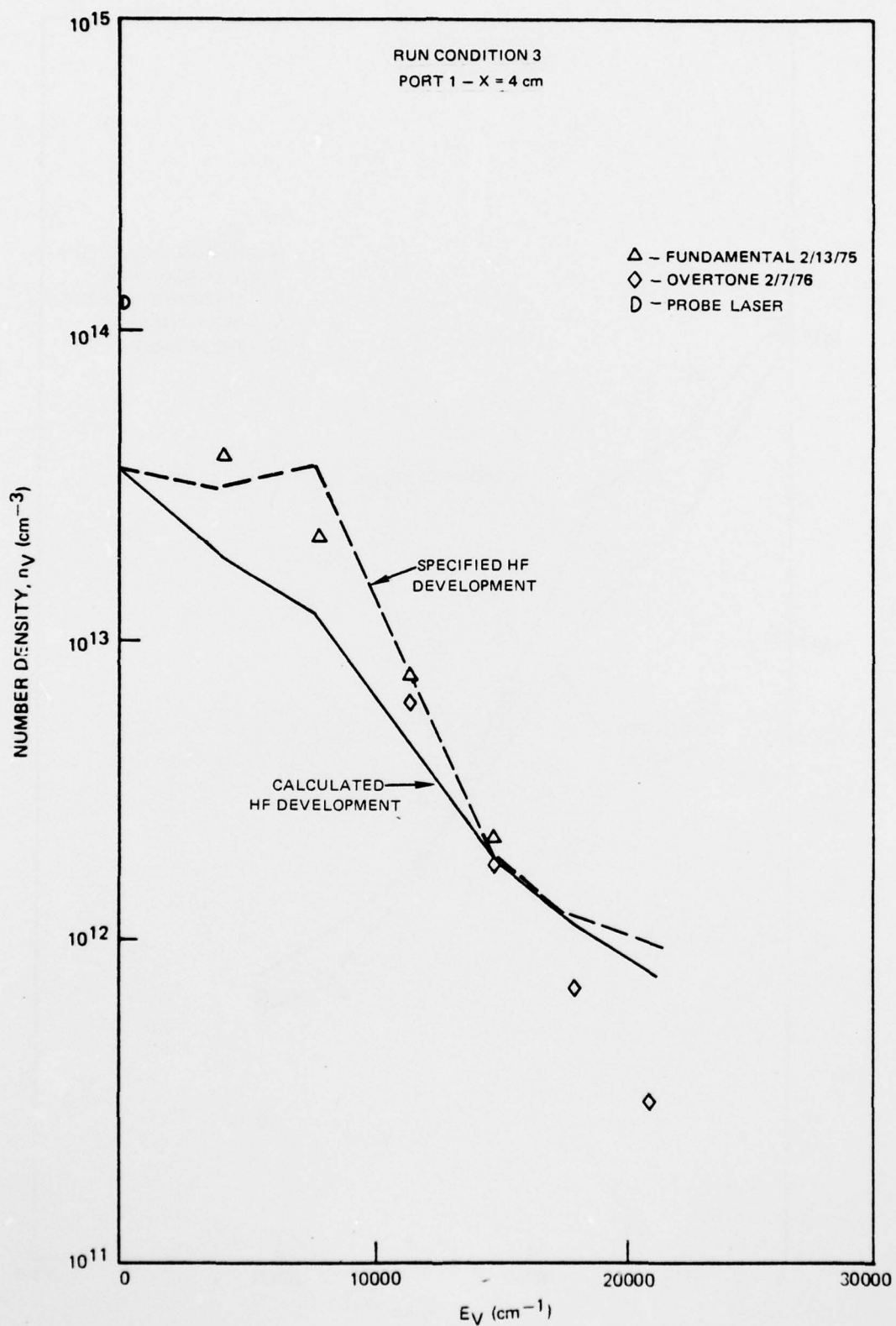


FIGURE 100 COMPARISON WITH MODEL

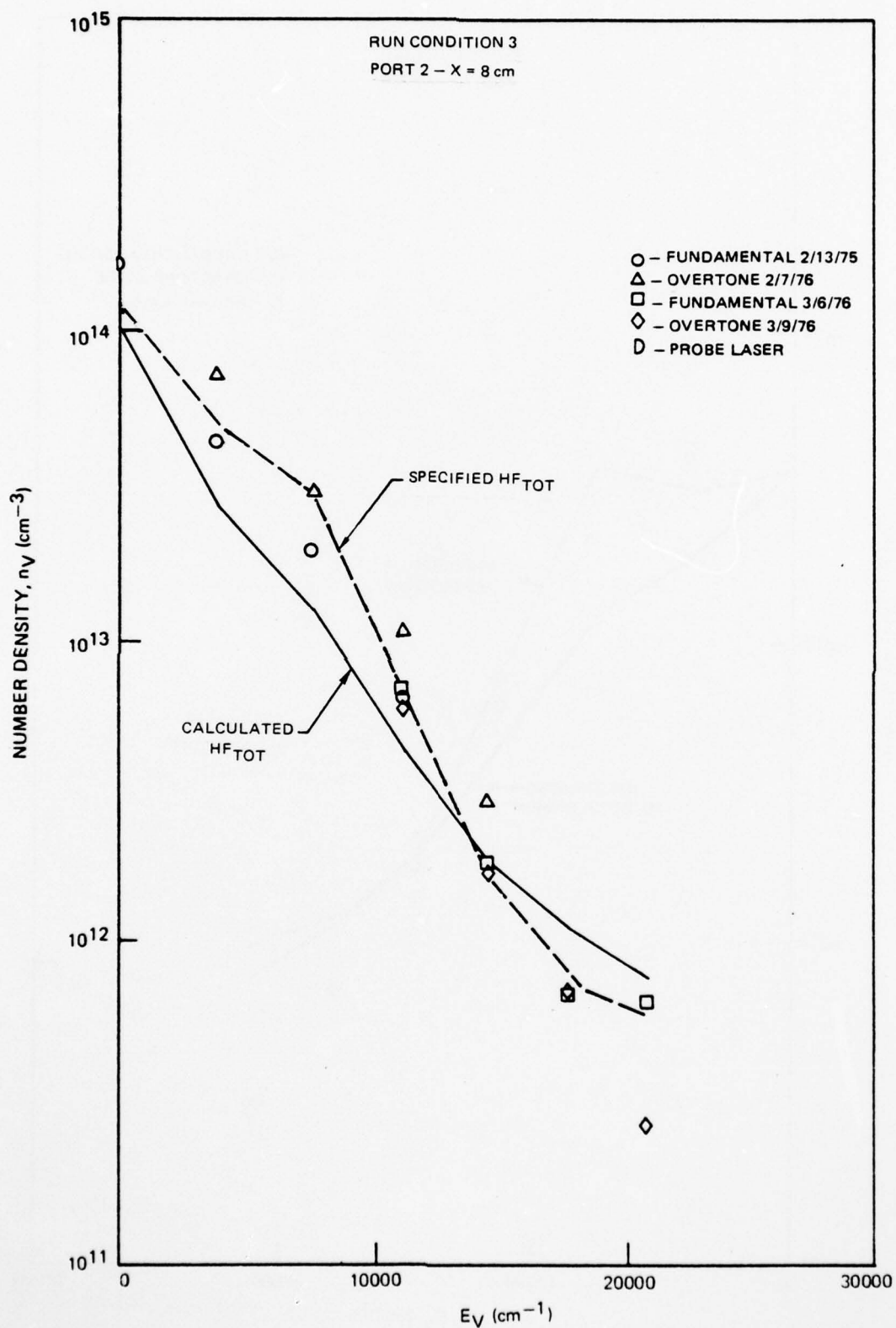


FIGURE 101 COMPARISON WITH MODEL

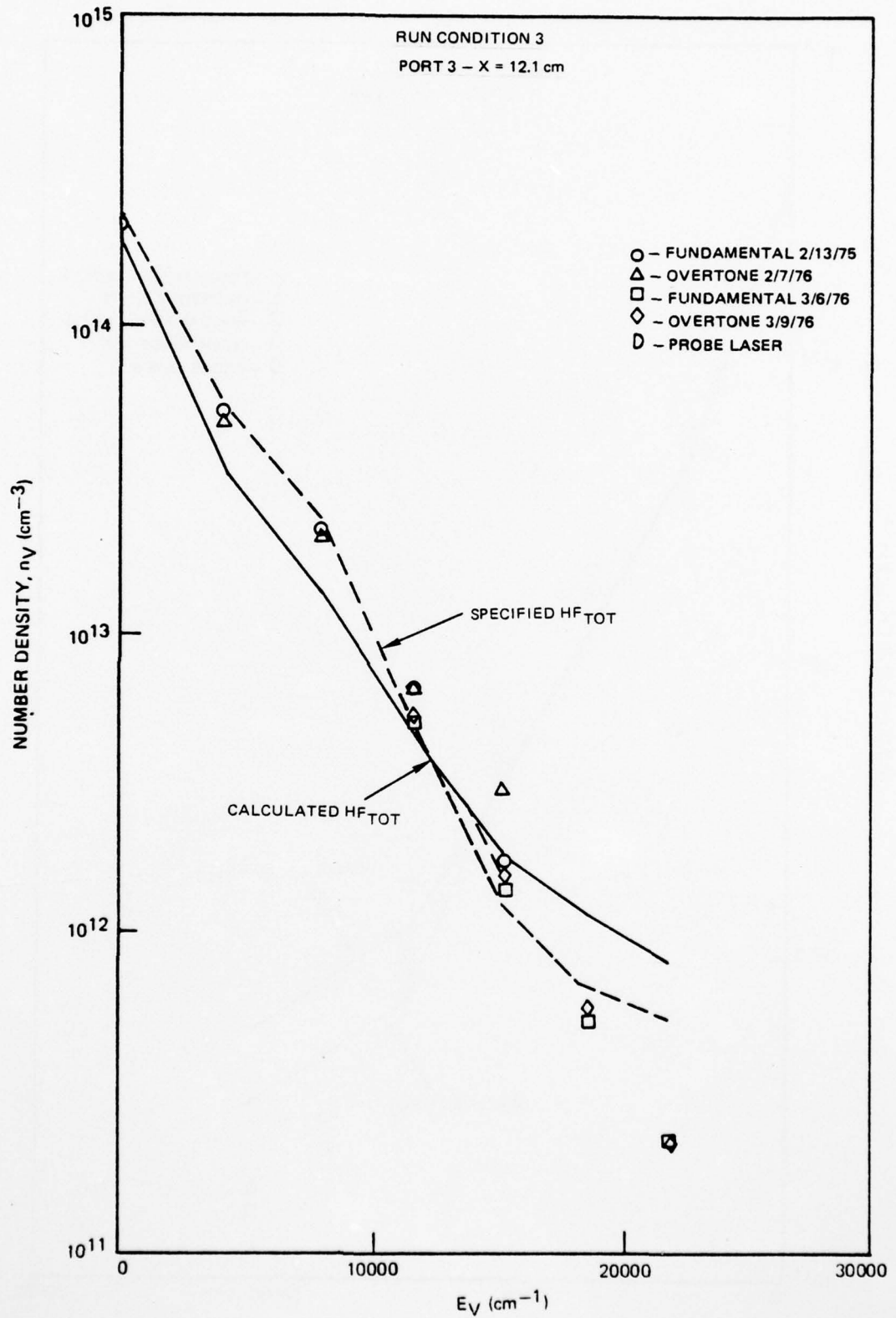


FIGURE 102 COMPARISON WITH MODEL

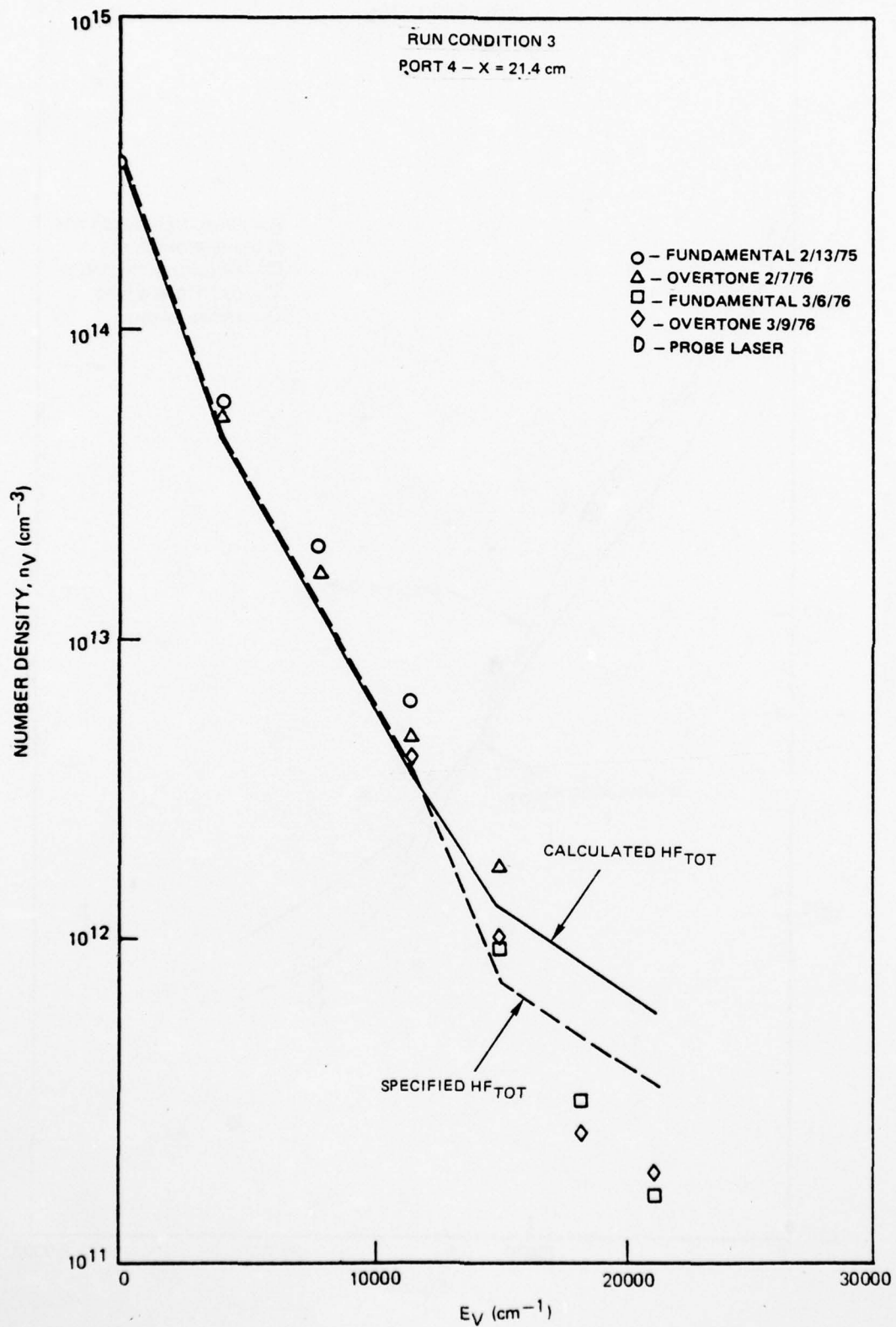


FIGURE 103 COMPARISON WITH MODEL

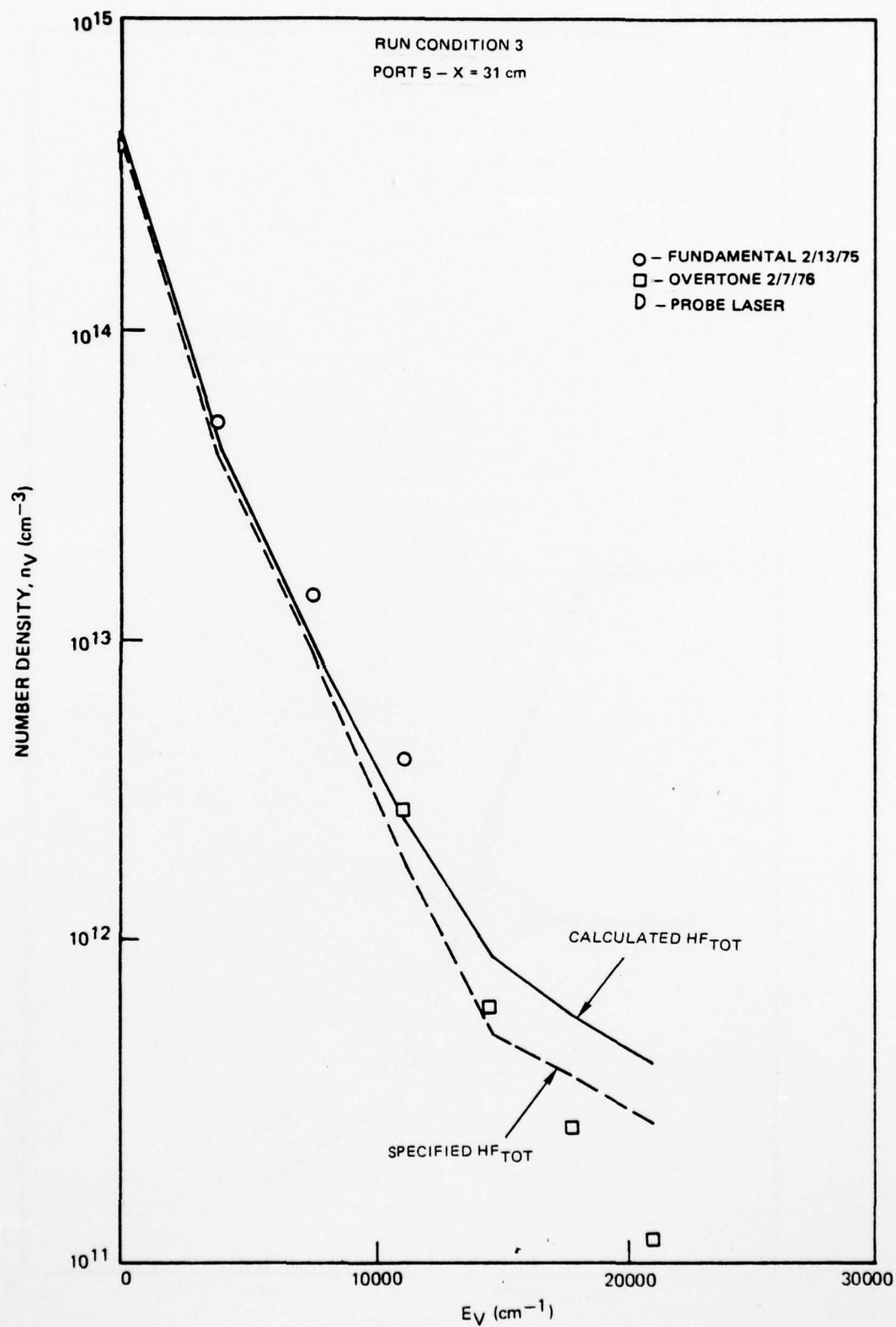


FIGURE 104 COMPARISON WITH MODEL

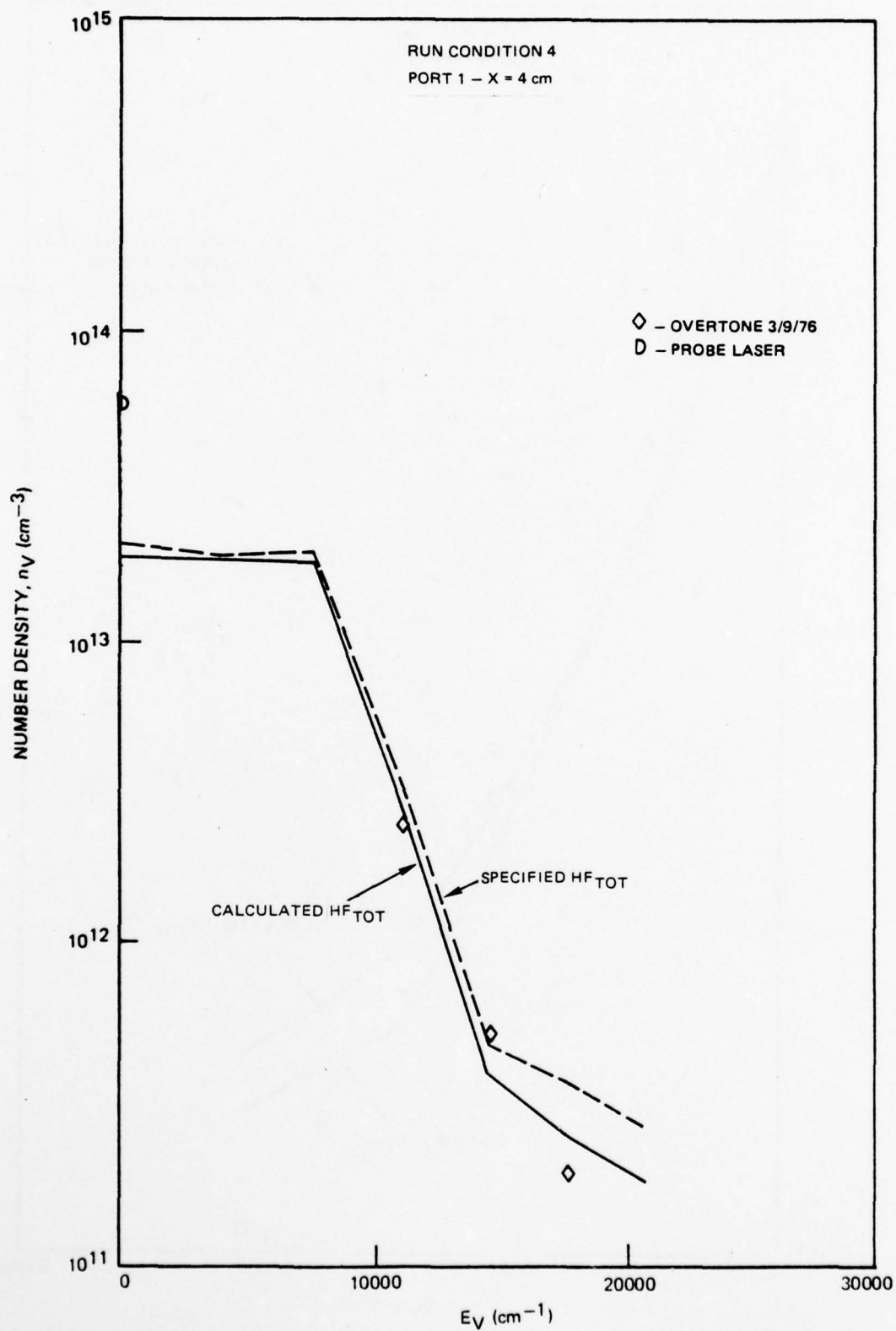


FIGURE 105 COMPARISON WITH MODEL

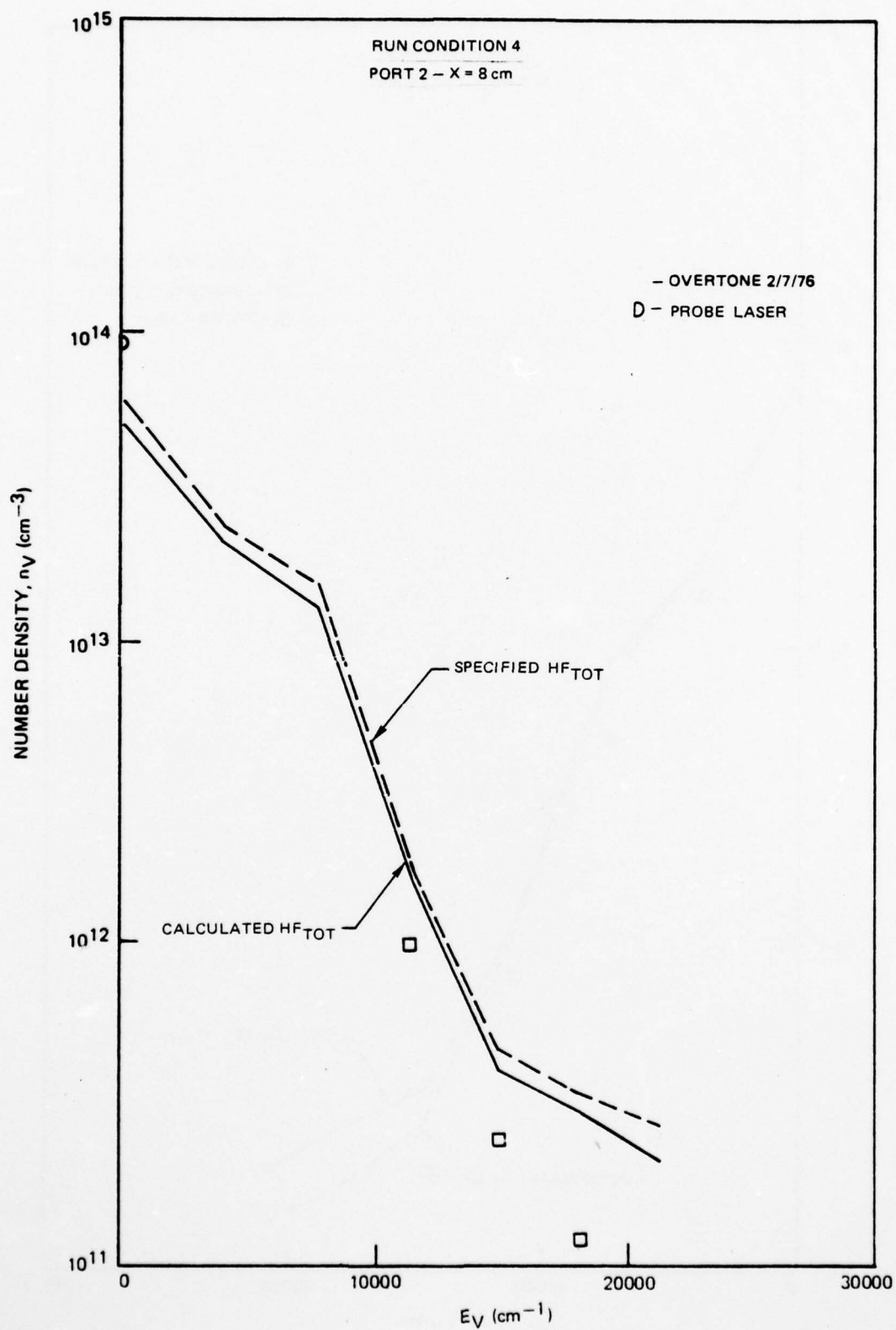


FIGURE 106 COMPARISON WITH MODEL

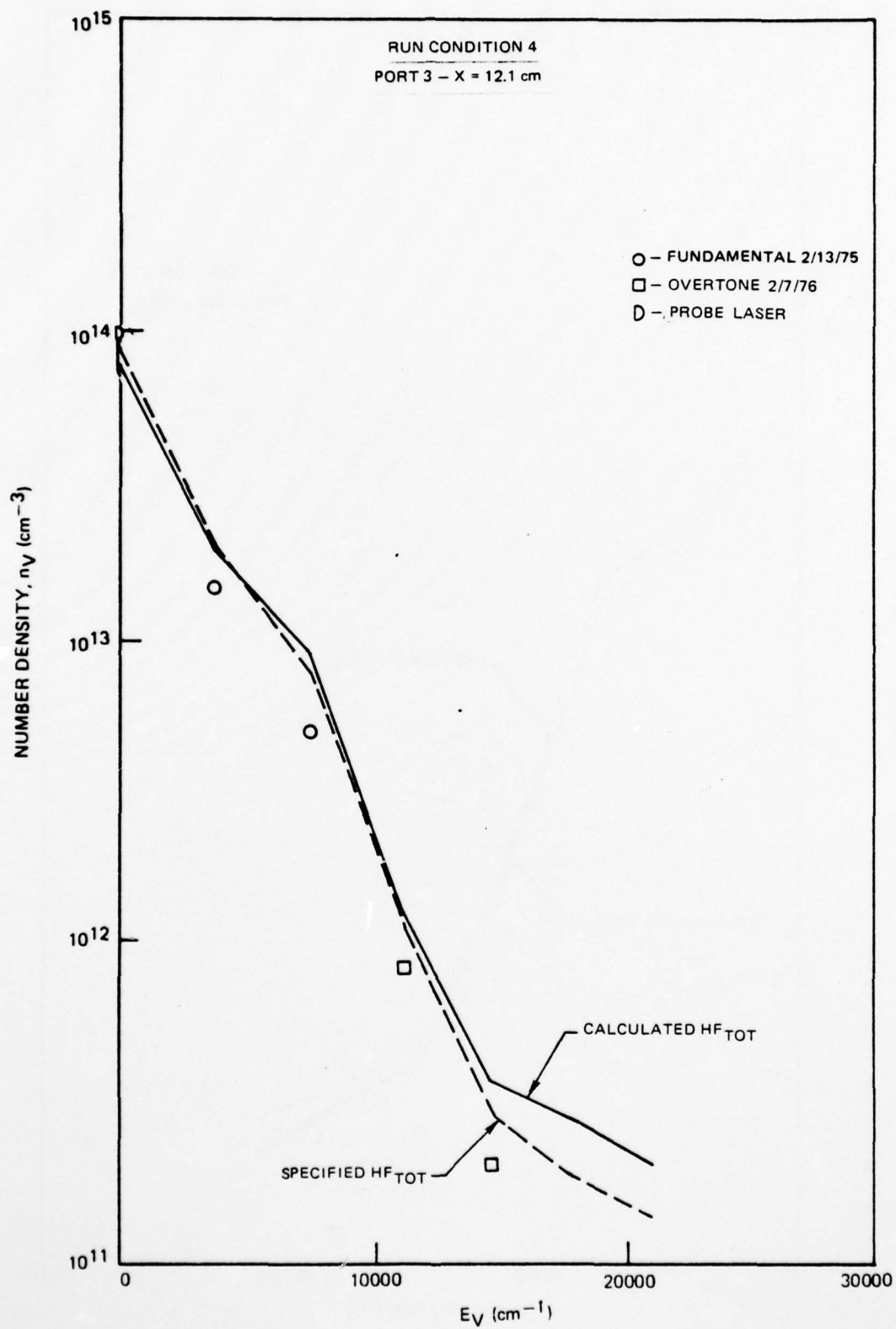


FIGURE 107 COMPARISON WITH MODEL

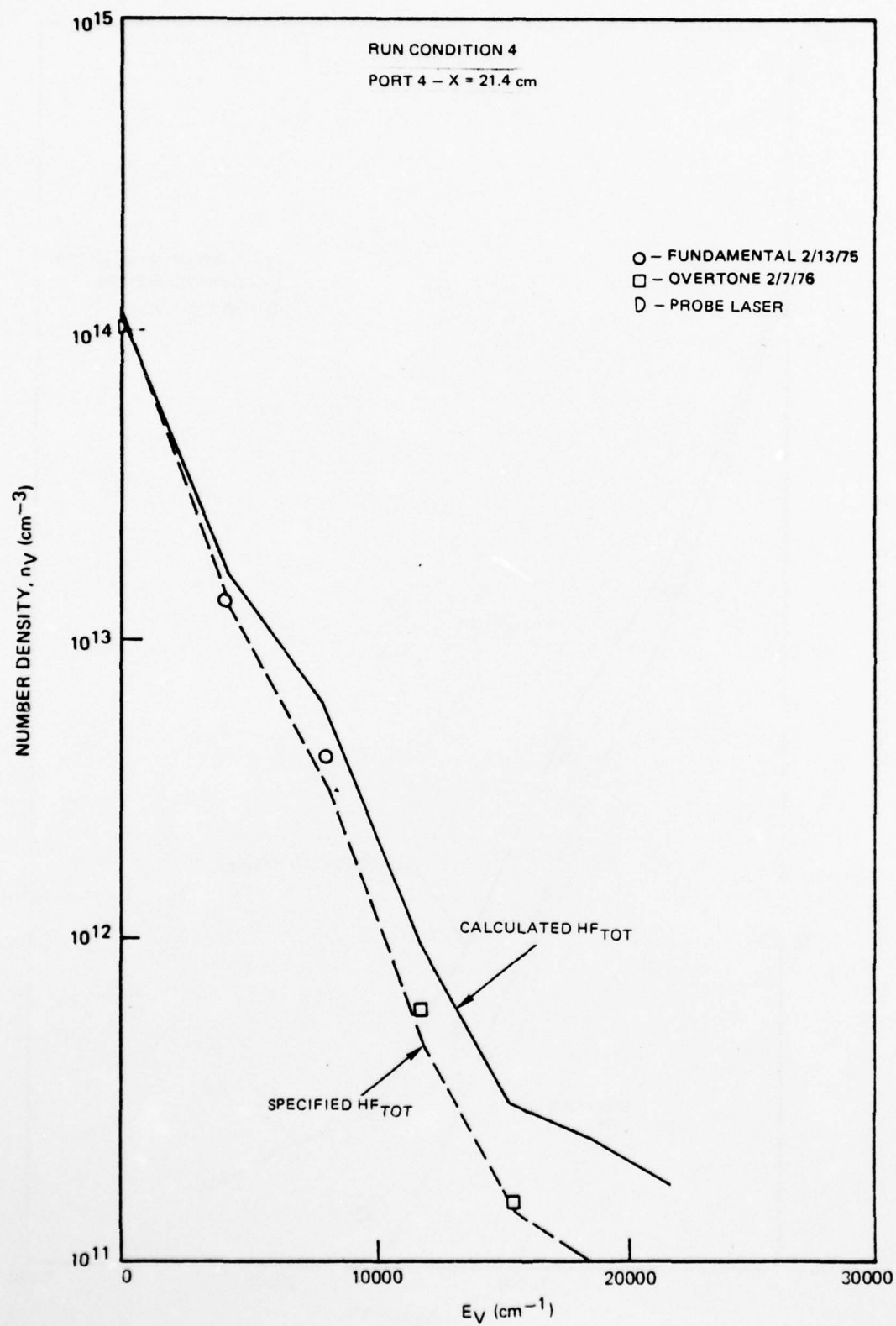


FIGURE 108 COMPARISON WITH MODEL

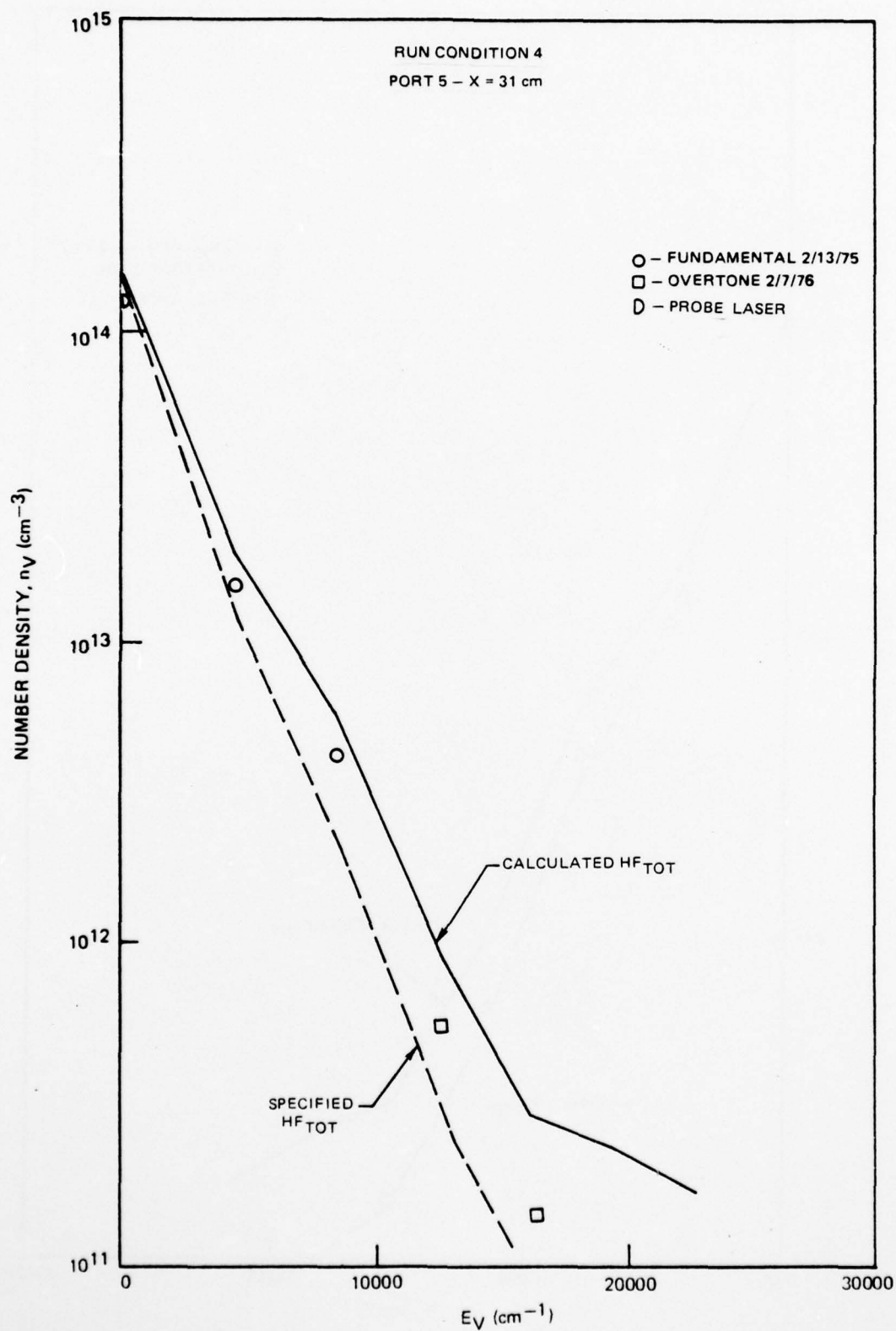


FIGURE 109 COMPARISON WITH MODEL

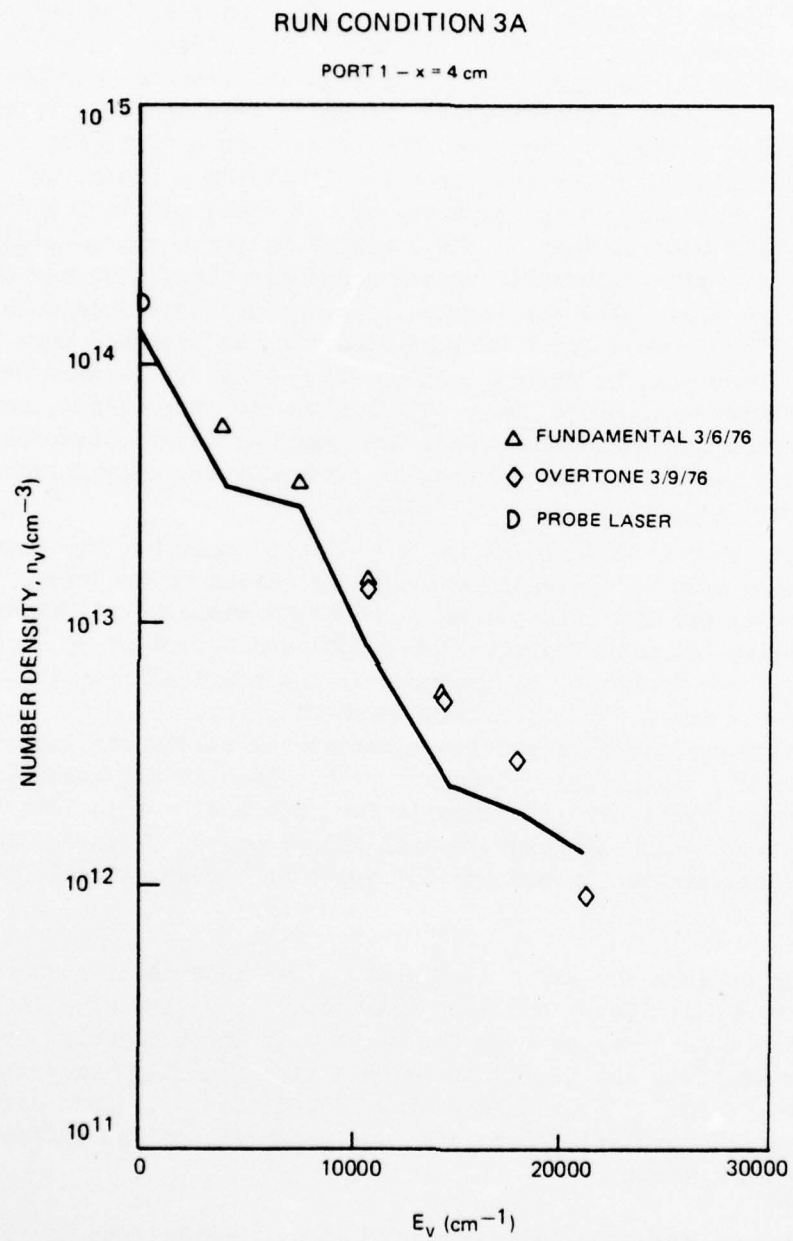


FIGURE 110 COMPARISON WITH MODEL

(Refs. 31 and 32). In the course of parameter variations to optimize the fit of the model to the data, linear scaling with v of the V-V rates was also tried. A typical comparison of the model with linear and $v^{-1/2}$ scaling is shown in Figures 111 and 112. The differences are seen to be relatively small, despite the large differences in the upper level probabilities. The faster V-V package generally tends to do a better job of matching the experimental distributions for the lower levels at short times, but for longer times it tends to overestimate the ground state population and those above $v = 5$, while underestimating the populations for $v = 1$ to 4 (Figs. 111 and 112). While this gives generally poorer agreement than, say, use of a $v^{-1/2}$ scaling for these flow tube tests, in power extraction calculations the faster V-V scaling tends to give more pessimistic (and perhaps more realistic) predictions. These will be described later on. This is in part because of the better agreement on the lower levels seen for short times, comparable to those in lasing systems. The poorer agreement at later times and on higher levels, which do not lase strongly, typically has only a secondary influence on predictions of power extraction.

To further test the model and isolate HF self deactivation tests a comparison was also made for cases in which HF was added to the flow. In particular 50 cc/sec and 100 cc/sec were added to run conditions 1 through 3. This is equivalent to initial mole fractions of 0.0002 and 0.0004 of HF in the flow, comparable with the amount of HF produced by the chemical reactions. A comparison of the model with experiment is shown in Figures 113 through 126. Since no $v = 0$ data are available to provide experimental values for the streamwise development of HF, calculated values are used. Even so the agreement remains generally good. The tendency is for the model predictions to fall along, or somewhat below the experimental measurements. This indicates that HF self deactivation is perhaps not quite as strong as included in the model.

To better isolate the effects of H atoms two additional sets of runs were performed (Conditions 5 and 6). These conditions are also listed in Table 9. The object was to find two cases with approximately the same rate of HF production, but having one with a significantly higher H-atom concentration (Condition 6) than the other (Condition 5). Thus differences in the vibrational populations would be due primarily to the differences in the H-atom concentration.

In order to assess the influence of H atoms, comparisons of the ratios of populations for given levels between the two cases were made at each port.

31. Kwok, M. private communication, August 1975.

32. Shin, H. K., "Vibration-Vibration Energy Transfer in HF Dimers," J. Chem. Phys., **63**, 2091, 1975.

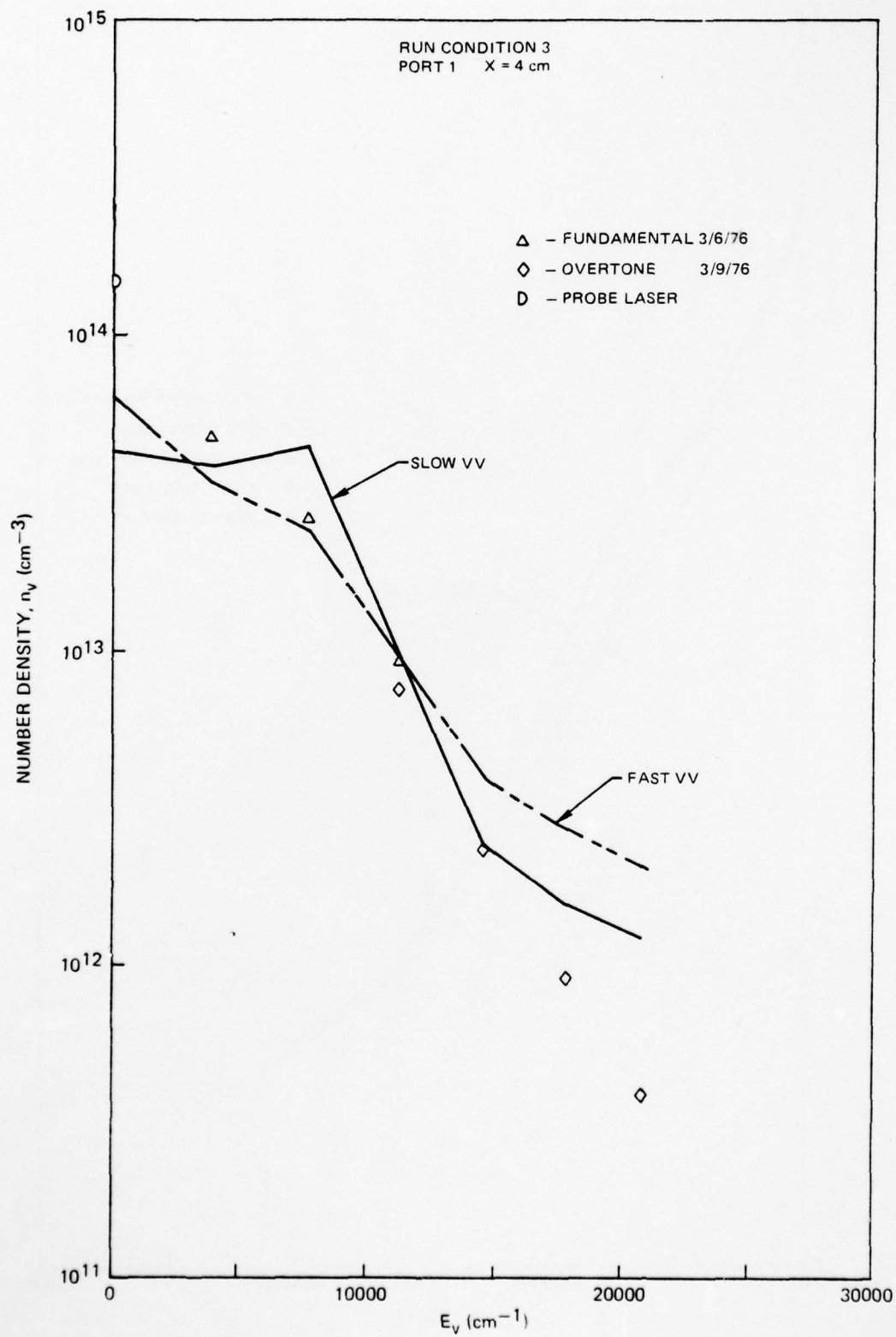


FIGURE 111 INFLUENCE OF V-V RATES

AD-A041 204

UNITED TECHNOLOGIES RESEARCH CENTER EAST HARTFORD CONN
LONG RANGE CHAIN LASER STUDIES, PHASE I STUDIES. (U)

F/G 20/5

JUN 77 L R BOEDEKER, P A BONZYK, J J HINCHEN F29601-75-C-0139

UNCLASSIFIED

UTRC/R77-952198-58

AFWL-TR-77-43

NL

3 OF 4
AD
A041204



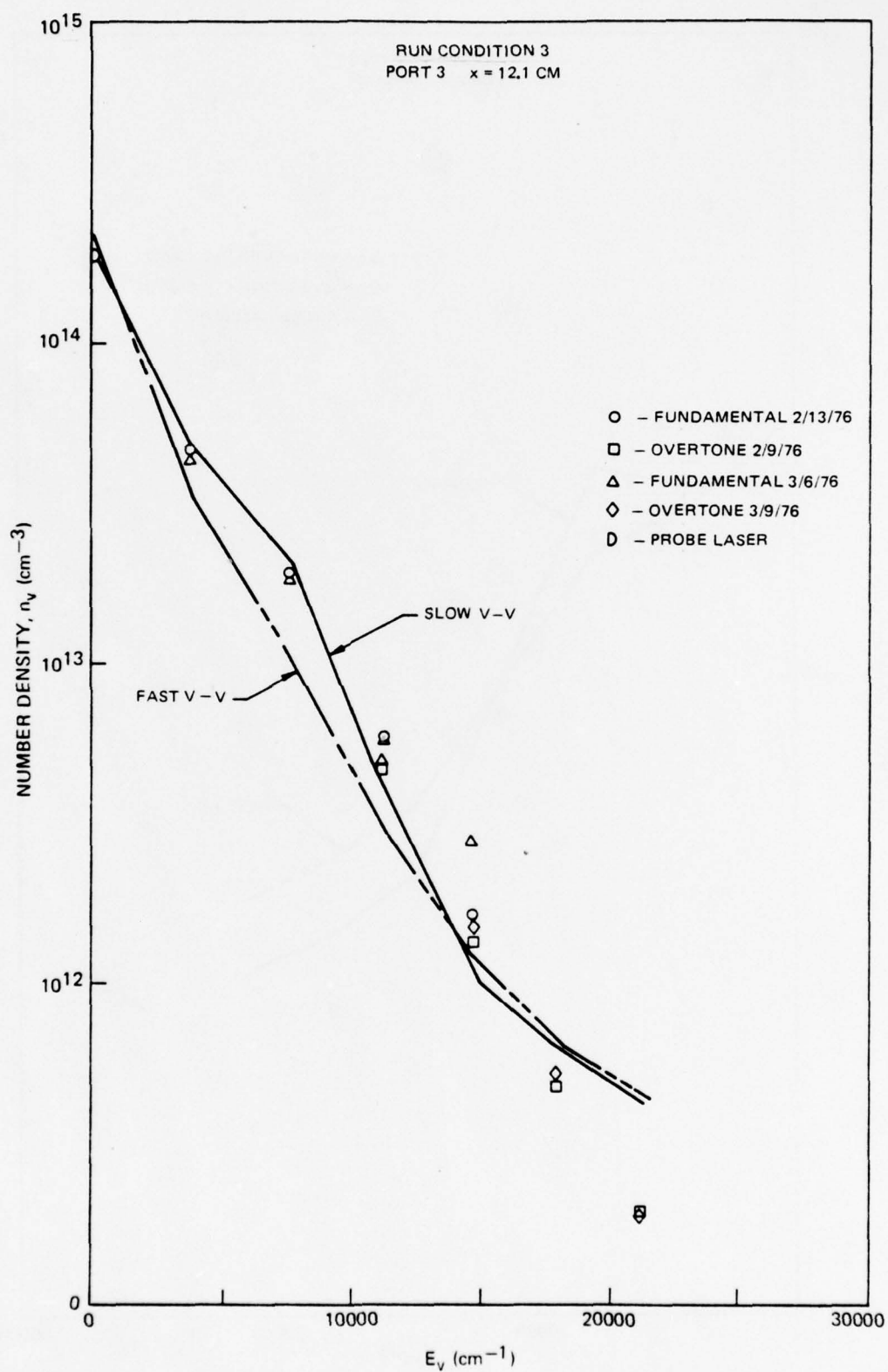


FIGURE 112 INFLUENCE OF V-V RATES

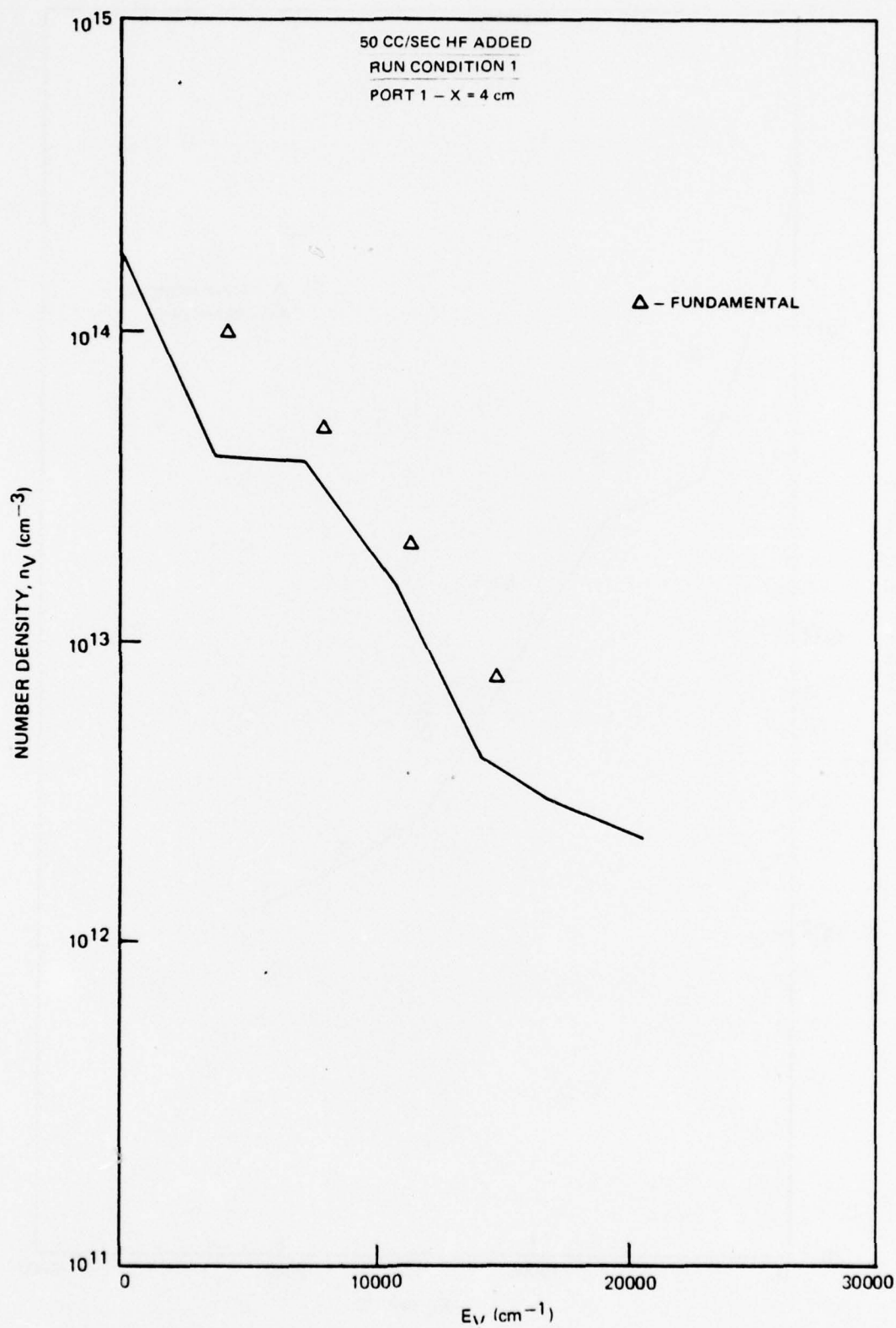


FIGURE 113 COMPARISON WITH MODEL

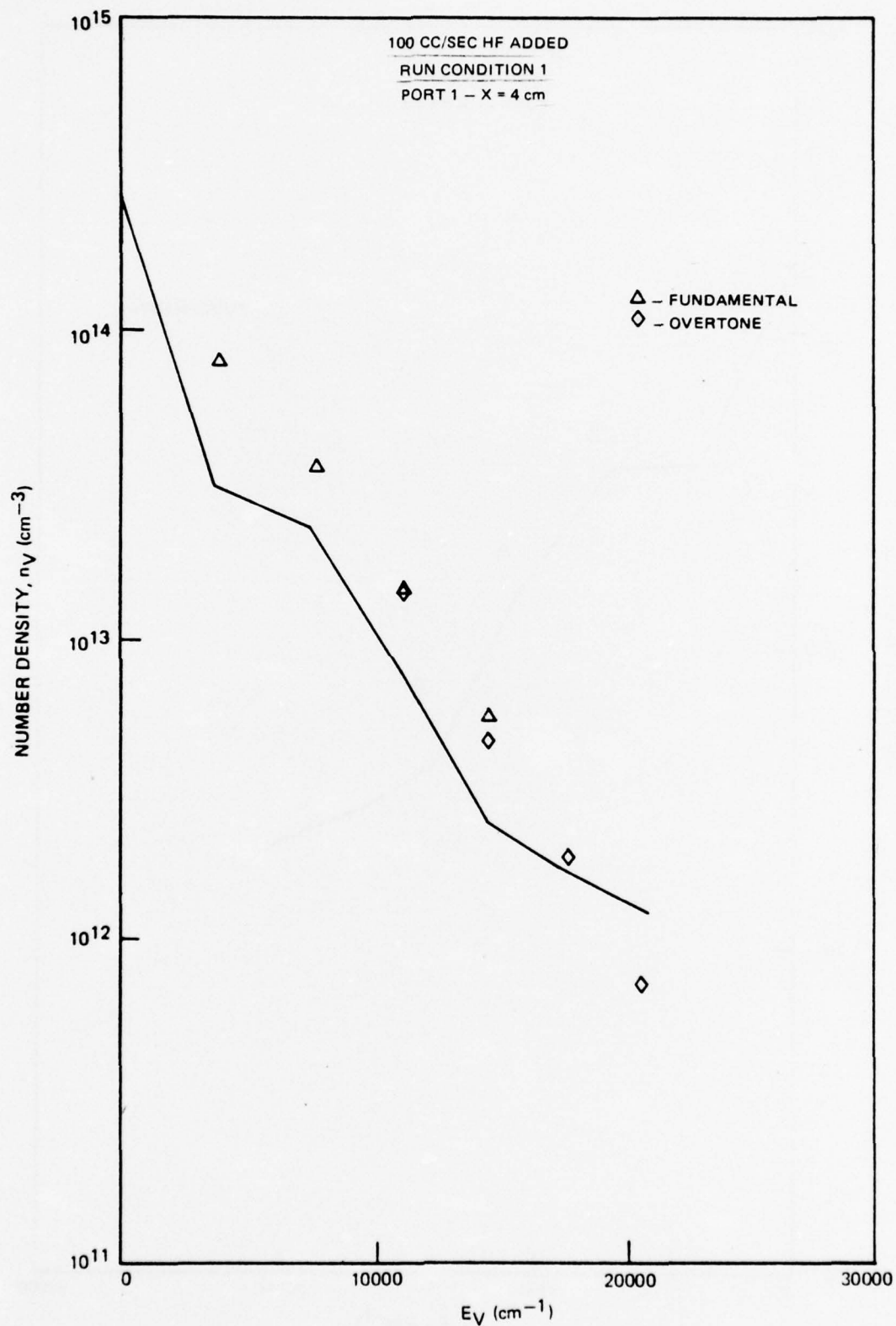


FIGURE 114 COMPARISON WITH MODEL

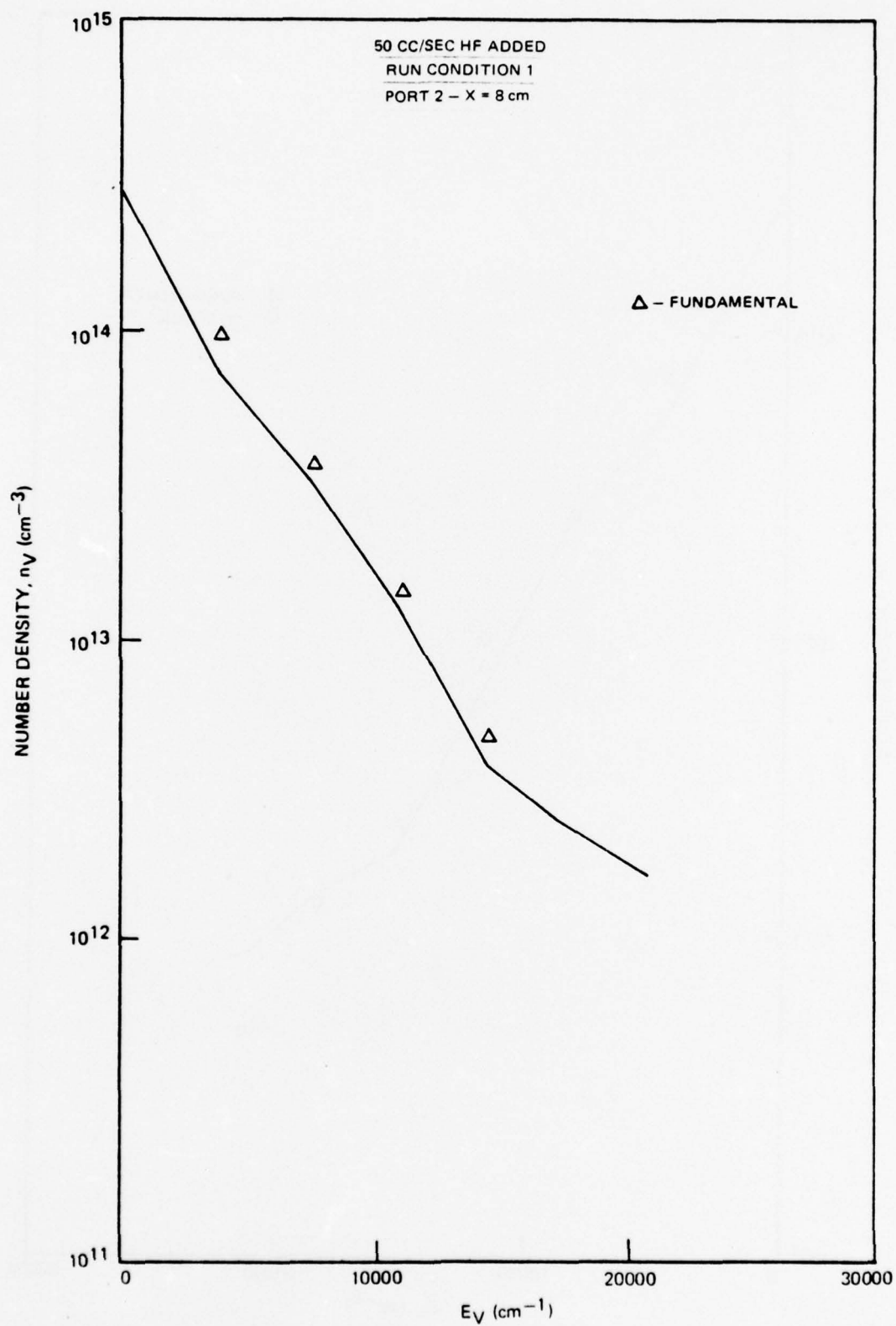


FIGURE 115 COMPARISON WITH MODEL

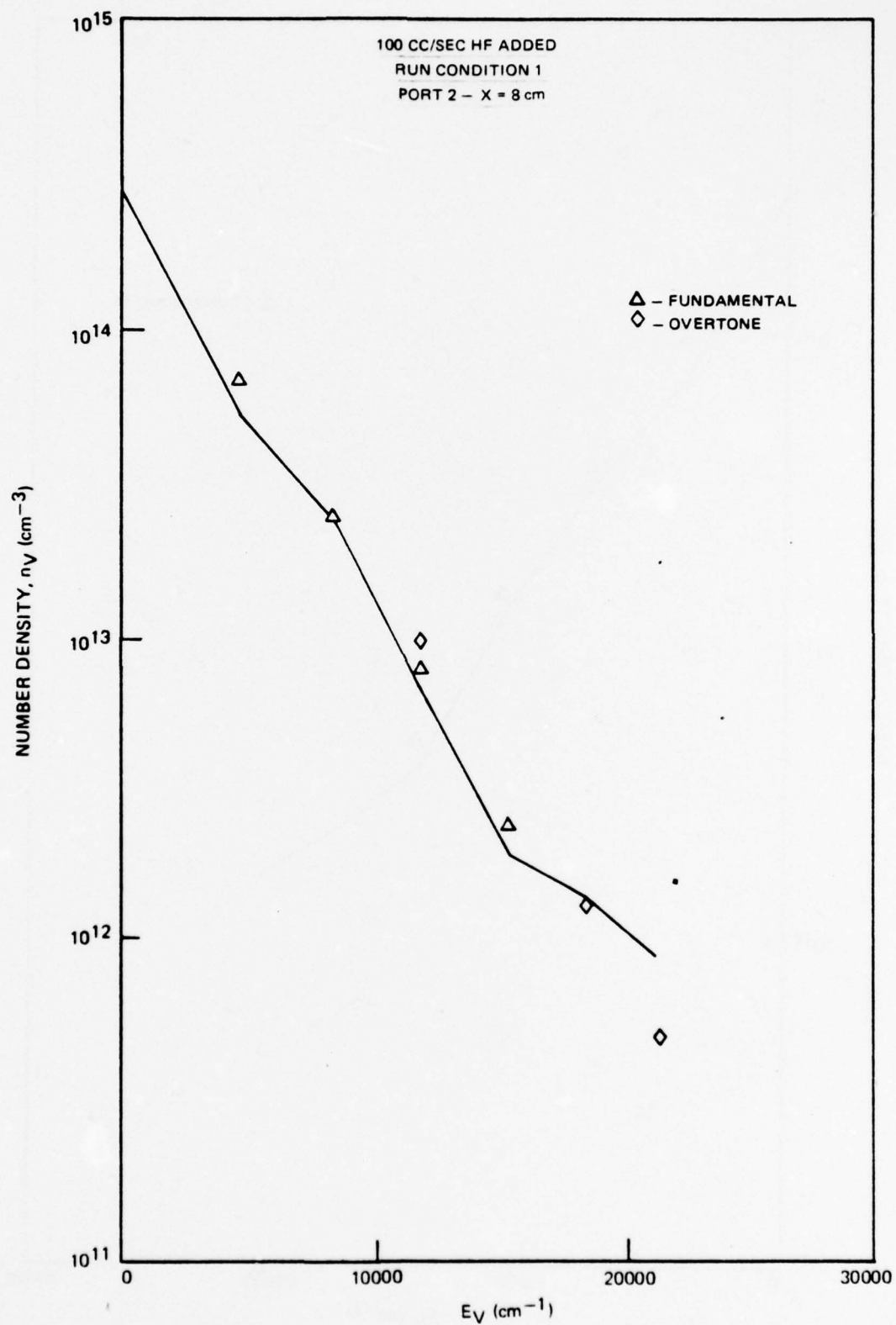


FIGURE 116 COMPARISON WITH MODEL

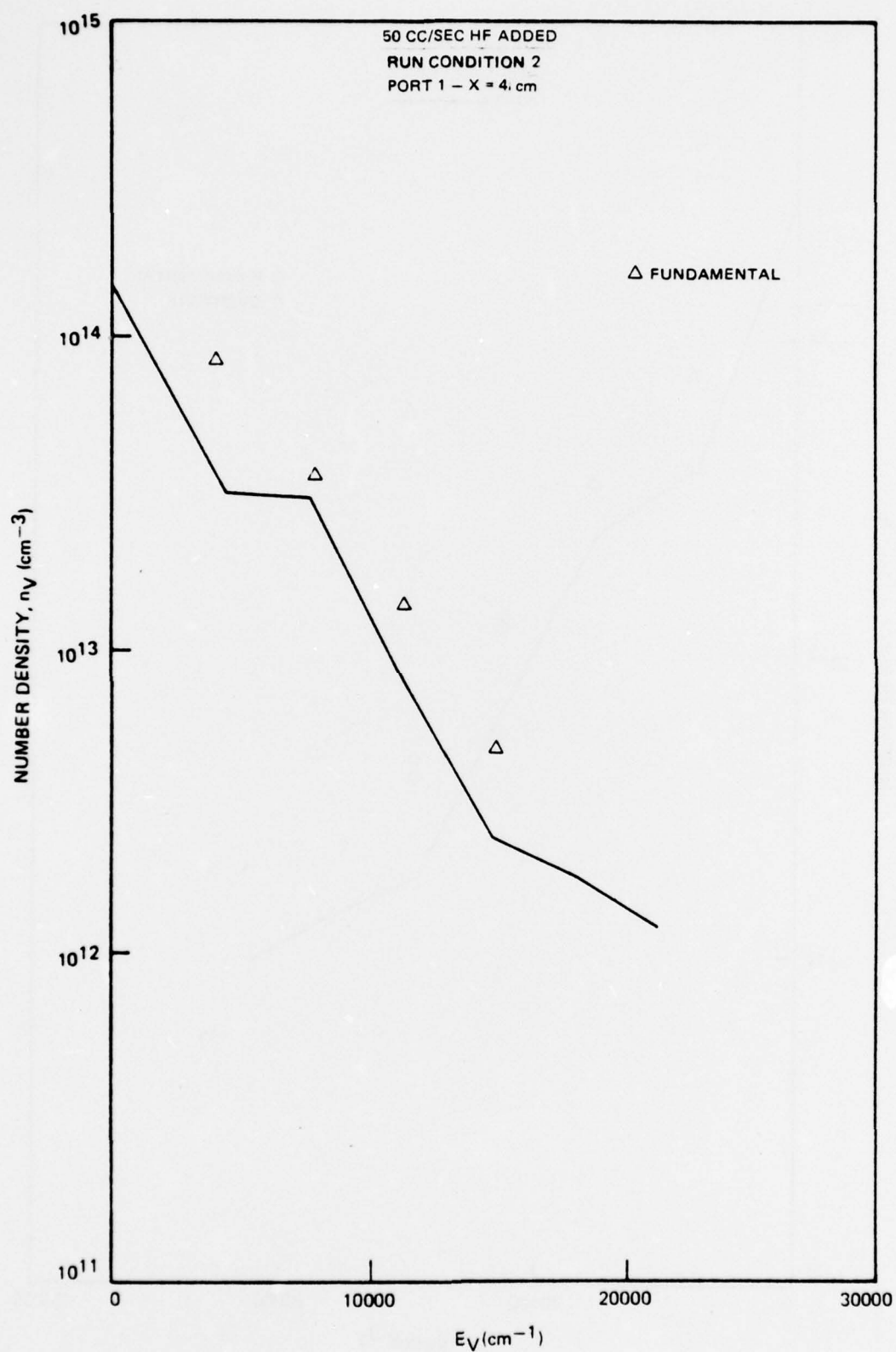


FIGURE 117 COMPARISON WITH MODEL

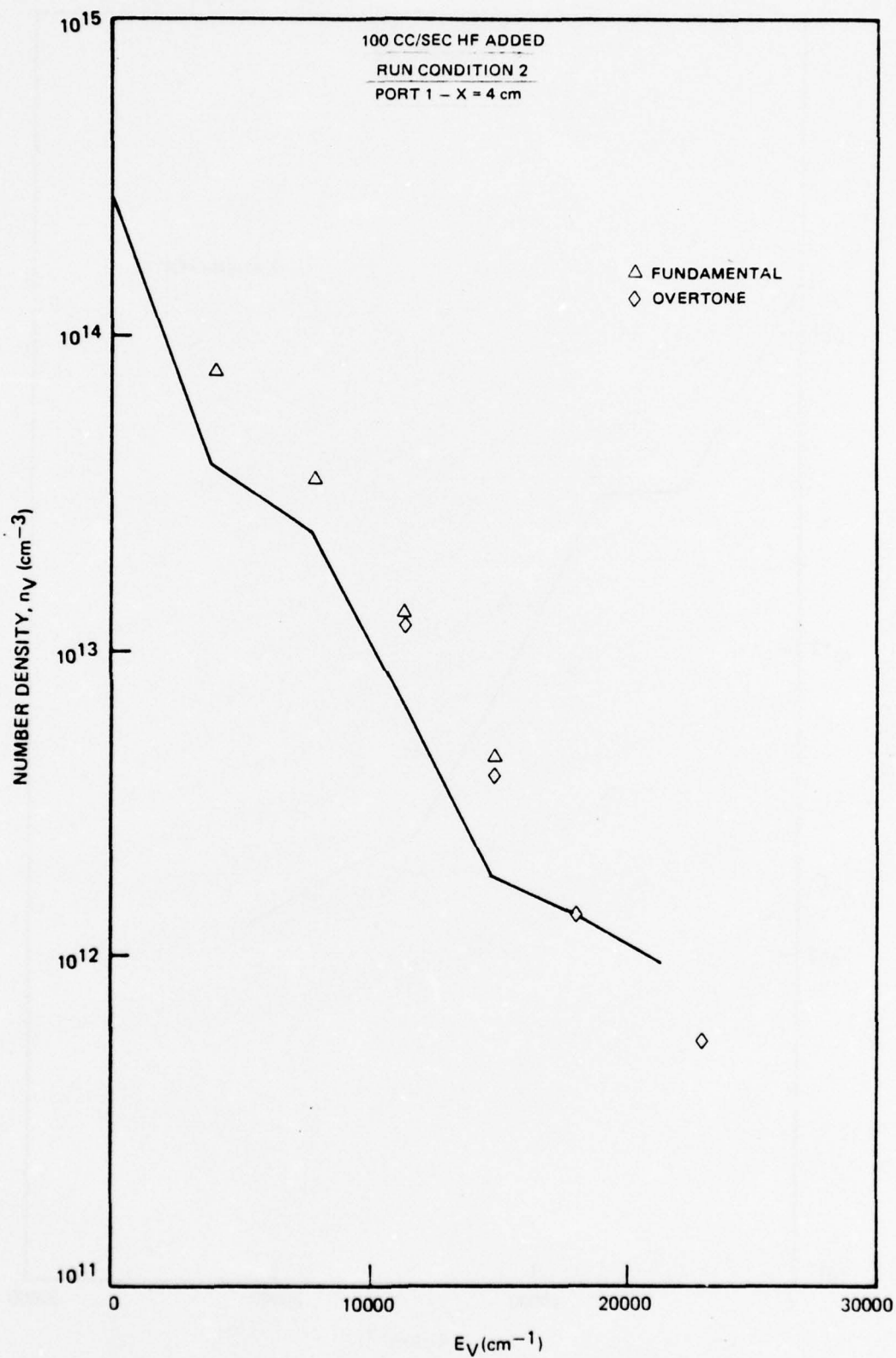


FIGURE 118 COMPARISON WITH MODEL

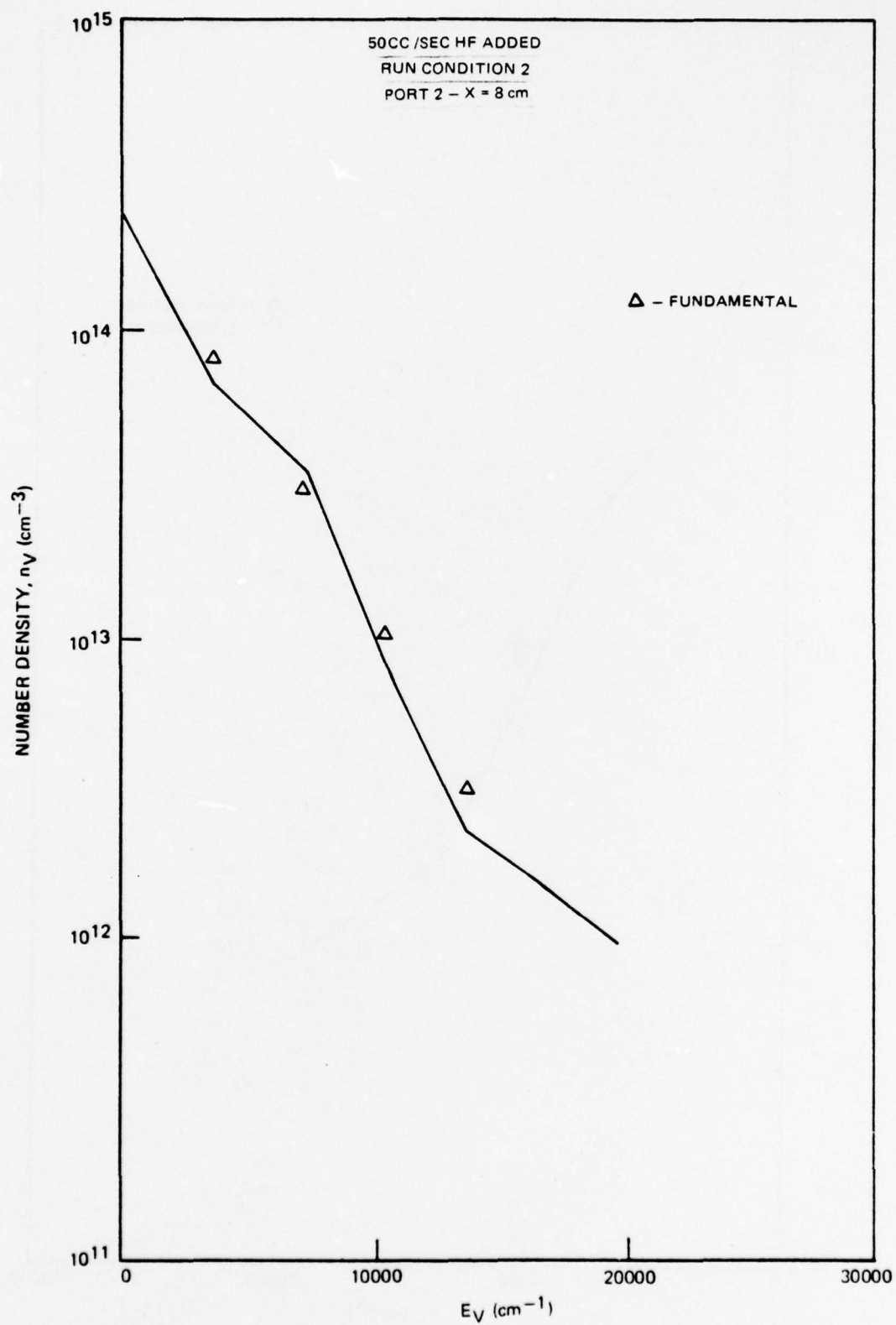


FIGURE 119 COMPARISON WITH MODEL

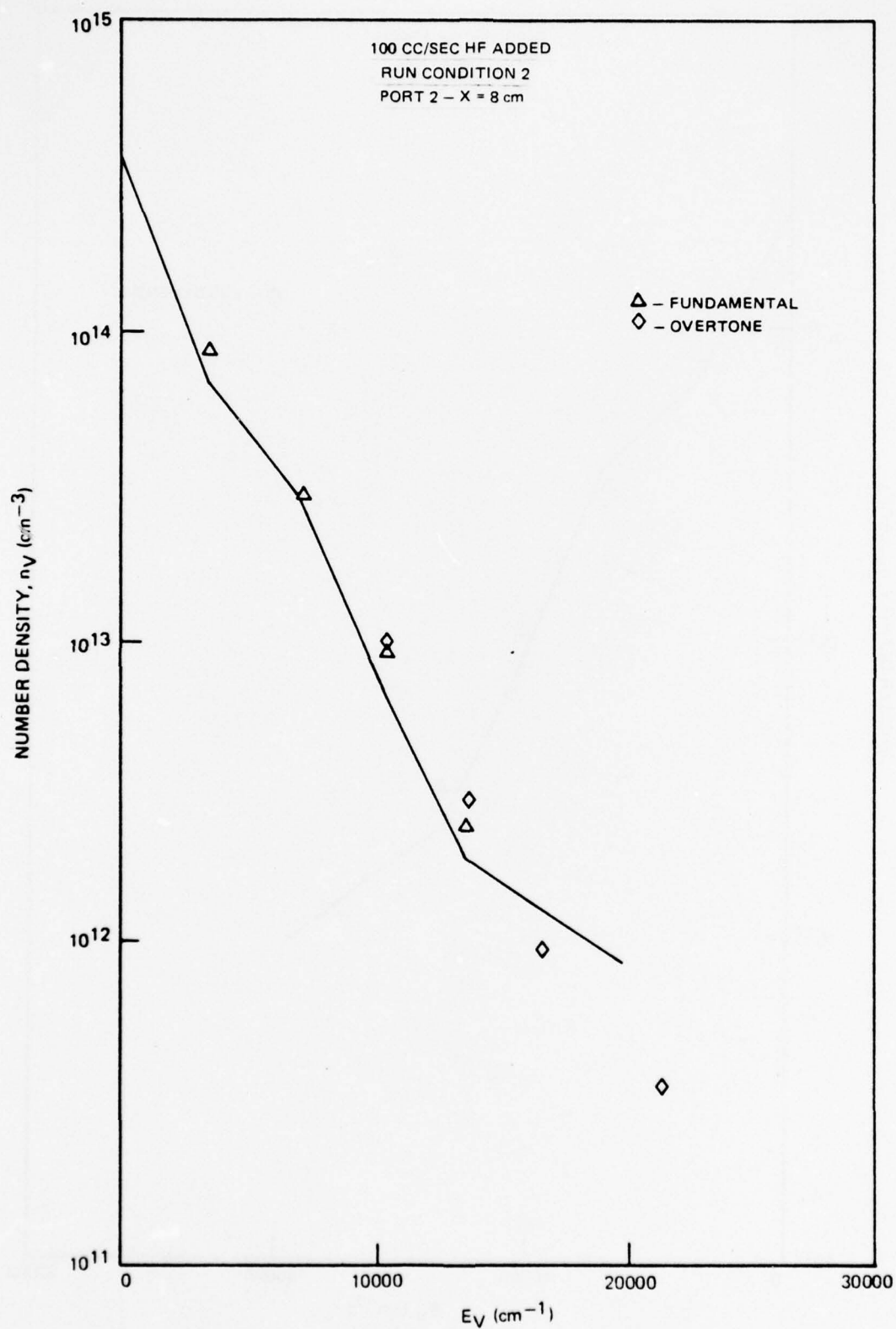


FIGURE 120 COMPARISON WITH MODEL

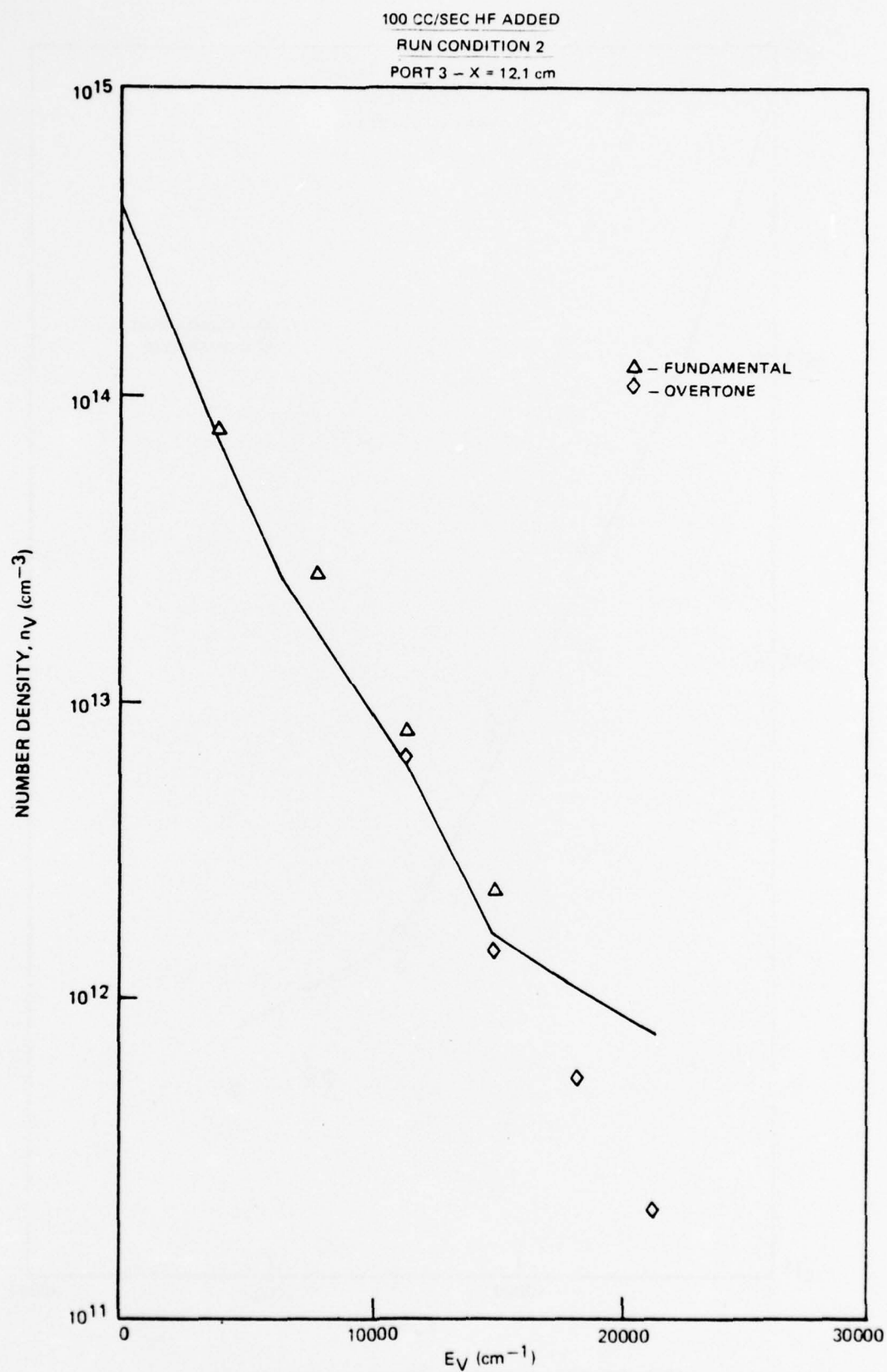


FIGURE 121 COMPARISON WITH MODEL

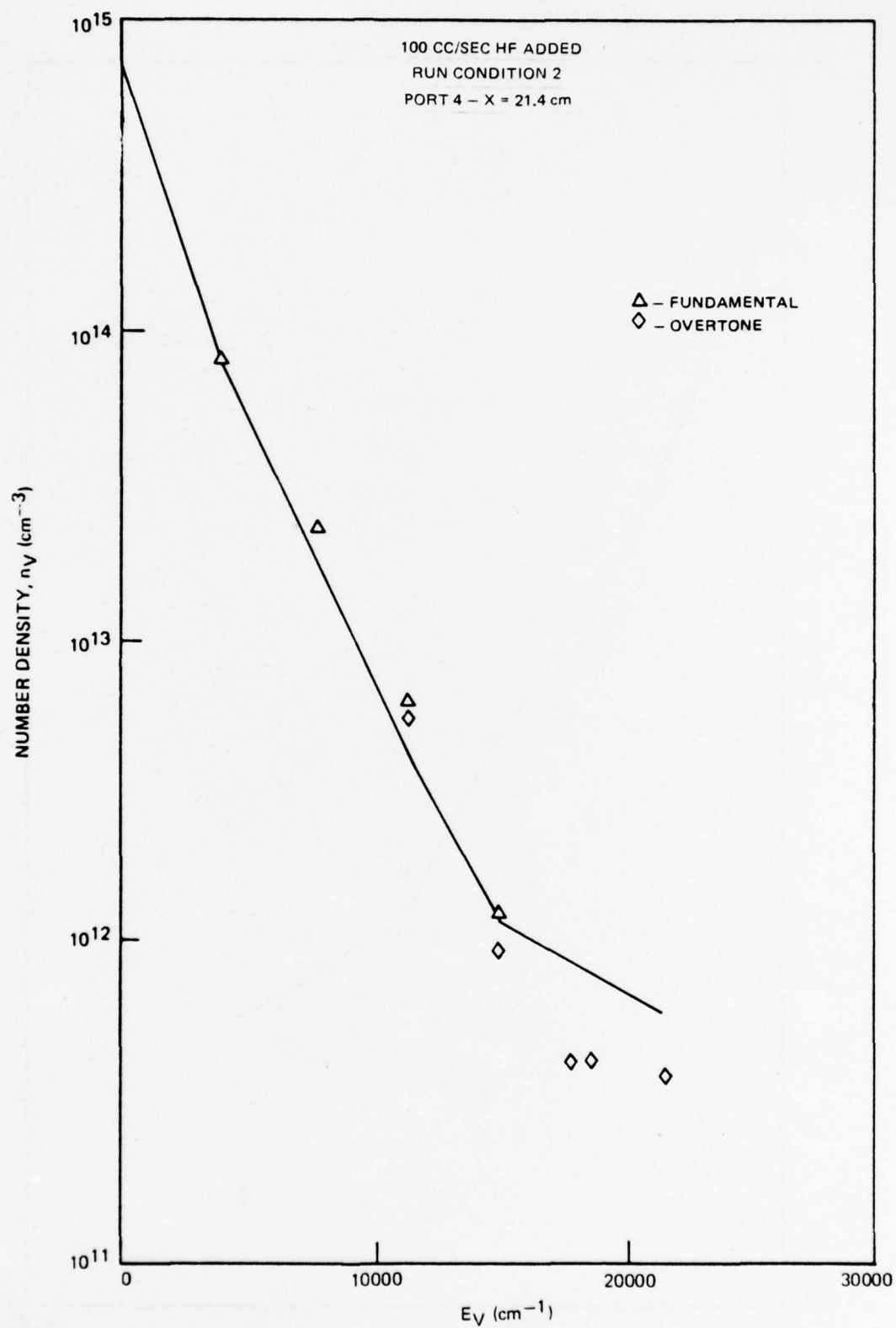


FIGURE 122 COMPARISON WITH MODEL

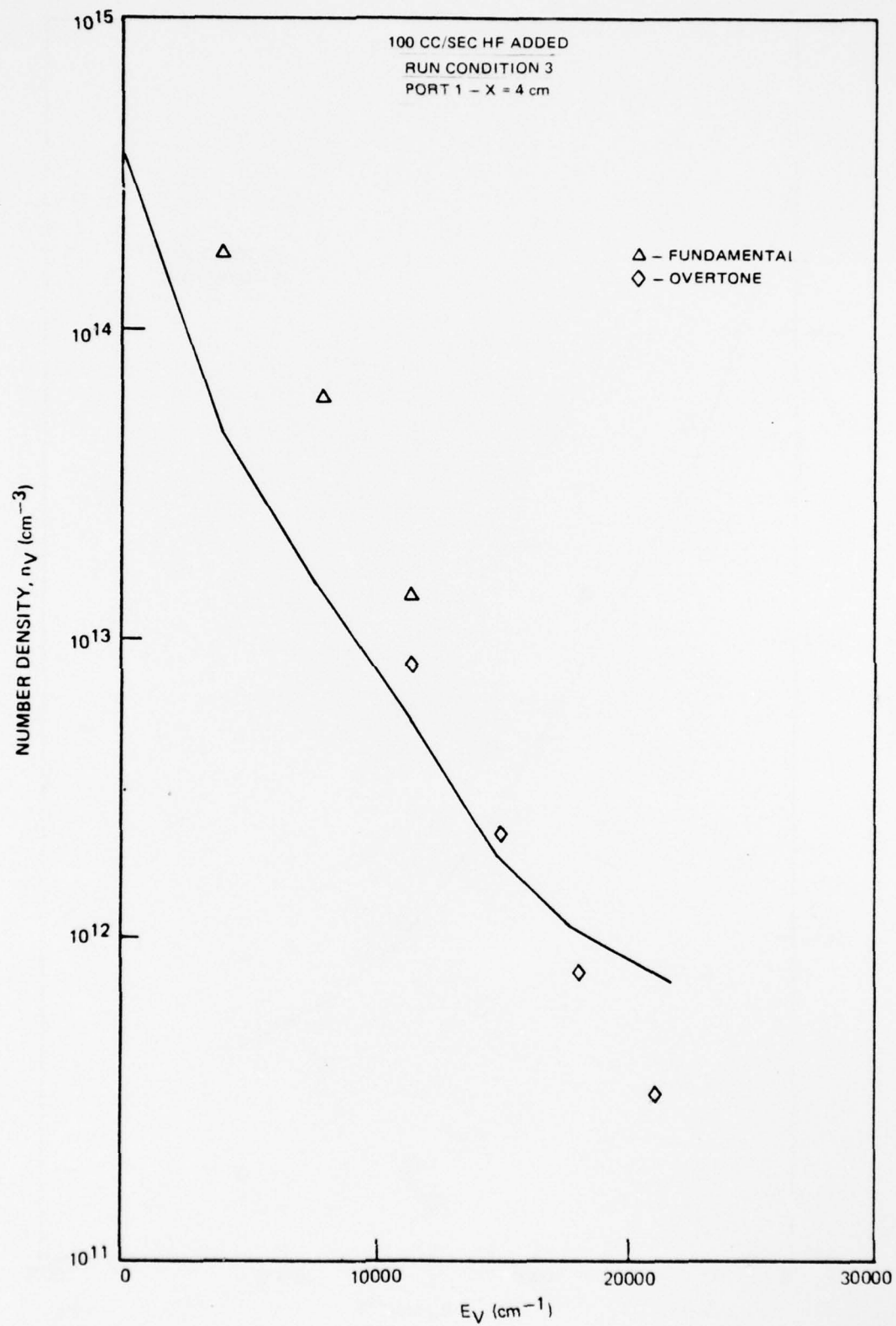


FIGURE 123 COMPARISON WITH MODEL

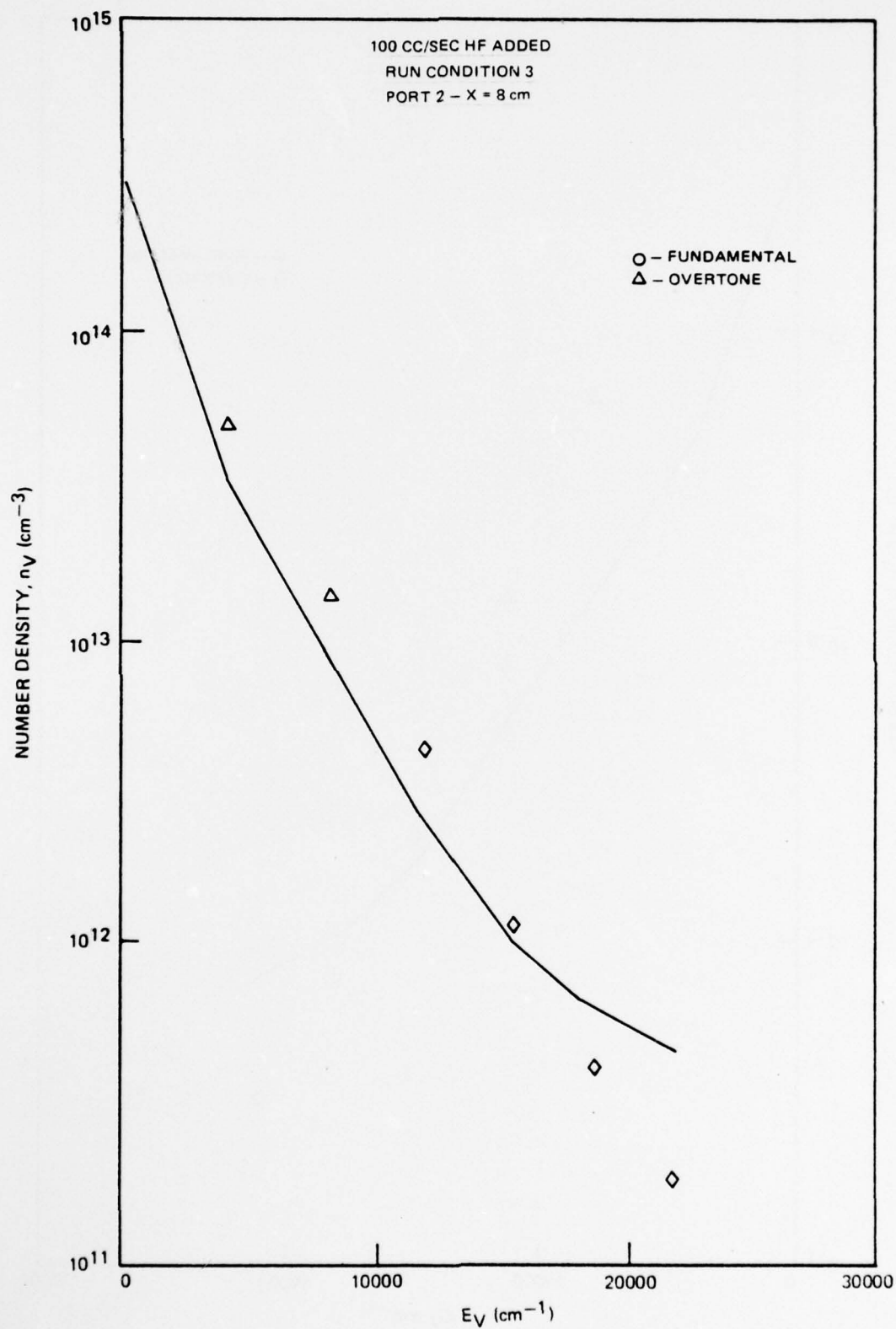


FIGURE 124 COMPARISON WITH MODEL

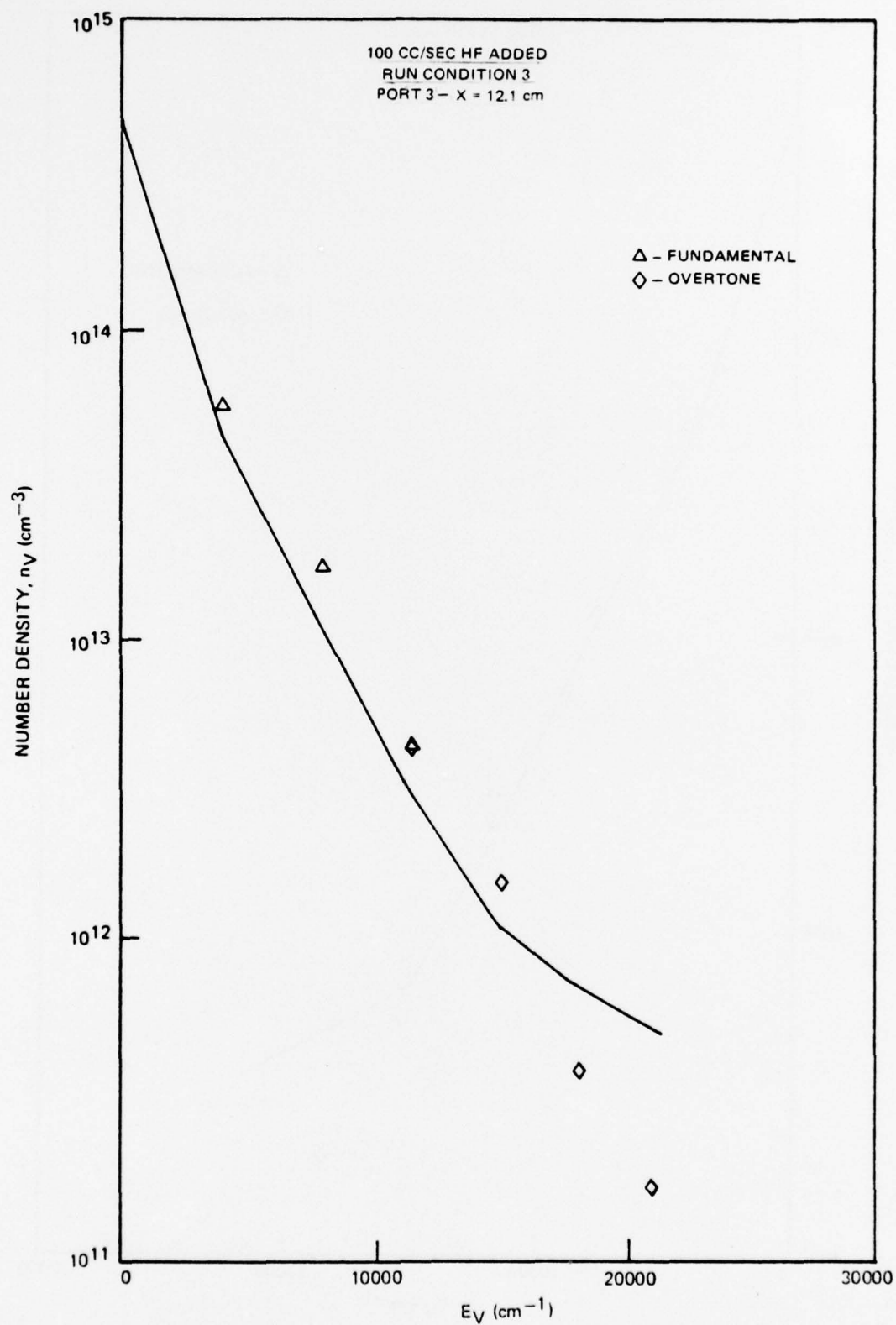


FIGURE 125 COMPARISON WITH MODEL

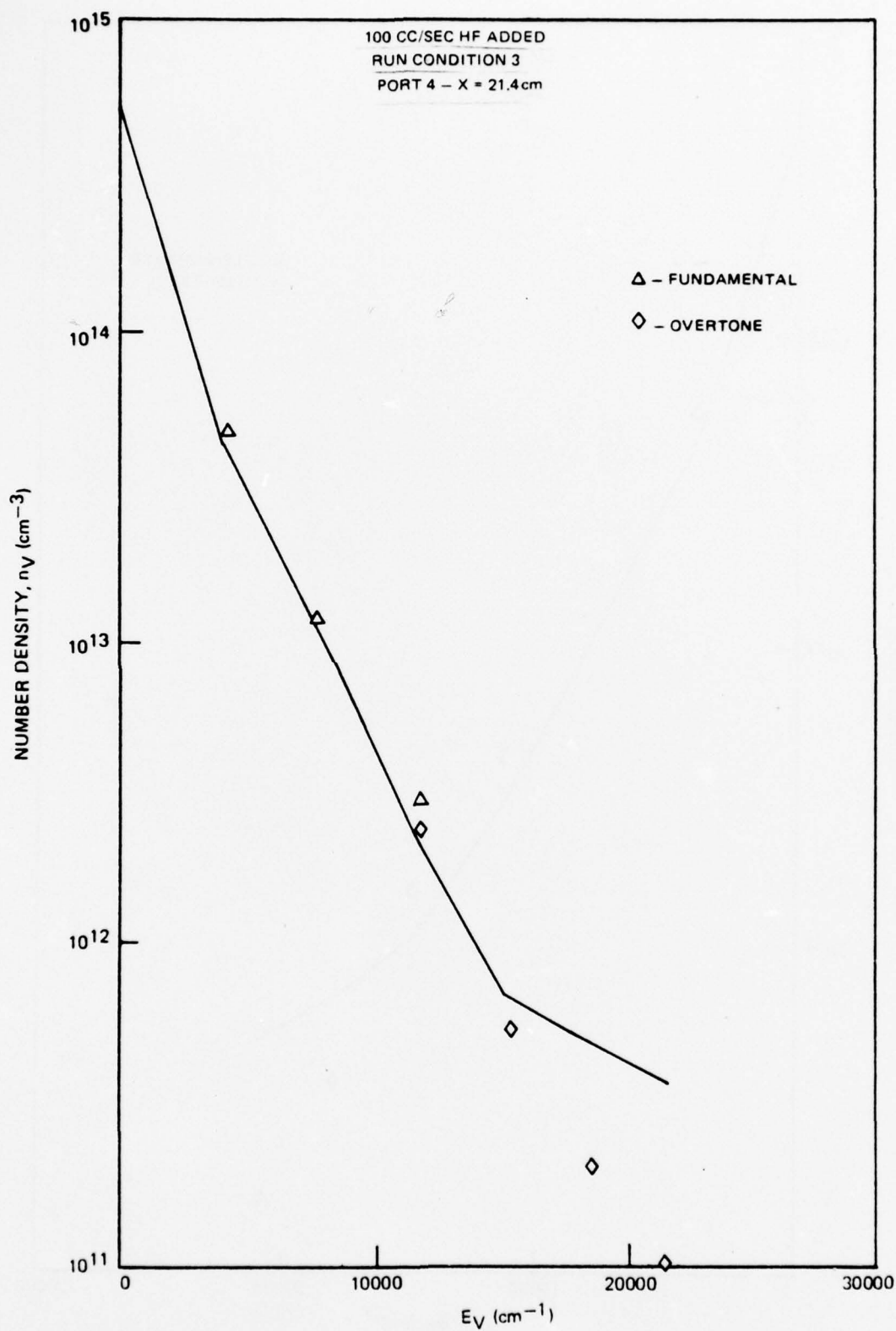


FIGURE 126 COMPARISON WITH MODEL

In the ideal situation the streamwise variation of HF would be the same for each case. Then any departure of the ratios from unity would be predominantly the result of H atom effects. If such effects were accurately modeled the calculations would compare well even if HF self deactivation were poorly modeled.

Figure 127 shows the measured development of HF for the two cases. Unfortunately differences in the initial reaction rates result initially in somewhat larger HF concentration for Condition 6, whereas at latter stages of the flow Condition 5 has high concentrations. Thus differences in the HF self relaxation will tend to mask the H atom effects. This problem is further complicated by the possibility that HF is initially present, as illustrated by the dashed lines in the figure.

The experimental population ratios were evaluated and compared with three sets of calculations: (1) H atom deactivation scaled to Bott's measurements, (2) H atom deactivation set at the nominal values, (3) H atom deactivation set to zero. The third set of calculations was performed to assess the influence of HF self relaxation alone. The results of the comparison are shown in Tables 12 through 16. An earlier comparison using calculated net HF development, had given fairly good agreement (Ref. 23). Now, however, with the HF variation specified from measurement, the comparison is less favorable. The predicted influence of HF self deactivation alone gives ratios comparable to those measured experimentally. Hence, little can be said about the influence of the H atoms.

A clearer illustration of the problem is available in Figures 128 through 131. These show vibrational distributions at $x = 8$ and $x = 31$ cm, respectively, for the two cases. As can be seen, the computation assuming no H atom deactivation under-predicts the upper level populations for both cases at the latter stages of the flow. It is apparent that either short comings still **exist** in the self-deactivation model or errors in the measured HF development preclude a valid assessment of H atom influences.

Pulsed-Fluorescence

The data available from the pulsed-fluorescence experiments that can be used to study vibrational relaxation are primarily qualitative in nature, in the form of fluorescence traces from the vibrational levels $v=1$ through 6. Some quantitative data, namely gain measurements, are also available.

Due to the short time scales and weak signals the fluorescence traces could not be calibrated to provide absolute number densities. Thus the traces were normalized to unity at the maximum. One case from each series

TABLE 12. $x = 4$ cm - PORT 1

V	Population Ratios: Cond 5/Cond 6			
	Exptl.	Bott H-Atom Deactivation	Nominal H- Atom Deactivation	No H-Atom Deactivation
3	1.3	1.5	1.3	1.0
4	2.0	2.4	2.1	1.5
5	2.9	2.3	2.2	2.0
6	2.7	2.2	2.0	1.9

TABLE 13. $x = 8$ cm - PORT 2

V	Population Ratios: Cond 5/Cond 6			
	Exptl.	Bott H-Atom Deactivation	Nominal H- Atom Deactivation	No H-Atom Deactivation
3	1.5	2.1	2.0	1.2
4	1.7	2.8	2.6	1.7
5	2.0	2.6	2.3	1.9
6	1.6	2.6	2.1	1.8

TABLE 14. $x = 12.1$ cm - PORT 3

V	Population Ratios: Cond 5/Cond 6			
	Exptl.	Bott H-Atom Deactivation	Nominal H- Atom Deactivation	No H-Atom Deactivation
3	2.0	3.1	2.9	1.6
4	3.3	3.6	3.1	2.1
5	2.7	3.3	2.6	2.2
6	2.1	3.2	2.4	2.1

TABLE 15. $x = 21.4$ cm - PORT 4

V	Population Ratios: Cond 5/Cond 6			
	Exptl.	Bott H-Atom Deactivation	Nominal H- Atom Deactivation	No H-Atom Deactivation
3	2.1	4.3	3.4	2.2
4	---	4.4	3.4	2.5
5	---	4.2	3.0	2.5
6	---	4.2	3.0	2.5

TABLE 16. $x = 31$ cm - PORT 5

V	Population Ratios: Cond 5/Cond 6			
	Exptl.	Bott H-Atom Deactivation	Nominal H- Atom Deactivation	No H-Atom Deactivation
3	1.9	4.1	3.2	2.2
4	---	4.0	3.0	2.4
5	---	3.7	2.7	2.2
6	---	3.6	2.5	2.1

FLOW TUBE EXPERIMENT

H-ATOM STUDY

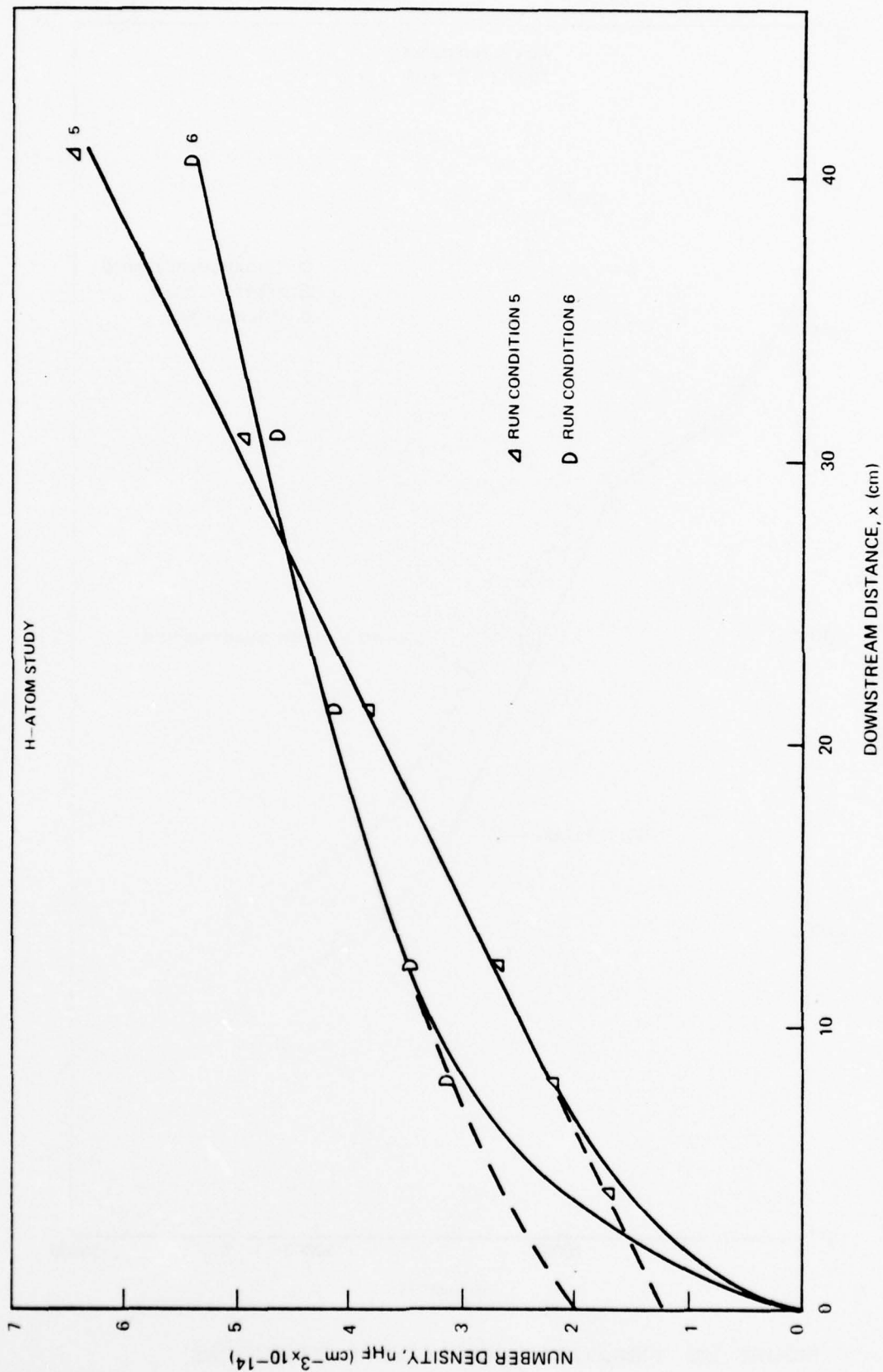


FIGURE 127 VARIATION OF TOTAL HF

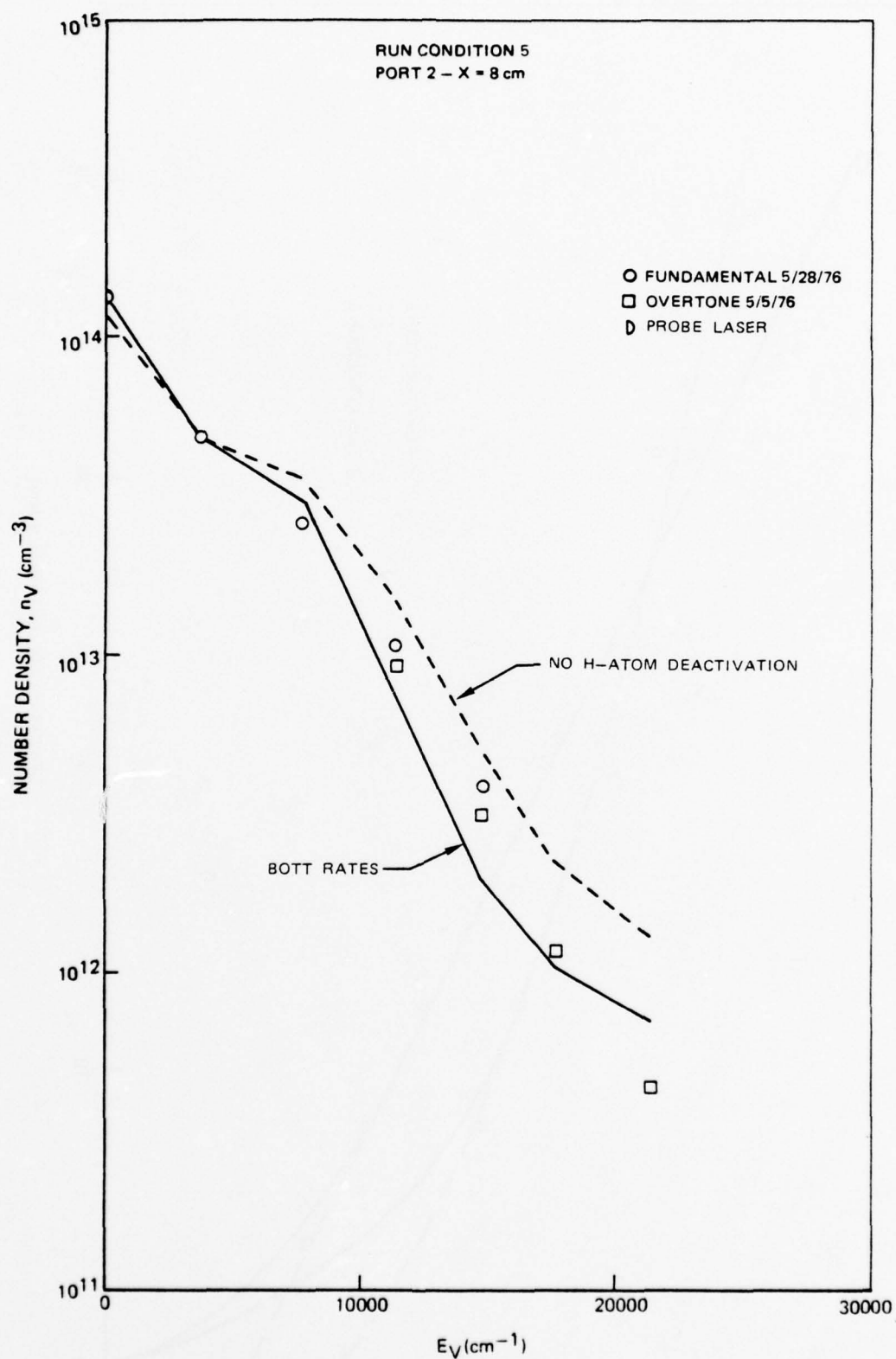


FIGURE 128 VIBRATIONAL POPULATION DISTRIBUTIONS

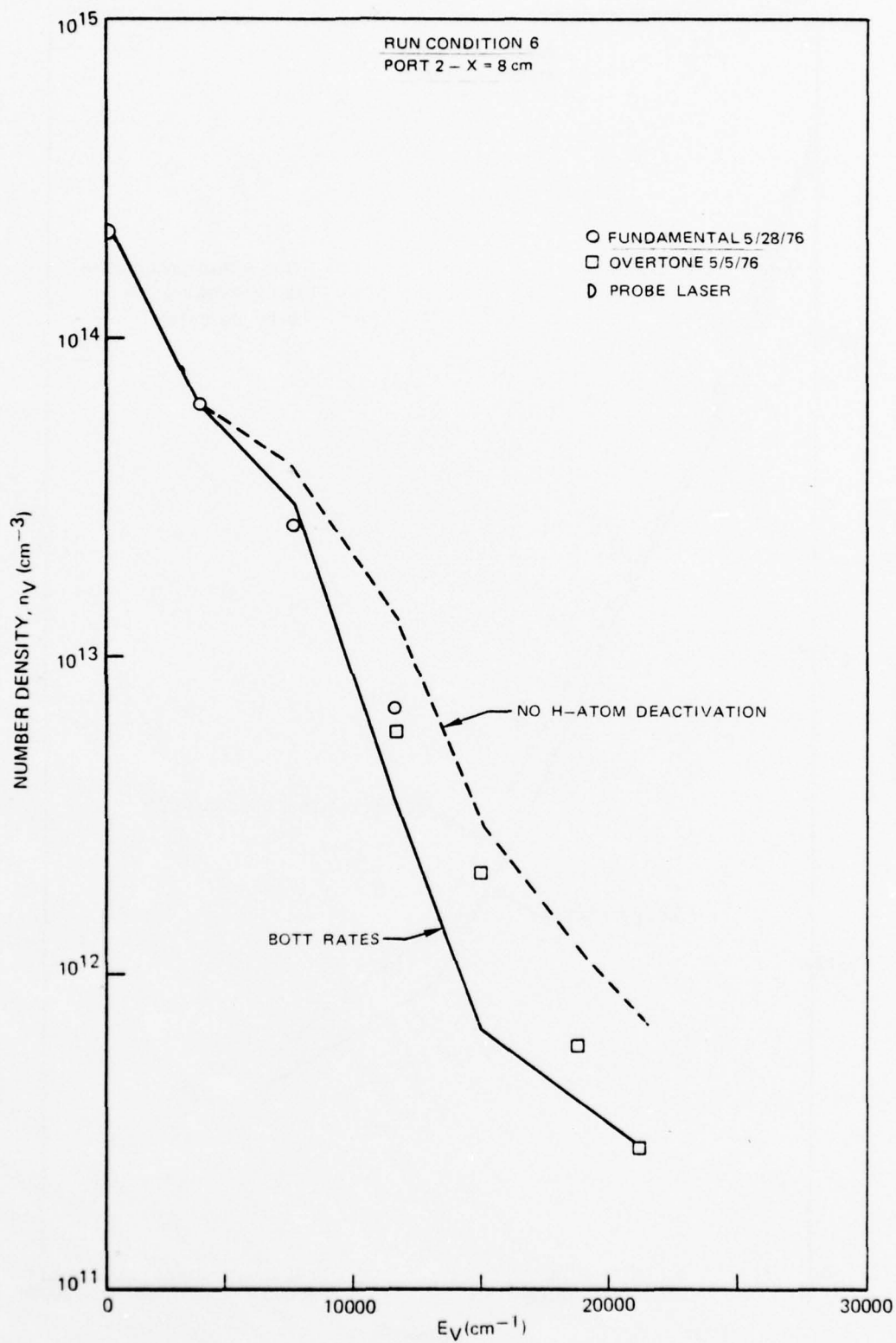


FIGURE 129 VIBRATIONAL POPULATION DISTRIBUTIONS

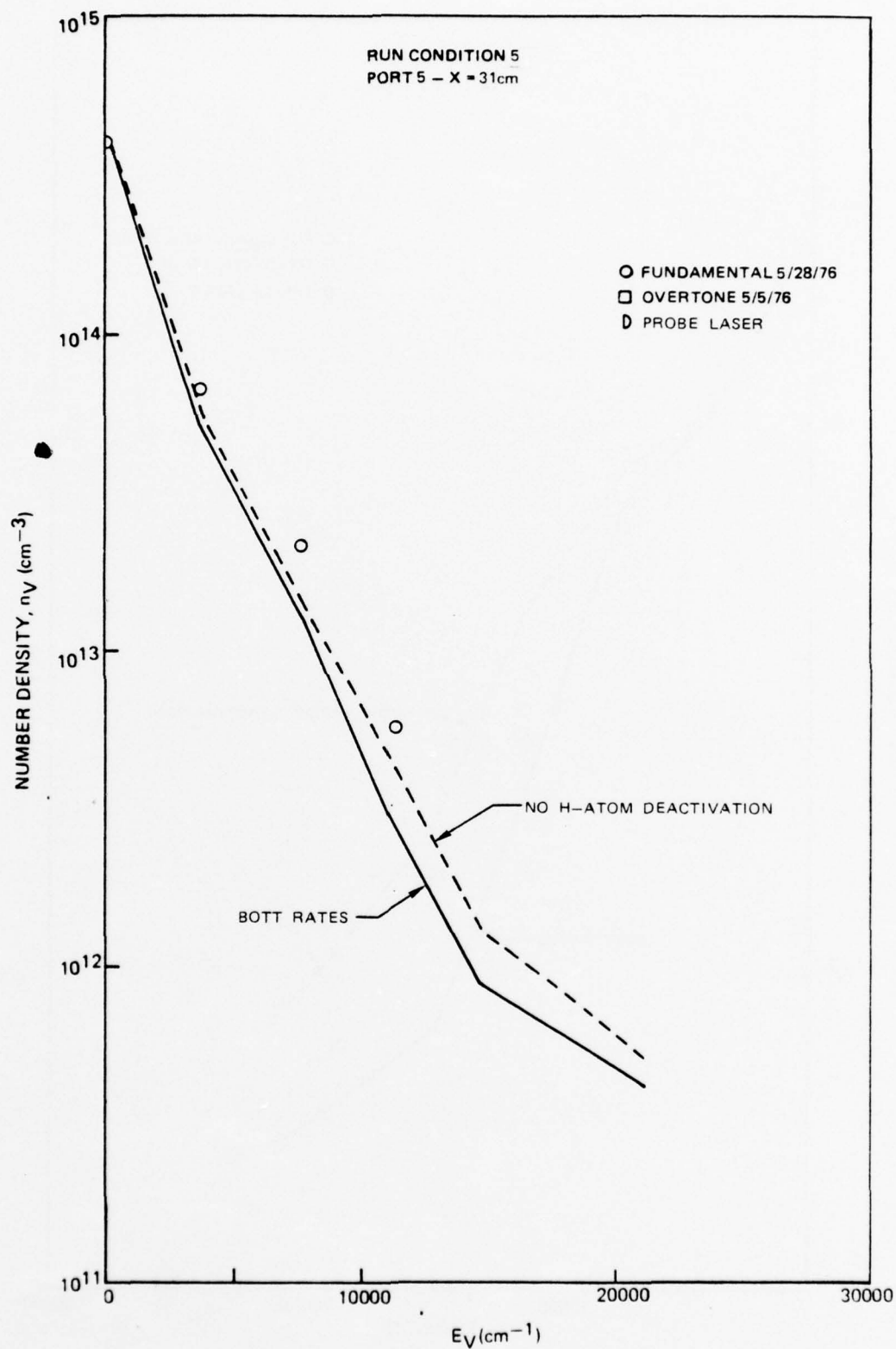


FIGURE 130 VIBRATIONAL POPULATION DISTRIBUTIONS

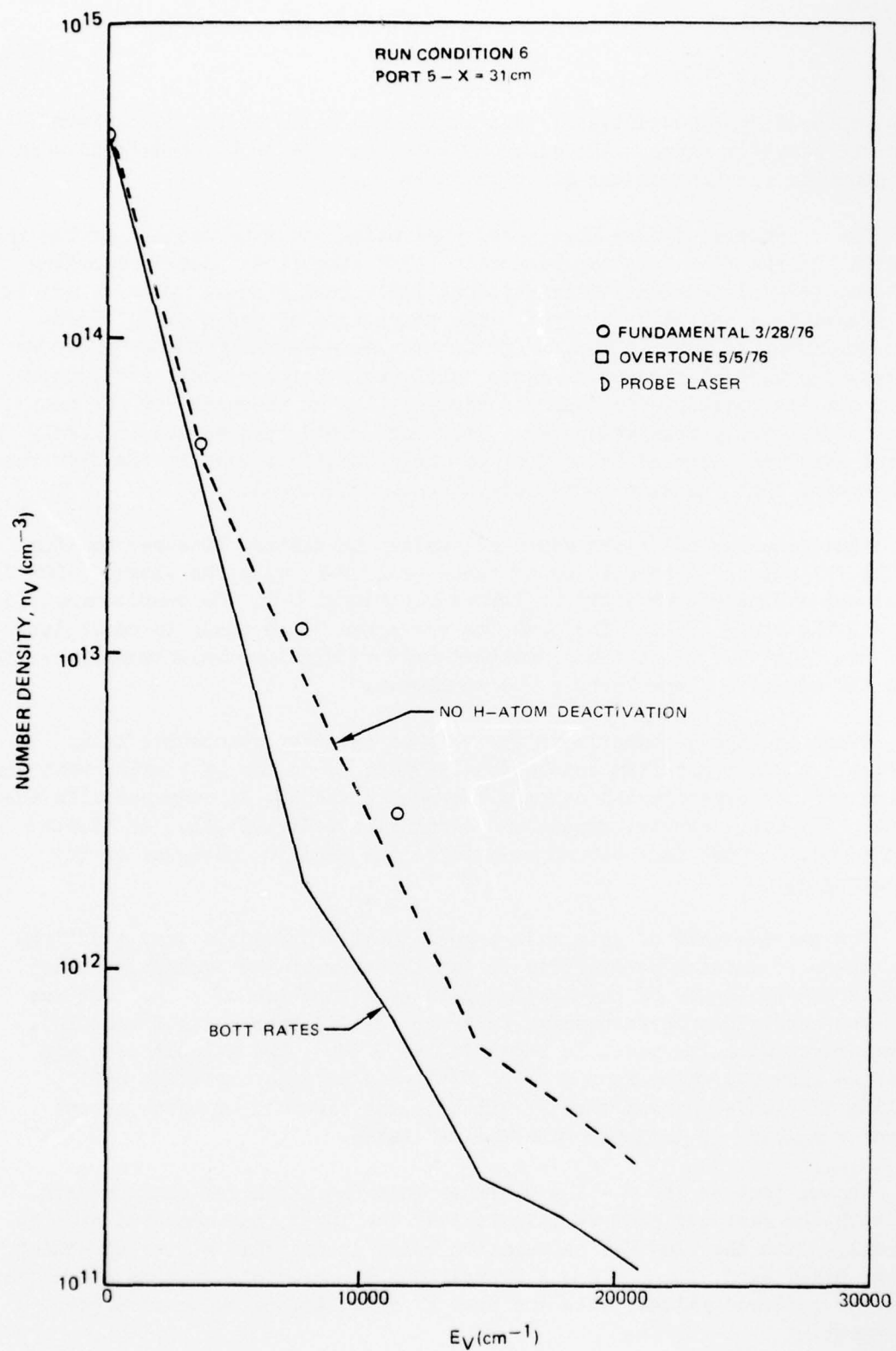


FIGURE 131 VIBRATIONAL POPULATION DISTRIBUTIONS

that appeared representative of that series was selected for comparison with the computer model. The cases selected and the input conditions used in the computer calculation are given in Table 17.

The calculations were first performed using the rate package giving the best fit in the flow tube experiments: (1) H atom rates scaled according to Bott, (2) Multiquanta V-T transitions individually scaled with v , and (3) V-V transitions scaled with $v^{-1/2}$. The comparison of these calculations with experiment is shown in Figures 132 through 148. Generally the slopes in the diminishing part of the curves agree fairly well between model and experiment, but the model predictions for the position of the peak lag far behind the experimentally observed peaks. This more rapid turn around is likely due to the same fast initial adjustment of the populations seen in the flow tube experiments that was also poorly simulated by the model.

Additional calculations were made using the faster, linear- v scaling on the V-V rates. A comparison of these (FAST V-V) with the slower (SLOW V-V) rates and experiments are shown in Figures 143 through 148. The results are typical for all the other cases. The peak for $v = 1$ and $v \geq 6$ tends to occur later than the "slow VV" predictions, and that for $v = 2$ through 5 tends to occur earlier. Also the negative slopes tend to be shallower.

Since the above comparisons are only of relative quantities it is difficult to draw any firm conclusions. There is no way of knowing what concentration the experimental maximum represents and how it compares with the model. It does, however, appear that population redistribution as treated in the model is not fast enough to produce the behavior observed in the experiments.

The measurements of gain made experimentally provide a more quantitative means of gaining perspective on the adequacy of the relaxation model. An experimental study of the maximum gain as a function of transition was made for conditions corresponding to series F (0.2 torr H_2 , 1.0 torr F_2). A comparison with the model is shown in Table 18. Two calculations are shown -- slow VV, which is the "best fit" rate package including $v^{-1/2}$ scaling of the V-V rates; fast VV which is the same set of rates except linear v scaling is employed with the V-V rates.

We see that on the $v = 1 \rightarrow 0$ transitions the predicted maximum gains for both the fast and slow VV calculations are lower than measured experimentally, with the slow V-V calculation being in somewhat better agreement. On the other hand, for $v = 2 \rightarrow 1$ transitions the predicted maxima are higher than the measured values, with the fast VV calculations being in closer agreement.

TABLE 17. INITIAL CONDITIONS - PULSED FLUORESCENCE
VIBRATIONAL STUDIES

Initial Pressure = 100 torr
Initial Temperature = 3000°K

Case	Mole Fractions				
	F	F ₂	H ₂	HF	Ar
A8	1.02×10^{-5}	0.008477	0.008677	0.001863	0.981003
B3	7.20×10^{-6}	0.009130	0.021180	0.002174	0.967509
C3	7.70×10^{-6}	0.009707	0.005336	0	0.984868
DH7	5.47×10^{-6}	0.004907	0.005497	0	0.989591
EF6	7.3×10^{-6}	0.004938	0.010155	0	0.984900
F7*	1.35×10^{-5}	0.01009	0.002345	0	0.987539

*The traces labeled G in the figures are for essentially the same conditions as F7.

TABLE 18. COMPARISON OF PREDICTED AND MEASURED GAIN

Line Variation

Mixture: 0.2 H₂, 1.0 F₂, 98.8 Ar

Line	Experiment		Model		
	Pulse Energy (J)	Gain %/cm	Pulse Energy (J)	Gain Slow VV	Gain Fast VV
1P2	.14	.98	.13	.66	.45
1P3	.13	.78	.13	.89	.67
1P4	.12	1.01	.13	.86	.63
1P6	.12-.14	.55	.13	.36	.22
1P7	.11	.26	.13	.16	.091
2P3	.13	1.2	.13	2.59	1.3
2P4	.12	.66	.13	2.36	1.15
2P5	.11	.48	.13	1.63	.70
2P6	.12-.14	.49	.13	.88	.34

RELATIVE POPULATION DEVELOPMENT

PULSE CASE A8
 $V = 1$

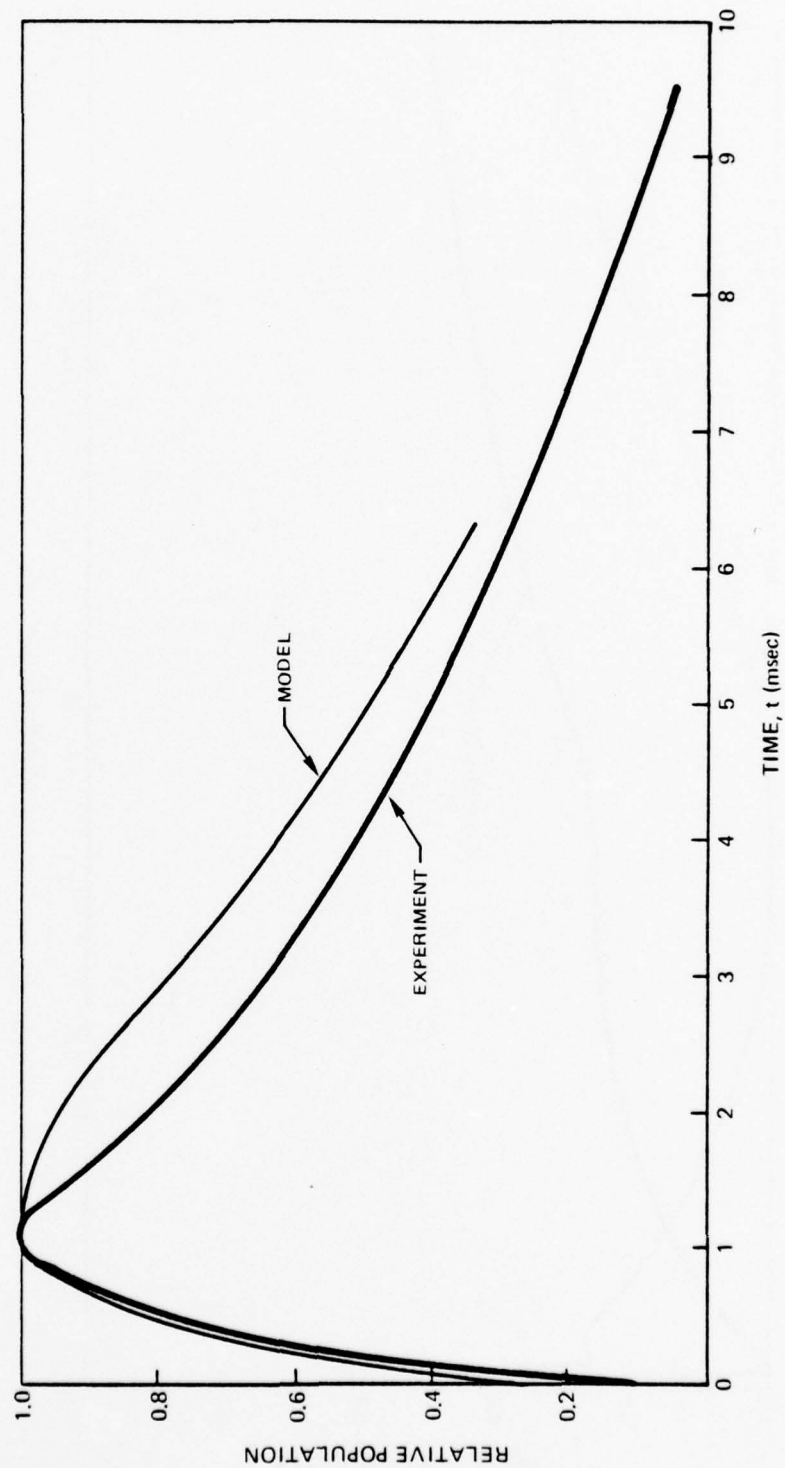


FIGURE 132 COMPARISON OF MODEL WITH EXPERIMENT

PULSE CASE A8
 $V = 2$

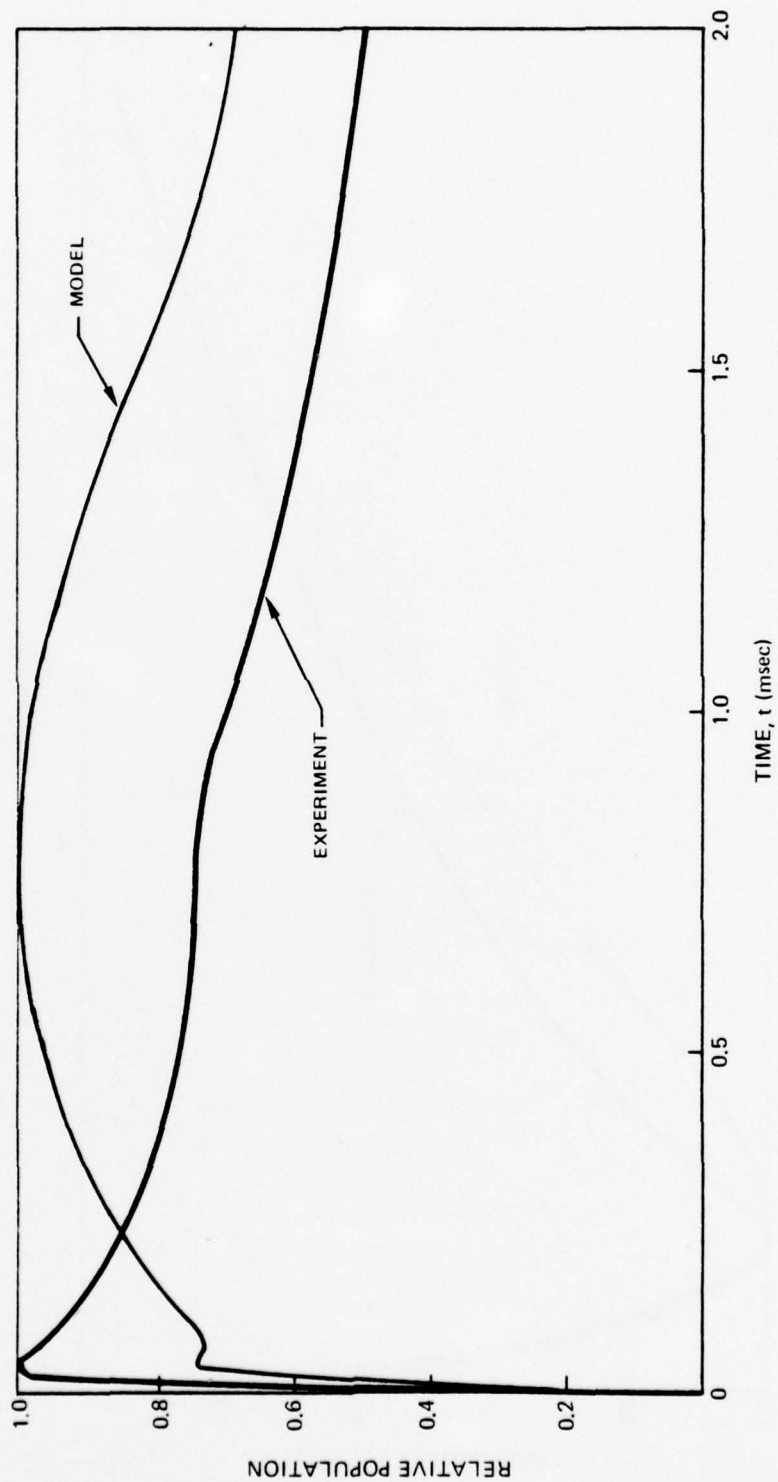


FIGURE 133 COMPARISON OF MODEL WITH EXPERIMENT
RELATIVE POPULATION DEVELOPMENT

PULSE CASE A8
 $V = 3$

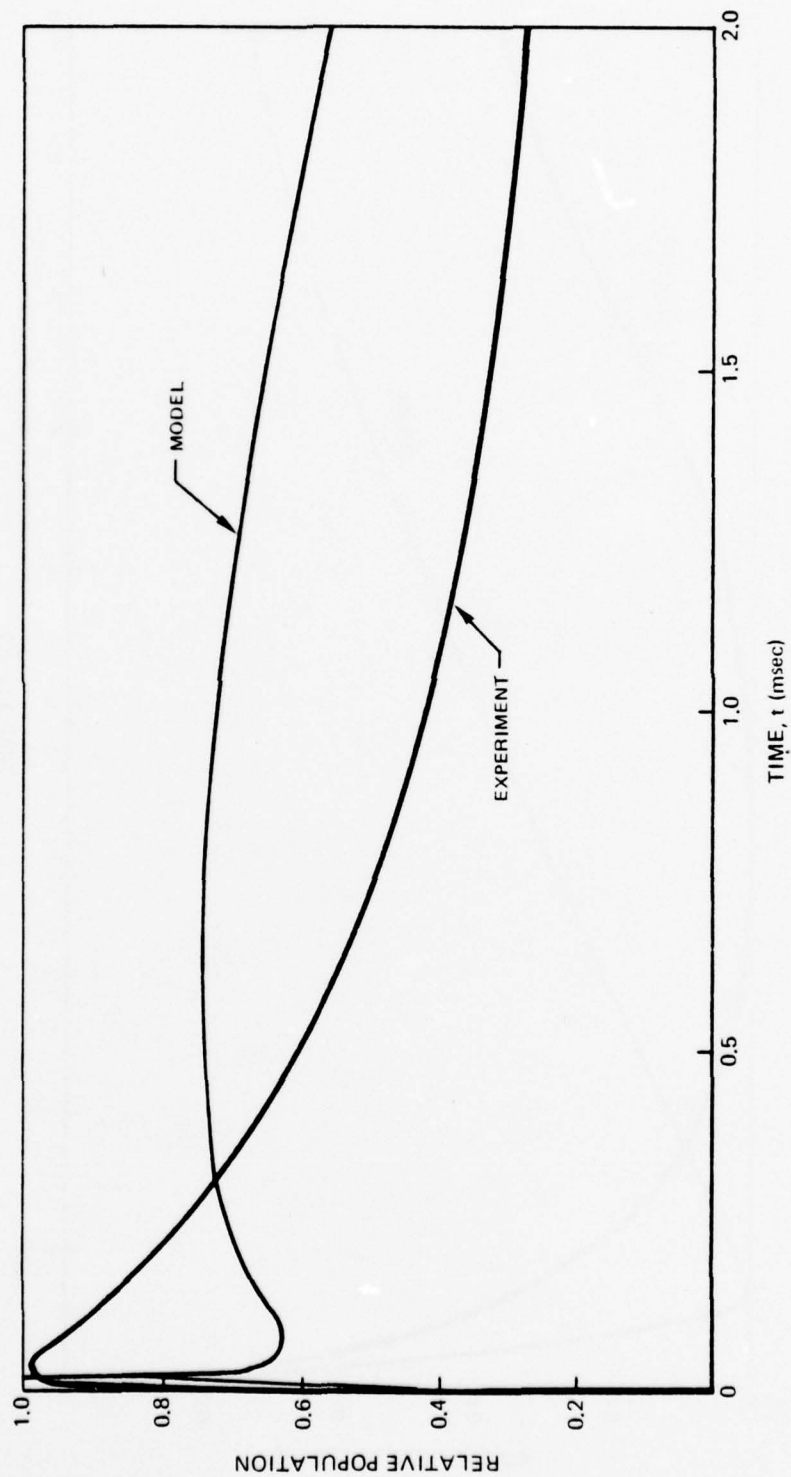


FIGURE 134 COMPARISON OF MODEL WITH EXPERIMENT
RELATIVE POPULATION DEVELOPMENT

PULSE CASE B3
 $V = 1$

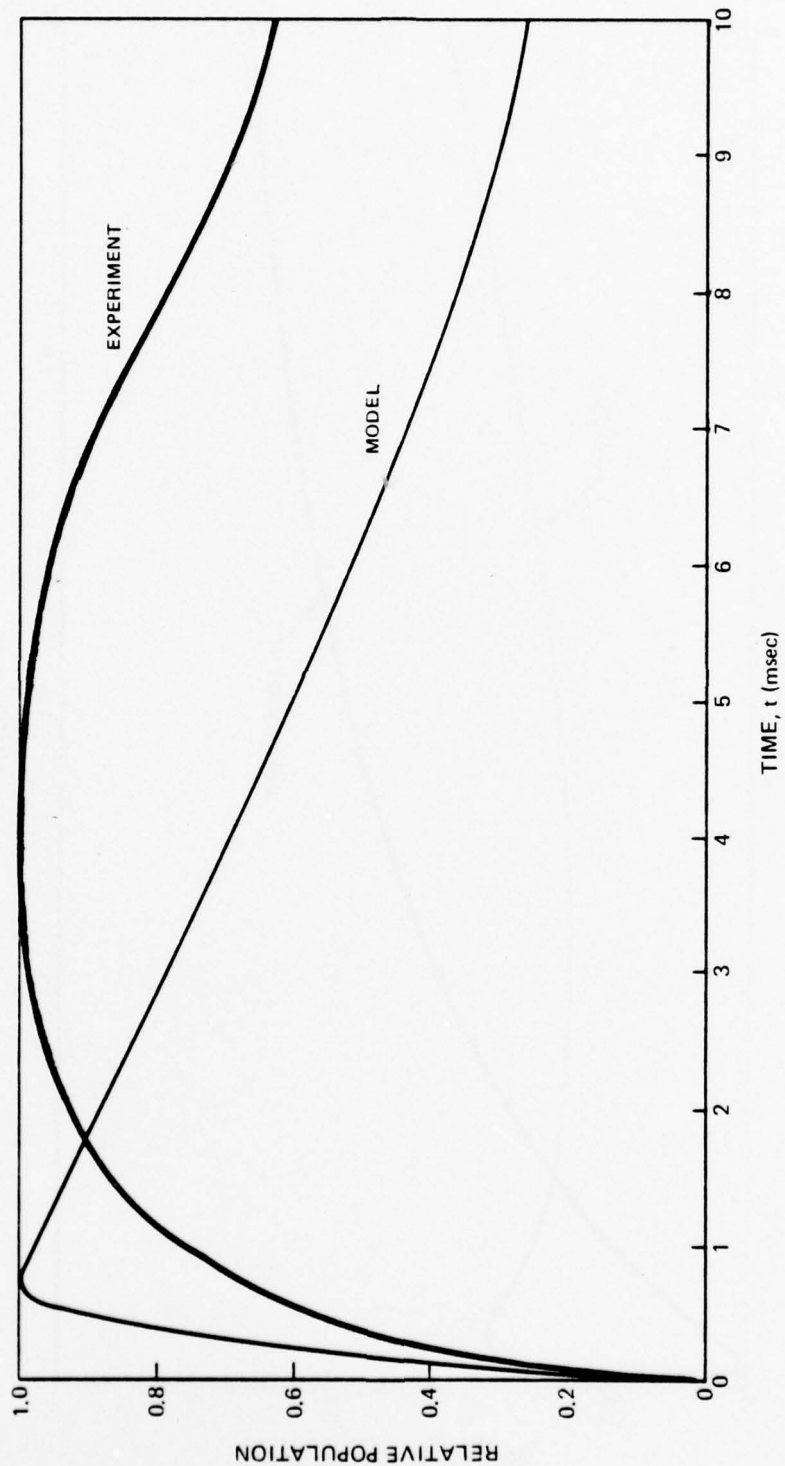


FIGURE 135 COMPARISON OF MODEL WITH EXPERIMENT
RELATIVE POPULATION DEVELOPMENT

PULSE CASE B3
 $v = 2$

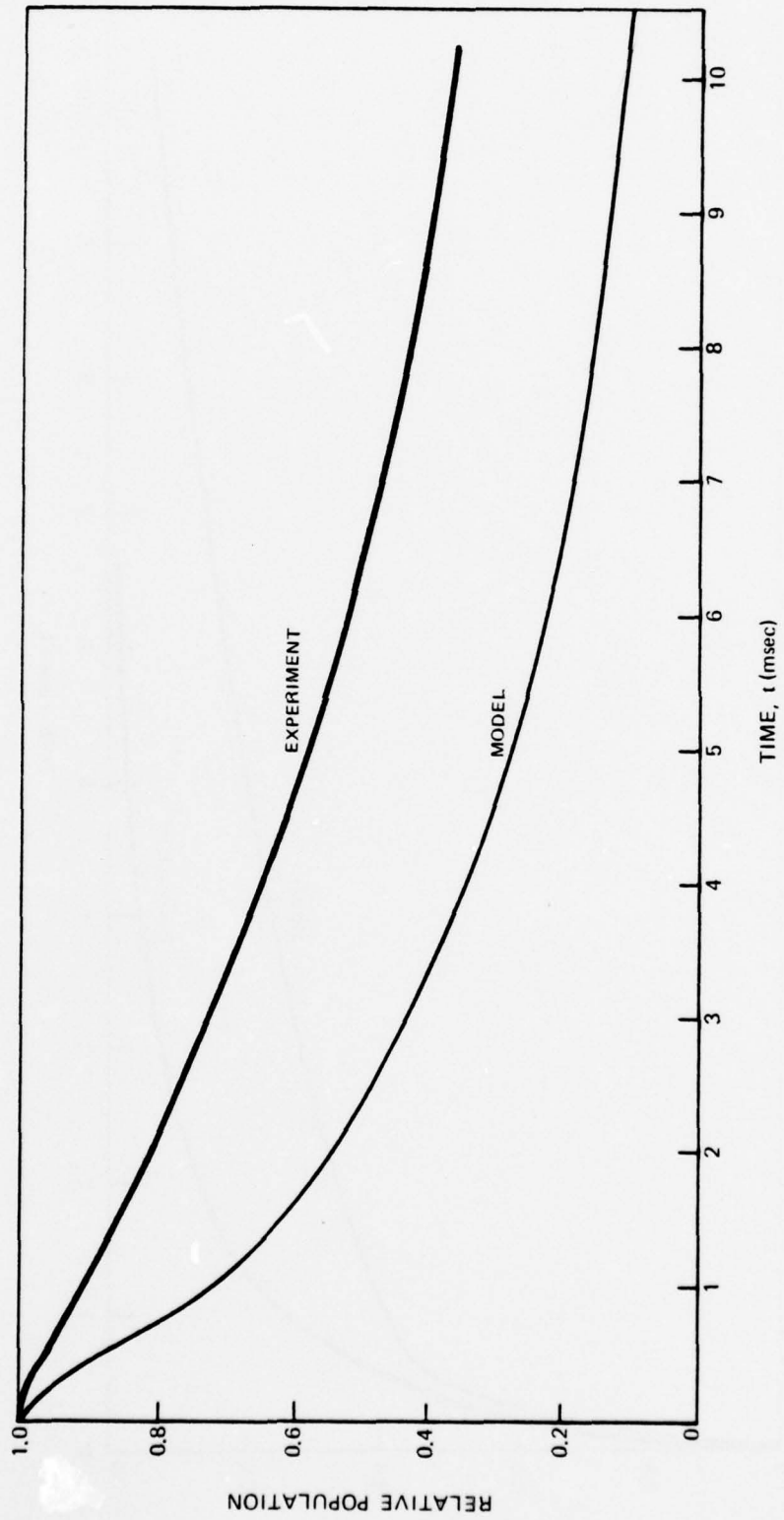


FIGURE 136 COMPARISON OF MODEL WITH EXPERIMENT
RELATIVE POPULATION DEVELOPMENT

PULSE CASE B3

$V = 3$

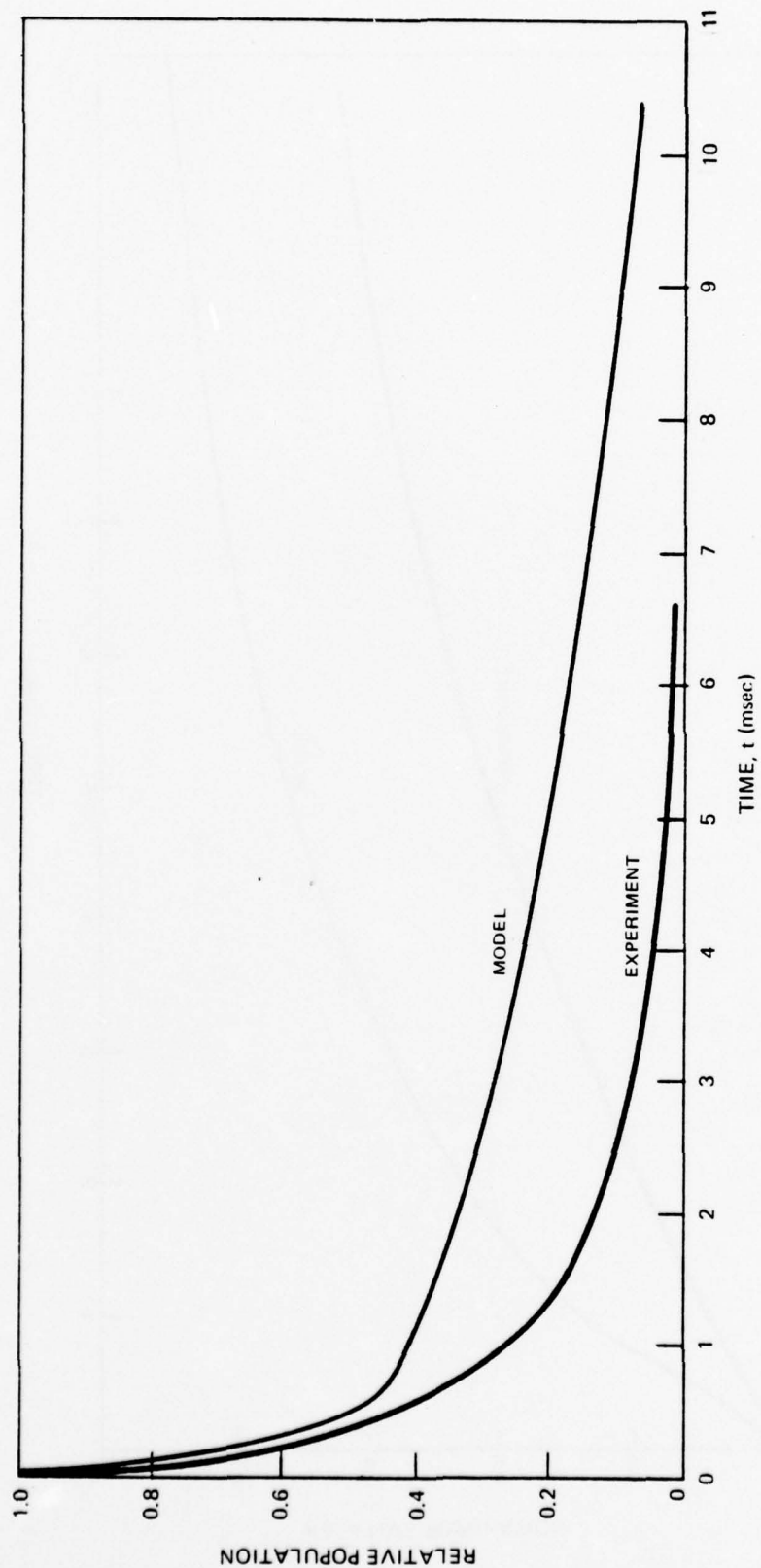


FIGURE 137 COMPARISON OF MODEL WITH EXPERIMENT
RELATIVE POPULATION DEVELOPMENT

PULSE CASE C3

$v = 1$

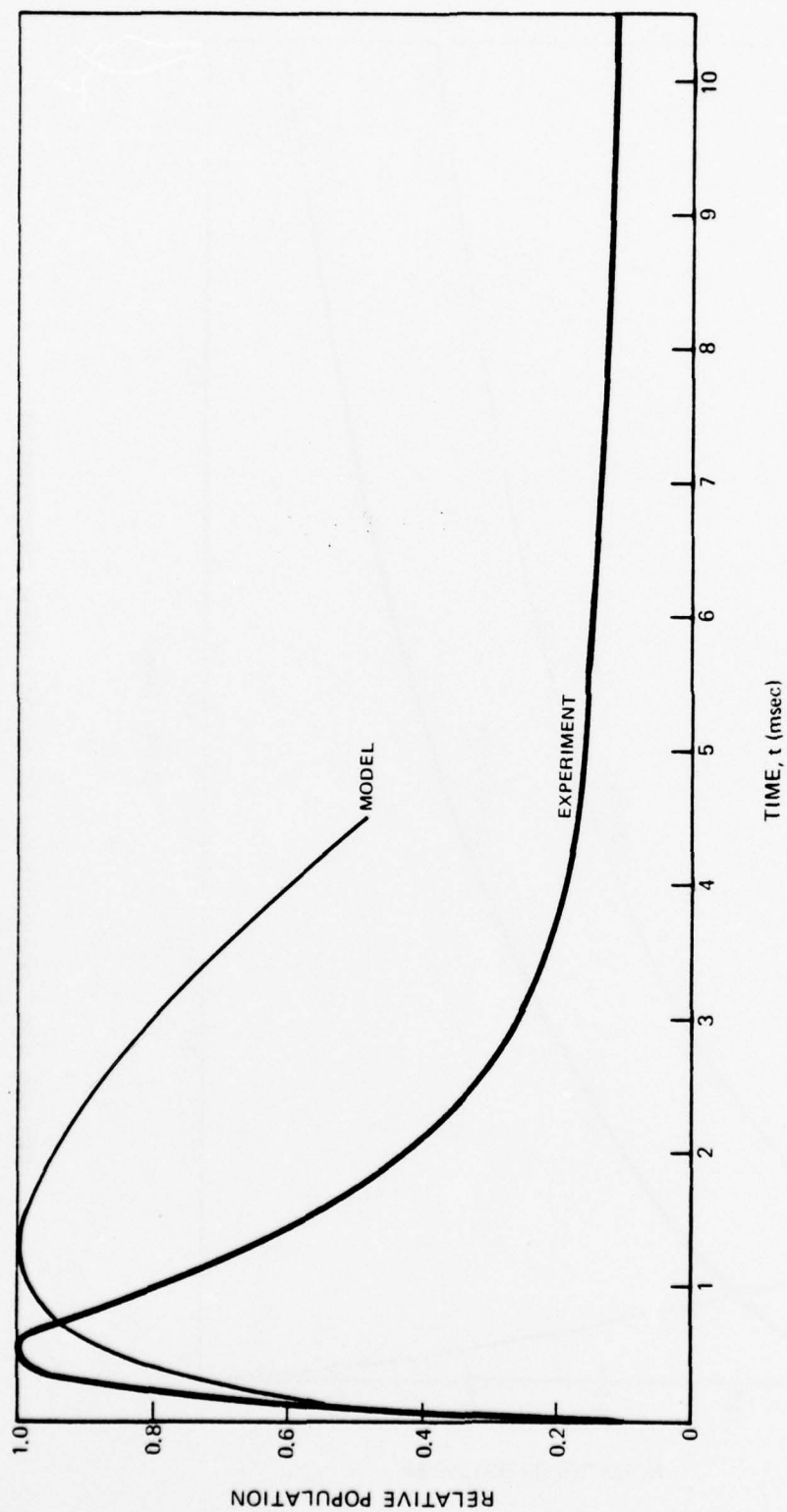


FIGURE 138 COMPARISON OF MODEL WITH EXPERIMENT RELATIVE POPULATION DEVELOPMENT

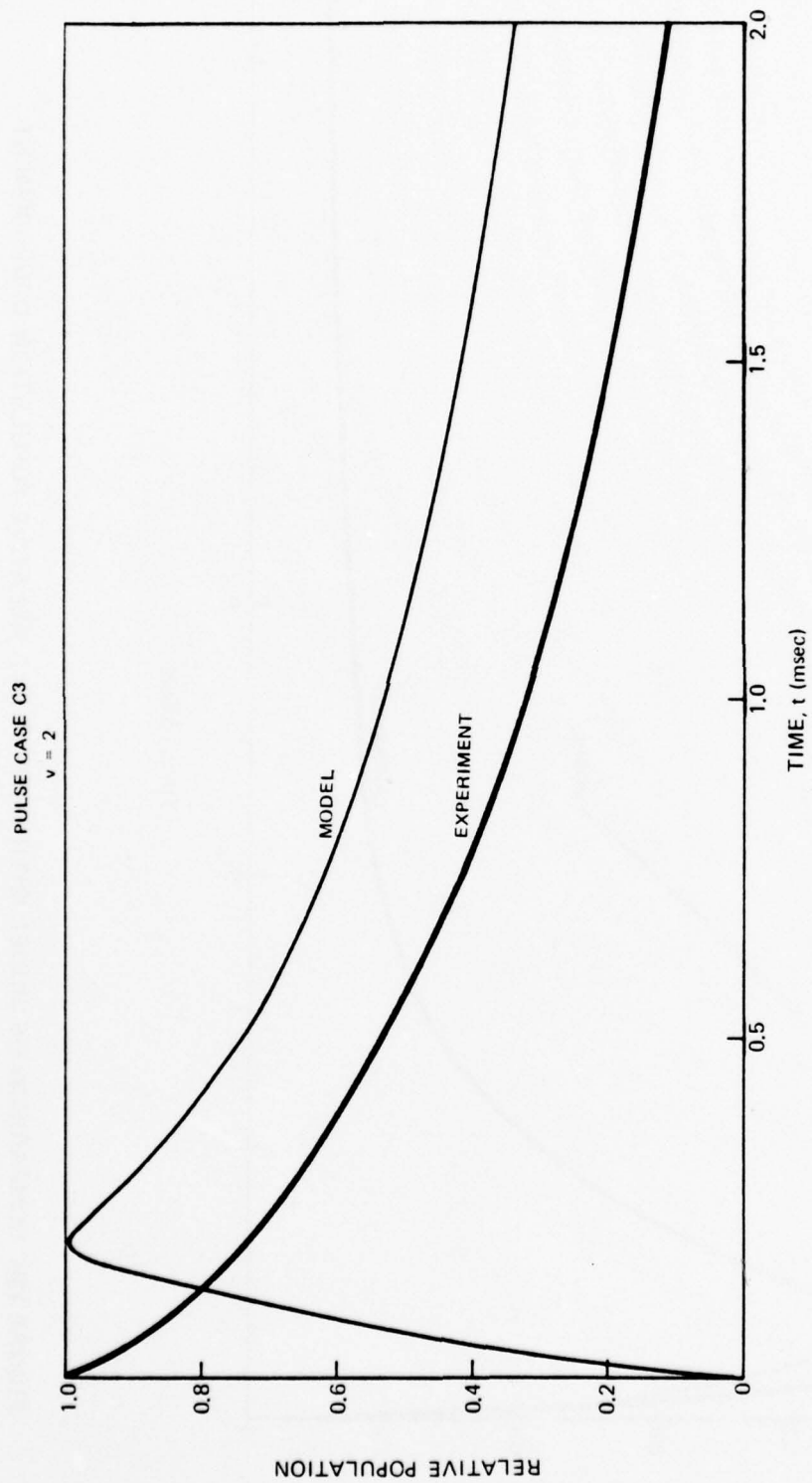


FIGURE 139 COMPARISON OF MODEL WITH EXPERIMENT
RELATIVE POPULATION DEVELOPMENT

PULSE CASE C3
 $V = 3$

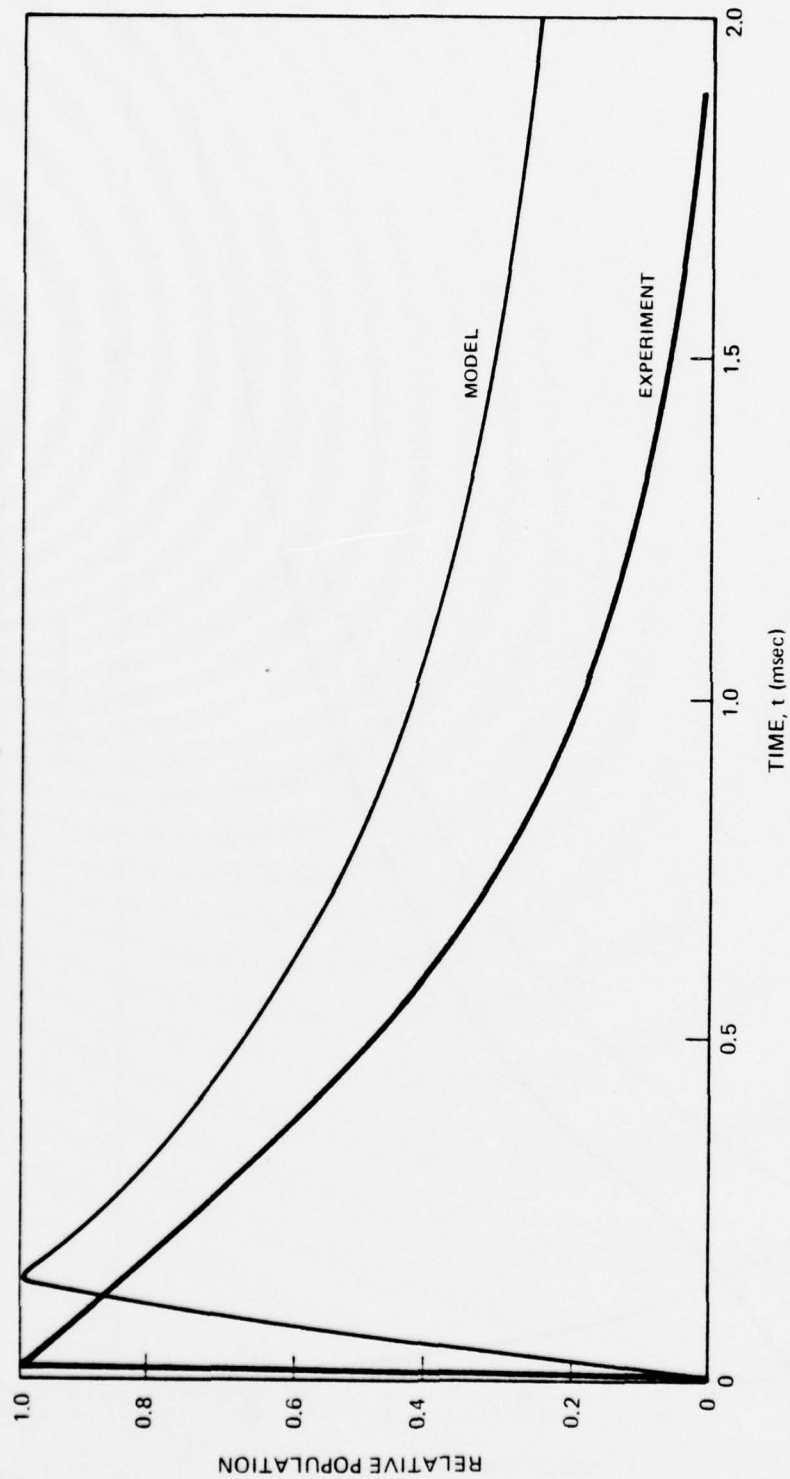


FIGURE 140 COMPARISON OF MODEL WITH EXPERIMENT
RELATIVE POPULATION DEVELOPMENT

PULSE CASE DH7
 $V = 1$

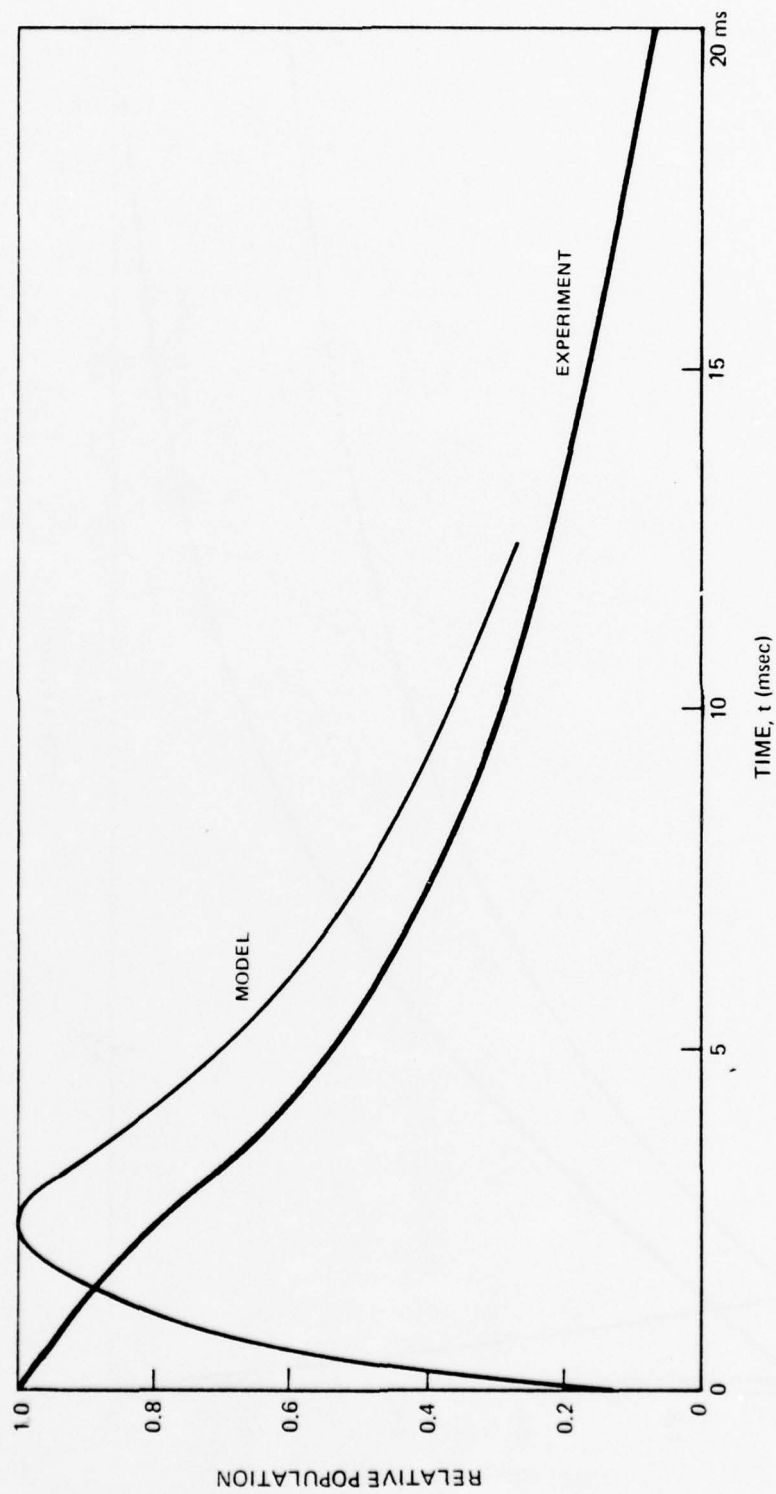


FIGURE 141 COMPARISON OF MODEL WITH EXPERIMENT
RELATIVE POPULATION DEVELOPMENT

PULSE CASE EF6
 $V = 1$

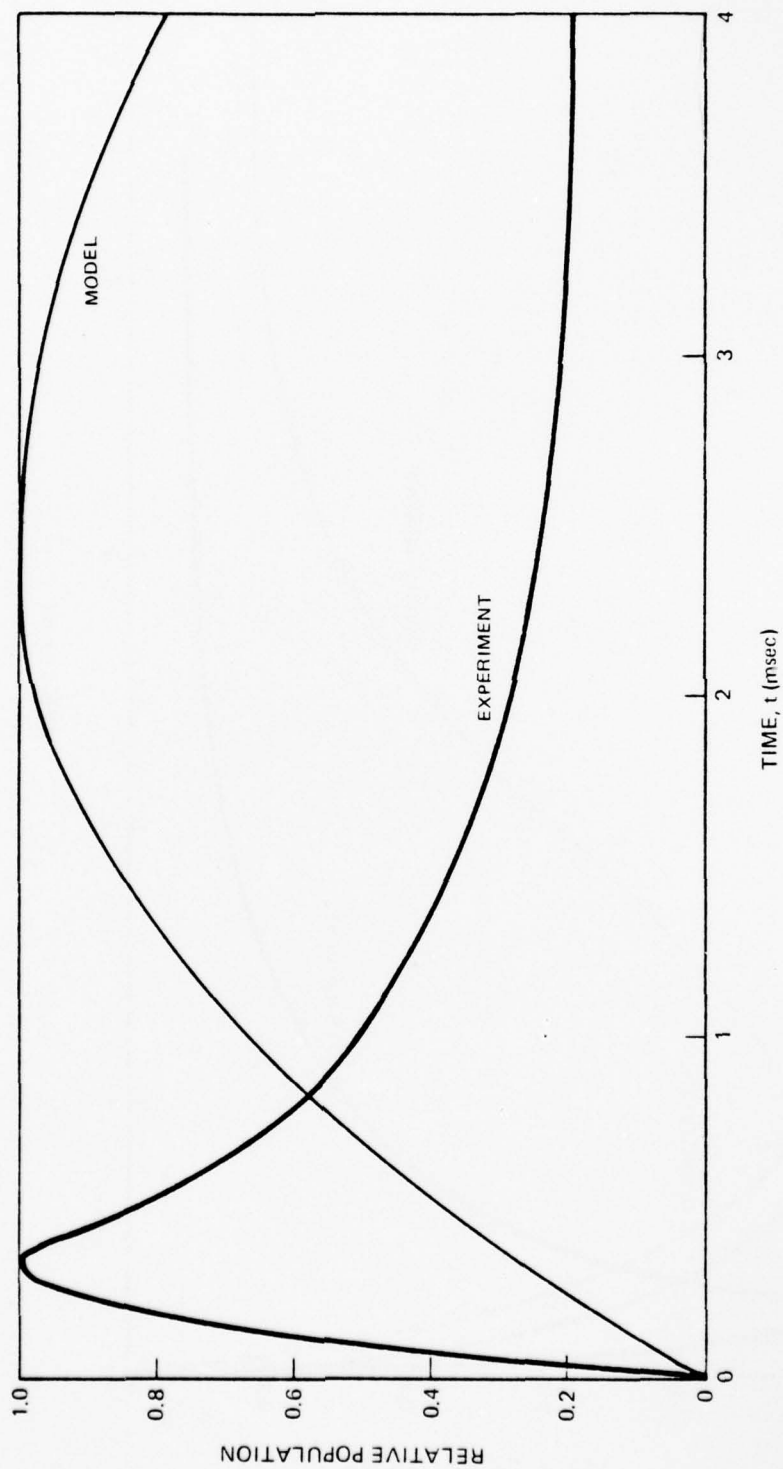


FIGURE 142 COMPARISON OF MODEL WITH EXPERIMENT
RELATIVE POPULATION DEVELOPMENT

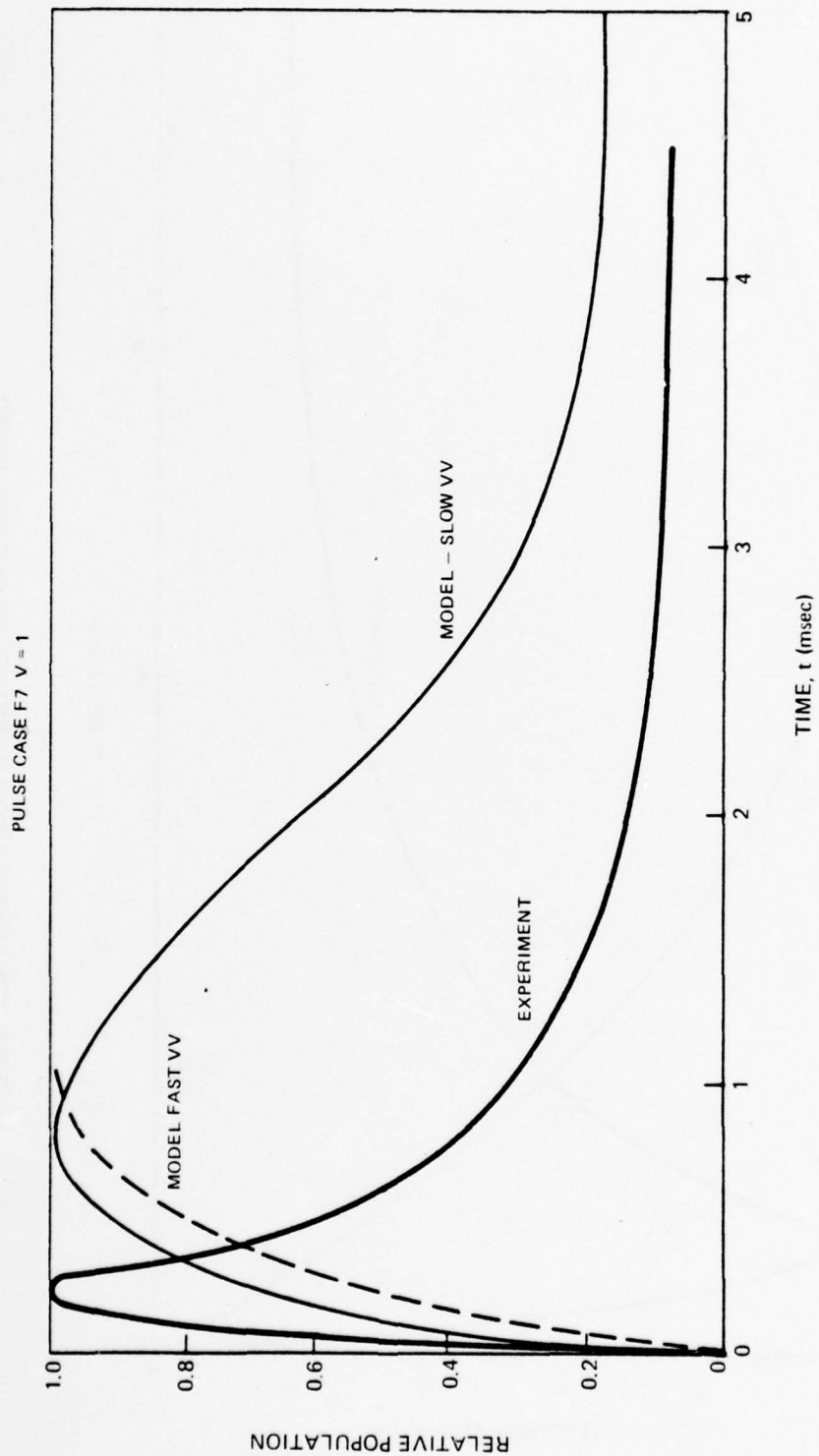


FIGURE 143 COMPARISON OF MODEL WITH EXPERIMENT
RELATIVE POPULATION DEVELOPMENT

PULSE CASE F7
 $V = 2$

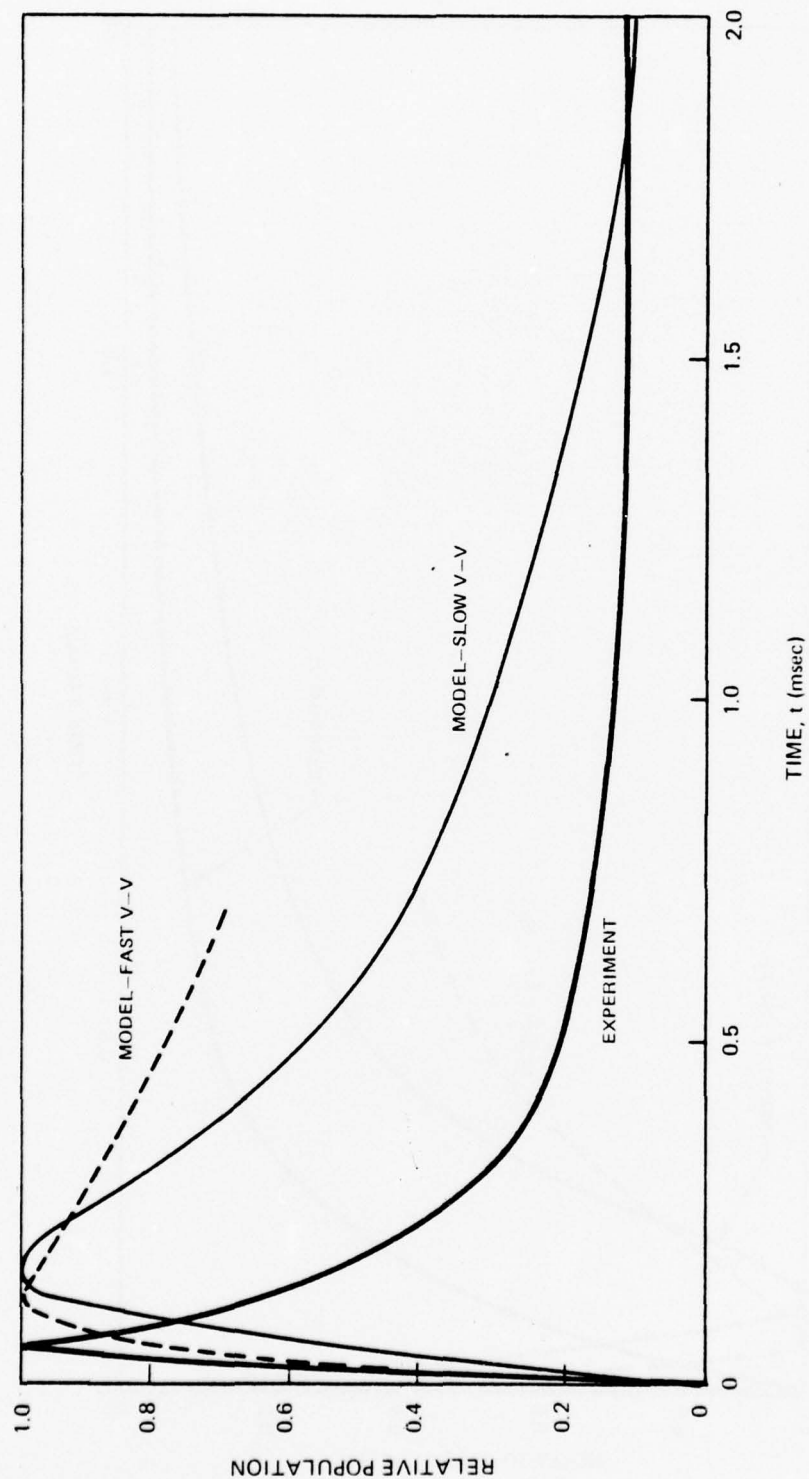


FIGURE 144 COMPARISON OF MODEL WITH EXPERIMENT
RELATIVE POPULATION DEVELOPMENT

PULSE CASE F7
 $V = 3$

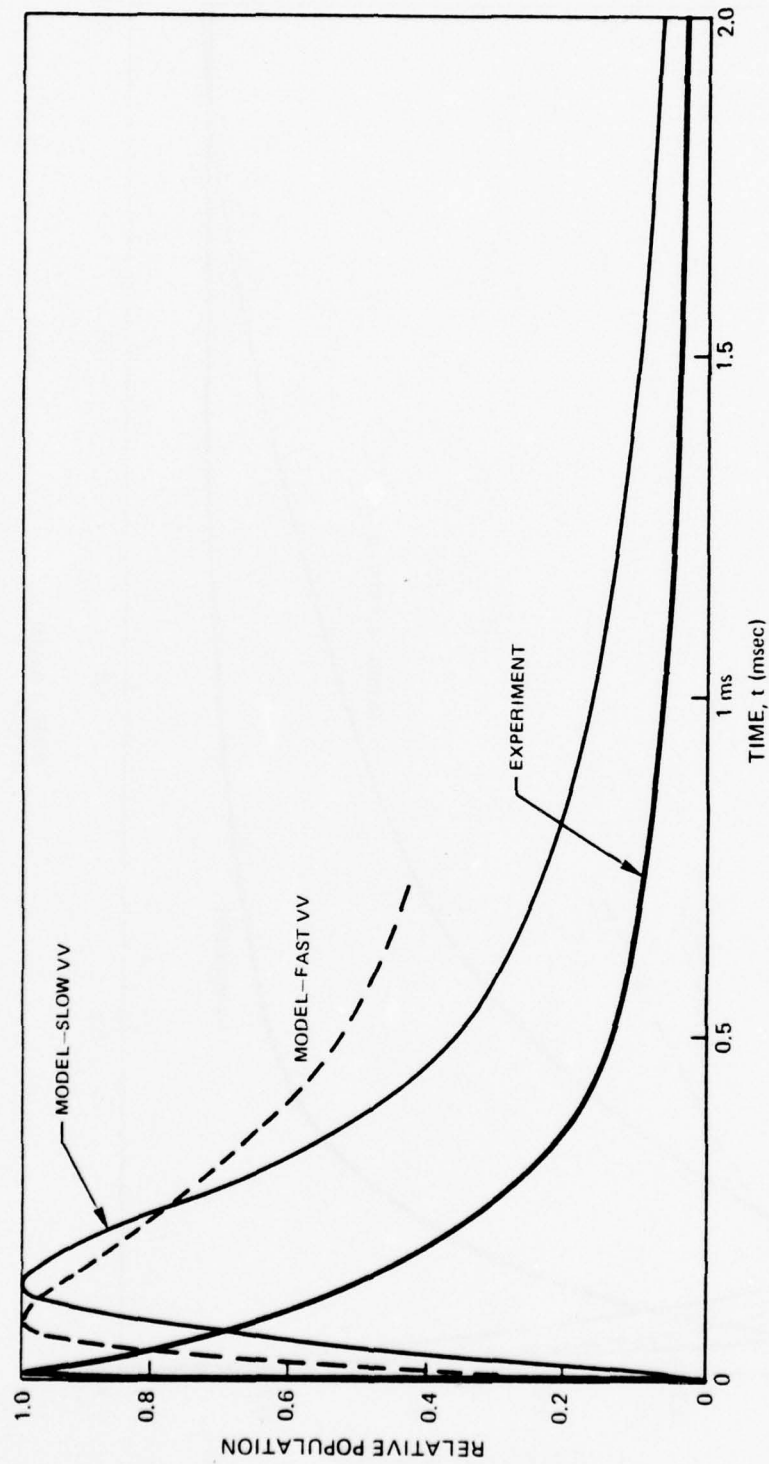


FIGURE 145 COMPARISON OF MODEL WITH EXPERIMENT
RELATIVE POPULATION DEVELOPMENT

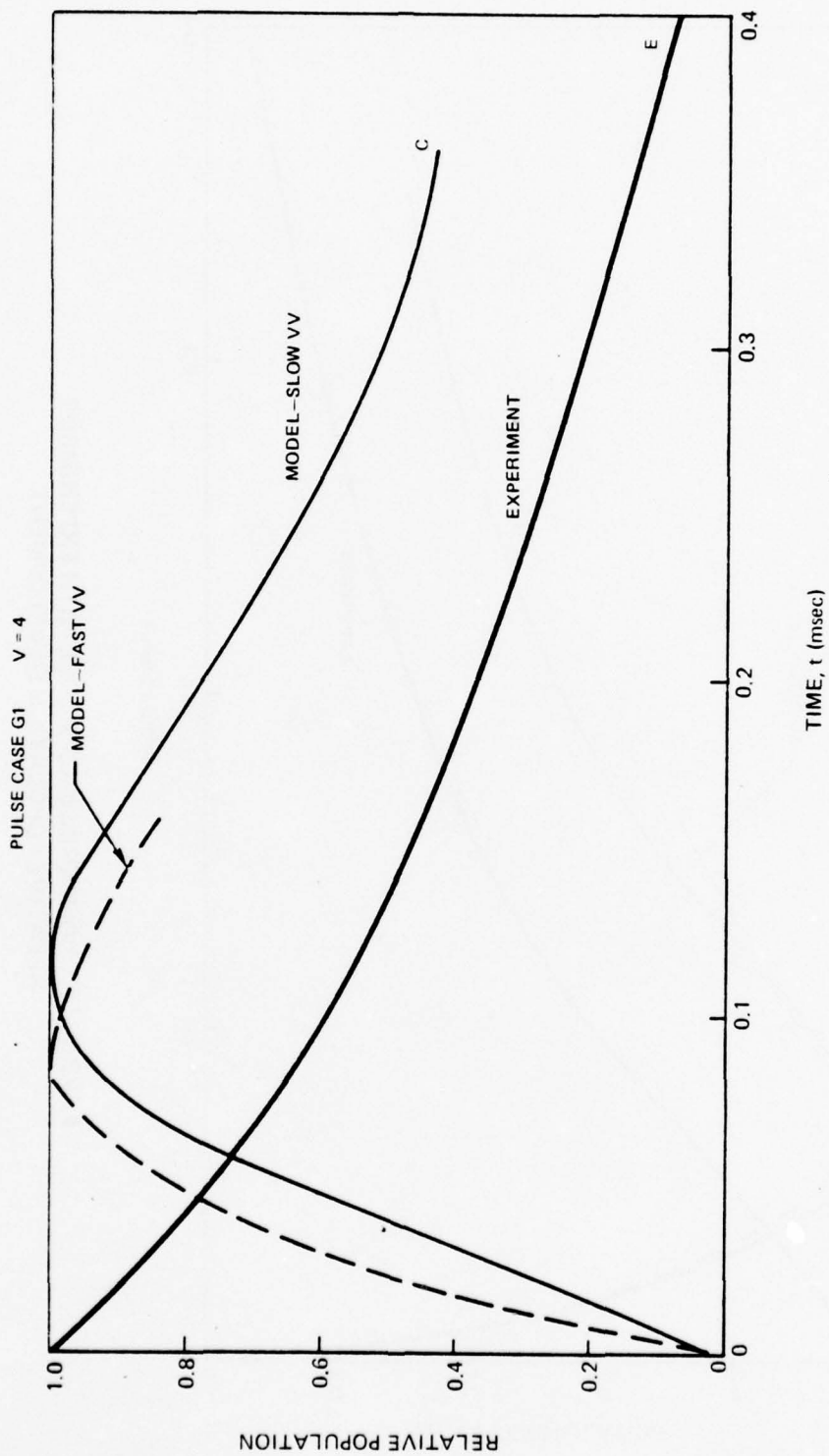


FIGURE 146 COMPARISON OF MODEL WITH EXPERIMENT
RELATIVE POPULATION DEVELOPMENT

PULSE CASE G4
 $V = 5$

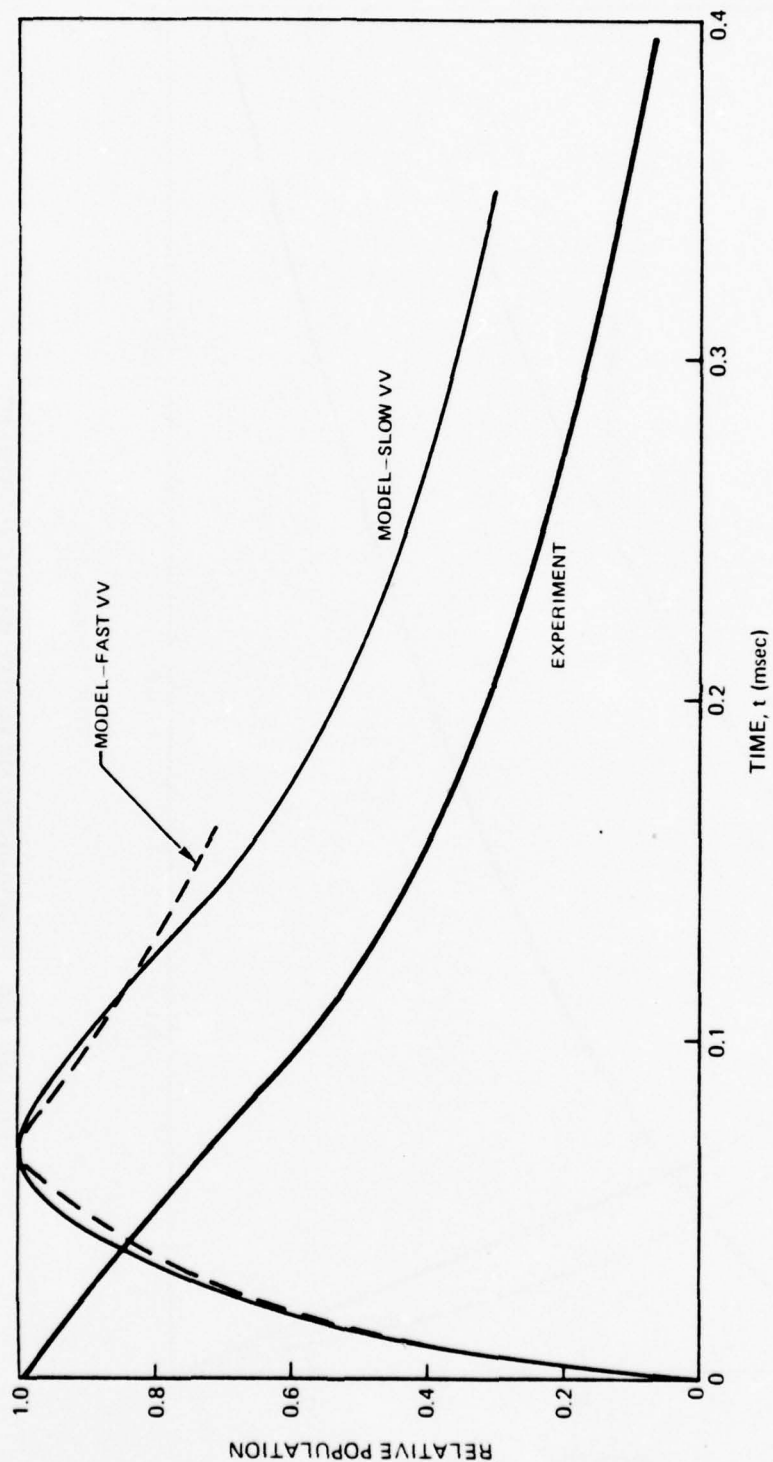


FIGURE 147 COMPARISON OF MODEL WITH EXPERIMENT
RELATIVE POPULATION DEVELOPMENT

PULSE CASE G3

$V = 6$

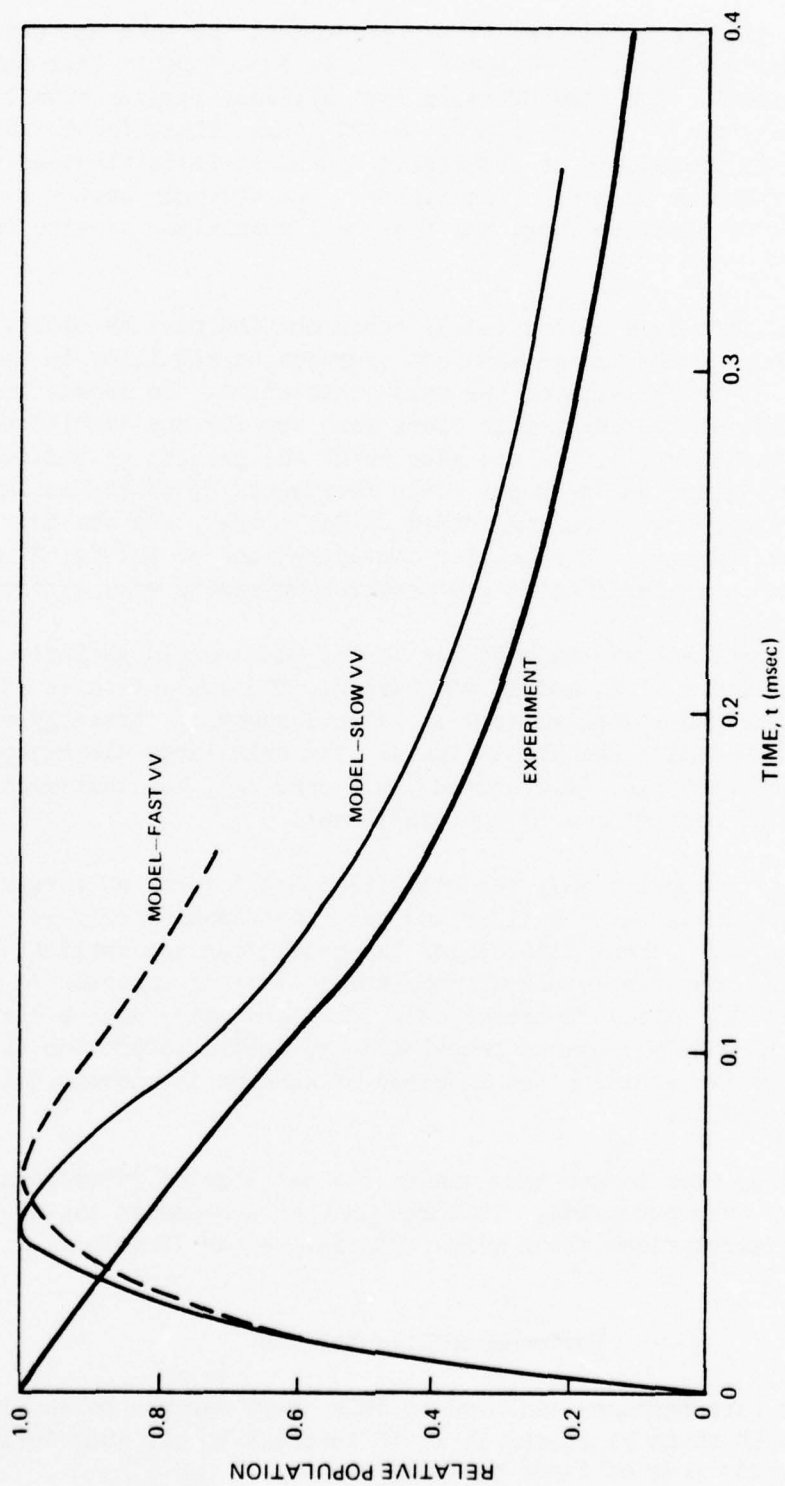


FIGURE 148 COMPARISON OF MODEL WITH EXPERIMENT RELATIVE POPULATION DEVELOPMENT

It should also be noted that in the experiment the gain was observed to have a duration of from 20 to 40 μ sec. This is considerably less than predicted by the model. The slow VV cases had durations ranging from 100 to 300 μ sec and the fast VV cases from 80 to 200 μ sec. These facts indicate that the model is inadequate in describing the rapid redistribution of the primitive distribution on short time scales. The strongly pumped $v = 2$ population remains too high too long, and the $v = 1$ population remains too low (relatively).

The strong influence of initial HF contamination must be noted. In some of the experiments there was an apparent prereaction resulting in small concentrations of HF at the time of the pulse initiation. To assess the possible influence of such HF, two comparable cases were run for run condition C3 (0.5 torr H_2 , 1.0 torr F_2). In one case no HF was present at initiation, and in the other 0.03 torr was present. This represents 3% of the maximum possible HF. The results are summarized in Table 19. We see that the effect is quite dramatic. Far smaller concentrations of initial HF could strongly influence measured gains and render comparisons very difficult.

A final comparison was made to see if the model could properly predict trends as the mixture of H_2 and F_2 was varied. The comparison is shown in Table 20. The model does quite well in this respect, correctly predicting which mixture would give the highest gain. The only large discrepancy is for the hydrogen rich case (1.0 torr H_2 , 0.5 torr F_2), but that might be the result of some HF contaminant in the experiment.

All in all it appears that the relaxation model does an adequate job of predicting vibrational distributions and net vibrational energy loss in most cases. However, over short time scales the model does not duplicate the rapid redistribution of vibrational populations that is apparent in experiment (flow tube and pulsed fluorescence). This indicates that a better VV model, including multiple-quanta transitions is needed to provide the rapid redistribution while avoiding the problems of anharmonic pumping evident in single quantum models.

Furthermore, over longer time scales the net loss of vibrational energy is occasionally over predicted. This implies that a somewhat slower V-T rate model might be appropriate along with revisions to the VV model.

Performance Calculations

While the rate packages employed in this study may not be the last word with regard to HF chain kinetics, it is of interest to see what influence they may have on predictions of laser performance.

TABLE 19. PREDICTED GAIN

Influence of Initial HF

Mixture: 0.5 H₂ 1.0 H₂ 98.5 Ar

Gain (%/cm)

Line	No Initial HF	0.3 Torr HF
1P2	1.10	Absorption ↓ 0.0027 0.0035 0.0041 0.0047
1P3	1.25	
1P4	1.07	
1P5	0.71	
1P6	0.37	
1P7	0.15	
2P3	3.70	
2P4	3.10	
2P5	2.00	
2P6	1.02	

TABLE 20. COMPARISON OF PREDICTED AND MEASURED GAIN

Mixture Variation
Line 1P4

Mixture	<u>Experiment</u>		<u>Model</u>	
	Pulse En. (J)	Gain %/cm	Pulse En. (J)	Gain %/cm
0.2 H ₂ 1.0 F ₂	.12	1.01	.13	0.86
0.5 H ₂ 0.5 F ₂	.11	0.54	.11	0.45
0.5 H ₂ 1.0 F ₂	.11	1.40	.09	1.10
1.0 H ₂ 0.5 F ₂	.08	0.09	.10	.62

Two sets of rates were used for the calculations, designated as C and C_F. These are rates designed to give the best overall fits to both the flow tube and pulsed fluorescence experiments. The set designated as C may be summarized as follows:

- (1) Hot reaction rate = 0.9 x nominal
- (2) Cold reaction rate = 1.5 x nominal
- (3) Multiquanta V-T deactivation scaled linearly with v
- (4) Single quantum Sharma-model VV exchange scaled with $v^{-1/2}$
- (5) H atom deactivation scaled according to the measurements of Bott.

The set designated C_F is identical except the V-V scaling is linear with v .

It was first of interest to assess the influence of the new rate packages on predicted performance of cold reaction lasers. Sample conditions of calculations for the long-range cold-reaction laser (matrix hole nozzle LRC1) are given in Table 21. The resulting calculations are summarized in Table 22. We see that generally little change in the predicted laser output results from use of the new rates. The largest variation is between the two V-V models for the 5 torr case. This is an indication that the V-V model selected can strongly influence power extraction predictions, even if there is little apparent difference in unloaded population distributions.

A comparison was also made with some calculations previously performed under a U.S. Army sponsored chain-reaction demonstration contract (Ref. 33). Two cases in particular were considered: (1) The initial design point, and (2) a later, more realistic design point. The input conditions for these are given in Tables 23 and 24. The resulting predictions are shown in Tables 25 and 26. These calculations are admittedly optimistic since aerodynamic and optical effects likely to degrade performance are not adequately included in the model. Even so the predicted performance is in the range which renders the chain reaction at best marginally competitive with the cold reaction as a laser pumping mechanism.

33. Kepler, C. E., et al., "Demonstration of HF Chain Reaction Laser," UTRC Technical Report RK-CR-75-4, UTRC, East Hartford, CT, July 1974.

TABLE 21. INPUT CONDITIONS - LONG RANGE COLD REACTION LASER

$$\alpha = 0.90$$

$$\text{He} = 0.157$$

$$p = 1.0, 5.0$$

$$g_0 = 0.003 \text{ cm}^{-1}$$

$$L_{\text{mix}} = 0.154, 0.77$$

Constant Pressure Option

Cavity Entrance Conditions

	<u>Primary</u>	<u>Secondary</u>
X_{He}	0.15652	---
X_{DF}	0.14311	---
X_{F2}	0.00626	---
X_{F}	0.11271	---
X_{H2}	---	0.58140
$u \text{ (cm/sec)}$	114345	364845
$T \text{ (°K)}$	268	339

TABLE 22. PREDICTED PERFORMANCE - COLD REACTION LASER

Case	Rate Package	X_L -cm	σ -J/g (kJ/lb)
p = 1	Nominal	0.79	723 (329)
	C	0.77	714 (325)
	C_F	0.71	688 (313)
p = 5	Nominal	0.66	271 (123)
	C	1.18	381 (173)
	C_F	0.78	275 (125)

TABLE 23. INPUT CONDITIONS - DESIGN POINT
CHAIN REACTION LASER

$$\alpha = 0.05$$

$$\text{He} = 0.85$$

$$p = 20 \text{ torr}$$

$$g_0 = 0.001 \text{ cm}^{-1}$$

$$L_{\text{mix}} = 5 \text{ cm}$$

Constant Pressure Option

Cavity Entrance Conditions

	<u>Primary</u>	<u>Secondary</u>
X_{He}	.63512	.21173
X_{F2}	.07098	---
X_{F}	.00747	---
X_{H2}	---	.07470
$u(\text{cm/sec})$	212000.	212000.
$T (^{\circ}\text{K})$	150	75

TABLE 24. INPUT CONDITIONS - REPRESENTATIVE
CHAIN REACTION LASER

$$\alpha = 0.10$$

$$\text{He} = 0.925$$

$$p = 20 \text{ torr}$$

$$g_0 = 0.001$$

$$L_{\text{mix}} = 10 \text{ cm}$$

Constant Pressure Option

Cavity Entrance Conditions

	<u>Primary</u>	<u>Secondary</u>
X_{He}	.69375	.23125
X_{F2}	.03068	---
X_{F}	.00682	---
X_{H2}	---	.03750
$u \text{ (cm/sec)}$	226600	195770
$T \text{ (°K)}$	157	75

TABLE 25. PREDICTED PERFORMANCE - DESIGN POINT
CHAIN REACTION LASER

Rate Package	X_L - cm	σ - J/g, (kJ/lb)	$\frac{\sigma_v}{\sigma} > 3$
Nominal	22	1012 (460)	0.39
C	20	572 (260)	0.21
C _F	20	480 (218)	0.28

TABLE 26. PREDICTED PERFORMANCE - REPRESENTATIVE
CHAIN REACTION LASER

Rate Package	X_L - cm	σ - J/g, (kJ/lb)	$\frac{\sigma_v}{\sigma} > 3$
Nominal	30	475 (216)	0.38
C	30	275 (125)	0.15
C _F	29	174 (79)	0.19

To see whether a more competitive set of conditions could be found for the chain reaction, some conditions were used in calculations over a range of higher pressures (to aid in recovery). The input conditions for these are shown in Table 27. Included are some fluorine rich cases reflecting the experimental observation that they produce the best gain. The results of these calculations are summarized in Tables 28 and 29. We see that, on paper at least, higher pressure performance, especially fluorine rich, provides more favorable performance from the chain, indicating a possible regime in which such lasers might have some specialized applications.

Discussion

Chemical Reactions

Some difficulty was encountered in trying to find a set of chemical reaction rates that would fit both the flow-tube and the pulsed fluorescence data. The flow-tube results implied somewhat lower rates than did the pulsed-fluorescence data. While some systematic error or unaccounted for reaction mechanism might explain the differences, we were unable to find a satisfactory resolution to the discrepancies. Consequently a fairly wide range must be applied to the values for the rate coefficients we have evaluated. For the hot reaction we find over the range $300 < T < 380^{\circ}\text{K}$

$$k_h = 1.8 \times 10^{-10} \exp(-2400/RT) \text{ cc/molecule-sec}$$

with an error band of ± 40 percent. This is 90 percent of the nominal value of Albright, et al. Because of the limited temperature range, no conclusion could be drawn about the temperature dependence of the rate, hence Albright's value has been used. There is a wide enough range in temperatures, however, to require the inclusion of temperature dependence in order to achieve a realistic fit to the data.

For the cold reaction we find that

$$k_c = 4.0 \times 10^{-10} \exp(-1600/RT) \text{ cc/molecule-sec}$$

with an error band of ± 35 percent. The nominal value of Hommann, et al., lies at the lower end of this range. Again, no conclusions could be drawn with regard to the temperature dependence.

In the pulse experiments, very fast back reaction rate coefficients that would be most important in the higher concentration cases (A, B, and C) and those with stronger upper level populations (C and F) can be invoked to

TABLE 27. INPUT CONDITIONS - CHAIN REACTION
PRESSURE VARIATION STUDIES

$$\alpha = 0.05$$

$$p = 20, 60 \text{ torr}$$

$$g_0 = 0.001$$

$$L_{\text{mix}} = 10, 30 \text{ cm}$$

Constant Pressure Option

CAVITY ENTRANCE CONDITIONS

Case - 92.5% He, $F_2/H_2 = 1$

	<u>Primary</u>	<u>Secondary</u>
X_{He}	.69375	.23125
X_{F_2}	.03393	---
X_{F}	.00357	---
X_{H_2}	---	0.03750
u	226600	195770
T	157	75

Case - 95% He, $F_2/H_2 = 1$

X_{He}	.7125	.2375
X_{F_2}	.02262	---
X_{F}	.00238	---
X_{H_2}	---	.002500
u	226600	195770
T	157	75

Case - 88.75% He, $F_2/H_2 = 2$ ($\alpha = 0.025$)

X_{He}	.55625	.23125
X_{F_2}	.07143	---
X_{F}	.00357	---
X_{H_2}	---	0.0375
u	226600	195770
T	157	75

TABLE 28. PREDICTED PERFORMANCE -
EFFECT OF PRESSURE VARIATION

Case	Rate Package	P (torr)	X _L (cm)	σ (J/g)	$\frac{\sigma_{v>3}}{\sigma}$	P _o (torr)	f _{HF}	T _e (°K)	M
92.5% He	C	20	56	229	0.20	74	0.88	808	1.48
		60	18	286	0.21	220	0.89	872	1.43
95% He		20	13	14	0	304	0.05	165	3.15
		60	48	128	0.32	250	0.93	654	1.58
92.5% He	C _F	20	51	136	0.27	95	0.62	614	1.70
		60	17	202	0.29	292	0.61	693	1.60
95% He		20	20	13	0	306	0.05	165	3.15
		60	39	77	0.46	289	0.75	561	1.60

TABLE 29. PREDICTED PERFORMANCE -
EFFECT OF FLUORINE

Case	Rate Package	P (torr)	X _L (cm)	σ (J/g)	$\frac{\sigma_{v>3}}{\sigma}$	P _o (torr)	f _{HF}	T _e (°K)	M
F ₂ /H ₂ =1	C _F	20	51	136	0.27	95	0.62	614	1.70
		60	17	202	0.29	292	0.61	693	1.60
F ₂ /H ₂ =2		20	33	341	0.36	96	0.85	783	1.70
		60	13	321	0.38	337	0.69	832	1.65

explain the anomalously fast reaction rates seen for the lower concentration cases (D and E). But that would require correspondingly faster forward rates. Furthermore the back reaction rates now are already taken to be nearly gas kinetic for the higher vibrational levels. While there is not enough firm evidence here to justify support of such a possibility, it is perhaps something that bears further study.

Supplemental chemical reactions were not found to be important. Hot atom effects could be important in specialized situations used to create F atoms and might come into play in pulsed devices. Such a situation could best be handled in a model by appropriately modifying the initial F atom concentration to reflect additional dissociation from F^*-F_2 collisions. Any hot atom effects arising from the chain reaction are likely to be masked in the overall hot and cold reaction rates. In the highly dilute cases tested here, such effects would be minimal. Less dilute situations might result in slightly faster effective rates (Ref. 34).

Wall interactions, which are highly specific to individual devices, can in some cases be important. At the very least in these experiments H-atom loss appears to have played a role in the flow tube and possibly also in the pulse cases (to help explain the lessening rate of reaction at later times). In any case care should be taken in evaluating any device to assess the influence of the walls if possible.

The currently recommended chemical reaction rates for H_2-F_2 chain reaction lasers are listed in Table 30.

Vibrational Deactivation

Since there are so many potential transitions involving HF vibrational states and since there is a fair amount of error in any experimental measurements, no set of rates that might be proposed is necessarily unique. Widely divergent approaches as to which transitions are important can lead to equally good fits of the available data.

In this program we have taken approach that assumes V-V interactions to be relatively unimportant for upper vibrational levels, while V-T deactivation scales up rapidly with increasing vibrational level. For such a model we find relatively good agreement with the experimental data. Some of the salient features of the model are summarized below.

-
34. Sullivan, J. H. and R. C. Feber, "The Kinetics of an H_2-F_2 Explosion as Initiated by a Pulse of Fluorine Atoms," Report LA-5409, Los Alamos Scientific Laboratory, Los Alamos, NM, 1974.

TABLE 30. RECOMMENDED CHEMICAL RATES

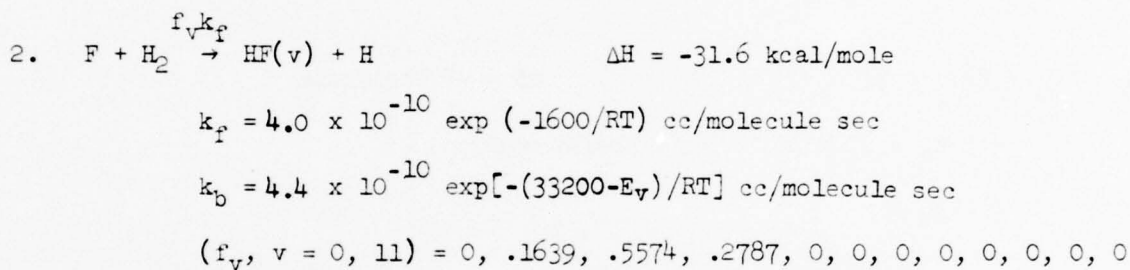
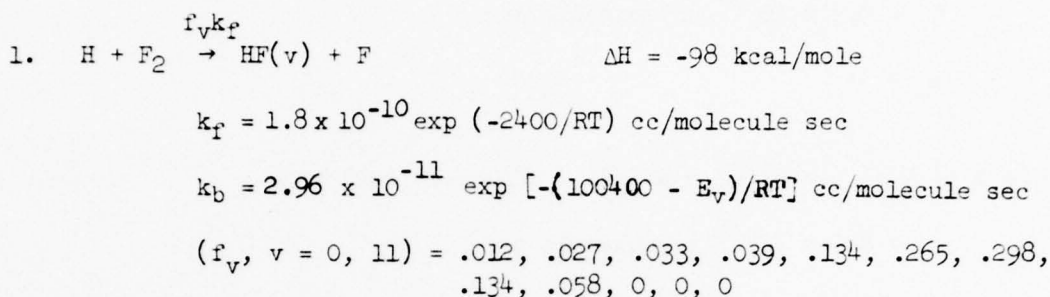
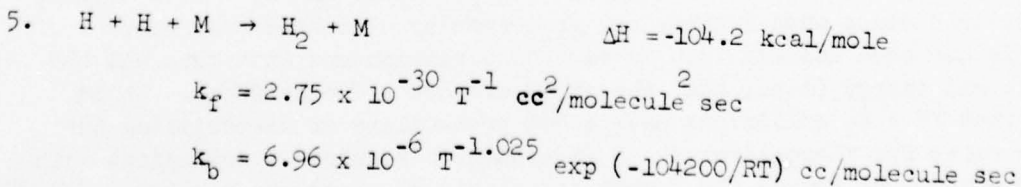
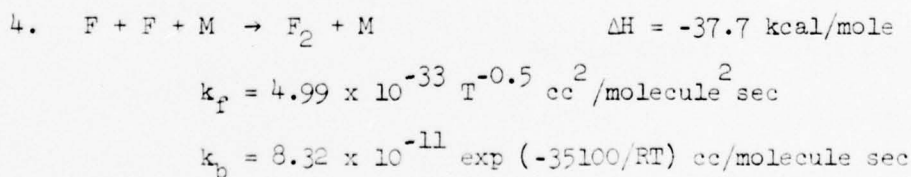
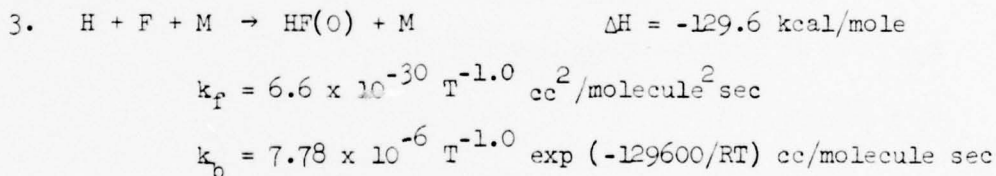
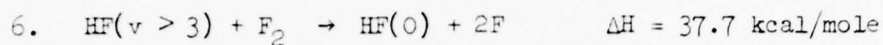
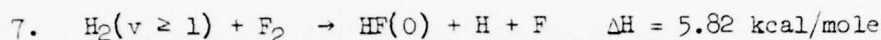
Optional

TABLE 30. RECOMMENDED CHEMICAL RATES (CONT'D)



$$k_f = 3.5 \times 10^{-17} \text{ cc/molecule sec}$$

$$k_b \equiv 0$$



$$k_f = 8.0 \times 10^{-19} \text{ cc/molecule sec}$$

$$k_b \equiv 0$$



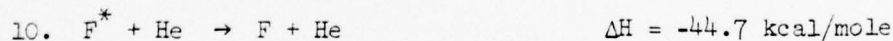
$$k_f = .7 \times 10^{-9} \text{ cc/molecule sec}$$

$$k_b = 0$$



$$k_f = 3 \times 10^{-10} \text{ cc/molecule sec}$$

$$k_b = 0$$



$$k_f = 1 \times 10^{-10} \text{ cc/molecule sec}$$

$$k_b = 0$$

Note: reactions 8-10 have been used as an upper limit on hot F atom effects in low diluent cases when F atoms are generated by a doubled ruby laser pulse. It has been assumed that in each dissociation one atom gets all the translational energy (i.e., half the atoms are hot - $T \approx 15000^\circ\text{K}$). It is assumed that $\text{F}^* + \text{F}_2$ collisions have a 50% probability of dissociating the F_2 . The rates for thermalization of F^* assume it requires 5 collisions with Ar or 10 with He to reduce the F atom translational energy to a value ($\sim 1500^\circ\text{K}$) at which enhanced dissociation would be minimal. In any situation in which the initiation of a pulsed laser might produce hot F atoms, a scheme of this sort (or more sophisticated) might be required to adequately model the results.

V-T deactivation of HF is treated as a multiquanta process. All transitions from a given level to lower levels are taken to have equal probability. Each is scaled linearly with vibrational quantum number. Upper level rate coefficients can thus be evaluated by scaling the best literature values for the 1-0 transition. An alternative approach that also gives good general agreement with these experiments is to treat the V-T deactivation as single quantum and scale upper level rate coefficients by $v^{2.3}$. Such an approach would be easier to implement in existing models.

With such fast V-T deactivation, the influence of single-quantum V-V exchange is not as strong as originally thought. Here we have modified our existing Sharma formulation by scaling with $v^{-1/2}$ rather than v . An equally good alternative would be to use a constant probability for all exothermic transitions. The probabilities for endothermic transitions would be found by applying detail balance. The appropriate rate coefficients would be obtained from measurements for lower level transitions (Refs. 35 and 36).

Direct assessment of H-atom deactivation proved difficult as the tests were too strongly influenced by differences in HF self deactivation. In the absence of convincing contrary evidence, H-atom rates scaled to Bott's measurements are being employed.

A summary of rates that gave the best overall fit to the vibrational population data within the constraints of the model used (in particular the limitation to single-quantum V-V exchange) is given in Table 31.

While the above described model gave fairly good general agreement with experiment, certain shortcomings were evident. First the model does not appear to adequately describe the rapid readjustment of primitive vibrational distributions to nearly Boltzmann distributions. Also, a "knee" which is not evident in experiment, appears in the predicted vibrational distributions for $v=5$ and $v=6$ that tends to persist regardless of how the various rates were modified. Finally there was the tendency in some flow-tube cases (3,4,5 and 6) to underpredict the populations of intermediate levels ($v = 2-4$) during the latter stages of the flow.

35. Airey, J. R. and I. W. M. Smith, "Quenching of Infrared Chemiluminescence Rates of Energy Transfer from HF ($v \leq 5$) to CO₂ and HF, and from DF ($v \leq 3$) to CO₂ and HF," J. Chem. Phys., **57**, 1669, 1972.
36. Osgood, R. M., et al., "Measurements of V-V Exchange Rates for Excited Vibrational Levels ($2 \leq v \leq 4$) in Hydrogen Fluoride Gas," J. Chem. Phys., **60**, 1464, 1974.

TABLE 31. RECOMMENDED CHANGES TO ORIGINAL
VIBRATIONAL RELAXATION RATE PACKAGE

I. V-T Multiple-Quanta Transitions; $v \rightarrow v-n$, n arbitrary

A. For H and F Atoms

$$k_{v \rightarrow v'} = aT^{-b} \exp(-c/RT) \text{ sec}^{-1} \text{ atm}^{-1}$$

(Note values for a in following tables are multiplied by 10^{-12})

	v'	H atoms			F atoms		
		a	b	c	a	b	c
$v=1$	0	.06	1.275	1172	29.87	1.766	3099
$v=2$	0	.045	1.084	896	0	1	1
	1	.0046	1.201	722	27.26	1.708	3077
$v=3$	0	1.88	1.063	761	0	1	1
	1	1.36	1.078	675	27.89	1.757	3718
	2	1.80	1.09	889	43.2	1.724	3645
$v=4$	0	7.16	1.324	806	0	1	1
	1	.321	.91	635	30	1.75	3700
	2	.608	.966	667	66	1.7	3600
	3	.786	1.001	519	100	1.7	3600
$v=5$	0	4.63	1.234	636	0	1	1
	1	1.92	1.149	610	30	1.75	3700
	2	.967	1.043	711	33	1.7	3700
	3	1.53	1.058	668	100	1.7	3700
	4	1.06	1.047	527	165	1.7	3700
$v=6$	0	3.69	1.189	620	0	1	1
	1	1.92	.837	568	30	1.75	3700
	2	1.97	1.155	751	34	1.658	3810
	3	.821	1.01	671	62.4	1.699	3589
	4	3.20	1.211	596	160	1.741	3638
	5	4.41	1.222	626	226	1.712	3644

TABLE 31. RECOMMENDED CHANGES TO ORIGINAL
VIBRATIONAL RELAXATION RATE PACKAGE (CONT'D)

		H atoms			F atoms			
		v'	a	b	c	a	b	c
v = 11 10 9 8 7		0	3.62	1.0	600	0	1.7	3600
		1	1.81	1.0	550	330		
		2	1.81		720			
		3	1.09		670			
		4	2.18		600			
		5	3.62					
		6						
		7						
		8						
		9						
		10						

B. All Other Species

$$k_{v,v'-n} = vk_{10}$$

k_{10} as given in Appendix CI

(alternative - single quantum with $k_{v,v-1} = v^{2.3}k_{10}$)

TABLE 31. RECOMMENDED CHANGES TO ORIGINAL
VIBRATIONAL RELAXATION RATE PACKAGE (CONT'D)

II. V-V Transitions

$$k_{r,r-1}^{s,s+1} = \left(\frac{r}{1-\epsilon r} \right)^{-\frac{1}{2}} \left(\frac{s+1}{1-(s+1)\epsilon} \right)^{-\frac{1}{2}} 2\sqrt{2} K$$

where $K = 0.8 \times 10^{-11}$ *

(Alternative - $k_{r,r-1}^{s,s+1} = 4.4K$ for all exothermic reactions)

*This value is selected such that the transition $(0,2) \rightarrow (1,1)$ has the value recommended by Cohen (Ref. 30).

Such problems illustrate the need to further improve the model. One such approach would be to employ arbitrary scaling of the V-T rates (e.g., a bit slower for $v = 2$ through 4 and faster for $v = 5$ and 6), but that would be tedious with little chance of general application. Arbitrary changes in the single-quantum V-V rates tend to introduce new problems while alleviating old ones. For example, faster V-V rates, which would help provide rapid early adjustment of primitive distributions, tend to depress intermediate level populations and enhance upper level populations too much.

It appears, in retrospect, that a new mechanism--namely multiquanta V-V exchange--will be required to improve theoretical predictions of vibrational distributions. An approach assuming multiquanta VV exchange in conjunction with less strongly scaled VT interactions has been proposed recently by Clendening, et al., (Ref. 37). This approach, based upon surprisal analysis, provides a rational means of evaluating all applicable transition rates. A model such as this should be applied to these experimental results in the near future.

Chain Reaction Laser Performance

Performance calculations with the new rate package do not indicate an optimistic future for the HF chain reaction laser, in basic agreement with the findings of Clendening (Ref. 38). However, it appears that a high-pressure fluorine-rich operating condition can provide reasonable performance that might be useful in some applications. Such a possibility should be examined in more detail.

-
37. Clendening, C., et al., "Information Theory Analysis of Deactivation Rates in Chemical Lasers," AFWL-TR-76-144, Kirtland AFB, NM, 1976.
 38. Clendening, C., "Current Status of HF/DF Chain Chemical Laser," AFWL-TR-76-194, Kirtland AFB, NM, 1976.

SECTION V. ESR TITRATION EXPERIMENT

Summary

It is shown that titration of F, F₂ with HCl is described principally by the reaction, $F + HCl \rightarrow HF + Cl$. Accordingly, F concentration may be determined by titration of F with a known quantity of HCl and a measurement of HF concentration. The required HF concentration may be determined by laser optical absorption methods (Refs. 39, 7). The F concentration is relevant to understanding the governing reaction sequences in HF/DF chain reaction lasers (Ref. 40). The conclusion concerning the above reaction is arrived at by observing the effect of HCl titration on the intensity of an F ESR (Electron Spin Resonance) signal, the intensity being proportional to concentration. It is found that the intensity decreases linearly with increasing HCl flow and that 1.07 ± 0.12 HCl molecules are required to remove 1 F atom. Since the flow contains F₂ as well as F, these latter results demonstrate the lesser importance of competing reactions, like $Cl + F_2 \rightarrow ClF + F$, to the titration method of F concentration determination. With regard to the latter reaction, present results verify that the rate constant associated with it is small, which is a conclusion reached by others earlier using a method different than the present one (Ref. 41).

Introduction

In order to verify that HCl titration of F is described by $F + HCl \rightarrow HF + Cl$, without significant interference from competing reactions, it is required that the relative amounts of F and HCl are known at the titration region. Since the species move in a flow tube, the flow rates in (Torr cc sec⁻¹) are compared, the latter unit being proportional to the number of molecules (or atoms) passing a given cross section of the tube per unit interval of time.

-
39. Bonczyk, P. A., "Determination of Einstein A and Linewidth Dependence on Pressure for 3.4 μ m DF Spectra. I. Absorption Measurements for Pure DF," Phys. Rev., 11A, 1522, 1975.
 40. Bronfin, B. R., Fifteenth Symposium (International) on Combustion, The Combustion Institute, Pittsburgh, 935-950, 1974.
 41. Ganguli, P. S. and M. Kaufman, "The Rate of Homogeneous Recombination of Fluorine Atoms," Chem. Phys. Lett., 25, 221, 1974.

The F concentration may be determined from intensities of F ESR spectra provided that calibration of the ESR spectrometer is done first with, for example, O_2 . The use of O_2 for calibration is known from earlier work by Ultee (Ref. 42) wherein a linear dependence of ESR signal intensity on O_2 pressure is demonstrated.

The relationship between species partial pressure and ESR signal intensity is contained in (Ref. 43)

$$P_i = \frac{2(kT)^2}{h\nu\beta} Q_i (f \int_0^\infty \chi_i'' dH) \quad (11)$$

In Eq. (11), P_i is species partial pressure, k is Boltzmann's constant, T is the gas temperature, h is Planck's constant, ν is the ESR transition frequency, β is one Bohr magneton, Q_i is a dimensionless quantity appropriate to species i , f is a spectrometer factor independent of i , χ_i'' is the imaginary part of the complex molecular susceptibility, and H is the variable external magnetic field strength. The quantity $\int_0^\infty \chi_i'' dH$ is in principle calculable, being independent of f . However, $A_i = f(\int_0^\infty \chi_i'' dH)$ is used herein, which is the area bounded by χ_i'' vs H , and is referred to as the ESR signal intensity. Accordingly, equation (11) may be rewritten in the form

$$P_i = \frac{2(kT)^2}{h\nu\beta} Q_i A_i \quad (12)$$

Appropriate expressions in the case of F and O_2 are

$$P_F = \frac{2(kT)^2}{h\nu\beta} Q_F A_F \quad (13)$$

and

$$P_{O_2} = \frac{2(kT)^2}{h\nu\beta} Q_{O_2} A_{O_2} \quad (14)$$

Dividing equation (13) by equation (14) and solving for P_F , it follows that

$$P_F = P_{O_2} \frac{Q_F}{Q_{O_2}} \frac{A_F}{A_{O_2}} \quad (15)$$

42. Ultee, C. J., "Determination of Absolute Concentrations by Gas Phase Electron Spin Resonance Spectroscopy," J. Appl. Phys. **37**, 1477, 1966.

43. Westenberg, A.A., Progress in Reaction Kinetics edited by K. R. Jennings and R. B. Cundall, Pergamon Press, New York, Vol. 7/1, p. 55, Eq. 20, 1973.

The quantities P_{O_2} and A_{O_2} are known from the spectrometer calibration. The factors Q_F and Q_{O_2} are conveniently tabulated in Reference 43. The A_F is determined from the measured F spectra. Having P_F and the F volume flow rate in cc/sec, the torr cc sec⁻¹ of F at the mixing region is known. This is then compared with the torr cc sec⁻¹ of HCl required to extinguish the F signal.

Apparatus

A schematic of the apparatus is given in Figure 149. The ($F_2 + Ar$) mixture is taken from a cylinder in which the concentration of F_2 is 10 percent. The volume flow rate of this mixture in cc/sec is measured at 1 atm pressure with a calibrated rotameter. The pressure at the HCl-F mixing region is considerably less than 1 atm owing to flow of the mixture. The pressure is determined by interpolating between values read from two Bourdon type gauges placed upstream and downstream from the mixing region. The volume flow rate at the mixing region falls within the range 112 to 334 cc/sec. The flow tube has a cross-sectional area of 0.5 cm²; hence, the molecular flow speed is 224 to 668 cm/sec.

The F_2 dissociation occurs in a microwave discharge with the nominal frequency and power being 2450 MHz and 100 W, respectively. The dissociation could be made to vary from 15 to 50 percent while retaining an F signal, but data for less than 15 percent dissociation are not obtainable owing to increased difficulty with the stability of the discharge.

The HCl apparatus consists of valves to control the HCl flow and a calibrated mass flowmeter. The Matheson 8116-0250 meter gives HCl flowrate directly. The calibration is checked before putting the instrument into use.

The ESR apparatus is a Varian V-4502 system. Listing of its components is omitted. Additions to the system include electronics for measuring the microwave frequency and power, and a NMR gaussmeter for calibration of the magnetic field sweep.

Results

(a) O_2 calibration spectra

An O_2 line is given in Figure 150. The signal corresponds to an O_2 pressure of 6.33 torr as measured with a McCleod type manometer. The signal shape is the derivative of a Lorentzian absorption signal. The derivative function is due to 100 KHz modulation of the variable magnetic field and, hence, the absorption line-shape, along with phase-sensitive detection of the result-

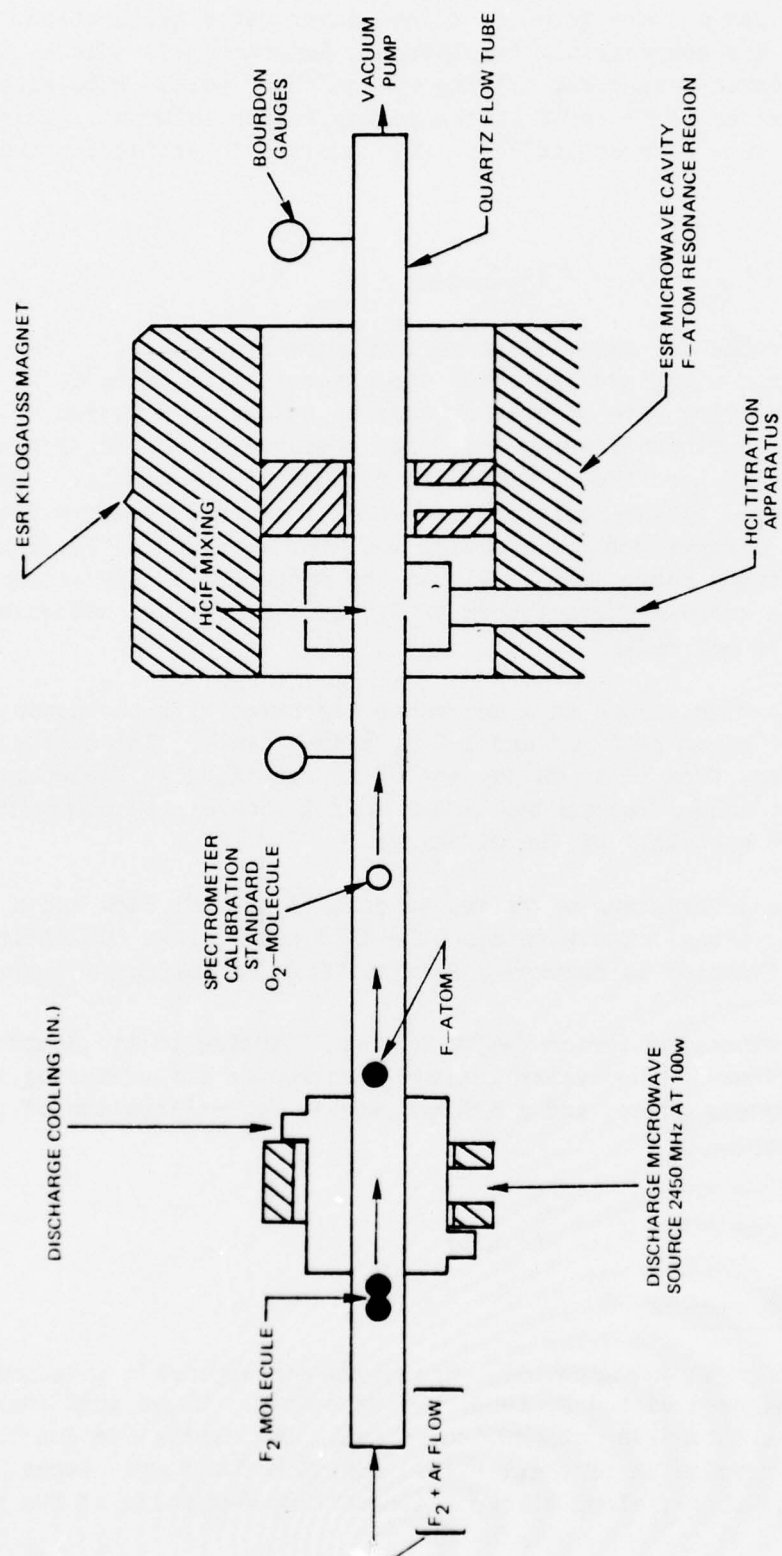


FIGURE 149 ESR F-ATOM TITRATION APPARATUS

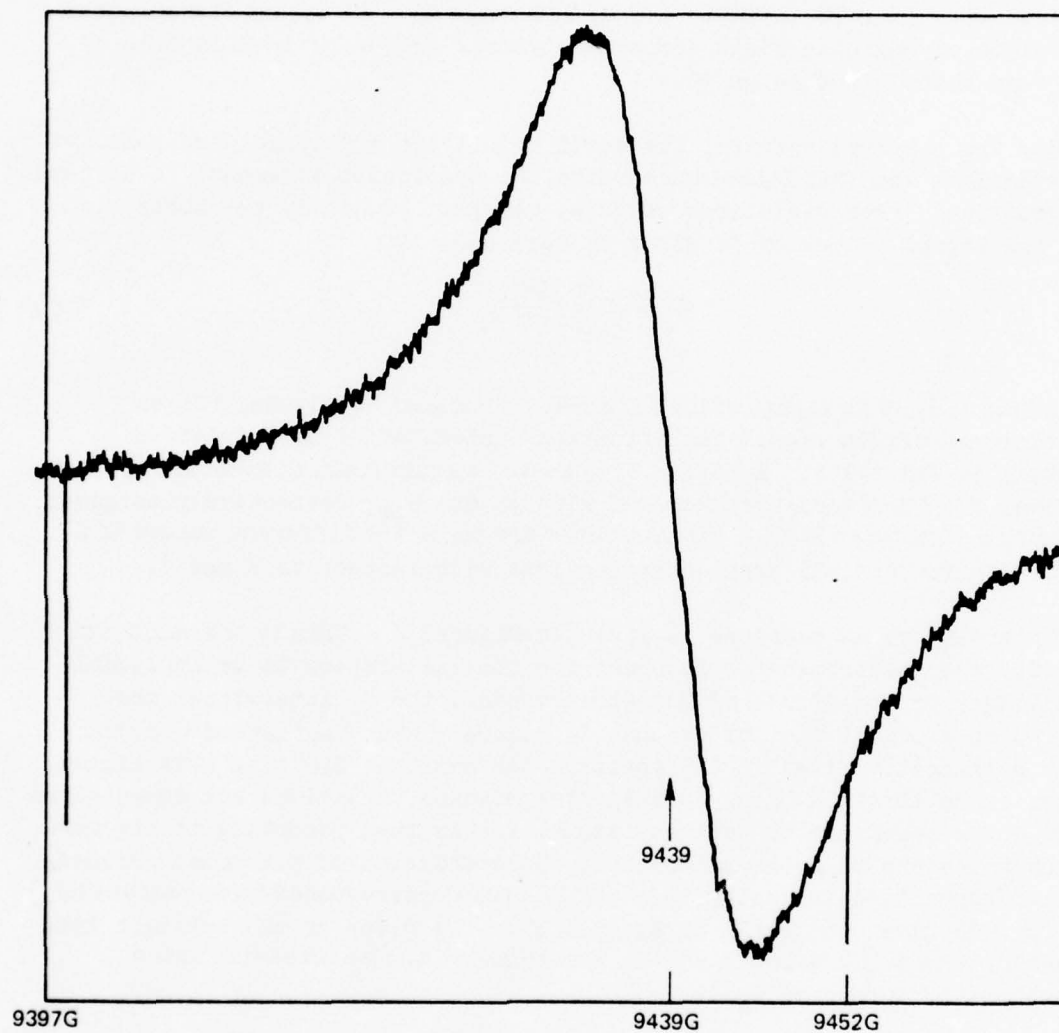


FIGURE 150 MOLECULAR OXYGEN ESR SIGNAL

ing modulated ESR signal. The calibration of the abscissa in Figure 150 is done with the NMR gaussmeter. From the magnetic field value at line center ($= 9439$ G) and the 9257 MHz klystron frequency, the transition is identified as $K = 3$, $J = 4$, $M_J \rightarrow M_J' = 3 \rightarrow 4$ in the O_2 ($3\Sigma_g^-$) spectrum. This line is identical with line 18 in Table III of Reference 42. It occurs at a somewhat lower value of magnetic field since the klystron frequency in this case is lower than that in Reference 42.

For the observed spectra, the small modulation amplitude used relative to the nominal spectral linewidth permits the absorption lineshape to be taken as Lorentzian. (For variations of this, see Ref. 42.) In the Lorentzian case, the signal intensity is given by Reference 42.

$$A_1 = f \frac{\pi}{\sqrt{3}} \left(\frac{W^2 L}{SV} \right)_1 \quad (16)$$

In Equation (16), W is signal width in Gauss, L is signal amplitude, S is an electronic-in-origin signal amplification factor, and V is modulation amplitude in rms volts. Equation (16) above is equivalent to Equation (18) of Reference 42. The W and L are identical with ΔH and S_{pp} , respectively as given in Figure 1 of Reference 42. Since spectra are taken for different values of S and V , we normalize all area determinations with respect to S and V .

Intensity vs O_2 pressure is given in Figure 151. This is the calibration curve for the spectrometer. In order for the calibration to be applicable for a longer period of use of the spectrometer, the O_2 intensities are referred to a signal similar to that in Figure 150 but due instead to a ruby sample permanently fixed in the spectrometer cavity. By using this signal, changes in calibration owing to daily temperature variations are compensated for by quick reference to the ruby signal rather than resorting to the more lengthy procedure of O_2 recalibration. Determination of a typical ordinate value of normalized intensity in Figure 151 which corresponds to a pressure of 6.33 torr is given in detail in Example 1. The slope of the straight line in Figure 151 is $5.108 \times 10^{-3} \text{ torr}^{-1}$. Accordingly, the O_2 intensity which corresponds to 1 torr of O_2 is

$$A_{O_2} = (5.108 \times 10^{-3}) A_{\text{ruby}} \quad (17)$$

where the resulting A_{O_2} is used in Equation (15) in order to determine P_F . In Equation (17), A_{ruby} is determined by a relationship among W , L , S , and V appropriate to ruby and given as in the case of O_2 by Equation (16). In this regard, see also Example 1.

(b) F-spectra

The F-line used in this work was $(M_J, M_I) \rightarrow (M_J', M_I') = (\frac{1}{2}, \frac{1}{2}) \rightarrow (3/2, \frac{1}{2})$ for the $F(2P_{3/2})$ state. This is line "A" in Table 13, Reference 43. As above, this identification is verified from the value of magnetic field at line



FIGURE 151 SPECTROMETER CALIBRATION CURVE

EXAMPLE 1

(Clarification of the Ordinate Values of Figure 151)

Values of W, L, S, and V for a typical O₂ line at 6.33 torr were:

$$W = 11.3 \text{ (div)} \times 1.724 \text{ (KHz/div)} \times 0.60437 \text{ (G/KHz)}$$

$$= 11.77 \text{ G (div} = 1 \text{ unit of recorder paper length)}$$

$$L = 62 \text{ div}$$

$$S = 262$$

$$V = 38.53 \text{ rms volts}$$

Accordingly, from Equation (14) and for this O₂ line, $(W^2L/SV) = [(11.77)^2 \times 62] / [262 \times 38.53] = 0.8508 \text{ G}^2$. At 6.33 torr, 9 such lines were measured and there resulted a final, average value of intensity given by, $(\frac{W^2L}{SV})_{O_2}$ [average] = 0.9346 G².

For the ruby signal, the values of W, L, S, and V were:

$$W = 16.6 \text{ (div)} \times 4.39 \text{ (KHz/div)} \times 0.23487 \text{ (G/KHz)}$$

$$= 17.12 \text{ G}$$

$$L = 80$$

$$S = 20.6$$

$$V = 38.38 \text{ r.m.s. volts}$$

Accordingly, the ruby intensity is $(\frac{W^2L}{SV})_{\text{ruby}} = [(17.12)^2 \times 80] / [20.6 \times 38.38] = 29.66 \text{ G}^2$. The ordinate of Figure 151 at 6.33 torr is then simply $A_{O_2}/A_{\text{ruby}} = 0.9346/29.66 = 31.5 \times 10^{-3}$.

center and the measured klystron frequency. A representative F-line is given in Figure 152. The area computation applied to it is identical in procedure to that given for O_2 and ruby above. The signal is appropriate to an F pressure of 0.233 torr. The details of this computation are outlined in Example 2.

(c) (F+HCl)-spectra

The effect of HCl titration on the intensity of an F signal is shown in Figure 153. The HCl is introduced into the flow tube through four 0.5 mm dia holes in the wall of the tube and at a point 12.5 cm upstream from the microwave cavity. The data of Figure 153 correspond to an F pressure of 0.233 torr at a flowrate of 334 cc/sec, which yields $0.233 \times 334 = 78$ [torr cc sec⁻¹] for the F "flow" at the mixing region. From the 77 [torr cc sec⁻¹] HCl "flow" required to extinguish fully the F signal, it follows that $77/78 = 0.99$ HCl molecules are required to remove one F atom from the flow stream. The linearity of F signal intensity with HCl flow and the above ratio of nearly unity validate the reaction $HCl + F \rightarrow HF + Cl$ and, moreover, the linearity excludes the significant presence of interfering reactions like $Cl + F_2 \rightarrow ClF + F$. (Ref. 41) Table 32 summarizes titration results for varying conditions of F and HCl flow.

Conclusion

Table 32 results and the linearity of F signal intensity with HCl "flow" demonstrate that the governing reaction is $HCl + F \rightarrow HF + Cl$ and, therefore, that HF determination by absorption of light measurement gives the F concentration.

The rate constant k associated with $HCl + F \xrightarrow{k} HF + Cl$ was determined earlier from the decay of HF chemical laser signals and was found to be $k = 1.5 \times 10^{13}$ [cm³ mole⁻¹ sec⁻¹] (Ref. 44). The rate k' associated with $Cl + F_2 \xrightarrow{k'} ClF + F$ was determined to be $k' < 1 \times 10^9$ [cm³ mole⁻¹ sec⁻¹] (Ref. 41). Hence, these latter results are consistent with conclusions reached herein.

44. Kompa, K. L. and J. Wanner, "Study of Some Fluorine Atom Reactions Using a Chemical Laser Method," Chem. Phys. Lett., **12**, 560, 1972.

EXAMPLE 2

(P_F Determination for a Typical Case)

For Figure 152 and 4 other similar lines, it follows that $(\frac{W^2 L}{SV}) = 0.8706 \text{ G}^2$. Since the ruby intensity was $(\frac{W^2 L}{SV})_{\text{ruby}} = 29.08 \text{ G}^2$, it follows that the O_2 intensity which corresponds to 1 torr of O_2 is

$$(\frac{W^2 L}{SV})_{O_2} = (5.108 \times 10^{-3}) \times 29.08 = 0.1485 \text{ G}^2.$$

Next, it follows from Equation (13) that

$$P_F = 1 \times \frac{2.14}{58.6} \times \frac{0.8706}{0.1485} = 0.214 \text{ Torr}$$

where values of Q_F and Q_{O_2} are taken from Reference 43.

The P_F above is the pressure at the microwave cavity, which is 12.5 cm downstream from the region of HCl mixing. What is required is pressure at the mixing region. In order to correct P_F to a point 12.5 cm upstream from the cavity, measurements of F intensity versus cavity-mixing separation are done, which give a 9 percent decrease in F intensity in going from the point of mixing to the cavity. Applying this correction, the F pressure at the point of mixing is $1.09 \times 0.214 = 0.233 \text{ torr}$.

TABLE 32. SUMMARY OF HCl TITRATION OF F VIA $\text{HCl} + \text{F} \rightarrow \text{HF} + \text{Cl}$.
 The HCl flow given in column 3 is that flow required to remove all the F atoms. The average result appropriate to column 4 is 1.07 ± 0.12 .

$\text{F}(\#/\text{cc}) \div \text{F}_2(\#/\text{cc})$	F-Flow(cc Torr sec ⁻¹) (1)	HCl-Flow(cc Torr sec ⁻¹) (2)	(2)÷(1)
0.35	24.6	24.1	0.98
0.54	77.9	77.0	0.99
0.43	43.2	48.8	1.13
0.42	21.3	20.9	0.98
0.15	11.8	15.2	1.29

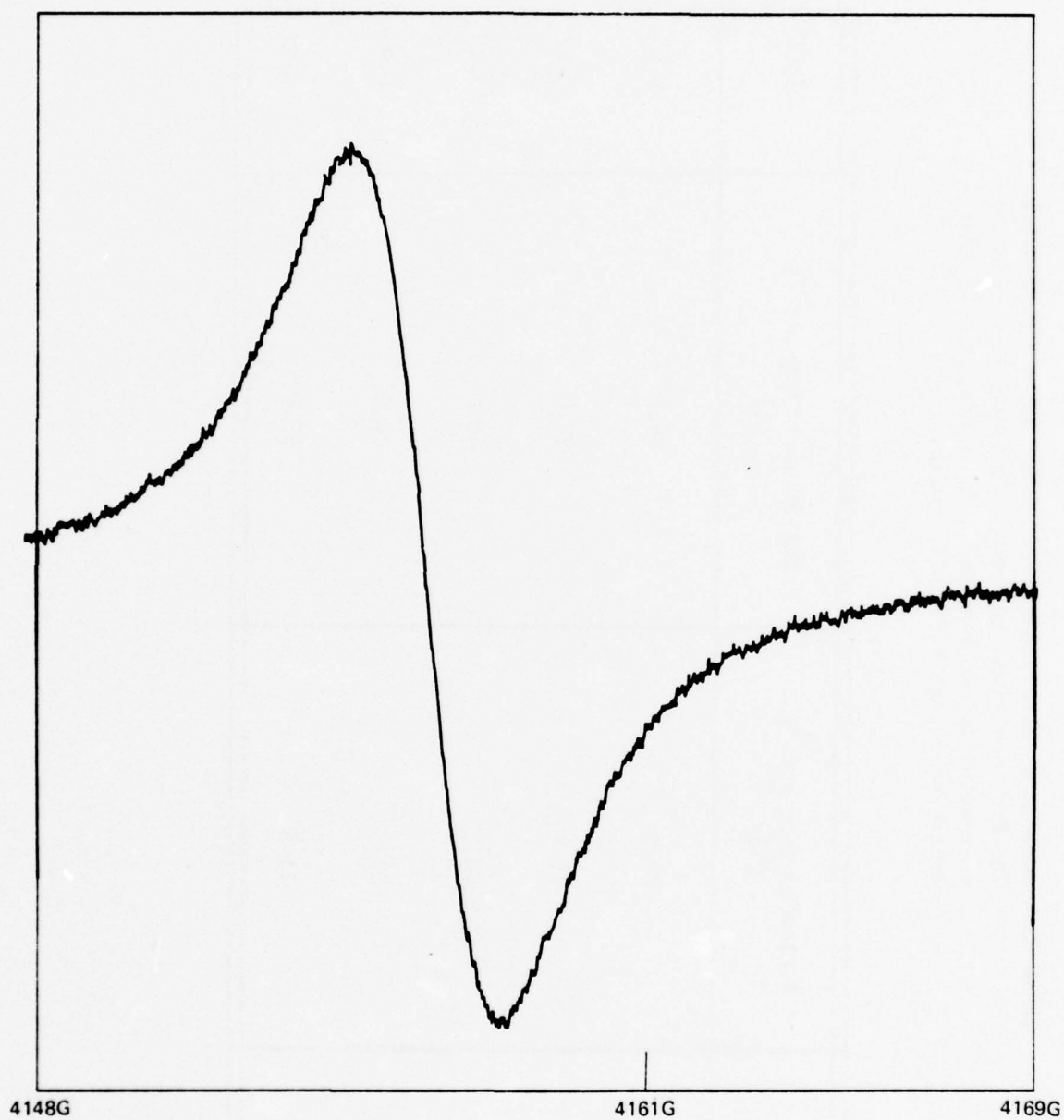


FIGURE 152 ATOMIC FLUORINE ESR SIGNAL

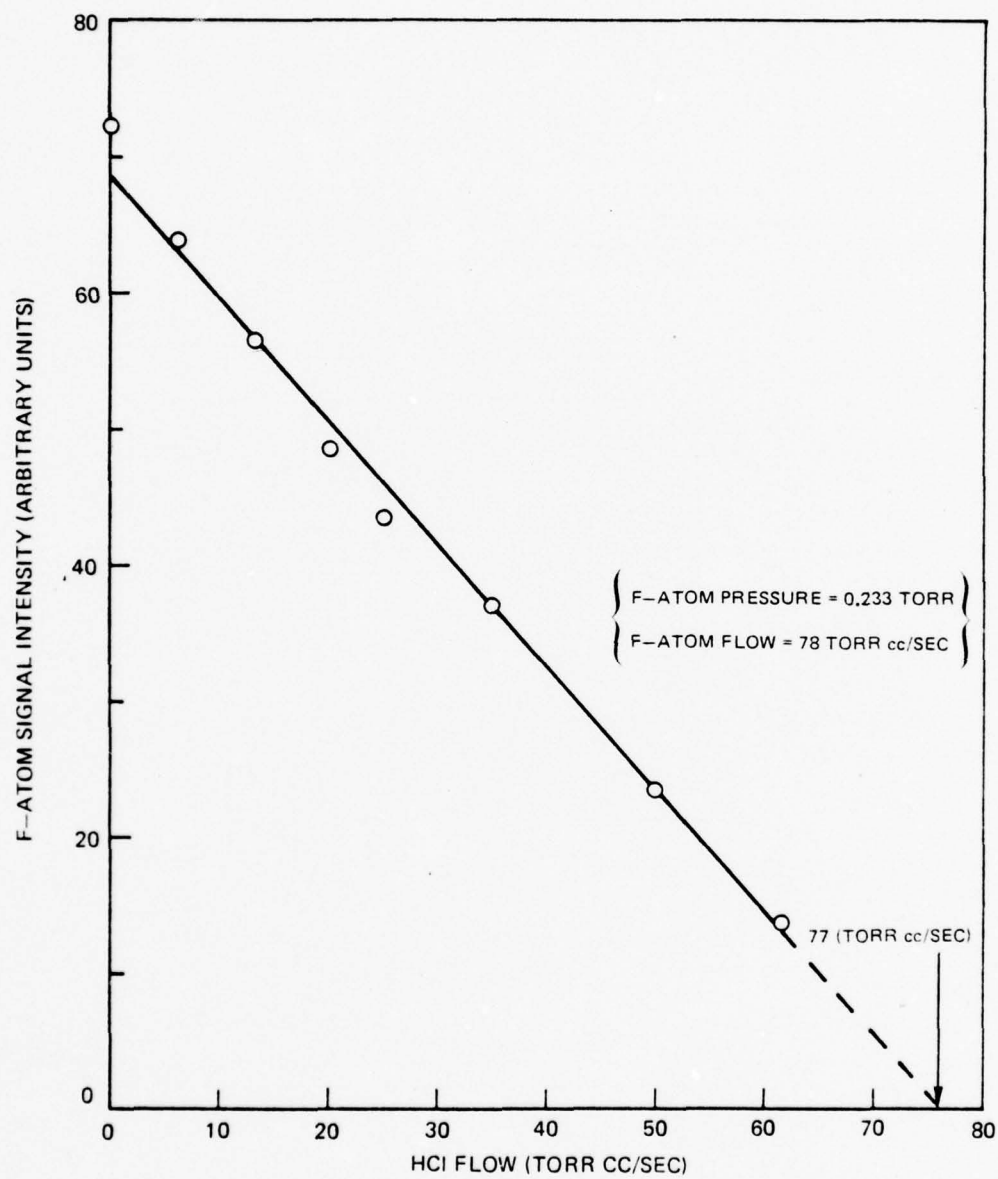


FIGURE 153 HCl TITRATION OF F-ATOM ESR SIGNAL

REFERENCES

1. UTRC Report P-R89, "Proposal for Long-Range HF Chain Laser Studies, Part I, Technical Proposal," and "Part II, Addendum," United Technologies Research Center, East Hartford, CT, April 1975.
2. UTRC Report P-R89-2, "Answers to Questions Addressed to United Technologies Research Center Concerning Proposal P-R89-1," United Technologies Research Center, East Hartford, CT, May 1975.
3. Boedeker, L. R., J. F. Verdieck, and R. J. Hall, "HF Chain Reaction Laser," Final Technical Report, Contract N00014-74-C-0379 (NRL/ONR), UTRC Report R75-951883-4, United Technologies Research Center, East Hartford, CT, May 1975.
4. Ultee, C. J., "HF Long-Range Chain Laser Studies, Proposed Research Plan," Contract F29601-75-C-0139, UTRC Report R75-952198-5, United Technologies Research Center, East Hartford, CT, August 1975.
5. Wood, R. J. and H. Wise, "Kinetics of Hydrogen Atom Recombination on Surfaces," J. Chem. Phys., 65, 1976, 1961.
6. Rizika, J. W. and W. M. Rohsenow, "Thermocouple Thermal Error," Industrial and Engineering Chemistry, 44, 1168, May-August, 1952.
7. Hinchey, J. J., "Determination of Vibration-Rotation Line Strengths for HF and DF by Use of an HF/DF CW Laser," J. Opt. Soc. Am., 64, 9, 1974.
8. Lynds, L., "Investigation of Master Oscillator Power Amplifier Systems for Chemical Lasers," Final Report, Contract F29601-73-C-0072, UTRC Report N911653-24, East Hartford, CT, August 1974.
9. Sileo, R. N. and T. A. Cool, "Overtone Emission Spectroscopy of HF and DF: Vibrational Matrix Elements and Dipole Moment Function," J. Chem. Phys., 65, 117, 1976.
10. Herbelin, J. M. and G. Emanuel, "Einstein Coefficients for Diatomic Molecules," J. Chem. Phys., 60, 689, 1974.
11. Steunenberg, R. K. and R. C. Vogel, "The Absorption Spectrum of Fluorine," J. Am. Chem. Soc., 78, 901, 1956.
12. Hinchey, J., "Operation of a Small Single-Mode Stable cw Hydrogen Fluoride Laser," J. Appl. Phys., 15, 4, April 1974.

REFERENCES (CONT'D)

13. Jaffe, J., et al., "Pressure Induced Shifts of Hydrogen Fluoride Lines Due to Noble Gases," J. Chem. Phys., 43, 1525, 1965 .
14. Bott, J. F., "Gas Dynamic Corrections Applied to Laser Induced Fluorescence Measurements of HF(v=1) and DF(v=1) Deactivation," J. Chem. Phys., 61, 3414, 1974.
15. Nichols, D. B., K. H. Wrolstad, and J. Doyle McClure, "Time-Resolved Spectroscopy of a Pulsed H₂-F₂ Laser with Well-Defined Initial Conditions," J. of Appl. Phys., 45, 12, December 1974.
16. Basov, N. G., L. V. Kulakov, E. P. Markin, A. I. Mikitin, A. N. Oraevskii, and P. N. Lebedev, "Emission Spectrum of a Chemical Laser Using an H₂ + F₂ Mixture," JETP Lett. 9, 375, 1969.
17. Dolgov-Savel'ev, G. G., V. F. Zharov, Yu. S. Neganov, and G. M. Chumak, "Vibrational-Rotational Transitions in an H₂ + F₂ Chemical Laser," JETP 34, 34, 1972.
18. Suchard, S. N., "Lasing from the Upper Vibrational Levels of a Flash-Initiated H₂-F₂ Laser," Appl. Phys. Lett., 23, 2, 15 July 1973.
19. Suchard, S. N., R. W. Gross and J. S. Whittier, "Time Resolved Spectroscopy of an Initiated H₂-F₂ Laser," Appl. Phys. Lett., 19, 411, 1971.
20. Albright, R. G., et al., "Mass Spectrometric Determination of Rate Constants for H-Atom Reactions with Cl₂ and F₂," J. Chem. Phys., 50, 3632, 1969.
21. Homann, K. H., et al., "Eine Methode zur Enzengang von Fluorstomer in Inerten Atmosphäre," Ber. Bunse. F. Phys. Chem., 74, 585, 1970.
22. Moore, W. J., Physical Chemistry, Prentice-Hall, Englewood Cliffs, NJ, 1955.
23. Boedeker, L. R., et al., "Long Range Chain Laser Studies Test Report," UTRC Report R76-952198-49, United Technologies Research Center, East Hartford, CT, October 1976.

REFERENCES (CONT'D)

24. Sullivan, J. H., et al., "Mechanisms and Types of Explosive Behavior in Hydrogen-Fluorine Systems," J. Chem. Phys., 62, 1714, 1975.
25. Kwok, M., "Studies of the Vibrational Relaxation of Upper Levels of HF ($v \leq 6$) in a Large Diameter, Medium Pressure Flow Tube," presented at the TriService Chemical Laser Symposium, Kirtland AFB, NM, February 1976.
26. Bott, J. F. and R. F. Heidner III, "A Study of the Vibrational Deactivation of HF($v=3$) by H Atoms," presented at the TriService Chemical Laser Symposium, Kirtland AFB, NM, February 1976.
27. Heidner, R. F. III and J. F. Bott, "Vibrational Deactivation of HF($v=1$) and DF($v=1$) by H and D Atoms," J. Chem. Phys., 63, 1810, 1975.
28. Wilkins, R. L., "Monte Carlo Calculations of Reaction Rates and Energy Distributions Among Reaction Products $H + HF(v) \rightarrow H_2(v') + F$ and $H + HF(v) \rightarrow HF(v') + H$," J. Chem. Phys., 58, 3038, 1973.
29. Wilkins, R. L., "Monte Carlo Calculations of Reaction Rates and Energy Distributions Among Reaction Products. IV. $F + HF(v) \rightarrow HF(v') + F$ and $F + DF(v) \rightarrow DF(v') + F$," J. Chem. Phys. 59, 698, 1973.
30. Cohen, N. and J. F. Bott, "A Review of Rate Coefficients in the H_2-F_2 Chemical Laser Systems," SAMSO Report TR-76-82, Aerospace Corporation, El Segundo, CA, 1976.
31. Kwok, M., private communication, August 1975.
32. Shin, H. K., "Vibration-Vibration Energy Transfer in HF Dimers," J. Chem. Phys., 63, 2091, 1975.
33. Kepler, C. E., et al., "Demonstration of HF Chain Reaction Laser," UARL Technical Report RK-CR-75-4, United Technologies Research Center, East Hartford, CT, July 1974.
34. Sullivan, J. H. and R. C. Feber, "The Kinetics of an H_2-F_2 Explosion as Initiated by a Pulse of Fluorine Atoms," Report LA-5409, Los Alamos Scientific Laboratory, Los Alamos, NM, 1974.
35. Airey, J. R. and I. W. M. Smith, "Quenching of Infrared Chemiluminescence Rates of Energy Transfer from HF ($v \leq 5$) to CO_2 and HF, and from DF ($v \leq 3$) to CO_2 and HF," J. Chem. Phys., 57, 1669, 1972).

REFERENCES (CONT'D)

36. Osgood, R. M., et al., "Measurement of V-V Exchange Rates for Excited Vibrational Levels ($2 \leq v \leq 4$) in Hydrogen Fluoride Gas," J. Chem. Phys., 60, 1464, 1974).
37. Clendening, C., et al., "Information Theory Analysis of Deactivation Rates in Chemical Lasers," AFWL-TR-76-144, Kirtland AFB, NM, 1976.
38. Clendening, C., "Current Status of HF/DF Chain Chemical Laser," AFWL-TR-76-194, Kirtland AFB, NM, 1976.
39. Bonczyk, P. A., "Determination of Einstein A and Linewidth Dependence on Pressure for 3.4 μ m DF Spectra. I. Absorption Measurements for Pure DF," Phys. Rev., 11A, 1522, 1975.
40. Bronfin, B. R., Fifteenth Symposium (International) on Combustion, The Combustion Institute, Pittsburgh, 935-950, 1974.
41. Ganguli, P. S. and M. Kaufman, "The Rate of Homogeneous Recombination of Fluorine Atoms," Chem. Phys. Lett., 25, 221, 1974.
42. Ultee, C. J., "Determination of Absolute Concentrations by Gas Phase Electron Spin Resonance Spectroscopy," J. Appl. Phys., 37, 1744, 1966.
43. Westenberg, A. A., Progress in Reaction Kinetics edited by K. R. Jennings and R. B. Cundall, Pergamon Press, New York, Vol. 7/1, p. 55, Eq. 20, 1973.
44. Kompa, K. L. and J. Wanner, "Study of Some Fluorine Atom Reactions Using a Chemical Laser Method," Chem. Phys. Lett., 12, 560, 1972.

APPENDIX A: NOMINAL RATE PACKAGE

Chemical Reactions

The possible reactions included in the model and their associated rate coefficients are listed in Table A1. For the cold reaction (1) the reaction rate used is that of Homann (Ref. 21). et.al. The reverse reaction rate, and that for all reactions (unless otherwise stated) is evaluated by using equilibrium constants derived from the JANAF Tables (Ref. A1). The division of products between thermal atoms, H and hot atoms H* is arbitrary. The vibrational product distribution is based upon the work of Jonathan, et al. (Ref. A2).

The "hot" reaction rate (2) used is from the work of Albright, et al. (Ref. 20), and the vibrational distribution is from Jonathan, et al. (Ref. A3). For reaction (3), the "hot" reaction with hot H atoms, Albright's expression is used, but with the assumption of no activation energy for the forward reaction.

Coupled with the hot H-atom reaction is the deactivation of the hot atoms, reaction (4). Here the assumption is made that the loss rate of hot H atoms to thermal H atoms occurs at 10 percent of the collision rate of the atoms with other gas molecules.

The chain branching reactions, (5) and (6), have rates based on the work of Sullivan, et al. (Ref. 11).

-
- A1. Stull, D. R. and Prophet, H., Project Directors JANAF Thermochemical Tables, 2nd Ed., U.S. Dept. of Commerce, National Bureau of Standards, June 1971.
 - A2. Jonathan, N., et al., "Initial Vibrational Energy Level Distributions Determined by Infrared Chemiluminescence," Mol. Phys., 22, 561, 1971.
 - A3. Jonathan, N., et al., "Initial Vibrational Energy Level Distributions Determined by Infrared Chemiluminescence," Mol. Phys., 24, 1143, 1972.

TABLE A1. CHEMICAL REACTIONS CONSIDERED AND NOMINAL RATES

1. $F + H_2 \xrightarrow{f_v k_f} HF(v) + H, H^* \quad \Delta H = -31.6 \text{ kcal/mole}$
 $k_f = 2.63 \times 10^{-10} \exp(-1600/RT) \text{ cc/molecule sec}$
 $k_b = 2.95 \times 10^{-10} \exp(-33200/RT) \text{ cc/molecule sec}$
 $(f_v, v = 0, 11) = 0, .1639, .5574, .2787, 0, 0, 0, 0, 0, 0, 0, 0$
 [Note - fractional division between H and H* (hot atoms) is arbitrary]
2. $H + F_2 \xrightarrow{f_v k_f} HF(v) + F \quad \Delta H = -98 \text{ kcal/mole}$
 $k_f = 2 \times 10^{-10} \exp(-2400/RT) \text{ cc/molecule sec}$
 $k_b = 3.29 \times 10^{-11} \exp(-100400/RT) \text{ cc/molecule sec}$
 $(f_v, v = 0, 11) = .012, .027, .033, .039, .134, .265, .298, .134, .058, 0, 0, 0$
3. $H^* + F_2 \xrightarrow{k_f f_v} HF(v) + F \quad \Delta H = -129.6 \text{ kcal/mole}$
 $k_f = 2 \times 10^{-10} \text{ cc/molecule sec}$
 $k_b = 3.29 \times 10^{-11} \exp(-129600/RT) \text{ cc/molecule sec}$
 f_v arbitrary, usually taken as for rxn 1.
4. $H^* + M \rightarrow H + M \quad \Delta H = -31.6 \text{ kcal/mole}$
 $k_f = 2.44 \times 10^{-12} T^{1/2} \text{ cc/molecule sec}$
 $k_b \equiv 0$

TABLE A1. CHEMICAL REACTIONS CONSIDERED AND NOMINAL RATES (CONT'D)

5. $\text{HF}(v>3) + \text{F}_2 \rightarrow \text{HF}(0) + 2\text{F} \quad \Delta H = 37.7 \text{ kcal/mole}$
 $k_f = 3.5 \times 10^{-17} \text{ cc/molecule sec}$
 $k_b \equiv 0$

6. $\text{H}_2(v \geq 1) + \text{F}_2 \rightarrow \text{HF}(0) + \text{H} + \text{F} \quad \Delta H = 5.82 \text{ kcal/mole}$
 $k_f = 8.0 \times 10^{-19} \text{ cc/molecule sec}$
 $k_b \equiv 0$

7. $\text{F} + \text{F} + \text{M} \rightarrow \text{F}_2 + \text{M} \quad \Delta H = -37.7 \text{ kcal/mole}$
 $k_f = 4.99 \times 10^{-33} T^{-0.5} (\text{cc/molecule sec})^2$
 $k_b = 8.32 \times 10^{-11} \exp(-35100/RT) \text{ cc/molecule sec}$

8. $\text{H} + \text{H} + \text{M} \rightarrow \text{H}_2 + \text{M} \quad \Delta H = -104.2 \text{ kcal/mole}$
 $k_f = 2.75 \times 10^{-30} T^{-1} (\text{cc/molecule sec})^2$
 $k_b = 6.96 \times 10^{-6} T^{-1.025} \exp(-104200/RT) \text{ cc/molecule sec}$

9. $\text{H} + \text{F} + \text{M} \rightarrow \text{HF}(0) + \text{M} \quad \Delta H = -129.6 \text{ kcal/mole}$
 $k_f = 6.6 \times 10^{-30} T^{-1.0} (\text{cc/molecule sec})^2$
 $k_b = 7.78 \times 10^{-6} T^{-1} \exp(-129600/RT) \text{ cc/molecule sec}$

The F_2 dissociation reaction rate (7) is based on the measurements of Shui (Ref. A4), et al. That for H_2 (8) is based on the work of Jacobs, et al. (Ref. A5). Finally, the HF dissociation (9) rate coefficient is based on the work of Blaur, et al. (Ref. A6) with a revised activation energy.

V-T Relaxation

The relaxation times for the 1-0 V-T transition are listed in Table A2. In all cases a Landau-Teller fit has been used. For HF-HF deactivation it has been necessary to fit the data in four temperature ranges due to the anomalous temperature dependence exhibited. The fit is based upon the composite data from many sources as summarized in Cohen (Refs. 28 and 29).

The H_2 V-T rate is based on the upper limit deduced by Bott (Ref. A7). Finally, the F_2 , Ar, and He relaxation times are conservative fits to the composite data summarized in Cohen (Refs. 28 and 29).

The special cases of relaxation by H and F atoms have been treated as multiple-quanta transition processes. The relaxation times, based on Wilkins (Ref. 27) calculations are summarized in Table A3.

V-V Relaxation

The V-V formulation for HF-HF self relaxation is based primarily on the long-range dipole-dipole interaction model of Sharma (Ref. A8) as adapted by

-
- A4. Shu, V. H., et al., Thirteenth Symposium (International) on Combustion, Combustion Institute, Pittsburgh, 1971.
- A5. Jacobs, T. A., et al., "Kinetics of Hydrogen Halides in Shock Waves, II. A New Measurement of the Hydrogen Dissociation Rate," J. Chem. Phys., 47, 54, 1967.
- A6. Blauer, J., "The Kinetics of Dissociation of Hydrogen Fluoride behind Incident Shock Waves," J. Phys. Chem., 72, 79, 1968.
- A7. Bott, J. F., "Vibrational Relaxation of HF ($V=1$) and DF ($V=1$) by H_2 and D_2 ," J. Chem. Phys., 61, 2530, 1974.
- A8. Sharma, R. D. and H. Schlossberg, "On the Assumptions Underlying the Near Resonant Theory of Energy Transfer," Chem. Phys. Lett., 20, 5, 1973.

TABLE A2. V-T RELAXATION TIMES

1. HF-HF - $k_{v,v-1} = v k_{10}$

Anomalous temp dependence treated by breaking up data into 4 separate regions and fitting each to a Landau-Teller form:

$$p\tau = a \exp(bT^{-1/3}) = 1/k$$

Temp Range	a (sec-atm)	b
$T \geq 1371$ °K	$.876 \times 10^{-9}$	65.6
$1351 \geq T \geq 751$	$.223 \times 10^{-7}$	29.5
$751 \geq T \geq 578$	$.87 \times 10^{-3}$	-66
$578 \geq T$.0256	-94.2

2. HF-M - $k_{v,v-1} = vk_{10}$

$$p\tau = a \exp(bT^{-1/3}) = 1/k$$

M	a(sec-atm)	b
H ₂	3.5×10^{-6}	0
F ₂	5.929×10^{-8}	79.4
Ar	5.929×10^{-8}	79.4
He	5.929×10^{-8}	79.4

TABLE A3. V-T MULTIPLE-QUANTA TRANSITIONS: $v \rightarrow v-n$, n ARBITRARY

For H and F Atoms

$$k_{v \rightarrow v'} = aT^{-b} \exp(-c/RT) \text{ sec}^{-1} \text{ atm}^{-1}$$

(Note values for a in following table are multiplied by 10^{-12})

	v'	H atoms		F atoms			
		a	b	c	a	b	c
$v=1$	0	1.219	1.275	1172	9.053	1.766	3099
$v=2$	0	.57	1.084	896	0	1	1
	1	.0583	1.201	722	8.26	1.708	3077
$v=3$	0	.52	1.063	761	0	1	1
	1	.376	1.078	675	8.45	1.757	3718
	2	.497	1.09	889	13.1	1.724	3645
$v=4$	0	1.98	1.324	806	0	1	1
	1	.0885	.91	635	9	1.75	3700
	2	.168	.966	667	20	1.7	3600
	3	.217	1.001	519	30	1.7	3600
$v=5$	0	1.28	1.234	636	0	1	1
	1	.53	1.149	610	9	1.75	3700
	2	.267	1.043	711	10	1.7	3700
	3	.423	1.058	668	30	1.7	3700
	4	.293	1.047	527	50	1.7	3700
$v=6$	0	1.02	1.189	620	0	1	1
	1	.53	.837	568	9	1.75	3700
	2	.545	1.155	751	10.3	1.658	3810
	3	.227	1.01	671	18.9	1.699	3589
	4	.885	1.211	596	48.6	1.741	3638
	5	1.22	1.222	626	68.6	1.712	3644

TABLE A3. V-T MULTIPLE-QUANTA TRANSITIONS: $v \rightarrow v-n$, n ARBITRARY

	v'	H atoms			F atoms		
		a	b	c	a	b	c
<p>$v = 11$ 10 9 8 7</p>	0	1.0	1.0	600	0	1.7	3600
	1	.5	1	550	100		
	2	.5		720			
	3	.3		670			
	4	.6		600			
	5	1.0					
	6						
	7						
	8						
	9						
	10						

Rockwood (Ref. A9). Both short and long range terms are included such that the net rate coefficient $K_{r,r-1}^{s,s+1} = L_{r,r-1}^{s,s+1} + S_{r,r-1}^{s,s+1}$. The short range term is given by

$$S_{r,r-1}^{s,s+1} = \left(\frac{r}{1-\epsilon r}\right) \left(\frac{s+1}{1-(s+1)\epsilon}\right) S_{10}^{01} \exp(\Delta E_{rs}/2kT) F((\omega\tau)_{rs}) \quad (A1)$$

where

ϵ = Molecular Anharmonicity

$$F = 1/2 (3 - \exp(-2/3 [\omega\tau])) \exp(-2/3 [\omega\tau])$$

$$\omega\tau = \frac{2\pi^2}{h} \Delta E_{rs} \left(\frac{\mu}{2\pi kT}\right)^{1/2}$$

$$\frac{S_{10}^{01}}{z} = \frac{\mu kT}{8\pi^2 M^2 (\nu_{10})^2 \lambda^2}$$

$$z = d^2 \left(\frac{8\pi kT}{\mu}\right)^{1/2}$$

$$d = \text{gas-kinetic collision diameter} = 2.7 \times 10^{-8} \text{ cm}$$

μ = reduced mass of collision pair

k = Boltzmann's constant

M = reduced mass of HF oscillator

ν_{10} = frequency of fundamental transition

λ = range parameter for repulsive interaction.

It turns out that this term makes only a small contribution.

The long range term is given by

$$L_{r,r-1}^{s,s+1} = \left(\frac{r}{1-\epsilon r}\right) \left(\frac{s+1}{1-(s+1)\epsilon}\right) L_{10}^{01} \exp(\Delta E_{rs}/2kT) \exp(-(\Delta E_{rs}/\delta)^2) \quad (A2)$$

A9. Rockwood, S. D., et al., "Time-Dependent Calculations of Carbon Monoxide Laser Kinetics," IEEE J. Quant. Elect., 9, 120, 1973.

where

$$\frac{L_{10}^{01}}{z} = \frac{A}{T}$$

and $\delta^2 = BT^{1/2}$

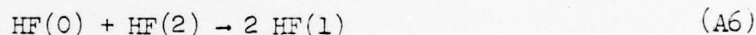
The parameters that can be adjusted in the model are the range parameter l used in the short range term, A , and δ^2 . The values we have used are

$$l = 2 \times 10^{-9} \text{ cm} \quad (\text{A3})$$

$$A = 27^\circ \text{K} \quad (\text{A4})$$

$$\delta^2 = 10^{-25} \quad (\text{A5})$$

These parameters were selected such that the rate of the transition



is pegged to the value reported by Airy and Fried (Ref. 33). Thus

$$K_{2,1}^{0,1} = K = 1.82 \times 10^{-11} \text{ cc/molecule-sec} \quad (\text{A7})$$

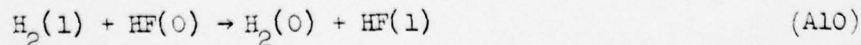
at 300°K .

A similar treatment is used for HF-H_2 V-V interactions. Here the short range term is taken as zero,

$$L_{10}^{01} = 5 \times 10^{-13} \quad (\text{A8})$$

$$\delta^2 = 1.6 \times 10^{-26} \quad (\text{A9})$$

in which the direction of the transition is endothermic. The exothermic rates are found from detail balance. The values used match the rate for the exothermic reaction



reported by Bott and Cohen (Ref. A10) (i.e., 1.33×10^{-12} cc/molecule-sec).

H₂ V-T Relaxation

The rate coefficients employed are derived from the recommendations of Cohen (Refs. 28 and 29). They are summarized in Table A4.

-
- A10. Bott, J. F. and N. Cohen, "Temperature Dependence of V-V and V-R, T Energy Transfer Measurements in Mixtures Containing HF," J. Chem. Phys., 58, 4539, 1973.

TABLE A4. H_2 DEACTIVATION

Collider	$k(\text{sec}^{-1})$
H	$1.22 \times 10^{-5} T^{3.3}$
H_2	$1.22 \times 10^{-3} T^{3.3}$
all other	$3.06 \times 10^{-6} T^{3.3}$

References

- A1. Stull, D. R. and Prophet, H., Project Directors. JANAF Thermochemical Tables, 2nd Ed., U.S. Dept. of Commerce, National Bureau of Standards, Publication NSRDS-NBS37, June 1971.
- A2. Jonathan, N., et al., "Initial Vibrational Energy Level Distributions Determined by Infrared Chemiluminescence," Mol. Phys., 22, 561, 1971.
- A3. Jonathan, N., et al., "Initial Vibrational Energy Level Distributions Determined by Infrared Chemiluminescence," Mol. Phys., 24, 1143, 1972.
- A4. Shu, V. H., et al., Thirteenth Symposium (International) on Combustion, Combustion Institute, Pittsburgh, 1971.
- A5. Jacobs, T. A., et al., "Kinetics of Hydrogen Halides in Shock Waves, II. A New Measurement of the Hydrogen Dissociation Rate," J. Chem. Phys., 47, 54, 1967.
- A6. Blauer, J., "The Kinetics of Dissociation of Hydrogen Fluoride behind Incident Shock Waves," J. Phys. Chem., 72, 79, 1968.
- A7. Bott, J. F., "Vibrational Relaxation of HF(V = 1) and DF(V = 1) by H₂ and D₂," J. Chem. Phys., 61, 2530, 1974.
- A8. Sharma, R. D. and H. Schlossberg, "On the Assumptions Underlying the Near Resonant Theory of Energy Transfer," Chem. Phys. Lett., 20, 5, 1973.
- A9. Rockwood, S. D., et al., "Time-Dependent Calculations of Carbon Monoxide Laser Kinetics," IEEE J. Quant. Elect., 9, 120, 1973.
- A10. Bott, J. F. and N. Cohen, "Temperature Dependence of V-V and V-R, T Energy Transfer Measurements in Mixtures Containing HF," J. Chem. Phys., 58, 4539, 1973.

APPENDIX B

STEADY-STATE SOLUTION

In complex systems such as HF chain reaction lasers a potentially useful but often neglected analytic tool is the development of approximate closed form solutions. For example, in typical chain reaction conditions computer calculations indicate, in the absence of significant atom loss processes, a quasi-steady state develops. In this steady-state condition the number of H and F atoms remain essentially constant. It happens that this situation is amenable to a closed form solution.

Consider a situation in which the relative rate of change of H_2 and F_2 is slow compared to the time scale over which steady state is achieved. Assume also that the temperature varies slowly and that only the forward hot and cold reactions are important (i.e., $H + F_2 \xrightarrow{k_h} HF + F$ and $F + H_2 \xrightarrow{k_c} HF + H$). Equations for the rate of change of H and F may be written:

$$\dot{[H]} = k_c [H_2] \cdot [F] - k_h [F_2] \cdot [H] \quad (B1)$$

$$\dot{[F]} = -[H] \quad (B2)$$

Now $k_c [H_2]$ and $k_h [F_2]$ may be taken as constants, thus allowing the simple solution of two linear differential equations with constant coefficients. The initial conditions are $[F] = [F]_0$, $[H] = 0$, $[F] = k_c [H_2] [F]_0$, $[H] = -[F]$. The solution becomes

$$\frac{[F]}{[F]_0} = \frac{K_h + K_c \exp(-[K_c + K_h]t)}{K_c + K_h} \quad (B3)$$

$$\frac{[H]}{[F]_0} = \frac{K_c - K_h \exp(-[K_c + K_h]t)}{K_c + K_h} \quad (B4)$$

where $K_c = k_c [H_2]$ and $K_h = k_h [F_2]$. As $(K_c + K_h)t$ becomes larger, the steady state solutions are achieved:

$$\frac{[F]}{[F]_0} = \frac{k_h [F_2]}{k_h [F_2] + k_c [H_2]} \quad (B5)$$

$$\frac{[H]}{[F]_0} = \frac{k_c [H_2]}{k_h [F_2] + k_c [H_2]} \quad (B6)$$

AD-A041 204

UNITED TECHNOLOGIES RESEARCH CENTER EAST HARTFORD CONN
LONG RANGE CHAIN LASER STUDIES, PHASE I STUDIES. (U)

F/G 20/5

JUN 77 L R BOEDEKER, P A BONZYK, J J HINCHEN F29601-75-C-0139

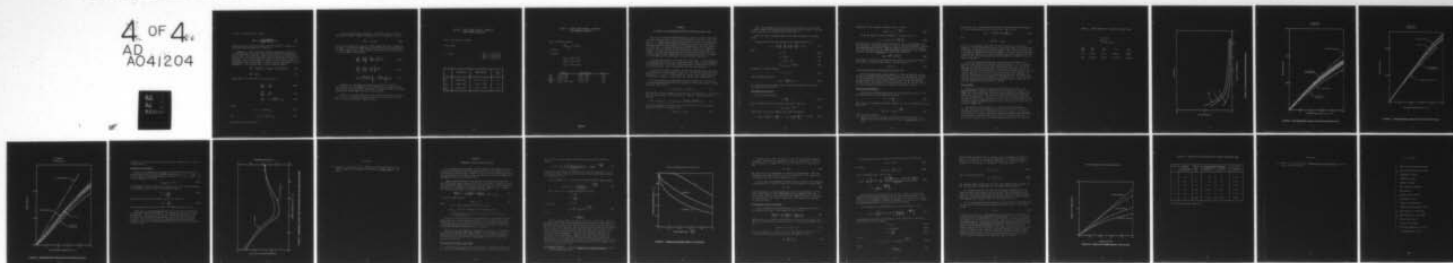
UNCLASSIFIED

UTRC/R77-952198-58

AFWL-TR-77-43

NL

4 OF 4
AD
A041204



END

DATE
FILMED
7-77

The rate of increase of HF is simply

$$[\dot{\text{HF}}] = 2 \frac{k_c[\text{H}_2]k_h[\text{F}_2]}{K_h[\text{F}_2] + k_c[\text{H}_2]} [\text{F}]_0 \quad (\text{B7})$$

The above solution could have equally well been achieved by equating B1 to zero with the constraint $[\text{F}]_0 = [\text{H}] + [\text{F}]$.

Comparison of this solution with computer calculations demonstrates excellent agreement (less than 1 percent error) when all back reactions are set equal to zero, and local values are used for k_c , k_h , $[\text{H}_2]$ and $[\text{F}_2]$. Inclusion of the back cold reaction in computer calculations can lead to significant error, depending upon the rates used for the upper levels of HF. Consequently it has been necessary to include the back cold reaction in the formulation. This is easily done. The rate equations become

$$[\dot{\text{H}}] = k_c[\text{H}_2] \cdot [\text{F}] - (k_h[\text{F}_2] + \sum_i [\text{HF}_i] k_{c_i}^-) [\text{H}] \quad (\text{B8})$$

$$[\dot{\text{F}}] = -[\dot{\text{H}}] \quad (\text{B9})$$

Equating (B8) to zero with $[\text{H}] + [\text{F}] = [\text{F}]_0$ leads to

$$\frac{[\text{F}]}{[\text{F}]_0} = \frac{K_h'}{D} \quad (\text{B10})$$

$$\frac{[\text{H}]}{[\text{F}]_0} = \frac{K_c}{D} \quad (\text{B11})$$

$$[\dot{\text{HF}}] = 2 \frac{K_c K_h}{D} [\text{F}]_0 \quad (\text{B12})$$

where

$$D = K_c + K_h + \sum [\text{HF}_i] k_{c_i}^- \quad (\text{B13})$$

and

$$K_h' = K_h + \sum [\text{HF}_i] k_{c_i}^- \quad (\text{B14})$$

K_h and K_c are as defined above.

One further refinement is possible. A simplified diffusive wall loss model may be treated. Suppose H atoms are lost to the walls at the rate

$$[\dot{H}]_w = -k_D [H] \quad (B15)$$

If the rate of change of F_2 and H is slow we again may treat the equations as linear. If we further assume that the loss of atoms is slow relative to the other reactions (i.e., $k_D/D = \delta \ll 1$) the equations may be solved simply to give the quasi-steady solution

$$\frac{[F]}{[F]_0} = \frac{K'_h}{D} \left[1 - \frac{K'_h - K_c}{D} \delta \right] e^{-K_c \delta t} \quad (B16)$$

$$\frac{[H]}{[F]_0} = \frac{K_c}{D} \left[1 - \frac{2K'_h}{D} \delta \right] e^{-K_c \delta t} \quad (B17)$$

$$[HF] = \frac{[F]_0 K_h K_c}{D} \left[2 - \frac{3K'_h - K_c}{D} \delta \right] e^{-K_c \delta t} \quad (B18)$$

Comparison of this model with computer calculations is excellent. Tables B1 and B2 show comparisons of the model with a corresponding computer calculation for cases with and without the loss of H atoms to the walls respectively. Local values are used for $[F_2]$ and $[H_2]$.

Thus we see that this simple model can serve well as a means of gaining quick insight into experimental results and provide guidance for efficient use of the more sophisticated computer models.

TABLE B1. STEADY STATE SOLUTION - COMPARISON
WITH COMPUTER CALCULATION

Case: Back reaction included

$x = 12.5$ cm

$T = 312$

$[F]_0 = 1.53 \times 10^{13}$
 $[H_2] = 1.40 \times 10^{15}$
 $[F_2] = 5.39 \times 10^{15}$

	Calculation	Approximation	Error (%)
[H]	6.23×10^{12}	6.16×10^{12}	1.1
[F]	9.09×10^{12}	9.15×10^{12}	0.6
[HF]	2.77×10^{17}	2.74×10^{17}	1.1

TABLE B2. STEADY STATE SOLUTION - COMPARISON
WITH COMPUTER CALCULATION

Case: Diffusion included

$$[\dot{H}]_{\text{Diff}} = -150 [H]$$

$x = 25 \text{ cm}$

$T = 334^\circ \text{K}$

$$[F] = 1.434 \times 10^{13}$$

$$[H_2] = 1.178 \times 10^{15}$$

$$[F_2] = 4.911 \times 10^{15}$$

	Computer	Approximation	Error
[H]	4.655×10^{12}	4.483×10^{12}	3.8%
[F]	8.023×10^{12}	8.007×10^{12}	0.2%
[H+F]	1.268×10^{13}	1.249×10^{13}	1.5%
[HF]	$2.415 \times 10^{17} \text{ sec}^{-1}$	2.330×10^{17}	3.6%

APPENDIX C

ACCOUNTING FOR TWO-DIMENSIONAL VELOCITY VARIATIONS IN PIPE FLOWS

The use of a quasi-one-dimensional model to analyze reacting flows within a circular pipe can lead to errors in interpretation of the data. First, the presence of boundary layers can strongly influence the pressure and mainstream velocity. A simple minded attempt to employ the true pressure distribution and mainstream velocity distribution in a one-dimensional calculator, however, will still lead to erroneous conclusions about the rates one is attempting to evaluate. The flow residing in the slower moving boundary layer tends to increase the effective reaction time for the gas found at a particular axial location. Thus a simple analysis based on the mainstream velocity would tend to overestimate the rate coefficient for the reaction of interest.

It is possible, however, to account for the effective rate of reaction in a two-dimensional flow with a one dimensional model. Under certain assumptions, a multiplying factor for the rate coefficients may be defined, based upon the 2-D velocity profile, that is incorporated into the rate equations.

Consider the following situation: (1) The rate equation can be expressed as linear function of the species of interest. (2) The velocity profile can be expressed as $u = u_c (1 - (r/R)^n)$, where u_c is the center line velocity and R the radius of the tube. (3) Diffusion is treated as for a binary system.

The first assumption is applicable to most relaxation rate equations and is also approximately applicable to the production of HF in the absence of back reactions. Then we have

$$\dot{HF} = [F][H_2] k_c + [H][F_2] k_n \quad (C1)$$

where k_n and k_c are the hot and cold reaction rate coefficients. We can re-express $[H_2]$ and $[F_2]$ as $([H_2]_0 - [HF]/2)$ and $([F_2]_0 - [HF]/2)$. This yields the rate equation

$$[HF] = \{ [F][H_2]_0 k_c - [H][F_2]_0 k_n \} - \frac{\{ [F] k_c + [H] k_n \}}{2} [HF] \quad (C2)$$

For quasi-steady state situations the terms in braces will be slowly varying and may be treated as constants so that

$$[HF] = K_1 - K_2 [HF] \quad (C3)$$

The second assumption reasonably represents the profiles of a pipe flow in various stages of development from an initially uniform velocity. Arbitrary profiles can also be treated as will be shown later.

Since our flow is primarily diluent, the third assumption is certainly valid.

We may now write the rate equation for an arbitrary species as

$$(1 - \hat{r}^n) \frac{\partial s}{\partial \hat{x}} = \frac{D}{kR^2} \frac{1}{\hat{r}} \frac{\partial}{\partial \hat{r}} \left(\hat{r} \frac{\partial s}{\partial \hat{r}} \right) + (K-s) \quad (C4)$$

where

$$\hat{r} = r/R \quad (C5)$$

$$\hat{x} = kx/u_E \quad (C6)$$

$$u = u_E (1 - \hat{r}^n) \quad (C7)$$

$$\dot{s}|_{\text{rate proc}} = k(K-s) \quad (C8)$$

We impose the initial condition

$$s = s_0 \text{ at } \hat{x} = 0 \quad (C9)$$

and the boundary condition

$$k_w s = - \frac{D}{r} \frac{\partial s}{\partial r} \text{ at } \hat{r} = 1 \quad (C10)$$

Let us now consider two limiting cases: (1) infinitely fast diffusion and (2) infinitely slow diffusion

Infinitely Fast Diffusion

For this case we define

$$\epsilon = \frac{kR^2}{D} \rightarrow 0 \quad (C11)$$

Then we assume the rate equation has a solution of the form

$$s = \varphi_0 + \epsilon \varphi_1 + O(\epsilon^2) \quad (C12)$$

Substitution of this into Equation (C4) yields the solution

$$s = \varphi_0(\hat{x}) + \epsilon \left\{ f(\hat{x}) + \frac{1}{4} \left(\frac{\partial \varphi_0}{\partial \hat{x}} - K + \varphi_0 \right) - \frac{1}{(n+2)^2} \frac{\partial \varphi_0}{\partial \hat{x}} \hat{r}^{n+2} + O(\epsilon^2) \right\} \quad (C12)$$

Application of the boundary condition with $k_w = 0$ gives

$$\varphi_0(\hat{x}) = K + C e^{-\frac{n+2}{n} \hat{x}} \quad (C14)$$

We may now apply the initial condition to find that as $\epsilon \rightarrow 0$

$$s = K + (s_0 - K) \exp \left\{ -\frac{n+2}{n} \frac{k}{u_E} x \right\} \quad (C15)$$

This solution is of the same form as the solution for a one-dimensional flow at velocity u_E . The only difference is that the exponential argument contains the additional factor $(n+2)/2$. Thus we consider the solution of our problem to be the solution of the one-dimensional problem referenced to the centerline velocity, but with an effective rate coefficient defined by

$$k_{eff} = \frac{n+2}{n} k = \beta_\infty(n) k \quad (C16)$$

where $\beta_\infty(n)$ is defined as the effective rate multiplier for infinite diffusion. In the limit of fully developed flow ($n = 2$) this reduces to

$$k_{eff} = 2k \quad (C17)$$

a solution previously obtained numerically (Ref. C1).

Strictly speaking this solution applies to a case in which the velocity profile is invariant with axial distance. However, we may apply the solution to a developing flow in which the fit parameter n varies by using the value for $\beta_\infty(n)$ appropriate to the local velocity profile. In the instantaneous diffusion limit, this approach is rigorously valid since the initial condition for every differential interval is a uniform concentration profile.

Infinitely Slow Diffusion

We now turn our attention to the case of no diffusion (i.e., $D \rightarrow 0$). In this limit we must solve the simplified equation

$$(1 - \hat{r}^n) \frac{\partial s}{\partial \hat{x}} = K - s \quad (C18)$$

Since there is no communication among streamlines we find an independent solution along each:

$$s(\hat{r}) = K + (s_0 - K) e^{-\frac{\hat{x}}{1 - \hat{r}^n}} \quad (C19)$$

-
- C1. Poirier, R. V. and R. W. Carr: "The Use of Tubular Flow Reactors for Kinetic Studies over Extended Pressure Ranges," J. Phys. Chem. **75**, 1593, 1971.

An effective rate coefficient may be defined by integrating $s(\hat{r})$ and equating it to the one-dimensional form of the solution. Thus we have

$$k_{\text{eff}} = - \ln \left\{ \int_0^1 2\hat{r} \exp \left(\frac{-\hat{x}}{1-\hat{r}^n} \right) d\hat{r} \right\} \quad (\text{C20})$$

and

$$\beta_0(n, \hat{x}) = k_{\text{eff}}/k \quad (\text{C21})$$

A plot of the variation of β_0 with n for various values of \hat{x} is shown in Figure C1. We see that as the extent of reaction increases the rate multiplier for any given velocity profile decreases towards unity. This is a consequence of the lack of communication between streamlines. As we move further and further downstream the reaction on the outer streamlines approaches completion and the effective rate of reaction becomes more a reflection of the chemistry near the center of the flow.

As for the infinite diffusion case, the solution above applies for a particular velocity profile, invariant with axial distance. It is possible to apply it to developing flows by using locally appropriate values for $\beta_0(n, \hat{x})$. This approach will not be rigorously correct in this case since the initial condition for any interval will not be a uniform concentration profile. Since our interest, however, is in bracketing the true solution, such an approach will suffice. The tendency will be to underestimate β_0 and thus overestimate the true rate coefficient k in an analysis of experimental data. The instantaneous diffusion solution, on the other hand, would underestimate k . Hence the two solutions should effectively bracket the results.

Test of Model

To test this approach to simulating reacting pipe flows with a one-dimensional model, a comparison was made with a two-dimensional computer code, MARBL, for a relatively simple case involving the chain reaction without any vibrational level detail. Two cases were considered (Table C1). Each had the same concentration of reactants, but in one case had an additional 15 torr of argon to bring the initial pressure up to 20 torr. The calculated velocity profiles from the 2-D MARBL program were used to develop β vs x curves for use in the 1-D CHEMIZ code.

The results of the calculations are shown in Figures C2 through C4. The first two show the HF variation for the 5 and 20 torr cases. The area between the infinite and zero diffusion solutions is shaded. Also shown are the solutions for two more simple minded one-dimensional approaches—a constant area solution and specification of the centerline velocity distribution. We see that the effective rate coefficient approach provides the best agreement

TABLE C1. INPUT CONDITIONS - EFFECTIVE RATE TEST CASES

$T = 300^{\circ}\text{K}$
 $L_{\text{mix}} = 0$
 $u = 10000 \text{ cm/sec}$

<u>Case</u>	<u>x_{H_2}</u>	<u>x_{F_2}</u>	<u>x_{F}</u>	<u>x_{Ar}</u>
p=5	0.0025	0.009	0.000025	0.98825
p=20	0.000625	0.00225	0.00000625	0.997063

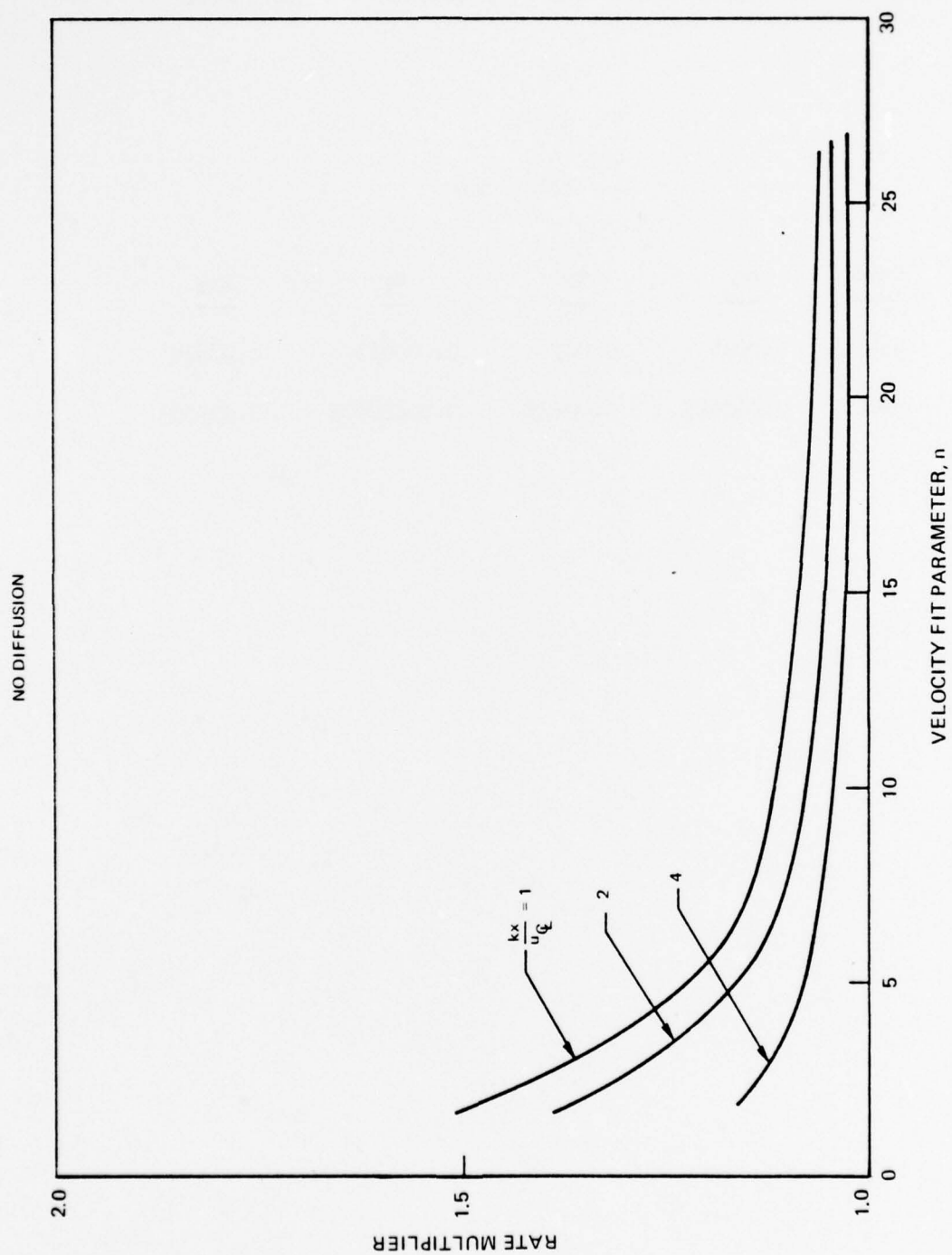


FIGURE C1 EFFECTIVE RATE COEFFICIENT MULTIPLIER

5 TORR CASE
HF PRODUCTION

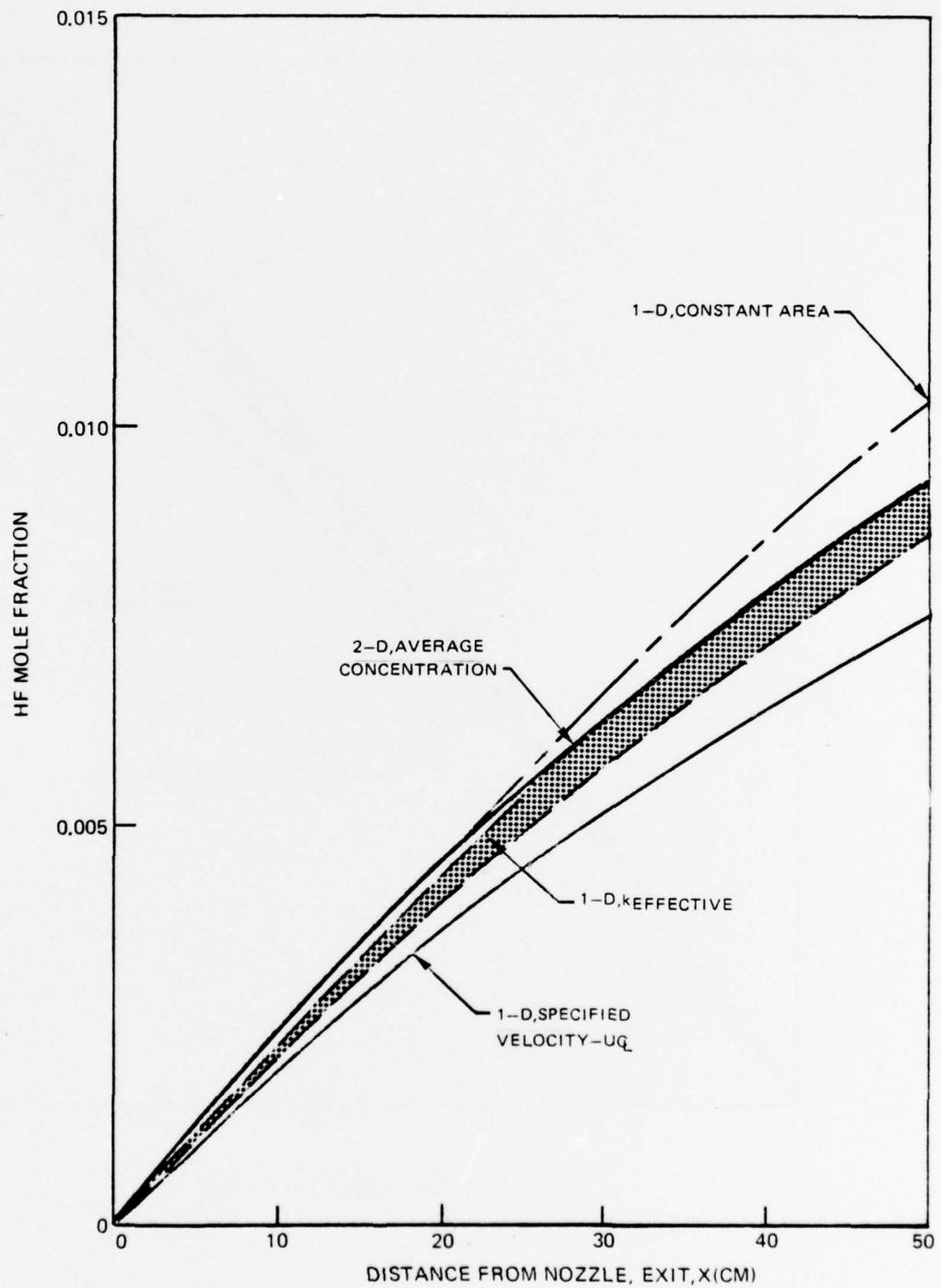


FIGURE C2 ONE DIMENSIONAL SIMULATION OF REACTING PIPE FLOW

20 TORR CASE
HF PRODUCTION

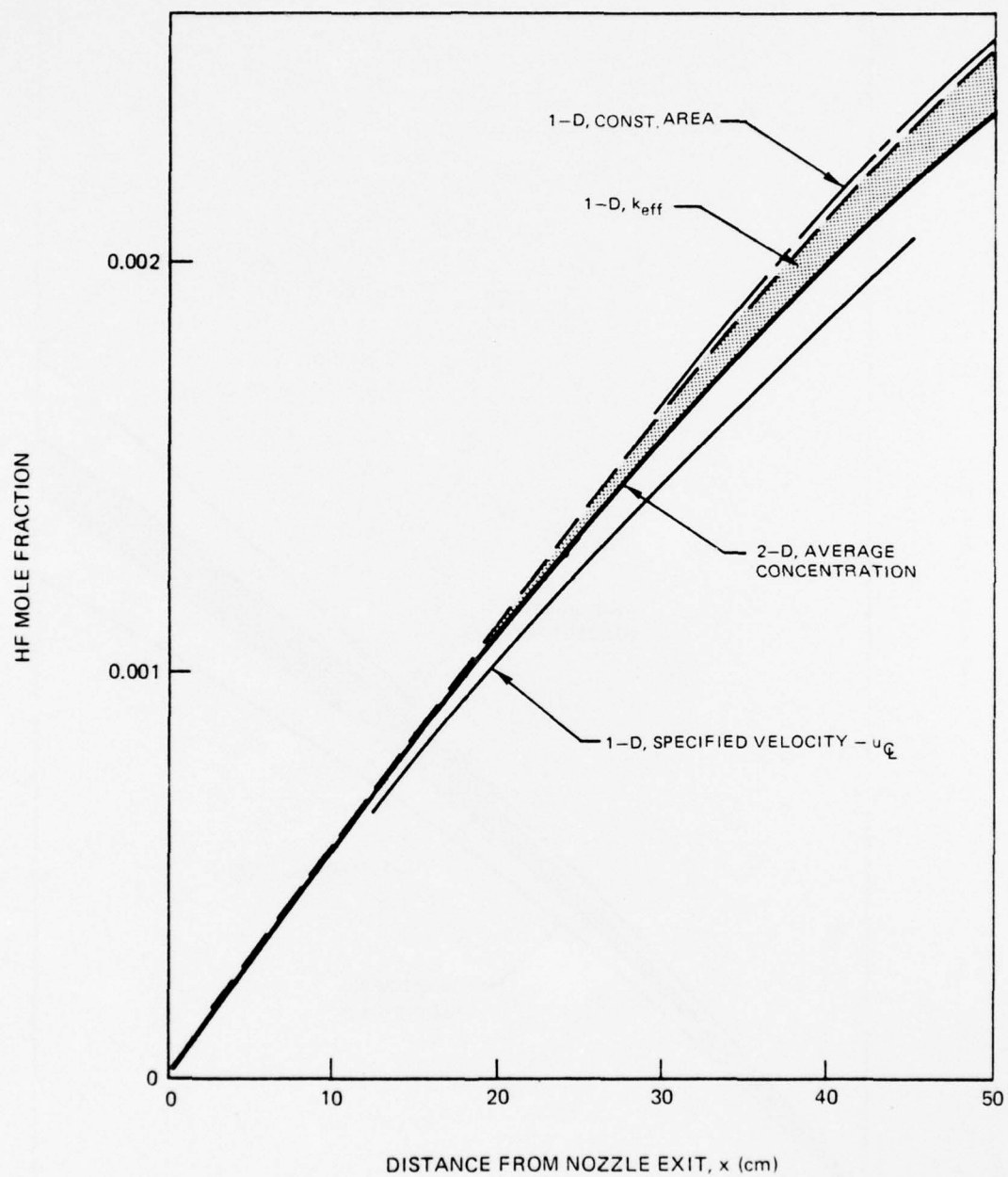


FIGURE C3 ONE DIMENSIONAL SIMULATION OF REACTING PIPE FLOW

20 TORR CASE
TEMPERATURE VS X

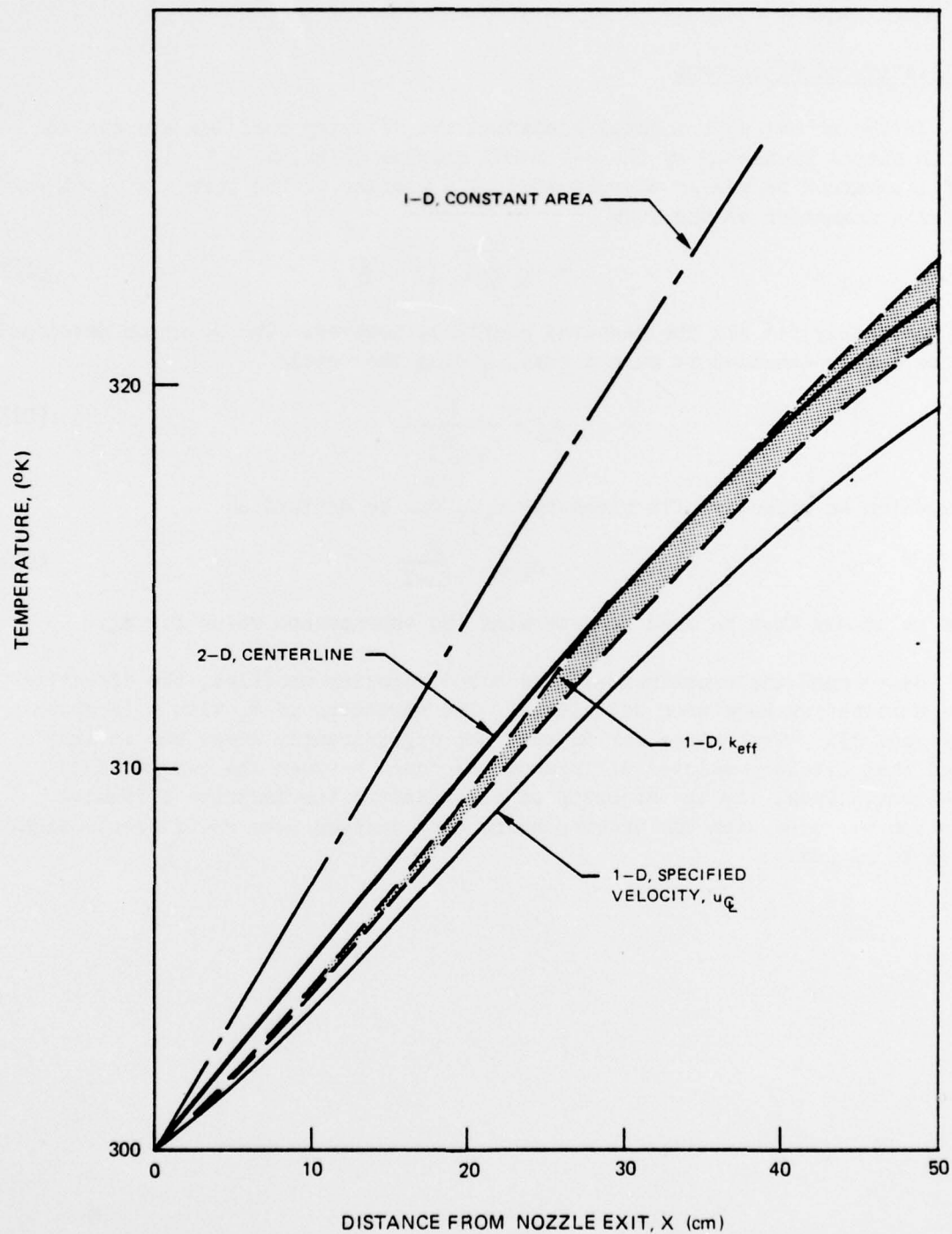


FIGURE C4 ONE DIMENSIONAL SIMULATION OF REACTING PIPE FLOW

in both cases. This is also true for the predicted temperature as is shown in the third figure.

Application to Experiment

In the actual experimental situation the velocity profiles are not the smooth shapes predicted by the 2-D MARBL program (Figs. 6 - 7). These profiles cannot be easily approximated by a profile of the form $u = u_L (1 - \hat{r}^n)$. A series summation of the form

$$u = u_L \sum_n a_n (1 - \hat{r}^n) \quad (C22)$$

can reasonably fit all the measured profiles, however. The solution developed can be easily extended to such a case, giving the result

$$\beta_\infty = \frac{1}{\sum \frac{na_n}{n+2}} \quad (C23)$$

from which an effective fit parameter n_{eff} can be defined as

$$n_{eff} = \frac{2}{\beta_\infty - 1} \quad (C24)$$

This value may then be used to determine the appropriate value for β_0 .

Based upon the experimentally measured velocity profiles, the effective rate multipliers have been calculated. The variation of β_∞ with x is shown in Figure C5. The values for β_0 were not significantly lower and it was found that little predicted difference was found between the two possible solutions. Thus, for the majority of calculations the infinite diffusion solution was used with the understanding that derived rate coefficients might be up to 5% low.

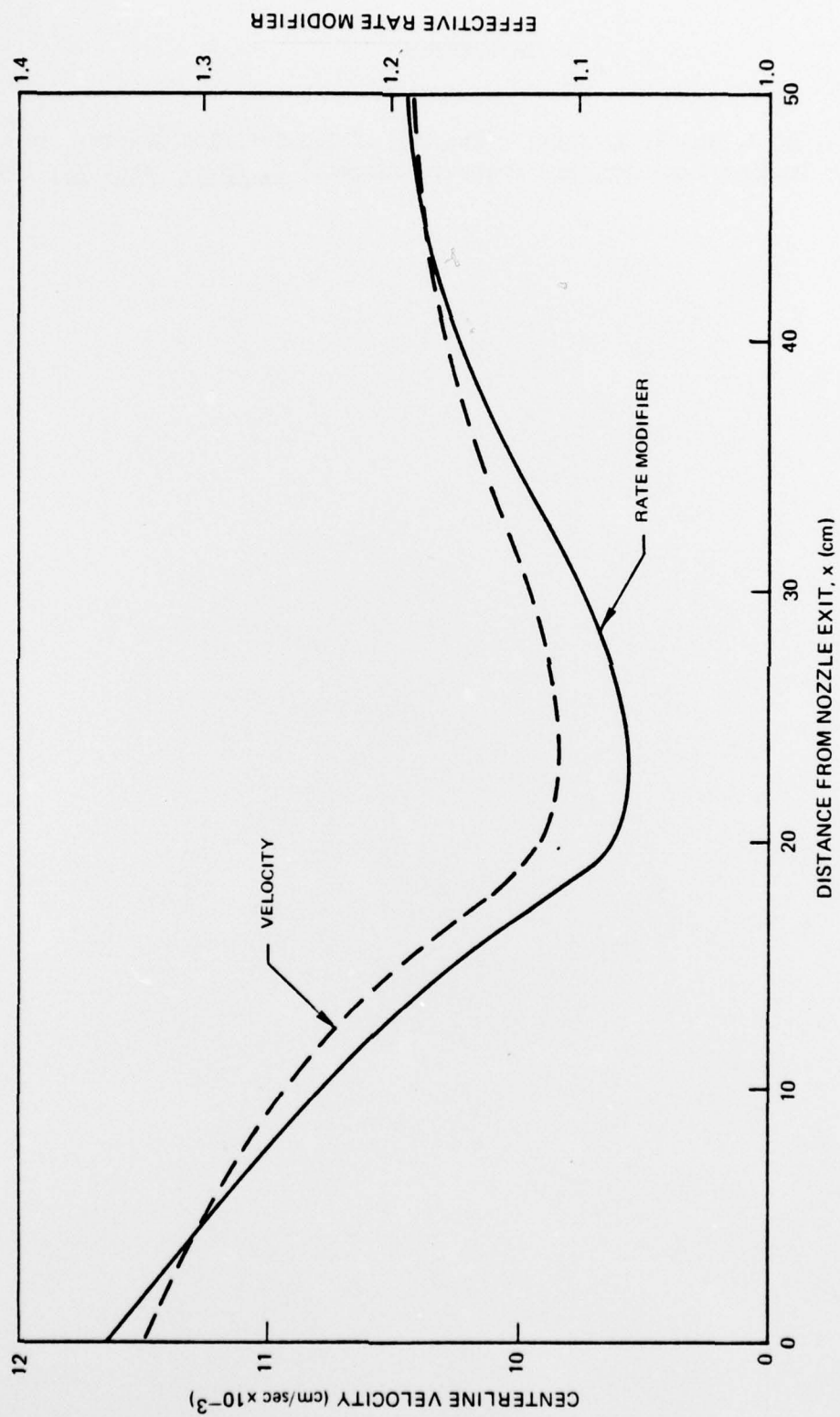


FIGURE C5 PRESCRIBED VELOCITY AND RATE MODIFIER FOR FLOW TUBE CALCULATIONS

References

- Cl. Poirier, R. V. and R. W. Carr: "The Use of Tubular Flow Reactors for Kinetic Studies over Extended Pressure Ranges," J. Phys. Chem. 75, 1593, 1971.

APPENDIX D

ESTIMATES OF WALL ADSORPTION EFFECTS

The experimental data available from the flow-tube and pulsed-fluorescence experiments has indicated that wall interactions may not be negligible. In particular the potential loss of atoms (H or F) or HF on the walls can influence the interpretation of the data. It is thus instructive to try to estimate the maximum possible loss by such processes.

Suppose that any molecule of the species of interest that strikes the walls of the test cell is adsorbed (or in effect destroyed). Suppose also that our cylindrically shaped test cells are very long relative to their diameter, and thus can be idealized as an infinite cylinder. Then the rate of change of the subject species will be described by the equation

$$\frac{\partial n(r,t)}{\partial t} - D \left(\frac{1}{r} \frac{\partial n(r,t)}{\partial r} + \frac{\partial^2 n(r,t)}{\partial r^2} \right) = \dot{n}(r,t)|_{\text{chem}} \quad (\text{D1})$$

with the boundary condition

$$n(R,t) = 0 \quad (\text{D2})$$

where

n = the number density of the subject species

$\dot{n}|_{\text{chem}}$ = the rate of production by chemical reactions

D = the diffusion coefficient of the subject species relative to the entire gas

Solution of this equation will, in principle, give the maximum adsorption that could occur for the conditions specified. Let us consider two highly simplified cases: (1) the species concentration is initially constant, with a zero chemical production rate; (2) the species concentration is initially zero and the chemical production rate is a constant.

The first case approximates the disappearance of the H or F atoms which would otherwise maintain essentially constant concentrations over a large fraction of the reaction time. The second case, if we restrict attention to the characteristic reaction time can approximate the loss of the HF being produced to the walls.

Potential Loss of Atoms to the Walls

We now obtain the solution for the first case. All that is required is the solution of the homogeneous part of equation (D1). This standard solution

may be found in any textbook on differential equations (Ref. D1) and is given by

$$n(r,t) = \frac{2}{R^2} \sum_{n=1}^{\infty} \frac{\int_0^R N_0(r) J_0(x_n r/R) dr}{[J_1(x_n)]^2} J_0\left(\frac{x_n r}{R}\right) e^{-\frac{x_n^2 D t}{R^2}} \quad (D3)$$

where $N_0(r)$ is the initial distribution of the species considered, J_0 is the zeroeth order Bessel function, J_1 is the first order Bessel function, and x_n is the n -th zero of J_0 .

If we let $N_0(r) = n_0 = \text{const}$, we may integrate equation (D3) to obtain

$$n(r,t) = 2n_0 \sum_{n=1}^{\infty} \frac{J_0(x_n r/R)}{x_n J_1(x_n r/R)} e^{-\frac{x_n^2 D t}{R^2}} \quad (D4)$$

This equation can be nondimensionalized by letting

$$\begin{aligned} \hat{r} &= r/R \\ \hat{t} &= \frac{x_1^2 D}{R^2} t \\ \hat{n} &= n/n_0. \end{aligned}$$

Then we have

$$\hat{n} = 2 \sum_{n=1}^{\infty} C_n J_0(x_n \hat{r}) e^{-\hat{t} \left(\frac{x_n}{x_1}\right)^2} \quad (D5)$$

where

$$C_n = \frac{1}{x_n J_1(x_n)}$$

With this nondimensional form of the equation it is possible to develop universal curves of the species distribution as a function of time. Then, with knowledge of the cylinder radius and gas diffusivity D , the time history of a specific case can be evaluated. The concentration profiles may also be averaged over the cylinder for various times to provide a plot of the average concentration in the cell as a function of time. This has indeed been done; the results are shown in Figure D1. Given are the centerline variation, the variation of the average along a diameter (called the linear average) and the average over a circular cross section (the cylindrical average). The linear average is essentially what one might observe using some radiative probe technique, whereas the cylindrical average represents the true average concentration for this idealized case.

D1. Martin, W. T. and E. Reissner, Elementary Differential Equation, Addison-Wesley, Reading, MA, 1961.

INFINITE CYLINDER, CONSTANT INITIAL POPULATION

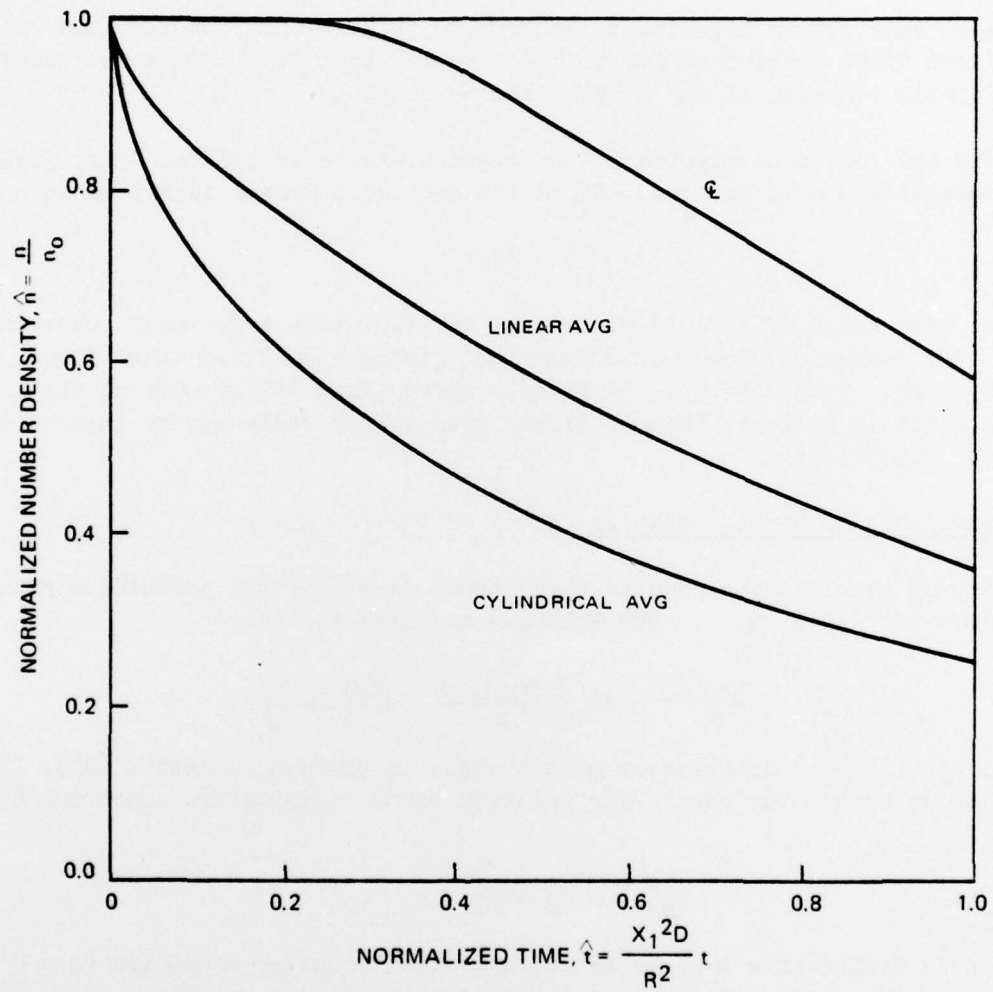


FIGURE D1 NORMALIZED NUMBER DENSITY TIME HISTORY

Consider now the cases of interest to us. For the pulsed-fluorescence experiment, the H atoms are immersed in a bath of Ar at 100 torr. For this the diffusivity is roughly $D \approx 8 \text{ cm}^2/\text{sec}$. The radius is 0.6 cm; hence, we have

$$\bar{t} = 122 \text{ } t \quad (\text{D6})$$

The time scale of the experiments is from 10 to 40 milliseconds. Thus the normalized times range from 1.2 to 5.0. We see that over such a time scale a considerable fraction of the H atoms can be lost.

For the flow tube experiment the argon pressure is only 20 torr, yielding a diffusivity $D \approx 40 \text{ cm}^2/\text{sec}$. Since the test cell radius is 2.5 cm we have

$$\bar{t} = 37 \text{ } t \quad (\text{D7})$$

Now the time scale of a fluid element in the flow tube experiments over the range of measurements is 4 to 6 milliseconds, giving normalized times from 0.15 to 0.22. Even for these relatively short times 30% or more of the atoms can potentially be lost. Hence, atomic loss to the walls may be important for both experiments.

Potential Loss of HF to the Walls

We now consider the case in which there is a constant production rate K over some time interval t . The equation to solve is then

$$\frac{\partial n(r,t)}{\partial t} - D \left(\frac{1}{r} \frac{\partial n(r,t)}{\partial r} + \frac{\partial^2 n(r,t)}{\partial r^2} \right) = K \quad (\text{D8})$$

The solution to the homogeneous part of this is given by equation (D3). In addition we obtain the particular solution for a steady state condition ($\partial n/\partial t = 0$):

$$n_p(r) = C_0 + C_1 \ln r + C_2 r^2 \quad (\text{D9})$$

Since n is finite at $r = 0$, we set $C_1 = 0$. The boundary condition ($n = 0$ on $r = R$) and the differential equation yield the complete solution

$$n_p = \frac{K}{4D} (R^2 - r^2) \quad (\text{D10})$$

We may superpose the two solutions and satisfy the initial condition

$$n(r,0) = n_0(r) \quad (D11)$$

by letting

$$N_0 = n_0(r) - \frac{K}{4D} (R^2 - r^2) \quad (D12)$$

in the homogeneous part. Thus we have

$$n(r,t) = \frac{K}{4D} \left\{ (R^2 - r^2) - \frac{2}{R^2} \frac{\sum_1^\infty \int_0^R \left[\frac{4Dr}{K} n_0(r) + r(r^2 - R^2) \right] J_0\left(\frac{x_n r}{R}\right) dr}{[J_1(x_n)]^2} \right. \\ \left. \times J_0\left(\frac{x_n r}{R}\right) e^{-\frac{x_n^2 Dt}{R^2}} \right\} \quad (D13)$$

In principle we could apply this in successive segments, each having a different average chemical production rate K , with the final profile of one segment used as the initial condition for the next. For our purposes, however, it will only be necessary to consider the simple case for which $n_0 = 0$, using an average chemical rate over the duration of the reaction.

For the case $N_0 = 0$ equation (D13) can be easily integrated to give

$$n(r,t) = \frac{K}{4D} \left\{ (R^2 - r^2) - 8R^2 \sum_1^\infty \frac{J_0(x_n r/R)}{x_n^3 J_1(x_n)} e^{-\frac{x_n^2 Dt}{R^2}} \right\} \quad (D14)$$

We may define a universal curve applicable to any combination of diffusivity D and reaction rate K by letting

$$\hat{r} = r/R \quad (D15)$$

$$\hat{t} = (x_1/R)^2 Dt \quad (D16)$$

$$\hat{n} = n / \frac{KR^2}{D} \quad (D17)$$

to give

$$\hat{n} = \frac{1}{4} [1 - \hat{r}^2 + \sum C_n J_0(x_n \hat{r}) e^{-\frac{(x_n)^2 \hat{t}}{x_1^2}}] \quad (D18)$$

where

$$C_n = \frac{-8}{x_n^3 J_1(x_n)} \quad (D19)$$

Equation (D18) can then be used to generate curves of \hat{n} against \hat{r} for various values of \hat{t} , and these in turn can be integrated to define average number densities as a function of \hat{t} . This has been done; the results are presented in Figure D2. Two averages are presented: the linear average

$$\langle \hat{n} \rangle = \int_0^1 \hat{n} \, d\hat{r} \quad (D20)$$

and the cylindrical average

$$\langle \hat{n} \rangle = 2 \int_0^1 \hat{r} \hat{n} \, d\hat{r} \quad (D21)$$

The "average" number density seen by a probe laser passing along a diameter of the cell with a finite beam width will lie between these two values.

It is expected that for the flow tube experiments HF adsorption on the walls will have little influence on the results. These experiments are performed over long time periods such that the walls would be saturated with HF. The pulsed fluorescence experiments, on the other hand, are of short duration, with emptying and refilling of the test cell between each run.

For the pulsed-fluorescence experiments the diffusivity of the HF through the argon is $D \approx 2 \text{ cm}^2/\text{sec}$ and the radius of the test cell is 0.6 cm. Thus we have

$$\hat{t} = 34t \quad (D22)$$

Consider now test series A. The maximum possible HF is $6.04 \times 10^{16} \text{ cm}^{-3}$; the reaction occurs over approximately 20 milliseconds at $\hat{t} = 0.64$. By referring to the figure we see that the average number density is between 55 and 65% of the maximum possible. This gives a number density range of 3.3×10^{16} to $3.3 \times 10^{16} \text{ cm}^{-3}$, well below the observed maxima. Similar we can consider the other test series. The results are summarized in Table D1. As can be seen, the observed number densities generally lie in a range for which HF could have been lost to the walls. A more realistic treatment, allowing for faster initial chemical rates and slower rates at later times would have given even lower predicted number densities. Hence even with diffusion coefficients as low as $2.0 \text{ cm}^2/\text{sec}$ the potential for significant wall loss exists.

INFINITE CYLINDER, CONSTANT CHEMICAL PRODUCTION

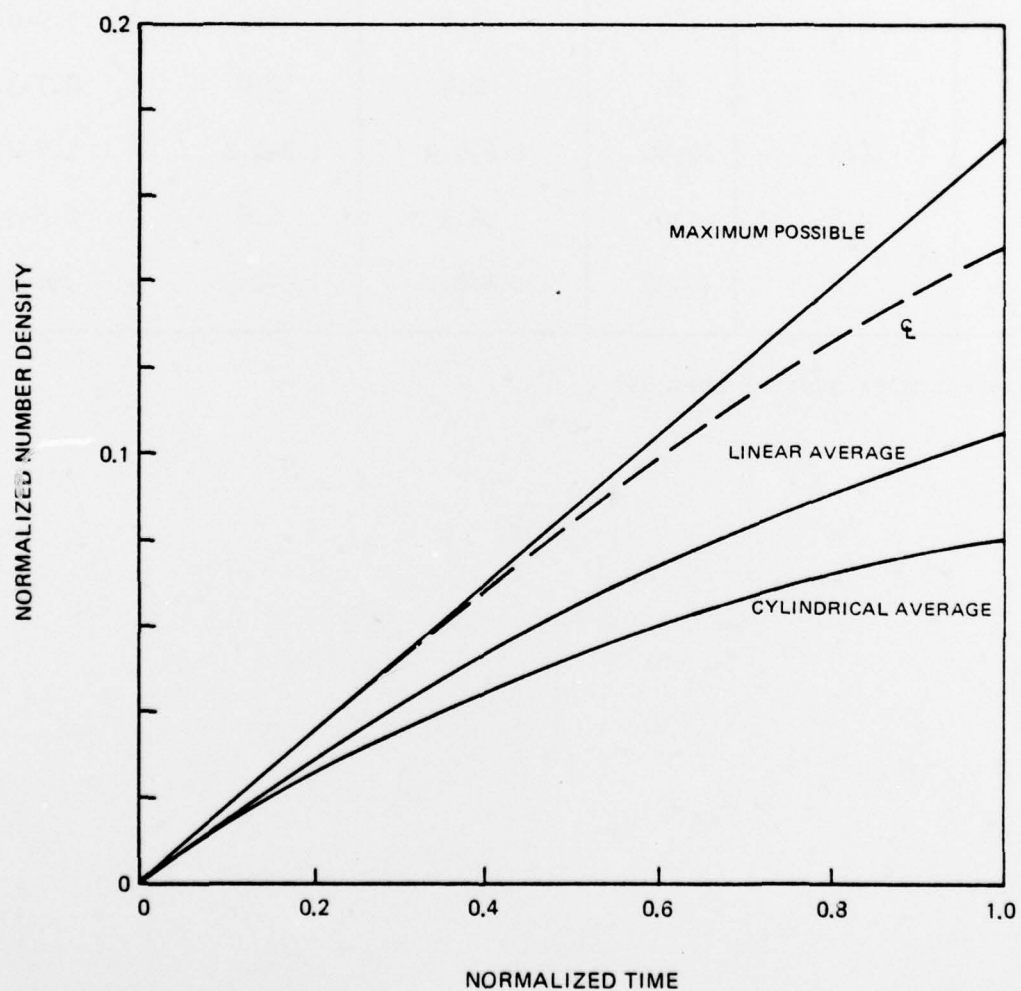


FIGURE D2. NORMALIZED NUMBER DENSITY TIME HISTORY

TABLE D1. POSSIBLE HF WALL LOSS EFFECTS IN PULSED-FLUORESCENCE TESTS

Series	Maximum No. Density ($\text{cm}^{-3} \times 10^{-16}$)	Reaction Time (ms)	Average Number Density		Observed* No. Densities ($\text{cm}^{-3} \times 10^{-16}$)
			Cylindrical ($\text{cm}^{-3} \times 10^{-16}$)	Linear ($\text{cm}^{-3} \times 10^{-16}$)	
A	6.04	20	3.3	3.9	5.2-6.1
B	6.6	20	3.6	4.3	5.9-6.5
C	3.5	10	2.4	2.8	2.7-3.3
D	2.8	20-40	1.6-0.9	1.8-1.2	1.5-2.0
E	3.2	10	2.1	2.6	2.6-3.2
F	1.5	20-30	0.8-0.7	1.0-0.9	.80-1.4

* Pulse energies greater than 0.1 J

References

- D1. Martin, W. T. and E. Reissner, Elementary Differential Equation, Addison-Wesley, Reading, MA, 1961.

LIST OF SYMBOLS

P_F	Atomic fluorine partial pressure
P_{O_2}	Molecular oxygen partial pressure
k	Boltzmann's constant
T	Temperature of gas
h	Planck's constant
ν	ESR transition frequency
β	Bohr magneton
H	Magnetic field strength
f	Spectrometer factor
χ''	Molecular susceptibility
Q	Theoretical ESR intensity factor
A_F	Area bounded by F ESR signal
A_{O_2}	Area bounded by O_2 ESR signal
W	Width of ESR signal
L	Height of ESR signal
S	ESR signal amplification factor
V	Field modulation voltage